Electronic transport in two-dimensional graphene

S. Das Sarma

Condensed Matter Theory Center, Department of Physics, University of Maryland, College Park, Maryland 20742-4111, USA

Shaffique Adam

Condensed Matter Theory Center, Department of Physics, University of Maryland, College Park, Maryland 20742-4111, USA and Center for Nanoscale Science and Technology, National Institute of Standards and Technology, Gaithersburg, Maryland 20899-6202, USA

E. H. Hwang

Condensed Matter Theory Center, Department of Physics, University of Maryland, College Park, Maryland 20742-4111, USA

Enrico Rossi[*]

Condensed Matter Theory Center, Department of Physics, University of Maryland, College Park, Maryland 20742-4111, USA

A broad review of fundamental electronic properties of two-dimensional graphene with the emphasis on density and temperature-dependent carrier transport in doped or gated graphene structures is provided. A salient feature of this review is a critical comparison between carrier transport in graphene and in two-dimensional semiconductor systems (e.g., heterostructures, quantum wells, inversion layers) so that the unique features of graphene electronic properties arising from its gapless, massless, chiral Dirac spectrum are highlighted. Experiment and theory, as well as quantum and semiclassical transport, are discussed in a synergistic manner in order to provide a unified and comprehensive perspective. Although the emphasis of the review is on those aspects of graphene transport where reasonable consensus exists in the literature, open questions are discussed as well. Various physical mechanisms controlling transport are described in depth including long-range charged impurity scattering, screening, short-range defect scattering, phonon scattering, many-body effects, Klein tunneling, minimum conductivity at the Dirac point, electron-hole puddle formation, *p-n* junctions, localization, percolation, quantum-classical crossover, midgap states, quantum Hall effects, and other phenomena.

CONTENTS

[*]Present address: Department of Physics, College of William and Mary, Williamsburg, VA 23187, USA.

I. INTRODUCTION

A. Scope

The experimental discovery of two-dimensional (2D) gated graphene in 2004 by Novoselov *et al.* (2004) is a seminal event in electronic materials science, ushering in a tremendous outburst of scientific activity in the study of electronic properties of graphene, which continued unabated up until the end of 2009 (with the appearance of more than 5000 articles on graphene during the 2005–2009 five-year period). The subject has now reached a level so vast that no single article can cover the whole topic in any reasonable manner, and most general reviews are likely to become obsolete in a short time due to rapid advances in the graphene literature.

The scope of the current review is transport in gated graphene with the emphasis on fundamental physics and conceptual issues. Device applications and related topics are not discussed (Avouris *et al.*, 2007), nor are graphene's mechanical properties (Bunch *et al.*, 2007; Lee, Wei *et al.*, 2008). The important subject of graphene materials science, which deserves its own separate review, is not discussed at all. Details of the band structure properties and related phenomena are also not covered in any depth, except in the context of understanding transport phenomena. What is covered in reasonable depth is the basic physics of carrier transport in graphene, critically compared with the corresponding well-studied 2D semiconductor transport properties, with the emphasis on scattering mechanisms and conceptual issues of fundamental importance. In the context of 2D transport, it is conceptually useful to compare and contrast graphene with the much older and well established subject of carrier transport in 2D semiconductor structures [e.g., Si inversion layers in metal-oxide-semiconductor-field-effect transistors (MOSFETs), 2D GaAs heterostructures, and quantum wells]. Transport in 2D semiconductor systems has a number of similarities and key dissimilarities with graphene. One purpose of this review is to emphasize the key conceptual differences between 2D graphene and 2D semiconductors in order to bring out the new fundamental aspects of graphene transport, which make it a truly novel electronic material that is qualitatively different from the large class of existing and well established 2D semiconductor materials.

Since graphene is a dynamically (and exponentially) evolving subject, with new important results appearing almost every week, the current review concentrates on only those features of graphene carrier transport where some qualitative understanding, if not a universal consensus, has been achieved in the community. As such, some active topics, where the subject is in flux, have been left out. Given the constraint of the size of this review, depth and comprehension have been emphasized over breadth; given the large graphene literature, no single review can attempt to provide a broad coverage of the subject at this stage. There have already been several reviews of graphene physics in the recent literature. We have made every effort to minimize overlap between our article and these recent reviews. The closest in spirit to our review is the one by Castro Neto *et al.* (2009) which was written 2.5 years ago (i.e. more than 3000 graphene publications have appeared in the literature since that review was written). Our review should be considered complimentary to Castro Neto *et al.* (2009), and we have tried avoiding too much repetition of the materials they already covered, concentrating instead on the new results arising in the literature following the older review. Although some repetition is necessary in order to make our review self-contained, we refer the interested reader to Castro Neto *et al.* (2009) for details on the history of graphene, its band structure considerations, and the early (2005–2007) experimental and theoretical results. Our material emphasizes the more mature phase (2007–2009) of 2D graphene physics.

For further background and review of graphene physics beyond the scope of our review, we mention in addition to the Rev. Mod. Phys. article by Castro Neto *et al.* (2009), the accessible reviews by Geim and his collaborators (Geim and Novoselov, 2007; Geim, 2009), the recent brief review by Mucciolo and Lewenkopf (2010), as well as two edited volumes of Solid State Communications (Das Sarma, Geim *et al.*, 2007; Fal'ko *et al.*, 2009), where the active graphene researchers have contributed individual perspectives.

B. Background

Graphene (or more precisely, monolayer graphene—in this review, we refer to monolayer graphene simply as "graphene") is a single 2D sheet of carbon atoms in a honeycomb lattice. As such, 2D graphene rolled up in the plane is a carbon nanotube, and multilayer graphene with weak

interlayer tunneling is graphite. Given that graphene is simply a single 2D layer of carbon atoms peeled off a graphite sample, early interest in the theory of graphene band structure was all worked out a long time ago. In this review we only consider graphene monolayers (MLG) and bilayers (BLG), which are both of great interest.

1. Monolayer graphene

Graphene monolayers have been rightfully described as the "ultimate flatland" (Geim and MacDonald, 2007), i.e., the most perfect 2D electronic material possible in nature, since the system is exactly one atomic monolayer thick, and carrier dynamics is necessarily confined in this strict 2D layer. The electron hopping in the 2D graphene honeycomb lattice is quite special since there are two equivalent lattice sites [*A* and *B* in Fig. 1(a)] which give rise to the "chirality" in the graphene carrier dynamics.

The honeycomb structure can be thought of as a triangular lattice with a basis of two atoms per unit cell, with 2D lattice vectors $\mathbf{A_0} = (a/2)(3, \sqrt{3})$ and $\mathbf{B_0} = (a/2)(3, -\sqrt{3})$ ($a \approx 0.142$ nm is the carbon-carbon distance). $\mathbf{K} = (2\pi/(3a), 2\pi/(3\sqrt{3}a))$ and $\mathbf{K'} = (2\pi/(3a), -2\pi/(3\sqrt{3}a))$ are the inequivalent corners of the Brillouin zone and are called Dirac points. These Dirac points are of great importance in the electronic transport of graphene, and they play a role similar to the role of Γ points in direct band-gap semiconductors such as GaAs. Essentially, all of the physics discussed in this review is the physics of graphene carriers (electrons and/or holes) close to the Dirac points (i.e., within a 2D wave vector $q = |\mathbf{q}| \ll 2\pi/a$ of the Dirac points) just as all the 2D semiconductor physics we discuss will occur around the Γ point.

The electronic band dispersion of 2D monolayer graphene was calculated by Wallace (1947) and others (McClure, 1957; Slonczewski and Weiss, 1958) a long time ago, within the tight-binding prescription, keeping up to the second-nearest neighbor hopping term in the calculation. The following approximate analytic formula is obtained for the conduction (upper, $+$, π^*) band and valence (lower, $-$, π) band:

$$E_{\pm}(q) \approx 3t' \pm \hbar v_F |\mathbf{q}| - \left(\frac{9t'a^2}{4} \pm \frac{3ta^2}{8} \sin(3\theta_q)\right)|\mathbf{q}|^2, \tag{1.1}$$

with $v_F = 3ta/2$, $\theta_q = \arctan^{-1}[q_x/q_y]$, and where t, t' are, respectively, the nearest-neighbor (i.e. intersublattice $A - B$) and next-nearest-neighbor (i.e. intrasublattice $A - A$ or $B - B$) hopping amplitudes, and $t(\approx 2.5$ eV$) \gg t'(\approx 0.1$ eV$)$.

The almost universally used graphene band dispersion at long wavelength puts $t' = 0$, where the band structure for small q relative to the Dirac point is given by

$$E_{\pm}(q) = \pm \hbar v_F q + \mathcal{O}(q/k)^2. \tag{1.2}$$

Further details on the band structure of 2D graphene monolayers can be found in the literature (Wallace, 1947; McClure, 1957; Slonczewski and Weiss, 1958; McClure, 1964; Reich *et al.*, 2002; Castro Neto *et al.*, 2009) and will not be discussed here. Instead, we provide below a thorough discussion of the implications of Eq. (1.2) for graphene carrier transport. Since much of the fundamental interest is in understanding graphene transport in the relatively low carrier density regime, complications arising from the large $q(\approx K)$ aspects of graphene band structure can be neglected.

The most important aspect of graphene's energy dispersion (and the one attracting the most attention) is its linear energy-momentum relationship with the conduction and valence bands intersecting at $q = 0$, with no energy gap. Graphene is thus a zero band-gap semiconductor with a linear, rather than quadratic, long-wavelength energy dispersion for both electrons (holes) in the conduction (valence) bands. The existence of two Dirac points at K and K', where the Dirac cones for electrons and holes touch [Fig. 2(b)] each other in momentum space, gives rise to a valley degeneracy $g_v = 2$ for graphene. The presence of any intervalley scattering between K and K' points lifts this valley degeneracy, but
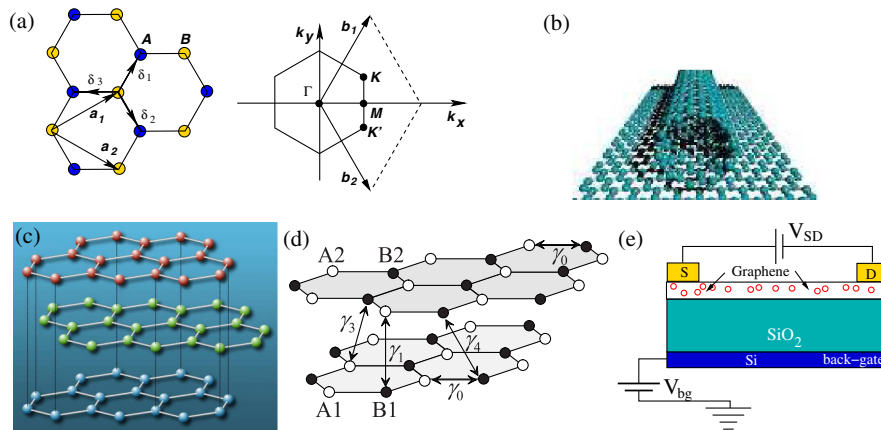
FIG. 1 (color online). (a) Graphene honeycomb lattice showing in different colors the two triangular sublattices. Also shown is the graphene Brillouin zone in momentum space. Adapted from Castro Neto *et al.*, 2009. (b) Carbon nanotube as a rolled up graphene layer. Adapted from Lee, Sharma *et al.*, 2008. (c) Lattice structure of graphite, graphene multilayer. Adapted from Castro Neto *et al.*, 2006. (d) Lattice structure of bilayer graphene. γ_0 and γ_1 are, respectively, the intralayer and interlayer hopping parameters t, $t_\perp$ used in the text. The interlayer hopping parameters γ_3 and γ_4 are much smaller than $\gamma_1 \equiv t_\perp$ and are normally neglected. Adapted from Mucha-Kruczynski *et al.*, 2010. (e) Typical configuration for gated graphene.
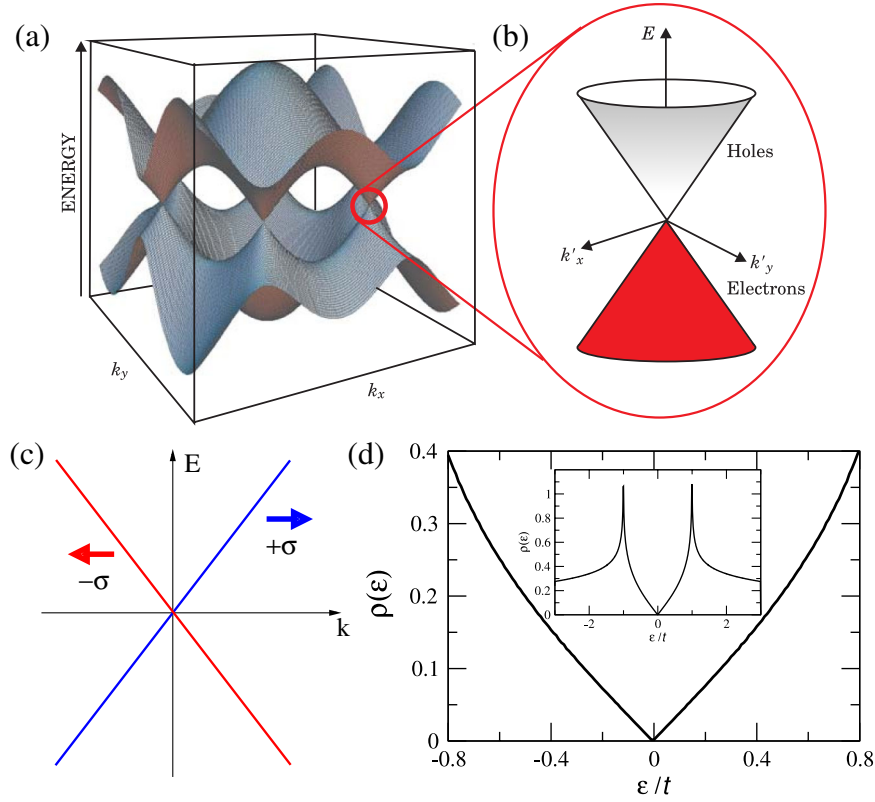
FIG. 2 (color online). (a) Graphene band structure. Adpated from Wilson, 2006. (b) Enlargment of the band structure close to the K and K' points showing the Dirac cones. Adpated from Wilson, 2006. (c) Model energy dispersion $E = \hbar v_F |\mathbf{k}|$. (d) Density of states of graphene close to the Dirac point. The inset shows the density of states over the full electron bandwidth. Adapted from Castro Neto *et al.*, 2009.

such effects require the presence of strong lattice scale scattering. Intervalley scattering seems to be weak and when they can be ignored, the presence of a second valley can be taken into account simply via the degenercy factor $g_v = 2$. Throughout this introduction, we neglect intervalley scattering processes.

The graphene carrier dispersion $E_{\pm}(q) = \hbar v_F q$ explicitly depends on the constant v_F, sometimes called the graphene (Fermi) velocity. In the literature different symbols (v_F, v_0, $\gamma/\hbar$) are used to denote this velocity. The tight-binding prescription provides a formula for v_F in terms of the nearest neighbor hopping t and the lattice constant $a_2 = \sqrt{3}a$: $\hbar v_F = 3ta/2$. The best estimates of $t \approx 2.5$ eV and $a = 0.14$ nm give $v_F \approx 10^8$ cm/s for the empty graphene band, i.e., in the absence of any carriers. The presence of carriers may lead to a many-body renormalization of the graphene velocity, which is, however, small for MLG but could, in principle, be substantial for BLG.

The linear long-wavelength Dirac dispersion, with a Fermi velocity that is roughly $1/300$ of the velocity of light, is the most distinguishing feature of graphene in addition to its strict 2D nature. It is therefore natural to ask about the precise applicability of the linear energy dispersion, since it is obviously a long-wavelength continuum property of graphene carriers valid only for $q \ll K \approx (0.1 \text{ nm})^{-1}$.

There are several ways to estimate the cutoff wave vector (or momentum) k_c above which the linear continuum Dirac dispersion approximation breaks down for graphene. The easiest is perhaps to estimate the carrier energy $E_c =$ $\hbar v_F k_c$ and to demand that $E_c < 0.4t(1.0 \text{ eV})$, so that one can ignore the lattice effects (which lead to deviations from pure Dirac-like dispersion). This leads to a cutoff wave vector given by $k_c \approx 0.25 \text{ nm}^{-1}$.

The mapping of graphene electronic structure onto the massless Dirac theory is deeper than the linear graphene carrier energy dispersion. The existence of two equivalent, but independent, sublattices A and B (corresponding to the two atoms per unit cell) leads to the existence of a novel chirality in graphene dynamics where the two linear branches of graphene energy dispersion (intersecting at Dirac points) become independent of each other, indicating the existence of a pseudospin quantum number analogous to electron spin (but completely independent of real spin). Thus, graphene carriers have a pseudospin index in addition to the spin and orbital index. The existence of the chiral pseudospin quantum number is a natural byproduct of the basic lattice structure of graphene comprising two independent sublattices. The long-wavelength, low energy effective 2D continuum Schrödinger equation for spinless graphene carriers near the Dirac point therefore becomes

$$- i\hbar v_F \boldsymbol{\sigma} \cdot \boldsymbol{\nabla} \Psi(\mathbf{r}) = E\Psi(\mathbf{r}), \qquad (1.3)$$

where $\boldsymbol{\sigma} = (\sigma_x, \sigma_y)$ is the usual vector of Pauli matrices (in 2D now), and $\Psi(\mathbf{r})$ is a 2D spinor wave function. Equation (1.3) corresponds to the effective low energy Dirac Hamiltonian:
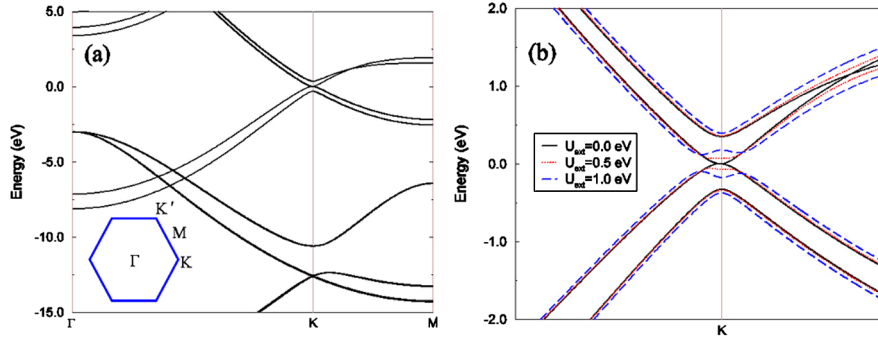
FIG. 3 (color online).   (a) Energy band of bilayer graphene for $V = 0$. (b) Enlargment of the energy band close to the neutrality point K for different values of V. Adapted from Min *et al.*, 2007.

$$\mathcal{H} = \hbar v_F \begin{pmatrix} 0 & q_x - iq_y \\ q_x + iq_y & 0 \end{pmatrix} = \hbar v_F \boldsymbol{\sigma} \cdot \mathbf{q}. \quad (1.4)$$

We note that Eq. (1.3) is simply the equation for massless chiral Dirac fermions in 2D (except that the spinor here refers to the graphene pseudospin rather than real spin), although it is arrived at starting purely from the tight-binding Schrödinger equation for carbon in a honeycomb lattice with two atoms per unit cell. This mapping of the low energy, long-wavelength electronic structure of graphene onto the massless chiral Dirac equation was discussed by Semenoff (1984) more than 25 years ago. It is a curious historical fact that although the actual experimental discovery of gated graphene (and the beginning of the frenzy of activities leading to this review) happened only in 2004, some of the key theoretical insights go back a long way in time and are as valid today for real graphene as they were for theoretical graphene when they were introduced (Wallace, 1947; McClure, 1957; Semenoff, 1984; Haldane, 1988; Gonzalez *et al.*, 1994; Ludwig *et al.*, 1994).

The momentum space pseudospinor eigenfunctions for Eq. (1.3) can be written as

$$\Psi(\mathbf{q}, K) = \frac{1}{\sqrt{2}} \begin{pmatrix} e^{-i\theta_q/2} \\ \pm e^{i\theta_q/2} \end{pmatrix},$$

$$\Psi(\mathbf{q}, K') = \frac{1}{\sqrt{2}} \begin{pmatrix} e^{i\theta_q/2} \\ \pm e^{-i\theta_q/2} \end{pmatrix},$$

where the $\pm$ signs correspond to the conduction (valence) bands with $E_{\pm}(q) = \pm \hbar v_F q$. It is easy to show using the Dirac equation analogy that the conduction (valence) bands come with positive (negative) chirality, which is conserved, within the constraints of the validity of Eq. (1.3). We note that the presence of real spin, ignored so far, would add an extra spinor structure to graphene's wave function (this real spin part of the graphene wave function is similar to that of ordinary 2D semiconductors). The origin of the massless Dirac description of graphene lies in the intrinsic coupling of its orbital motion to the pseudospin degree of freedom due to the presence of A and B sublattices in the underlying quantum-mechanical description.

2. Bilayer graphene

The case of bilayer graphene is interesting in its own right, since with two graphene monolayers that are weakly coupled

by interlayer carbon hopping, it is intermediate between graphene monolayers and bulk graphite.

The tight-binding description can be adapted to study the bilayer electronic structure assuming specific stacking of the two layers with respect to each other (which controls the interlayer hopping terms). Considering the so-called A-B stacking of the two layers [which is the three-dimensional (3D) graphitic stacking], the low energy, long-wavelength electronic structure of bilayer graphene is described by the following energy dispersion relation (Brandt *et al.*, 1988; Dresselhaus and Dresselhaus, 2002; McCann, 2006; McCann and Fal'ko, 2006):

$$E_{\pm}(q) = [V^2 + \hbar^2 v_F^2 q^2 + t_{\perp}^2/2 \pm (4V^2 \hbar^2 v_F^2 q^2 + t_{\perp}^2 \hbar^2 v_F^2 q^2 + t_{\perp}^4/4)^{1/2}]^{1/2}, \quad (1.5)$$

where $t_{\perp}$ is the effective interlayer hopping energy (and t, v_F are the intralayer hopping energy and graphene Fermi velocity for the monolayer case) (see Fig. 3). We note that $t_{\perp} (\approx 0.4 \text{ eV}) < t (\approx 2.5 \text{ eV})$, and we have neglected several additional interlayer hopping terms since they are much smaller than $t_{\perp}$. The quantity V with dimensions of energy appearing in Eq. (1.5) for bilayer dispersion corresponds to the possibility of a real shift (e.g. by an applied external electric field perpendicular to the layers, $\hat{z}$ direction) in the electrochemical potential between the two layers, which would translate into an effective band-gap opening near the Dirac point (Castro *et al.*, 2007; Ohta *et al.*, 2006; Oostinga *et al.*, 2008; Zhang, Tang *et al.*, 2009).

Expanding Eq. (1.5) to leading order in momentum, and assuming $V \ll t$, we get

$$E_{\pm}(q) = \pm [V - 2\hbar^2 v_F^2 V q^2/t_{\perp}^2 + \hbar^4 v_F^4 q^4/(2t_{\perp}^2 V)]. \quad (1.6)$$

We conclude the following (i) For $V \neq 0$, bilayer graphene has a minimum band gap of $\Delta = 2V - 4V^3/t_{\perp}^2$ at $q = \sqrt{2}V/\hbar v_F$; and (ii) for $V = 0$, bilayer graphene is a gapless semiconductor with a parabolic dispersion relation $E_{\pm}(q) \approx \hbar^2 v_F^2 q^2/t_{\perp} = \hbar^2 q^2/(2m)$, where $m = t_{\perp}/(2v_F^2)$ for small q. The parabolic dispersion (for $V = 0$) applies only for small values of q satisfying $\hbar v_F q \ll t_{\perp}$; whereas, in the opposite limit $\hbar v_F q \gg t_{\perp}$, we get a linear band dispersion $E_{\pm}(q) \approx \pm \hbar v_F q$, just as in the monolayer case. We note that using the best estimated values for v_F and $t_{\perp}$, the bilayer effective mass
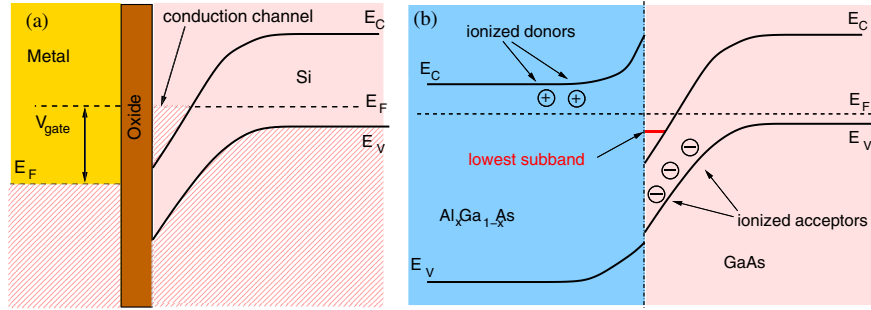
FIG. 4 (color online). (a) Diagram showing the bands at the interfaces of a metal-oxide-silicon structure. (b) Band diagram showing the bending of the bands at the interface of the semiconductors and the two-dimensional subband.

is $m \approx (0.03–0.05)m_e$, which corresponds to a very small effective mass.

To better understand the quadratic to linear crossover in the effective BLG band dispersion, it is convenient to rewrite the BLG band dispersion (for $V = 0$) in the following hyperbolic form:

$$E_{\mathrm{BLG}} = \mp m v_F^2 \pm m v_F^2 [1 + (k/k_0)^2]^{1/2}, \qquad (1.7)$$

where $k_0 = t_\perp/(2\hbar v_F)$ is a characteristic wave vector. In this form it is easy to see that $E_{\mathrm{BLG}} \rightarrow k^2(k)$ for $k \rightarrow 0(\infty)$ for the effective BLG band dispersion with $k \ll k_0$ ($k \gg k_0$) being the parabolic (linear) band dispersion regimes, $k_0 \approx 0.3$ nm^{-1} for $m \approx 0.03 m_e$. Using the best available estimates from band structure calculations, we conclude that for carrier densities smaller (larger) than 5×10^{12} cm^{-2}, the BLG system should have parabolic (linear) dispersion at the Fermi level.

What about chirality for bilayer graphene? Although the bilayer energy dispersion is non-Dirac–like and parabolic, the system is still chiral due to the A/B sublattice symmetry giving rise to the conserved pseudospin quantum index. The detailed chiral 4-component wave function for the bilayer case, including both layer and sublattice degrees of freedom, can be found in the literature (McCann, 2006; McCann and Fal'ko, 2006; Nilsson *et al.*, 2006a, 2006b, 2008).

The possible existence of an external bias-induced band gap and the parabolic dispersion at long wavelength distinguish bilayer graphene from monolayer graphene, with both possessing chiral carrier dynamics. We note that bilayer graphene should be considered a single 2D system, quite distinct from "double-layer" graphene (Hwang and Das Sarma, 2009a), which is a composite system consisting of two parallel single layers of graphene, separated by a distance in the $\hat{z}$ direction. The 2D energy dispersion in double-layer graphene is massless Dirac-like (as in the monolayer case), and the interlayer separation is arbitrary; whereas, bilayer graphene has the quadratic band dispersion with a fixed interlayer separation of 0.3 nm similar to graphite.

3. 2D Semiconductor structures

Since one goal of this review is to understand graphene electronic properties in the context of extensively studied (for more than 40 years) 2D semiconductor systems (e.g., Si inversion layers in MOSFETs, GaAs-AlGaAs heterostructures, quantum wells, etc.), we summarize in this section the basic electronic structure of 2D semiconductor systems which are of relevance in the context of graphene physics, without giving much details, which can be found in the literature (Ando *et al.*, 1982; Bastard, 1991; Davies, 1998).

There are, broadly speaking, four qualitative differences between 2D graphene and 2D semiconductor systems (see Fig. 4). (We note that there are significant quantitative and some qualitative differences between different 2D semiconductor systems themselves). These differences are sufficiently important in order to be emphasized right at the outset.

(i) First, 2D semiconductor systems typically have very large (> 1 eV) band gaps so that 2D electrons and 2D holes must be studied using completely different electron-doped or hole-doped structures. By contrast, graphene (except biased graphene bilayers that have small band gaps) is a gapless semiconductor with the nature of the carrier system changing at the Dirac point from electrons to holes (or vice versa) in a single structure. A direct corollary of this gapless (or small gap) nature of graphene is of course the "always metallic" nature of 2D graphene, where the chemical potential (Fermi level) is always in the conduction or the valence band. By contrast, the 2D semiconductor becomes insulating below a threshold voltage, as the Fermi level enters the band gap.

(ii) Graphene systems are chiral, while 2D semiconductors are nonchiral. Chirality of graphene leads to some important consequences for transport behavior, as we discuss later in this review. (For example, $2k_F$ backscattering is suppressed in MLG at low temperature.)

(iii) Monolayer graphene dispersion is linear, while 2D semiconductors have quadratic energy dispersion. This leads to substantial quantitative differences in the transport properties of the two systems.

(iv) Finally, the carrier confinement in 2D graphene is ideally two dimensional, since the graphene layer is precisely one atomic monolayer thick. For 2D semiconductor structures, the quantum dynamics is two dimensional by virtue of confinement induced by an external electric field, and as such, 2D semiconductors are quasi-2D systems, and always have an average width or thickness $\langle z \rangle$ (≈ 5 to 50 nm) in the third direction with $\langle z \rangle \lesssim \lambda_F$, where λ_F is the 2D Fermi wavelength (or equivalently the carrier de Broglie wavelength). The condition $\langle z \rangle < \lambda_F$ defines a 2D electron system.

The carrier dispersion of 2D semiconductors is given by $E(q) = E_0 + \hbar^2 q^2/(2m^*)$, where E_0 is the quantum confinement energy of the lowest quantum confined 2D state, and

$\mathbf{q} = (q_x, q_y)$ is the 2D wave vector. If more than one quantum 2D level is occupied by carriers (usually called "subbands") the system is no longer, strictly speaking, two-dimensional, and therefore a 2D semiconductor is no longer two-dimensional at high enough carrier density when higher subbands get populated.

The effective mass m^* is known from band structure calculations, and within the effective mass approximation $m^* = 0.07m_e$ (electrons in GaAs), $m^* = 0.19m_e$ (electrons in Si 100 inversion layers), $m^* = 0.38m_e$ (holes in GaAs), and $m^* = 0.92m_e$ (electrons in Si 111 inversion layers). In some situations, e.g., Si 111, the 2D effective mass entering the dispersion relation may have anisotropy in the x-y plane and a suitably averaged $m^* = \sqrt{m_x m_y}$ is usually used.

The 2D semiconductor wave function is nonchiral, and is derived from the effective mass approximation to be

$$\Phi(\mathbf{r}, z) \sim e^{i\mathbf{q}\cdot\mathbf{r}} \xi(z), \tag{1.8}$$

where $\mathbf{q}$ and $\mathbf{r}$ are the 2D wave vector and position, and $\xi(z)$ is the quantum confinement wave function in the $\hat{z}$ direction for the lowest subband. The confinement wave function defines the width or thickness of the 2D semiconductor state with $\langle z \rangle = |\langle \xi | z^2 | \xi \rangle|^{1/2}$. The detailed form for $\xi(z)$ usually requires a quantum-mechanical self-consistent local density approximation calculation using the confinement potential, and we refer the interested reader to the extensive existing literature for the details on the confined quasi-2D subband structure calculations (Ando *et al.*, 1982; Stern and Das Sarma, 1984; Bastard, 1991; Davies, 1998).

Finally, we note that 2D semiconductors may also in some situations carry an additional valley quantum number similar to graphene. But the valley degeneracy in semiconductor structures, e.g., Si-MOSFET 2D electron systems, have nothing whatsoever to do with a pseudospin chiral index. For Si inversion layers, the valley degeneracy ($g_v = 2$, 4, and 6, respectively, for Si 100, 110, and 111 surfaces) arises from the bulk indirect band structure of Si which has 6 equivalent ellipsoidal conduction band minima along the 100, 110, and 111 directions about 85% to the Brillouin zone edge. The valley degeneracy in Si MOSFETs, which is invariably slightly lifted (≈ 0.1 meV), is a well established experimental fact.

C. Elementary electronic properties

We describe, summarize, and critically contrast the elementary electronic properties of graphene and 2D semiconductor-based electron gas systems based on their long-wavelength effective 2D energy dispersion discussed in the earlier sections (see Table II). Except where the context is obvious, we abbreviate the following from now on: MLG, BLG, and semiconductor-based 2D electron gas systems (2DEG). The valley degeneracy factors are typically $g_v = 2$ for graphene and Si 100 based 2DEGs, whereas $g_v = 1(6)$ for 2DEGs in GaAs (Si 111). The spin degeneracy is always $g_s = 2$, except at high magnetic fields. The Fermi wave vector for all 2D systems is given simply by filling up the noninteracting momentum eigenstates up to $q = k_F$:

$$n = g_s g_v \int_{|\mathbf{q}|\leq k_F} \frac{d\mathbf{q}}{(2\pi)^2} \rightarrow k_F = \sqrt{\frac{4\pi n}{g_s g_v}}, \tag{1.9}$$

where n is the 2D carrier density in the system. Unless otherwise stated, we will mostly consider electron systems (or the conduction band side of MLG and BLG). Typical experimental values of $n \approx 10^9$ to 5×10^{12} cm^{-2} are achievable in graphene and Si-MOSFETs; whereas, in GaAs-based 2DEG systems $n \approx 10^9$ to 5×10^{11} cm^{-2}.

1. Interaction parameter r_s

The interaction parameter—also known as the Wigner-Seitz radius, the coupling constant, or the effective fine-structure constant—is denoted here by r_s, which in this context is the ratio of the average interelectron Coulomb interaction energy to the Fermi energy. Noting that the average Coulomb energy is simply $\langle V \rangle = e^2/\kappa\langle r \rangle$, where $\langle r \rangle = (\pi n)^{-1/2}$ is the average interparticle separation in a 2D system with n particles per unit area, and κ is the background dielectric constant, we obtain $r_s \sim n^0$ for MLG and $r_s \sim n^{-1/2}$ for BLG and 2DEG.

A note of caution about the nomenclature is in order here, particularly since we have kept the degeneracy factors $g_s g_v$ in the definition of the interaction parameter. Putting $g_s g_v = 4$, the usual case for MLG, BLG, and Si 100 2DEG, and $g_s g_v = 2$ for GaAs 2DEG, we get $r_s = e^2/(\kappa\hbar v_F)$ (MLG), $r_s = 2me^2/(\kappa\hbar^2\sqrt{\pi n})$ (BLG and Si 100 2DEG), and $r_s = me^2/(\kappa\hbar^2\sqrt{\pi n})$ (GaAs 2DEG). The traditional definition of the Wigner-Seitz radius for a metallic Fermi liquid is the dimensionless ratio of the average interparticle separation to the effective Bohr radius $a_B = \kappa\hbar^2/(me^2)$. This gives for the Wigner-Seitz radius $r_s^{WS} = me^2/(\kappa\hbar^2\sqrt{\pi n})$ (2DEG and BLG), which differs from the definition of the interaction parameter r_s by the degeneracy factor $g_s g_v/2$. We emphasize that the Wigner-Seitz radius from the above definition is meaningless for MLG, because the low energy linear dispersion implies a zero effective mass (or more correctly the concept of an effective mass for MLG does not apply). For MLG, therefore, an alternative definition widely used in the literature defines an effective fine-structure constant (α) as the coupling constant $\alpha = e^2/(\kappa\hbar v_F)$, which differs from the definition of r_s by the factor $\sqrt{g_s g_v}/2$. Putting $\sqrt{g_s g_v} = 2$ for MLG gives the interaction parameter r_s equal to the effective fine-structure constant α, just as setting $g_s g_v = 2$ for GaAs 2DEG gave the interaction parameter equal to the Wigner-Seitz radius. Whether the definition of the interaction parameter should or should not contain the degeneracy factor is a matter of taste and has been discussed in the literature in the context of 2D semiconductor systems (Das Sarma *et al.*, 2009).

A truly significant aspect of the monolayer graphene interaction parameter, which follows directly from its equivalence with the fine-structure constant definition, is that it is a carrier density independent constant, unlike the r_s parameter for the 2DEG (or BLG), which increases with decreasing carrier density as $n^{-1/2}$. In particular, the interaction parameter for MLG is bounded, i.e., $0 \leq r_s \lesssim 2.2$, since $1 \leq \kappa \leq \infty$, and as discussed earlier, $v_F \approx 10^8$ cm/s is set by the carbon hopping parameters and lattice spacing. This is in sharp contrast to 2DEG systems where $r_s \approx 13$ (for electrons in

GaAs with $n \approx 10^9$ cm^{-2}) and $r_s \approx 50$ (for holes in GaAs with $n \approx 2 \times 10^9$ cm^{-2}) have been reported (Das Sarma *et al.*, 2005; Huang *et al.*, 2006; Manfra *et al.*, 2007).

Monolayer graphene is thus, by comparison, always a fairly weakly interacting system, while bilayer graphene could become a strongly interacting system at low carrier density. We point out, however, that the real low-density regime in graphene (both MLG and BLG) is dominated entirely by disorder in currently available samples, and therefore a homogeneous carrier density of $n \lesssim 10^{10}$ cm^{-2} (10^9 cm^{-2}) is unlikely to be accessible for gated (suspended) samples in the near future. Using the BLG effective mass $m = 0.03 m_e$, we get the interaction parameter for BLG: $r_s \approx 68.5/(\kappa \sqrt{\tilde{n}})$, where $\tilde{n} = n/10^{10}$ cm^{-2}. For comparison, the r_s parameters for GaAs 2DEG ($\kappa = 13$, $m^* = 0.67 m_e$) and Si 100 on SiO$_2$ ($\kappa = 7.7$, $m^* = 0.19 m_e$, $g_v = 2$) are $r_s \approx 4/\sqrt{\tilde{n}}$, and $r_s \approx 13/\sqrt{\tilde{n}}$, respectively.

For the case when the substrate is SiO$_2$, $\kappa = (\kappa_{\text{SiO}_2} + 1)/2 \approx 2.5$ for MLG and BLG, we have $r_s \approx 0.8$ and $r_s \approx 27.4/(\sqrt{\tilde{n}})$, respectively. In vacuum, $\kappa = 1$ and $r_s \approx 2.2$ for MLG and $r_s \approx 68.5/(\sqrt{\tilde{n}})$ for BLG.

2. Thomas-Fermi screening wave vector q_{TF}

Screening properties of an electron gas depend on the density of states D_0 at the Fermi level. The simple Thomas-Fermi theory leads to the long-wavelength Thomas-Fermi screening wave vector

$$q_{\text{TF}} = \frac{2\pi e^2}{\kappa} D_0. \tag{1.10}$$

The density independence of long-wavelength screening in BLG and 2DEG is the well-known consequence of the density of states being a constant (independent of energy); whereas, the property that $q_{\text{TF}} \sim k_F \sim n^{1/2}$ in MLG is a direct consequence of the MLG density of states being linear in energy.

A key dimensionless quantity determining the charged impurity scattering limited transport in electronic materials is $q_s = q_{\text{TF}}/k_F$ which controls the dimensionless strength of quantum screening. From Table I, we have $q_s \sim n^0$ for MLG and $q_s \sim n^{-1/2}$ for BLG and 2DEG. Using the usual substitutions $g_s g_v = 4(2)$ for Si 100 (GaAs) based 2DEG system, and taking the standard values of m and κ for graphene-SiO$_2$, GaAs-AlGaAs, and Si-SiO$_2$ structures, we get (for $\tilde{n} = n/10^{10}$ cm^{-2})

$$\text{MLG: } q_s \approx 3.2, \quad \text{BLG: } q_s \approx 54.8/\sqrt{\tilde{n}}, \tag{1.11a}$$

$$n\text{-GaAs: } q_s \approx 8/\sqrt{\tilde{n}}, \ p\text{-GaAs: } q_s \approx 43/\sqrt{\tilde{n}}. \tag{1.11b}$$

We point out two important features of the simple screening considerations described above: (i) In MLG, q_s being a constant implies that the screened Coulomb interaction has exactly the same behavior as the unscreened bare Coulomb interaction. The bare 2D Coulomb interaction in a background with dielectric constant κ is given by $v(q) = 2\pi e^2/(\kappa q)$ and the corresponding long-wavelength screened interaction is given by $u(q) = 2\pi e^2/\kappa(q + q_{\text{TF}})$. Putting $q = k_F$ in the above equation, we get $u(q) \sim (k_F + q_{\text{TF}})^{-1} \sim k_F^{-1}(1 + q_{\text{TF}}/k_F)^{-1} \sim k_F^{-1}$ for MLG. Thus, in MLG, the functional dependence of the screened Coulomb scattering on the carrier density is exactly the same as unscreened Coulomb scattering, a most peculiar phenomenon arising from the Dirac linear dispersion. (ii) In BLG (but not MLG, see above) and in 2DEG, the effective screening becomes stronger as the carrier density decreases since $q_s = q_{\text{TF}}/k_F \sim n^{-1/2} \to \infty(0)$ as $n \to 0(\infty)$. This counterintuitive behavior of 2D screening, which is true for BLG systems also, means that in 2D systems effects of Coulomb scattering on transport properties increases with increasing carrier density, and at very high density, the system behaves as an unscreened system. This is in sharp contrast to 3D metals where the screening effect increases monotonically with increasing electron density.

Finally, in the context of graphene, it is useful to give a direct comparison between screening in MLG versus screening in BLG: $q_{\text{TF}}^{\text{BLG}}/q_{\text{TF}}^{\text{MLG}} \approx 16/\sqrt{\tilde{n}}$, showing that as carrier density decreases, BLG screening becomes much stronger than MLG screening.

3. Plasmons

Plasmons are self-sustaining normal mode oscillations of a carrier system, arising from the long-range nature of the interparticle Coulomb interaction. The plasmon modes are defined by the zeros of the corresponding frequency and wave vector dependent dynamical dielectric function. The long-wavelength plasma oscillations are essentially fixed by the particle number (or current) conservation, and can be obtained from elementary considerations. We write down the long-wavelength plasmon dispersion ω_p:

$$\text{MLG: } \omega_p(q \to 0) = \left(\frac{e^2 v_F q}{\kappa \hbar}\sqrt{\pi n g_s g_v}\right)^{1/2}, \tag{1.12a}$$

$$\text{BLG and 2DEG: } \omega_p(q \to 0) = \left(\frac{2\pi n e^2}{\kappa m} q\right)^{1/2}. \tag{1.12b}$$

A rather intriguing aspect of MLG plasmon dispersion is that it is nonclassical [i.e., $\hbar$ appears explicitly in Eq. (1.12), even in the long-wavelength limit]. This explicit quantum nature of long-wavelength MLG plasmon is a direct manifestation of

TABLE I. Elementary electronic quantities. Here E_F, $D(E)$, r_s, and q_{TF} represent the Fermi energy, the density of states, the interaction parameter, and the Thomas-Fermi wave vector, respectively. $D_0 = D(E_F)$ is the density of states at the Fermi energy and $q_s = q_{\text{TF}}/k_F$.

	E_F	$D(E)$	$D_0 = D(E_F)$	r_s	q_{TF}	q_s
MLG	$\hbar v_F \sqrt{\frac{4\pi n}{g_s g_v}}$	$\frac{g_s g_v E}{2\pi(\hbar v_F)^2}$	$\frac{\sqrt{g_s g_v n}}{\sqrt{\pi}\hbar v_F}$	$\frac{e^2}{\kappa \hbar v_F}\frac{\sqrt{g_s g_v}}{2}$	$\frac{\sqrt{4\pi g_s g_v n}e^2}{\kappa \hbar v_F}$	$\frac{g_s g_v e^2}{\kappa \hbar v_F}$
BLG and 2DEG	$\frac{2\pi \hbar^2 n}{m g_s g_v}$	$\frac{g_s g_v m}{2\pi \hbar^2}$	$\frac{g_s g_v m}{2\pi \hbar^2}$	$\frac{me^2}{2\kappa \hbar^2}\frac{g_s g_v}{\sqrt{\pi n}}$	$\frac{g_s g_v me^2}{\kappa \hbar^2}$	$\frac{(g_s g_v)^{3/2}me^2}{\kappa \hbar^2 \sqrt{4\pi n}}$

its linear Dirac-like energy-momentum dispersion, which has no classical analogy (Das Sarma and Hwang, 2009).

4. Magnetic field effects

Although magnetic field-induced phenomena in graphene and 2D semiconductors [e.g., quantum Hall (QH) effect and fractional quantum Hall effect] are briefly covered in Sec. V, we mention at this point a few elementary electronic properties in the presence of an external magnetic field perpendicu-

lar to the 2D plane leading to the Landau orbital quantization of the system.

a. Landau level energetics

The application of a strong perpendicular external magnetic field (B) leads to a complete quantization of the orbital carrier dynamics of all 2D systems leading to the following quantized energy levels E_n, the so-called Landau levels:

$$\text{MLG: } E_n = \text{sgn}(n)v_F\sqrt{2e\hbar B|n|}, \quad \text{with } n = 0, \pm1, \pm2, \ldots, \tag{1.13a}$$

$$\text{BLG: } E_n = \frac{\text{sgn}(n)}{\sqrt{2}}[(2|n| + 1)(2eBv_F^2\hbar) + 4m^2v_F^4 - \sqrt{(2mv_F^2)^4 + 2(2|n| + 1)(2eBv_F^2\hbar)(2mv_F^2)^2 + (2eBv_F^2\hbar)^2}],$$
$$\text{with } n = 0, \pm1, \pm2, \ldots, \tag{1.13b}$$

$$\text{2DEG: } E_n = (n + 1/2)\left(\frac{eB\hbar}{mc}\right), \quad \text{with } n = 0, 1, 2, \ldots \tag{1.13c}$$

The hallmark of the Dirac nature of graphene is the existence of a true zero-energy [$n = 0$ in Eq. (1.13a)] Landau level, which is equally shared by electrons and holes. The experimental verification of this zero-energy Landu level in graphene is definitive evidence for the long-wavelength Dirac nature of the system (Miller *et al.*, 2009; Novoselov, Geim *et al.*, 2005; Zhang *et al.*, 2005).

b. Cyclotron resonance

External radiation induced transitions between Landau levels give rise to the cyclotron resonance in a Landau quantized system, which has been extensively studied in 2D semiconductor (Ando *et al.*, 1982) and graphene systems (Jiang *et al.*, 2007; Henriksen *et al.*, 2008, 2010). The cyclotron resonance frequency in MLG and 2DEG is given by

$$\text{MLG: } \omega_c = v_F\sqrt{2e\hbar B}(\sqrt{n + 1} - \sqrt{n}), \tag{1.14a}$$

$$\text{2DEG: } \omega_c = \frac{eB}{mc}. \tag{1.14b}$$

For BLG, the cyclotron frequency should smoothly interpolate from the formula for MLG for very large n, so that E_n in Eq. (1.13) is much larger than $2mv_F^2$, to that of the 2DEG for small n so that $E_n \ll 2mv_F^2$ (where $m \approx 0.033$ is the approximate $B = 0$ effective mass of the bilayer parabolic-band dispersion). Experimental BLG cyclotron resonance studies (Henriksen *et al.*, 2010) indicate the crossover from the quadratic band dispersion (i.e., 2DEG-like) for smaller q to the linear band dispersion (i.e., MLG-like) at larger q seems to happen at lower values of q than that implied by simple band theory considerations.

A particularly interesting and important feature of cyclotron resonance in graphene is that it is affected by electron-electron interaction effects unlike the usual parabolic 2DEG, where the existence of Kohn's theorem prevents the long-wavelength cyclotron frequency from being renormalized by electron-electron interactions (Kohn, 1961; Ando *et al.*, 1982). For further discussion of this important topic, we refer

the interested reader to the recent literature on the subject (Henriksen *et al.*, 2010; Shizuya, 2010.

c. Zeeman splitting:

In graphene, the spin splitting can be large since the Landé g factor in graphene is the same ($g = 2$) as in vacuum. The Zeeman splitting in an external magnetic field is given by (μ_B is the Bohr magneton) $E_z = g\mu_B B = 0.12B[\text{T}]$ meV, for $g = 2$ (MLG, BLG, Si 2DEG) and $E_z = -0.03B[\text{T}]$ meV for $g = -0.44$ (GaAs 2DEG). We note that the relative value of E_z/E_F is rather small in graphene, $E_z/E_F \approx 0.01(B[\text{T}]/\sqrt{\tilde{n}}) \rightarrow 0.01$ for $B = 10$ T and $n = 10^{12}$ cm^{-2}. Thus, the spin splitting is only 1% even at high fields. Of course, the polarization effect is stronger at low carrier densities, since E_F is smaller.

D. Intrinsic and extrinsic graphene

It is important to distinguish between intrinsic and extrinsic graphene because gapless graphene (either MLG or BLG) has a charge neutrality point (CNP), i.e., the Dirac point, where its character changes from being electronlike to being holelike. Such a distinction is not meaningful for a 2DEG (or BLG with a large gap) since the intrinsic system is simply an undoped system with no carriers (and as such is uninteresting from the electronic transport properties perspective).

In monolayer and bilayer graphene, the ability to gate (or dope) the system by putting carriers into the conduction or valence band by tuning an external gate voltage enables one to pass through the CNP where the chemical potential (E_F) resides precisely at the Dirac point. This system, with no free carriers at $T = 0$, and E_F precisely at the Dirac point is called intrinsic graphene with a completely filled (empty) valence (conduction) band. Any infinitesimal doping (or, for that matter, any finite temperature) makes the system "extrinsic" with electrons (holes) present in the conduction (valence) band (Müller *et al.*, 2009). Although the intrinsic system is a set of measure zero (since E_F has to be precisely at the Dirac point), the routine experimental ability to tune the

TABLE II.   Electronic quantities for monolayer graphene. Note that the graphene Fermi velocity ($v_F = 10^8$ cm/s) and the degeneracy factor $g = g_s g_v = 4$, i.e., the usual spin degeneracy ($g_s = 2$) and a valley degeneracy ($g_v = 2$), are used in this table. Here $\bar{n} = n/(10^{10} \text{ cm}^{-2})$, and B, q, and σ are measured in T, cm^{-1}, and σ are measured in T, cm^{-1}, and $e^2/h = 38.74$ μS (or $h/e^2 = 25.8$ kΩ), respectively.

Quantity	Scale values
Fermi wave vector (k_F)	$1.77 \times 10^5 \sqrt{\bar{n}}$ [cm^{-1}]
Thomas-Fermi wave vector (q_{TF})	$1.55 \times 10^6 \sqrt{\bar{n}}/\kappa$ [cm^{-1}]
Interaction parameter (r_s)	$2.19/\kappa$
DOS at E_F [$D_0 \equiv D(E_F)$]	$1.71 \times 10^9 \sqrt{\bar{n}}$ [meV^{-1} cm^{-2}]
Fermi energy (E_F)	$11.65\sqrt{\bar{n}}$ [meV]
Zeeman splitting (E_z)	$0.12B$ [meV]
Cyclotron frequency (ω_c)	$5.51 \times 10^{13}\sqrt{B}$ [s^{-1}]
Landau level energy (E_n)	sgn(l)$36.29\sqrt{B|l|}$ [meV], $l = 0, \pm1, \pm2, \ldots$
Plasma frequency ($\omega_p(q)$)	$5.80 \times 10^{-2}\sqrt{\sqrt{\bar{n}}q/\kappa}$ [meV]
Mobility (μ)	$2.42 \times 10^4 \sigma/\bar{n}$ [cm^2/V s]
Scattering time (τ)	$2.83 \times 10^{-14}\sigma/\sqrt{\bar{n}}$ [s]
Level broadening (Γ)	$11.63\sqrt{\bar{n}}/\sigma$ [meV]

system from being electronlike to to being holelike by changing the external gate voltage, manifestly establishes that one must be going through the intrinsic system at the CNP. If there is an insulating regime in between, as there would be for a gapped system, then intrinsic graphene is not being accessed.

Although it is not often emphasized, the achievement of Novoselov *et al.* (2004) in producing 2D graphene in the laboratory is not just fabricating (Novoselov, Jiang *et al.*, 2005) and identifying (Ferrari *et al.*, 2006; Ferrari, 2007) stable monolayers of graphene flakes on substrates, but also establishing its transport properties by gating the graphene device using an external gate, which allows one to simply tune an external gate voltage and thereby continuously controlling the 2D graphene carrier density as well as their nature (electron or hole). If all that could be done in the laboratory was to produce 2D graphene flakes, with no hope of doping or gating them with carriers, then the subject of graphene would be many orders of magnitude smaller and less interesting. What led to the exponential growth in graphene literature is the discovery of gatable and density tunable 2D graphene in 2004.

Taking into account the quantum capacitance in graphene, the doping induced by the external gate voltage V_g is given by the following relation (Fang *et al.*, 2007; Fernandez-Rossier *et al.*, 2007):

$$n = \frac{CV_g}{e} + n_Q\left[1 - \sqrt{1 + \frac{CV_g}{en_Q}}\right], \qquad (1.15)$$

where C is the gate capacitance, e the absolute value of the electron charge, and $n_Q \equiv (\pi/2)(C\hbar v_F/e^2)^2$. The second term on the right-hand side (r.h.s.) of (1.15) is analogous to the term due to the so-called quantum capacitance in regular 2DEG. Note that in graphene, due to the linear dispersion, contrary to parabolic 2D electron liquids, the *quantum capacitance* depends on V_g. For a background dielectric constant $\kappa \approx 4$ and gate voltages larger than few millivolts, the second term on the r.h.s. of (1.15) can be neglected for thicknesses of the dielectric larger than few angstroms. In current experiments on exfoliated graphene on SiO$_2$ the oxide

is 300 nm thick, and therefore quantum-capacitance effects are completely negligible. In this case, a simple capacitance model connects the 2D carrier density (n) with the applied external gate voltage V_g, $n \approx CV_g$, where $C \approx 7.2 \times 10^{10}$ cm^{-2}/V for graphene on SiO$_2$ with roughly 300 nm thickness. This approximate value of the constant C seems to be pretty accurate, and the following scaling should provide n for different dielectrics:

$$n[10^{10} \text{ cm}^{-2}] = 7.2 \times \frac{t \text{ [nm]}}{300} \frac{\kappa}{3.9} V_g[\text{V}], \qquad (1.16)$$

where t is the thickness of the dielectric (i.e., the distance from the gate to the graphene layer) and κ is the dielectric constant of the insulating substrate.

It is best, therefore, to think of 2D graphene on SiO$_2$ [see Fig. 1(e)] as a metal-oxide-graphene-field-effect-transistor similar to the well-known Si-MOSFET structure, with Si replaced by graphene where the carriers reside. In fact, this analogy between graphene and Si 100 inversion layer is operationally quite effective: Both have the degeneracy factor $g_s g_v = 4$ and both typically have SiO$_2$ as the gate oxide layer. The qualitative and crucial difference is, of course, that graphene carriers are chiral, massless, with linear dispersion and with no band gap, so that the gate allows one to go directly from being n-type to a p-type carrier system through the charge neutral Dirac point. Thus, a graphene metal-oxide-graphene-field-effect-transistor is not a transistor at all (at least for MLG), since the system never becomes insulating at any gate voltage (Avouris *et al.*, 2007).

We will distinguish between extrinsic (i.e., doped) graphene with free carriers and intrinsic (i.e., undoped) graphene with the chemical potential precisely at the Dirac point. All experimental systems (since they are always at $T \neq 0$) are necessarily extrinsic, but intrinsic graphene is of theoretical importance since it is a critical point. In particular, intrinsic graphene is a non-Fermi liquid in the presence of electron-electron interactions (Das Sarma, Hwang, and Tse, 2007), while extrinsic graphene is a Fermi liquid. Since the non-Fermi-liquid fixed point for intrinsic graphene is unstable to the presence of any finite carrier density, the non-Fermi-liquid nature of this fixed point is unlikely to have any

experimental implication. But it is important to keep this non-Fermi-liquid nature of intrinsic graphene in mind when discussing graphene's electronic properties. We also mention (see Sec. IV) that disorder, particularly long-ranged disorder induced by random charged impurities present in the environment, is a relevant strong perturbation affecting the critical Dirac point, since the system breaks up into spatially random electron-hole puddles, thus masking its zero-density intrinsic nature.

E. Other topics

There are several topics that are of active current research which we could not cover in this review. Some remain controversial, and others are still poorly understood. Yet these subjects are important, in terms of both fundamental physics and for the application of graphene for useful devices. Here we sketch the status of these subjects. For example, several novel methods of fabricating graphene recently emerged, including chemical vapor deposition on nickel (Kim, Zhao *et al.*, 2009) and copper (Li *et al.*, 2009), as well as directly unzipping carbon nanotubes (Kosynkin *et al.*, 2009; Sinitskii *et al.*, 2009) and other chemical methods (Jiao *et al.*, 2009). As of early 2010, all of these other fabrication processes are just in their infancy. The notable exception is "epitaxial graphene" manufactured by heating SiC wafers, causing the Si atoms to desorb, resulting in several graphene layers at the surface (Berger *et al.*, 2004; Berger *et al.*, 2006; Emtsev *et al.*, 2009; de Heer *et al.*, 2010; First *et al.*, 2010) that are believed to be very weakly coupled and of very good quality (Rutter *et al.*, 2007; Hass *et al.*, 2008; Orlita *et al.*, 2008; Miller *et al.*, 2009). We note that graphene can be used as a component of more complicated structures by exploiting its spin (Hill *et al.*, 2006; Cho *et al.*, 2007; Tombros *et al.*, 2007; Han *et al.*, 2009; Huertas-Hernando *et al.*, 2006, 2009; Józsa *et al.*, 2009) or valley (Rycerz *et al.*, 2007b) degeneracy or by patterning gates with a periodic superpotential (Park, *et al.*, 2008; Brey and Fertig, 2009a). Graphene can also be made to superconduct through the proximity effect by coupling it to superconducting leads (Beenakker, 2006, 2008; Heersche *et al.*, 2007; Du, Skachko, and Andrei, *et al.*, 2008) or other novel proposals (Feigel'man *et al.*, 2008; Lutchyn *et al.*, 2008). This review could not cover these topics in any reasonable depth.

1. Optical conductivity

It was pointed out as early as 1994 by Ludwig *et al.* (1994) that if one examined the conductivity of Dirac fermions in linear response theory, keeping a finite frequency, i.e., $\sigma(\omega)$ while taking the limit of zero temperature ($T \rightarrow 0$) and vanishing disorder ($\Gamma \rightarrow 0$), then one obtained a universal and frequency independent optical conductivity (i.e., electrical conductivity at finite frequency):

$$\sigma(\omega) = g_s g_v \frac{\pi e^2}{8h}. \tag{1.17a}$$

Ludwig *et al.* (1994) also noted that this result did not commute with the dc conductivity in which one first took the limit $\omega \rightarrow 0$ and then $\Gamma \rightarrow 0$, in which case one obtained

$$\sigma_{\min} = g_s g_v \frac{e^2}{\pi h}. \tag{1.17b}$$

These $T = 0$ results apply to intrinsic graphene, where E_F is precisely at the Dirac point. The crossover between these two theoretical intrinsic limits remains an open problem (Katsnelson, 2006; Ostrovsky *et al.*, 2006).

The optical conductivity [Eq. (1.17a)] has been measured experimentally both by infrared spectroscopy (Li *et al.*, 2008) and by measuring the absorption of suspended graphene sheets (Nair *et al.*, 2008). In the IR measurements, $\sigma(\omega)$ is close to the predicted universal value for a range of frequencies $4000 < \omega < 6500$ cm^{-1}. While in the absorption experiment, the attenuation of visible light through multilayer graphene scales as $\pi \alpha$ per layer. They claimed that this was an accurate measurement of the fine-structure constant α and is a direct consequence of having $\sigma(\omega)$ as a universal and frequency independent constant. In some sense, it is quite remarkable that disorder and electron-electron interactions do not significantly alter the value of the optical conductivity. This has attracted considerable theoretical interest (Gusynin and Sharapov, 2006; Mishchenko, 2007; Herbut *et al.*, 2008; Katsnelson, 2008; Kuzmenko *et al.*, 2008; Peres *et al.*, 2008; Peres and Stauber, 2008; Stauber, Peres, and Geim, *et al.*, 2008; Min and MacDonald, 2009; Mishchenko, 2009; Sheehy and Schmalian, 2009), where it has been argued that it is a fortuitous cancellation of higher order terms that explains the insensitivity of $\sigma(\omega)$ to interaction effects. We refer the interested reader to these works for a detailed discussion of how interaction effects and disorder change $\sigma(\omega)$ from the universal value, although a consensus is yet to emerge on whether these effects could be observed experimentally or how accurate $\sigma(\omega)$ is for a measure of the fine-structure constant (Mak *et al.*, 2008; Gusynin *et al.*, 2009).

2. Graphene nanoribbons

It was realized in the very first graphene transport experiments that the finite minimum conductivity [Eq. (1.17)] would be an obstacle for making a useful transistor since there is no "off" state. One way to circumvent this problem is to have a quasi-one-dimensional (1D) geometry that confines the graphene electrons in a strip of (large) length L and a finite (small) width W. The confinement gap typically scales as $1/W$ (Wakabayashi *et al.*, 1999); however, this depends on the imposed boundary conditions. This is quite similar to carbon nanotubes (since a nanotube is just a nanoribbon with periodic boundary conditions). The nomenclature in graphene is slightly different from carbon nanotubes, where a zigzag-edge nanoribbon is similar to an armchair nanotube in that it is always metallic within the tight-binding approximation. Similarly, an armchair nanoribbon is similar to a zigzag nanotube in that it can be either metallic or semiconducting depending on the width. Early theoretical calculations (Son, *et al.*, 2006a, 2006b; Yang *et al.*, 2007) used a density functional theory to calculate the band gap of armchair graphene nanoribbons and found that just as in carbon nanotubes, the energy gaps come in three families that are all semiconducting (unlike the tight-binding calculation, which gives one of the families as metallic). Brey and Fertig (2006) showed that simply quantizing the Dirac Hamiltonian (the

low energy effective theory) gave quantitatively similar results for the energy gaps as the tight-binding calculation, while Son, *et al.* (2006a) showed that the density functional results could be obtained from the tight-binding model with some added edge disorder. By considering arbitrary boundary conditions, Akhmerov and Beenakker (2008) demonstrated that the behavior of the zigzag edge is the most generic for graphene nanoribbons. These theoretical works gave a simple way to understand the gap in graphene nanoribbons.

The first experiments on graphene nanoribbons (Han *et al.*, 2007), however, presented quite unexpected results. As shown in Fig. 5 the transport gap for narrow ribbons is much larger than that predicted by theory (with the gap diverging at widths of ≈ 15 nm), while wider ribbons have a much smaller gap than expected. Surprisingly, the gap showed no dependence on the orientation (i.e., zigzag or armchair direction) as required by the theory. These discrepancies have prompted several studies (Areshkin *et al.*, 2007; Chen *et al.*, 2007; Sols *et al.*, 2007; Abanin and Levitov, 2008; Adam, Cho *et al.*, 2008; Basu *et al.*, 2008; Biel, Blase *et al.*, 2009; Biel, Triozon *et al.*, 2009; Dietl *et al.*, 2009; Martin and Blanter, 2009; Stampfer *et al.*, 2009; Todd *et al.*, 2009). In particular, Sols *et al.* (2007) argued that fabrication of the nanoribbons gave rise to very rough edges breaking the nanoribbon into a series of quantum dots. Coulomb blockade of charge transfer between the dots (Ponomarenko *et al.*, 2008) explains the larger gaps for smaller ribbon widths. In a similar spirit, Martin and Blanter (2009) showed that edge disorder qualitatively changed the picture from that of the disorder-free picture presented earlier, giving a localization length comparable to the sample width. For larger ribbons, Adam, Cho *et al.* (2008) argued that charged impurities in the vicinity of the graphene would give rise to inhomogeneous puddles so that the transport would be governed by percolation [as shown in Fig. 5, the points are experimental data, and the solid lines, for both electrons and holes, show fits to $\sigma \sim (V - V_c)^\nu$, where ν is close to 4/3, the theoretically expected value for percolation in 2D systems]. The large gap for small

ribbon widths would then be explained by a dimensional crossover as the ribbon width became comparable to the puddle size. A numerical study including the effect of quantum localization and edge disorder was done by Mucciolo *et al.* (2009) who found that a few atomic layers of edge roughness were sufficient to induce transport gaps to appear, which are approximately inversely proportional to the nanoribbon width. Two recent and detailed experiments (Gallagher *et al.*, 2010; Han *et al.*, 2010) seem to suggest that a combination of these pictures might be at play (e.g., transport through quantum dots that are created by the charged impurity potential), although as of now, a complete theoretical understanding remains elusive. The phenomenon that the measured transport gap is much smaller than the theoretical band gap seems to be a generic feature in graphene, occurring not only in nanoribbons but also in biased bilayer graphene where the gap measured in transport experiments appears to be substantially smaller than the theoretically calculated, band gap (Oostinga *et al.*, 2008) or even the measured optical gap (Mak *et al.*, 2009; Zhang, Tang *et al.*, 2009).

3. Suspended graphene

Since the substrate affects both the morphology of graphene (Ishigami *et al.*, 2007; Meyer *et al.*, 2007; Stolyarova *et al.*, 2007) and provides a source of impurities, it became clear that one needed to find a way to have electrically contacted graphene without the presence of the underlying substrate. The making of "suspended graphene" or "substrate-free" graphene was an important experimental milestone (Bolotin, Sikes, Jiang *et al.*, 2008; Bolotin, Sikes, Hone *et al.*, 2008; Du *et al.*, 2008) where after exfoliating graphene and making electrical contact, one then etches away the substrate underneath the graphene so that the graphene is suspended over a trench that is approximately 100 nm deep. As a historical note, we mention that suspended graphene without electrical contacts was made
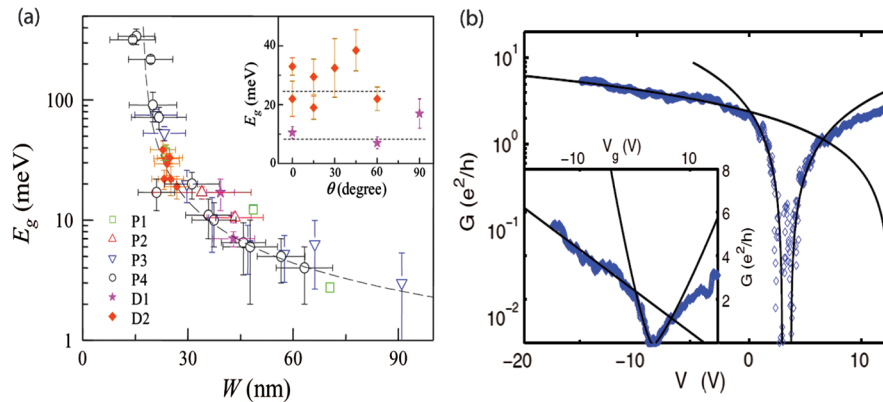
FIG. 5 (color online).   (a) Graphene nanoribbon energy gaps as a function of width. Adapted from Han *et al.*, 2007. Four devices (P1–P4) were orientated parallel to each other with varying width, while two devices (D1–D2) were oriented along different crystallographic directions with uniform width. The dashed line is a fit to a phenomenological model with $E_g = A/(W - W^*)$ where A and W^* are fit parameters. The inset shows that contrary to predictions, the energy gaps have no dependence on crystallographic direction. The dashed lines are the same fits as in the main panel. (b) Evidence for a percolation metal-insulator transition in graphene nanoribbons. Adapted from Adam, Cho *et al.*, 2008. Main panel shows graphene ribbon conductance as a function of gate voltage. Solid lines are a fit to percolation theory, where electrons and holes have different percolation thresholds (seen as separate critical gate voltages V_c). The inset shows the same data in a linear scale, where even by eye the transition from high-density Boltzmann behavior to the low-density percolation transport is visible.

earlier by Meyer *et al.* (2007). Quite surprisingly, the suspended samples as prepared did not show much difference from unsuspended graphene, until after current annealing (Moser *et al.*, 2007; Barreiro *et al.*, 2009). This suggested that most of impurities limiting the transport properties of graphene were stuck to the graphene sheet and not buried in the substrate. After removing these impurities by driving a large current through the sheet, the suspended graphene samples showed both ballistic and diffusive carrier transport properties. Away from the charge neutrality point, suspended graphene showed near-ballistic transport over hundreds of nm, which prompted much theoretical interest (Adam and Das Sarma, 2008b; Fogler, Guinea, and Katsnelson, 2008; Stauber, Peres, and Neto, *et al.*, 2008; Müller *et al.*, 2009). One problem with suspended graphene is that only a small gate voltage ($V_g \approx 5$ V) could be applied before the graphene buckles due to the electrostatic attraction between the charges in the gate and on the graphene sheet, and binds to the bottom of the trench that was etched out of the substrate. This is in contrast to graphene on a substrate that can support as much as $V_g \approx 100$ V and a corresponding carrier density of $\approx 10^{13}$ cm^{-2}. To avoid the warping, it was proposed that one should use a top gate with the opposite polarity, but currently, this has yet to be demonstrated experimentally. Despite the limited variation in carrier density, suspended graphene has achieved a carrier mobility of more than $200\,000$ cm^2/V s (Bolotin, Sikes, Jiang *et al.*, 2008; Bolotin, Sikes, Hone *et al.*, 2008; Du *et al.*, 2008). Recently suspended graphene bilayers were demonstrated experimentally (Feldman *et al.*, 2009).

4. Many-body effects in graphene

The topic of many-body effects in graphene is itself a large subject, and one that we could not cover in this transport review. As discussed earlier, for intrinsic graphene the many-body ground state is not even a Fermi liquid (Das Sarma, Hwang, and Tse, 2007), an indication of the strong role played by interaction effects. Experimentally, one can observe the signature of many-body effects in the compressibility (Martin *et al.*, 2007) and using angle resolved photoemission spectroscopy (ARPES) (Bostwick *et al.*, 2007; Zhou *et al.*, 2007). Away from the Dirac point, where graphene behaves as a normal Fermi liquid, the calculation of the electron-electron and electron-phonon contribution to the quasiparticle self-energy was studied by several groups (Barlas *et al.*, 2007, Calandra and Mauri, 2007, E. H. Hwang *et al.*, 2007a, 2007b; Park *et al.*, 2007, 2009; Polini *et al.*, 2007; Tse and Das Sarma, 2007; Hwang and Das Sarma, 2008c; Polini, Asgari *et al.*, 2008; Carbotte *et al.*, 2010), and shows reasonable agreement with experiments (Bostwick *et al.*, 2007; Brar *et al.*, 2010). For both bilayer graphene (Min, Borghi *et al.*, 2008) and double-layer graphene (Min, Bistritzer *et al.*, 2008), an instability towards an excitonic condensate has been proposed. In general, monolayer graphene is a weakly interacting system since the coupling constant ($r_s \leq 2$) is never large (Muller *et al.*, 2009). In principle, bilayer graphene could have arbitrarily large coupling at low carrier density where disorder effects are also important. We refer the interested reader to these works for details on this subject.

5. Topological insulators

There is a deep connection between graphene and topological insulators (Kane and Mele, 2005a; Sinitsyn *et al.*, 2006). Graphene has a Dirac cone where the "spin" degree of freedom is actually related to the sublattices in real space; whereas, it is the real electron spin that provides the Dirac structure in the topological insulators (Hasan and Kane, 2010) on the surface of BiSb and BiTe (Hsieh *et al.*, 2008; Chen *et al.*, 2009). Graphene is a weak topological insulator because it has two Dirac cones (by contrast, a strong topological insulator is characterized by a single Dirac cone on each surface), but in practice the two cones in graphene are mostly decoupled and it behaves like two copies of a single Dirac cone. Therefore, many of the results presented in this review, although intended for graphene, should also be relevant for the single Dirac cone on the surface of a topological insulator. In particular, we expect the interface transport properties of topological insulators to be similar to the physics described in this review as long as the bulk is a true gapped insulator.

F. 2D nature of graphene

As the concluding section of the Introduction, we ask the following: what precisely is meant when an electronic system is categorized as 2D, and how can one ensure that a specific sample or system is 2D from the perspective of electronic transport phenomena?

The question is not simply academic, since 2D does not necessarily mean a thin film (unless the film is literally one atomic monolayer thick as in graphene, and even then, one must consider the possibility of the electronic wave function extending somewhat into the third direction). Also, the definition of what constitutes a 2D may depend on the physical properties or phenomena that one is considering. For example, for the purpose of quantum localization phenomena, the system dimensionality is determined by the width of the system being smaller than the phase coherence length L_ϕ (or the Thouless length). Since L_ϕ could be very large at low temperature, metal films and wires can, respectively, be considered 2D and 1D for localization studies at ultralow temperature. For our purpose, however, dimensionality is defined by the 3D electronic wave function as "free" plane-wave–like (i.e., carrying a conserved 2D wave vector) in a 2D plane, while it is a quantized bound state in the third dimension. This ensures that the system is quantum mechanically 2D.

Considering a thin film of infinite (i.e., very large) dimension in the *x-y* plane and a finite thickness *w* in the *z* direction, where *w* could be the typical confinement width of a potential well creating the film, the system is considered 2D if $\lambda_F = 2\pi/k_F > w$. For graphene, we have $\lambda_F \approx (350/\sqrt{\tilde{n}})$ nm, where $\tilde{n} = n/(10^{10}$ cm$^{-2})$, and since $w \approx$ 0.1 to 0.2 nm (the monolayer atomic thickness), the condition $\lambda_F \gg w$ is always satisfied, even for unphysically large $n = 10^{14}$ cm^{-2}.

Conversely, it is essentially impossible to create 2D electronic systems from thin metal films since the very high electron density of metals provides $\lambda_F \approx 0.1$ nm, so that even for a thickness of $w \approx 1$ nm (the thinnest metal film

that one can make), $\lambda_F < w$, making them effectively 3D. By virtue of the much lower carrier densities in semiconductors, the condition $\lambda_F > w$ can be easily satisfied for $w = 5$ to 50 nm for $n = 10^9$ to 10^{12} cm^{-2}, making it possible for 2D semiconductor systems to be readily available since confinement potentials with a width of ≈ 10 nm can be implemented by external gate voltage or band structure engineering.

We now address the question of the experimental verification of the 2D nature of a particular system or sample. The classic technique is to show that the orbital electronic dynamics is sensitive only to a magnetic field perpendicular to the 2D plane (i.e., B_z) (Practically, there could be complications if the spin properties of the system affect the relevant dynamics, since the Zeeman splitting is proportional to the total magnetic field). Therefore, if either the magnetoresistance oscillations (Shubnikov–de Hass effect) or the cyclotron resonance properties depend only on B_z, then the 2D nature is established.

Both of these are true in graphene. The most definitive evidence for 2D nature, however, is the observation of the quantum Hall effect, which is a quintessentially 2D phenomenon. Any system manifesting an unambiguous quantized Hall plateau is 2D in nature, and therefore the observation of the quantum Hall effect in graphene in 2005 by Novoselov, Geim *et al.* (2005) and Zhang *et al.* (2005) absolutely clinched its 2D nature. In fact, the quantum Hall effect in graphene persists to room temperature (Novoselov *et al.*, 2007), indicating that graphene remains a strict 2D electronic material even at room temperature.

Finally, we remark on the strict 2D nature of graphene from a structural viewpoint. The existence of finite 2D flakes of graphene with crystalline order at finite temperature does not in any way violate the Hohenberg-Mermin-Wagner-Coleman theorem which rules out the breaking of a continuous symmetry in two dimensions. This is because the theorem only asserts a slow power law decay of the crystalline (i.e., positional order) correlation with distance, and hence, very large flat 2D crystalline flakes of graphene (or for that matter of any material) are manifestly allowed by this theorem. In fact, a 2D Wigner crystal, i.e., a 2D hexagonal classical crystal of electrons in a very low-density limit, was experimentally observed more than 30 years ago (Grimes and Adams, 1979) on the surface of liquid ^{4}He (where the electrons were bound by their image force). A simple back of the envelope calculation shows that the size of the graphene flake has to be unphysically large for this theorem to have any effect on its crystalline nature (Thompson-Flagg *et al.*, 2009). There is nothing mysterious or remarkable about having finite 2D crystals with quasi-long-range positional order at finite temperatures, which is what we have in 2D graphene flakes.

II. QUANTUM TRANSPORT

A. Introduction

The phrase ''quantum transport'' usually refers to the charge current induced in an electron gas in response to a vanishing external electric field in the regime where quantum interference effects are important (Rammer, 1988;

Akkermans and Montambaux, 2007). This is relevant at low temperatures where the electrons are coherent and interference effects are not washed out by dephasing. Theoretically, this corresponds to the systematic application of diagrammatic perturbation theory or field-theoretic techniques to study how quantum interference changes the conductivity. For diffusive transport in two dimensions (including graphene), to lowest order in this perturbation theory, interference can be neglected, and one recovers the Einstein relation $\sigma_0 = e^2 D(E_F)\mathcal{D}$, where $D(E_F)$ is the density of states at E_F, and $\mathcal{D} = v_F^2 \tau / 2$ is the diffusion constant. This corresponds to the classical motion of electrons in a diffusive random walk scattering independently off the different impurities.

Since the impurity potential is typically calculated using the quantum-mechanical Born approximation, this leading order contribution to the electrical conductivity is known as the semiclassical transport theory and is the main subject of Sec. III.A. Higher orders in perturbation theory give quantum corrections to this semiclassical result, i.e., $\sigma = \sigma_0 + \delta\sigma$, where $\delta\sigma \ll \sigma$. In some cases these corrections can be divergent, a result that simultaneously implies a formal breakdown of the perturbation theory itself, while suggesting a phase transition to a nonperturbatively accessible ground state.

For example, it is widely accepted that quantum interference between forward and backward electron trajectories is the microscopic mechanism responsible for the Anderson metal-insulator transition (Abrahams *et al.*, 1979). For this reason, the leading quantum correction to the conductivity is called ''weak localization'' and is interpreted as the precursor to Anderson localization.

Weak localization is measured experimentally by using a magnetic field to break the symmetry between the forward and backward trajectories causing a change in the resistance. In this case the zero-field conductivity $\sigma(B = 0) = \sigma_0 + \delta\sigma$ includes the quantum corrections while $\sigma(B > B^*) = \sigma_0$ has only the semiclassical contribution. (B^* is approximately the magnetic field necessary to thread the area of the sample with one flux quantum.)

The second hallmark of quantum transport is mesoscopic conductance fluctuations. If one performed the low-temperature magnetotransport measurement discussed above, one would notice fluctuations in the magnetoresistance that would look like random noise. However, unlike noise, these traces are reproducible and are called magneto-fingerprints. These magneto-fingerprints depend on the positions of the random impurities as seen by the electrons. Annealing the sample relocates the impurities and changes the fingerprint. The remarkable feature of these conductance fluctuations is that their magnitude is universal (depending only on the global symmetry of the system), and notwithstanding the caveats discussed below, they are completely independent of any microscopic parameters such as material properties or type of disorder.

While the general theory for weak localization and universal conductance fluctuations is now well established (Lee and Ramakrishnan, 1985), in Sec. II.C.3 we discuss its application to graphene.

The discussion so far has concerned diffusive transport; in what follows, we also consider the ballistic properties of

noninteracting electrons in graphene. Early studies on the quantum-mechanical properties of the Dirac Hamiltonian revealed a peculiar feature—Dirac carriers could not be confined by electrostatic potentials (Klein, 1929).

An electron facing such a barrier would transmute into a hole and propagate through the barrier. In Sec. II.B we study Klein tunneling of Dirac carriers and discuss how this formalism can be used to obtain graphene's ballistic universal minimum conductivity. There is no analog of this type of quantum-limited transport regime in two-dimensional semiconductors. The ''metallic nature'' of graphene gives rise to several interesting and unique properties that we explore in this section, including the absence of Anderson localization for Dirac electrons and a metal-insulator transition induced by atomically sharp disorder (such as dislocations). We note that many of the results in this section can be also obtained using field-theoretic methods (Fradkin, 1986; Ludwig *et al.*, 1994; Altland, 2006; Ostrovsky *et al.*, 2006; Ryu, Mudry, Obuse, and Furusaki, 2007; Fritz *et al.*, 2008; Schuessler *et al.*, 2009).

B. Ballistic transport

1. Klein tunneling

In classical mechanics, a potential barrier, whose height is greater than the energy of a particle, will confine that particle. In quantum mechanics, the notion of quantum tunneling describes the process whereby the wave function of a non-relativistic particle can leak out into the classically forbidden region. However, the transmission through such a potential barrier decreases exponentially with the height and width of the barrier. For Dirac particles, the transmission probability depends only weakly on the barrier height, approaching unity with increasing barrier height (Katsnelson *et al.*, 2006). One can understand this effect by realizing that the Dirac Hamiltonian allows for both positive energy states (called electrons) and negative energy states (called holes). While a positive potential barrier is repulsive for electrons, it is attractive for holes (and vice versa). For any potential barrier, one needs to match the electron states outside the barrier with the hole states inside the barrier. Since the larger the barrier is, the greater the mode matching between electron and hole states is, the transmission is also greater. For an infinite barrier, the transmission becomes perfect. This is called Klein tunneling (Klein, 1929).

By solving the transmission and reflection coefficients for both the graphene *p-n* junction (Cheianov and Fal'ko, 2006b; Low and Appenzeller, 2009) and the *p-n-p* junction (Katsnelson *et al.*, 2006), it was found that for graphene the transmission at an angle normal to the barrier was always perfect (although there could be some reflection at other angles). This can be understood in terms of pseudospin conservation. At normal incidence, the incoming electron state and the reflected electron state are of opposite chirality, resulting in vanishing probability for reflection.

At finite angles of incidence, the transmission depends on the sharpness of the barrier. In the limit of a perfectly sharp step, the transmission probability is determined only by pseudospin conservation and is given by $T_{\text{step}}(\theta) = \cos^2\theta$. For a smooth variation in the electrostatic potential that defines the *p-n* junction (characterized by a length scale ξ), the transmission probability was shown by Cheianov and Fal'ko (2006b) to be $T_\xi(\theta) = \exp[-\pi(k_F\xi)\sin^2\theta]$. This implies that for both sharp and smooth potential barriers, a wave packet of Dirac fermions will collimate in a direction perpendicular to the *p-n* junction. One can estimate the conductance of a single *p-n* junction (of width W) to be

$$G_{p\text{-}n} = \frac{4e^2}{h}(k_F W)\int \frac{d\theta}{2\pi} T_\xi(\theta) \xrightarrow{k_F\xi \gg 1} \frac{2e^2}{\pi h}\sqrt{\frac{k_F}{\xi}}W. \quad (2.1)$$

Although the conductance of smooth *p-n* junctions are smaller by a factor of $\sqrt{k_F\xi}$ compared to sharp ones, this result suggests that the presence of *p-n* junctions would make a small contribution to the overall resistivity of a graphene sample (see also Sec. IV.D), i.e., graphene *p-n* junctions are essentially transparent.

The experimental realization of *p-n* junctions came shortly after the theoretical predictions (Huard *et al.*, 2007; Lemme *et al.*, 2007; Özyilmaz *et al.*, 2007; Williams *et al.*, 2007). At zero magnetic field, the effect of creating a *p-n* junction was to modestly change the device resistance. More dramatic was the change at high magnetic field in the quantum Hall regime (see Sec. V).

More detailed calculations of the zero-field conductance of the *p-n* junction were performed by taking into account the effect of nonlinear electronic screening. This tends to make the *p-n* junction sharper, and for $r_s \ll 1$, increases the conductance by a factor $r_s^{1/6}$ (Zhang and Fogler, 2008), and thereby further reduces the overall contribution of *p-n* junctions to the total resistance. The effect of disorder was examined by Fogler, Novikov *et al.* (2008) who studied how the *p-n* junction resistance changed from its ballistic value in the absence of disorder to the diffusive limit with strong disorder. More recently, Rossi, Bardarson, Brouwer, and Das Sarma (2010) used a microscopic model of charged impurities to calculate the screened disorder potential and solved for the conductance of such a disordered *n-p-n* junction numerically.

The broad oscillations visible in Fig. 6 arise from resonant tunneling of the few modes with the smallest transverse momentum. These results demonstrate that the signatures of the Klein tunneling are observable for impurity densities as high as 10^{12} cm^{-2} and would not be washed away by disorder as long as the impurity limited mean free path is greater than length of the middle region of the opposite polarity. This implies that at zero magnetic field, the effects of Klein tunneling are best seen with a very narrow top gate. Indeed, recent experiments have succeeded in using an ''air bridge'' (Gorbachev *et al.*, 2008; Liu *et al.*, 2008) or very narrow top gates (Stander *et al.*, 2009; Young and Kim, 2009). The observed oscillations in the conductivity about the semiclassical value are in good agreement with the theory of Rossi, Bardarson, Brouwer, and Das Sarma (2010).

There is a strong similarity between the physics of phase-coherent ballistic trajectories of electrons and that of light waves which is often exploited (Ji *et al.*, 2003; Cheianov, Fal'ko, and Altshuler, 2007; Shytov *et al.*, 2008). In particular, Liang *et al.* (2001) demonstrated that one could construct a Fabry-Pérot resonator of electrons in a carbon nanotube. This relies on the interference between electron paths in the
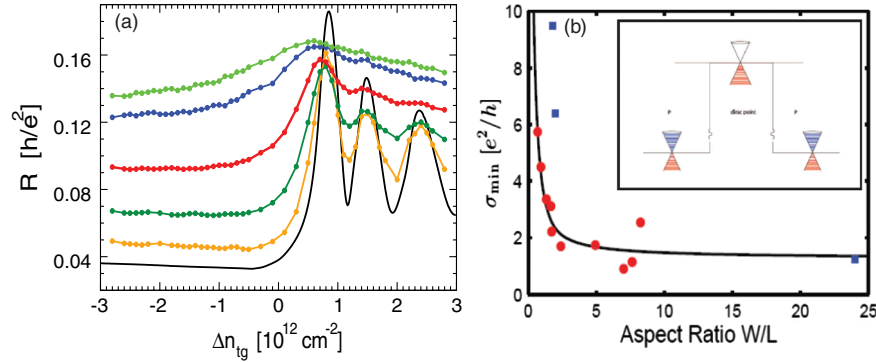
FIG. 6 (color online).   (a) Disorder averaged resistance as a function of top gate voltage for a fixed back gate density $n_{bg} = 5 \times 10^{11}$ cm^{-2} and several values of the impurity density (from bottom to top $n_{imp} = 0, 1, 2.5, 5, 10$, and 15×10^{11} cm^{-2}). Results were obtained using 10^3 disorder realizations for a square samples of size $W = L = 160$ nm in the presence of a top gate placed in the middle of the sample 10 nm above the graphene layer, 30 nm long, and of width W. The charge impurities were assumed at a distance $d = 1$ nm and the uniform dielectric constant κ was taken equal to 2.5. Adapted from Rossi, Bardarson, Brouwer, and Das Sarma, 2010. (b) Solid line is Eq. (2.4) for armchair boundary conditions showing the aspect ratio dependence of the Dirac point ballistic conductivity (Tworzydło *et al.*, 2006). For $W \gg L$, the theory approaches the universal value $4e^2/\pi h$. Circles show experimental data taken from Miao *et al.* (2007), and squares show the data from Danneau *et al.* (2008). Inset: Illustration of the configuration used to calculate graphene's universal minimum conductivity. For $V_g > 0$, one has a *p-p-p* junction, while for $V_g < 0$, one has a *p-n-p* junction. This illustrates the ballistic universal conductivity that occurs at the transition between the *p-p-p* and *p-n-p* junctions when $V_g = 0$.

different valleys K and K'. The same physics has been observed in "ballistic" graphene, where the device geometry is constructed such that the source and drain electrodes are closer than the typical electronic mean free path (Miao *et al.*, 2007; Cho and Fuhrer, 2009).

2. Universal quantum-limited conductivity

An important development in the understanding of graphene transport is the use of the formalism of Klein tunneling to address the question of graphene's minimum conductivity (Katsnelson, 2006; Tworzydło *et al.*, 2006). This of course considers noninteracting electrons at zero temperature and in the limit of no disorder. As shown in the inset of Fig. 6(b), the insight is to consider the source-graphene-drain configuration as the *n-p-n* or *n-n-n* junction, i.e., the leads are heavily electron doped, while the graphene sheet in the middle could be electron doped, hole doped, or pinned at the Dirac point with zero doping. Since there is no disorder, the electronic mean free path is much longer than the distance between the source and drain ($\ell \gg L$). We have this situation in mind when we talk about graphene's "ballistic conductivity."

For a non-Dirac metal, at finite carrier density, the absence of scattering would imply that the semiclassical electrical conductivity is infinite, since there is nothing to impede the electron motion. However, the conductance would then vanish as the carrier density is tuned to zero. This metal-insulator transition will be discussed in more detail later in the context of two-dimensional semiconductors.

The situation is quite different for graphene. From studying the Klein tunneling problem, we already know that both the *n-p-n* junction and the *n-n-n* junction have finite transmission coefficients. An interesting question follows: What is the tunneling at the precise point where the junction changes from a *n-p-n* junction to a *n-n-n* junction? The conductivity at this transition point would then be the quantum-limited (ballistic) conductivity of graphene at the Dirac point.

The solution is obtained by finding the transmission probabilities and obtaining the corresponding ballistic conductivity. This is analogous to the quantum mechanics exercise of computing the transmission through a potential barrier, but now instead for relativistic electrons. Using the noninteracting Dirac equation

$$[\hbar v_F \boldsymbol{\sigma} \cdot \mathbf{k} + eV(x)]\Psi(\mathbf{r}) = \varepsilon\Psi(\mathbf{r}), \qquad (2.2)$$

with the boundary conditions corresponding to $V(x < 0) = V(x > L) = V_\infty$ to represent the heavily doped leads and $V(x) = V_g$ for $0 < x < L$. For the case of $V_\infty \to \infty$ and at the Dirac point ($V_g = \varepsilon = 0$), the transmission probability (i.e., the square of the transmission amplitude) is given by purely evanescent modes (Tworzydło *et al.*, 2006):

$$T_n = \left| \frac{1}{\cosh(q_n L)} \right|^2. \qquad (2.3)$$

This is in contrast to the nonrelativistic electrons (i.e., with the usual parabolic dispersion), where for fixed q_n the analogous calculation gives vanishing transmission probability $T_n \sim 1/V_\infty$. The remaining subtle point is determining the transverse wave vector q_n. While it is clear that $q_n \sim nW^{-1}$ for large n, the choice of the boundary condition changes the precise relation, e.g., $q_n = n\pi/W$ for metallic armchair edges and $q_n = (n \pm 1/3)\pi/W$ for semiconducting armchair edges. Following Tworzydło *et al.* (2006), we use twisted boundary conditions $\Psi(y = 0) = \sigma_x\Psi(y = 0)$ and $\Psi(y = W) = -\sigma_x\Psi(y = W)$, which give $q_n = (n + 1/2)\pi/W$. This boundary condition is equivalent to having massless Dirac fermions inside the strip of width W, but infinitely massive Dirac fermions outside of the strip, thereby confining the electrons (Ryu, Mudry, Furusaki, and Ludwig, 2007).

The Landauer conductivity is then given by

$$\sigma = \frac{L}{W} \frac{g_s g_v e^2}{h} \sum_{n=0}^{\infty} T_n$$

$$= \frac{4e^2}{h} \sum_{n=0}^{\infty} \frac{L}{W \cosh^2[\pi(n + 1/2)L/W]} \xrightarrow{W \gg L} \frac{4e^2}{\pi h}. \tag{2.4}$$

Since at the Dirac point (zero energy) there is no energy scale in the problem, the conductivity (if finite) can only depend on the aspect ratio L/W. The remarkable fact is that for $W \gg L$, the sum in Eq. (2.4) converges to a finite and universal value—giving for ballistic minimum conductivity $\sigma_{\min} = 4e^2/\pi h$. This result also agrees with that obtained using linear response theory in the limit of vanishing disorder, suggesting that the quantum-mechanical transport through evanescent modes between source and drain (or equivalently the transport across two *p-n* junctions with heavily doped leads) is at the heart of the physics behind the universal minimum conductivity in graphene.

Miao *et al.* (2007) and Danneau *et al.* (2008) probed this ballistic limit experimentally using the two-probe geometry. Their results, shown in Fig. 6(b), are in good agreement with the theoretical predictions. Although it is not clear what role contact resistance (Blanter and Martin, 2007; Giovannetti *et al.*, 2008; Huard *et al.*, 2008; Lee, Balasubramanian *et al.*, 2008; Blake *et al.*, 2009; Cayssol *et al.*, 2009; Golizadeh-Mojarad and Datta, 2009) played in these two-probe measurements.

3. Shot noise

Shot noise is a type of fluctuation in electrical current caused by the discreteness of charge carriers and from the randomness in their arrival times at the detector or drain electrode. It probes any temporal correlation of the electrons carrying the current, quite distinct from thermal noise (or Johnson-Nyquist noise) which probes their fluctuation in energy. Shot noise is quantified by the dimensionless Fano factor $\mathcal{F}$, defined as the ratio between noise power spectrum and the average conductance. Scattering theory gives (Büttiker, 1990)

$$\mathcal{F} = \frac{\sum_n T_n(1 - T_n)}{\sum_n T_n}. \tag{2.5}$$

Some well-known limits include $\mathcal{F} = 1$ for "Poisson noise" when $T_n \ll 1$ (e.g., in a tunnel junction), and $\mathcal{F} = 1/3$ for disordered metals (Beenakker and Büttiker, 1992). For graphene at the Dirac point, we can use Eq. (2.3) to get $\mathcal{F} \to 1/3$ for $W \gg L$ (Tworzydło *et al.*, 2006). One should emphasize that obtaining the same numerical value for the Fano factor $\mathcal{F} = 1/3$ for ballistic quantum transport in graphene as that of diffusive transport in disordered metals could be nothing more than a coincidence (Dragomirova *et al.*, 2009). Cheianov and Fal'ko (2006b) found that the shot noise of a single *p-n* junction was $\mathcal{F} = 1 - \sqrt{1/2}$, which is numerically quite close to $1/3$.

Since several different mechanisms all give $\mathcal{F} \approx 1/3$, this makes shot noise a complicated probe of the underlying physical mechanism. Recent numerical studies by San-Jose *et al.* (2007), Lewenkopf *et al.* (2008), and Sonin (2008, 2009) treated the role of disorder to examine the crossover from the $\mathcal{F} = 1/3$ in ballistic graphene to the diffusive regime (see Sec. IV.B). Within the crossover, or away from the Dirac point, the Fano factor is no longer universal and shows disorder dependent deviations. The experimental situation is less clear. Danneau *et al.* (2008) measured the Fano factor decrease from $\mathcal{F} \approx 1/3$ with increasing carrier density to claim agreement with the ballistic theory. While DiCarlo *et al.* (2008) found that $\mathcal{F}$ was mostly insensitive to carrier type and density, temperature, aspect ratio, and the presence of a *p-n* junction, suggesting diffusive transport in the dirty limit.

Since shot noise is, in principle, an independent probe of the nature of the carrier dynamics, it could be used as a separate test of the quantum-limited transport regime. However, in practice, the coincidence in the numerical value of the Fano factor with that of diffusive transport regime makes this prospect far more challenging.

C. Quantum interference effects

1. Weak antilocalization

Over the past 50 years, there has been much progress towards understanding the physics of Anderson localization [for a recent review, see Evers and Mirlin (2008)]. Single particle Hamiltonians are classified according to their global symmetry. Since the Dirac Hamiltonian (for a single valley) $\mathcal{H} = \hbar v_F \boldsymbol{\sigma} \cdot \mathbf{k}$ is invariant under the transformation $\mathcal{H} = \sigma_y \mathcal{H}^* \sigma_y$ [analogous to spin-rotation symmetry (SRS) in pseudospin space] it is in the AII class (also called the symplectic Wigner-Dyson class). The more familiar physical realization of the symplectic class is the usual disordered electron gas with strong spin-orbit coupling:

$$\mathcal{H}_{\alpha\beta} = \frac{\hbar^2 k^2}{2m} \delta_{\alpha\beta} + \mathcal{V}_{\alpha\beta},$$
$$\mathcal{V}_{\alpha\mathbf{k},\beta\mathbf{k}'} = V_{\mathbf{k}-\mathbf{k}'} - i V_{\mathbf{k}-\mathbf{k}'}^{\text{so}}(\hat{\mathbf{k}}' \times \hat{\mathbf{k}}) \cdot \boldsymbol{\sigma}_{\alpha\beta}, \tag{2.6}$$

where α and β are (real) spin indices, $\boldsymbol{\sigma}_{\alpha\beta}$ a vector of Pauli matrices. Note that this Hamiltonian is also invariant under SRS, $\mathcal{H} = \sigma_y \mathcal{H}^* \sigma_y$. We have

$$\langle V_{\mathbf{q}} V_{\mathbf{q}'} \rangle = \frac{\delta(\mathbf{q} - \mathbf{q}')}{2\pi\nu\tau}, \quad \langle V_{\mathbf{q}}^{\text{so}} V_{\mathbf{q}'}^{\text{so}} \rangle = \frac{\delta(\mathbf{q} - \mathbf{q}')}{2\pi\nu\tau_{\text{so}}}. \tag{2.7}$$

It was shown by Hikami *et al.* (1980) that when the classical conductivity is large ($\sigma_0 \gg e^2/h$), the quantum correction to the conductivity is positive

$$\delta\sigma = \frac{e^2}{\pi h} \ln(L/\ell). \tag{2.8}$$

Equivalently, one can define a one-parameter scaling function (Abrahams *et al.*, 1979)

$$\beta(\sigma) = \frac{d \ln \sigma}{d \ln L}, \tag{2.9}$$

where for the symplectic class it follows from Eq. (2.8) that $\beta(\sigma) = 1/(\pi\sigma)$ for large σ. To have $\beta > 0$ means that the

conductivity increases as one goes to larger system sizes or adds more disorder. This is quite different from the usual case of an Anderson transition where a negative β function means that for those same changes, the system becomes more insulating.

Since perturbation theory only gives the result for $\beta(\sigma \gg e^2/h)$, the real question becomes what happens to the β function at small σ. If the β function crosses zero and becomes negative as $\sigma \to 0$, then the system exhibits the usual Anderson metal-insulator transition. Numerical studies of the Hamiltonian [Eq. (2.6)] show that for the spin-orbit system, the β function vanishes at $\sigma^* \approx 1.4$ and below this value, the quantum correction to the classical conductivity is negative resulting in an insulator at zero temperature. σ^* is an unstable fixed point for the symplectic symmetry class.

As we have seen in Sec. II.B.2, however, graphene has a minimum ballistic conductivity $\sigma_{\min} = 4e^2/\pi h$ and does not become insulating in the limit of vanishing disorder. This makes graphene different from the spin-orbit Hamiltonian discussed above, and the question of what happens with increasing disorder becomes interesting.

Bardarson *et al.* (2007) studied the Dirac Hamiltonian [Eq. (2.2)] with the addition of a Gaussian correlated disorder term $U(\mathbf{r})$, where

$$\langle U(\mathbf{r})U(\mathbf{r}')\rangle = K_0 \frac{(\hbar v_F)^2}{2\pi\xi^2} \exp\left[\frac{-|\mathbf{r}-\mathbf{r}'|^2}{2\xi^2}\right]. \qquad (2.10)$$

One should think of K_0 as parametrizing the strength of the disorder and ξ as its correlation length. If the theory of one-parameter scaling holds for graphene, then it should be possible to rescale the length $L^* = f_0(K_0)L$, where f_0 is a scaling function inversely proportional to the effective electronic mean free path. Their numerical results are shown in Fig. 7 and demonstrate that (i) graphene does exhibit one-parameter scaling (i.e., there exists a β function) and (ii) the β function is always positive unlike the spin-orbit case. Therefore, Dirac fermions evade Anderson localization and are always metallic. Similar conclusions were obtained by Nomura *et al.* (2007), San-Jose *et al.* (2007), Titov (2007), and Tworzydło *et al.* (2008).

The inset of Fig. 7 shows an explicit computation of the β function comparing Dirac fermions with the spin-orbit model. The difference between these two classes of the AII symmetry class has been attributed to a topological term (i.e., two possible choices for the action of the field theory describing these Hamiltonians). Since it allows for only two possibilities, it has been called a Z_2 topological symmetry (Kane and Mele, 2005b; Evers and Mirlin, 2008). The topological term has no effect at $\sigma \gg e^2/h$ but is responsible for the differences at $\sigma \approx e^2/h$ and determines the presence or absence of a metal-insulator transition. Nomura *et al.* (2007) presented an illustrative visualization of the differences between Dirac fermions and the spin-orbit symplectic class shown in Fig. 8. By imposing a twist boundary condition in the wave functions such that $\Psi(x=0) = \exp[i\phi]\Psi(x=L)$ and $\Psi(y=0) = \Psi(y=W)$, one can examine the single particle spectrum as a function of the twist angle ϕ. For $\phi = 0$ and $\phi = \pi$, the phase difference is real and eigenvalues come in Krammer's degenerate pairs. For other values of ϕ, this degeneracy is lifted. As seen in the figure, for massless Dirac fermions all energy states are connected by a continuous variation in the boundary conditions. This precludes creating a localized state, which would require the energy variation with boundary condition (also called Thouless energy) be smaller than the level spacing. Since this is a topological effect, Nomura *et al.* (2007) argued that this line of reasoning should be robust to disorder.

The situation for the spin-orbit case is very different. The same Krammer's pairs that are degenerate at $\phi = 0$ reconnect at $\phi = \pi$. In this case, there is nothing to prevent localization if the disorder would push the Krammer's pairs past the mobility edge. Similar considerations regarding the Z_2 symmetry also hold for topological insulators where the metallic surface state should remain robust against localization in the presence of disorder.
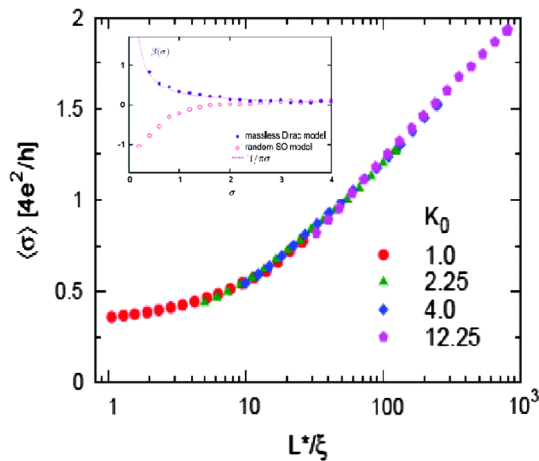

FIG. 7 (color online). Demonstration of one-parameter scaling at the Dirac point. From Bardarson *et al.*, 2007. Main panel shows the conductivity as a function of L^*/ξ, where $L^* = f(K_0)L$ is the scaled length and ξ is the correlation length of the disorder potential. Note that $\beta = d\ln\sigma/d\ln L > 0$ for any disorder strength. The inset shows explicit comparison of the β function for the Dirac fermion model and for the symplectic (AII) symmetry class. From Nomura *et al.*, 2007.
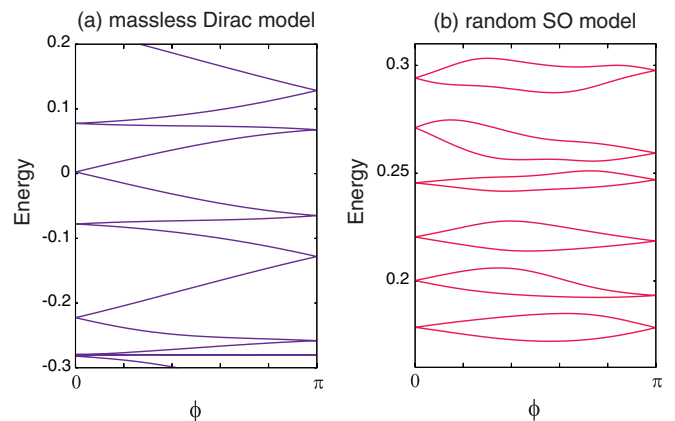

FIG. 8 (color online). Picture proposed by Nomura *et al.* (2007) to understand the difference in topological structure between the massless Dirac model and the random spin-orbit symmetry class.

2. Crossover from the symplectic universality class

It is already apparent in the preceding discussion that each Dirac cone is described by the Dirac Hamiltonian $\mathcal{H} = \sigma \cdot \mathbf{p}$. The effective SRS $\mathcal{H} = \sigma_y \mathcal{H}^* \sigma_y$ is preserved in each cone, and for most purposes graphene can be viewed as two degenerate copies of the AII symplectic symmetry class. However, as Suzuura and Ando (2002a) first pointed out, a material defect such as a missing atom would couple the two Dirac cones (and since each cone is located in a different "valley," this type of interaction is called intervalley scattering). One can appreciate intuitively why such scattering is expected to be small. The two valleys at points K and K' in the Brillouin zone are separated by a large momentum vector that is inversely proportional to the spacing between two neighboring carbon atoms. This means that the potential responsible for such intervalley coupling would have to vary appreciably on the scale of 0.12 nm in order to couple the K and K' points.

We note that while such defects and the corresponding coupling between the valleys are commonly observed in scanning tunneling microscopy (STM) studies on epitaxial graphene (Rutter *et al.*, 2007), they are virtually absent in all similar studies in exfoliated graphene (Ishigami *et al.*, 2007; Stolyarova *et al.*, 2007; Zhang *et al.*, 2008). In the presence of such atomically sharp disorder, Suzuura and Ando (2002a) proposed a model for the two-valley Hamiltonian that captures the effects of intervalley scattering. The particular form of the scattering potential is not important, and in Sec. II.C.3 we will discuss a generalized Hamiltonian that includes all nonmagnetic (static) impurities consistent with the honeycomb symmetry and is characterized by five independent parameters (Aleiner and Efetov, 2006; McCann *et al.*, 2006). Here the purpose is simply to emphasize the qualitative difference between two types of disorder: long-range (i.e., diagonal) disorder $\mathcal{U}^{\mathrm{LR}}$ that preserves the effective SRS and a short-range potential $\mathcal{U}^{\mathrm{SR}}$ that breaks this symmetry.

We note that with the intervalley term $\mathcal{U}^{\mathrm{SR}}$, the Hamiltonian belongs to the Wigner-Dyson orthogonal symmetry class, while as discussed in Sec. II.C.1 including only the diagonal disorder $\mathcal{U}^{\mathrm{LR}}$, one is in the Wigner-Dyson symplectic class.

A peculiar feature of this crossover is that it is governed by the concentration of short-range impurities thus questioning the notion that the universality class is determined only by the global symmetries of the Hamiltonian and not by microscopic details. However, a similar crossover was observed by Miller *et al.* (2003) where the strength of the spin-orbit interaction was tuned by carrier density, moving from weak localization at low density and a weak spin-orbit interaction, to weak antilocalization at high density and a strong spin-orbit interaction.

From symmetry considerations, one should expect that without atomically sharp defects, graphene would exhibit weak antilocalization (where $\delta\sigma > 0$) and no Anderson localization (see Sec. II.C.1). However, with intervalley scattering, graphene should have weak localization ($\delta\sigma < 0$) and be insulating at zero temperature. These conclusions were verified by Suzuura and Ando (2002a) from a microscopic Hamiltonian by calculating the Cooperon (see Fig. 9) and

obtaining the corrections to the conductivity from the bare Hikami box (see Sec. II.C.3 for a more complete discussion).

For the case of no intervalley scattering $\mathcal{U} = \mathcal{U}^{\mathrm{LR}}$, the resulting Cooperon is

$$C^{\mathrm{LR}}_{\mathbf{k}_\alpha \mathbf{k}_\beta}(Q) = \frac{n_i u^2}{A} e^{i(\psi_{\mathbf{k}_\alpha} - \psi_{\mathbf{k}_\beta})} \frac{1}{(v_F \tau Q)^2}, \tag{2.11}$$

with area $A = LW$, $Q = \mathbf{k}_\alpha + \mathbf{k}_\beta$, and $e^{i(\psi_{\mathbf{k}_\alpha} - \psi_{\mathbf{k}_\beta})} \approx -1$, giving $\delta\sigma_{\mathrm{LR}} = (2e^2/\pi^2\hbar)\ln(L_\phi/\ell)$. As expected for the symplectic class, without intervalley scattering, the quantum correction to the conductivity is positive.

With intervalley scattering, $\mathcal{U} = \mathcal{U}^{\mathrm{SR}}$ calculating the same diagrams gives

$$C^{\mathrm{SR}}_{\mathbf{k}_\alpha \mathbf{k}_\beta}(Q) = \frac{n_i u^2}{A} j_\alpha j_\beta e^{i(\psi_{\mathbf{k}_\alpha} - \psi_{\mathbf{k}_\beta})} \frac{1}{(v_F \tau Q)^2}, \tag{2.12}$$

with current $j_\alpha = -j_\beta$ and $\delta\sigma_{\mathrm{SR}} = -e^2/(2\pi^2\hbar)\ln(L_\phi/\ell)$. This negative $\delta\sigma$ is consistent with the orthogonal symmetry class. The explicit microscopic calculation demonstrates the crossover from weak antilocalization to weak localization induced by atomically sharp microscopic defects providing intervalley coupling.

This crossover was recently observed experimentally (Tikhonenko *et al.*, 2009). They noted empirically that for their samples the scattering associated with short-range defects is stronger at high carrier density. In fact, this is what one expects from the microscopic theory discussed in Sec. III. Because of the unique screening properties of graphene, long-range scatterers dominate transport at low carrier density while short-range scatterers dominate at high density. Assuming that these short-range defects are also the dominant source of intervalley scattering, one would expect to have weak localization at high carrier density (due to the large intervalley scattering), and weak antilocalization at low carrier density where transport is dominated by "atomically smooth" defects such as charged impurities in the substrate. This is precisely what was seen experimentally. Figure 10 shows a comparison of the magnetoconductance at three different carrier densities. At the lowest carrier density, the data show the weak antilocalization characteristic of the symplectic symmetry class, while at high density, one finds weak localization signaling a crossover to the orthogonal universality class.

A second crossover away from the symplectic universality class was examined by Morpurgo and Guinea (2006). As discussed, a magnetic field breaks time reversal symmetry and destroys the leading quantum corrections to the conductivity $\delta\sigma(B > B^*) = 0$. This can also be understood as a crossover from the symplectic (or orthogonal) universality class to the unitary class. The unitary class is defined by the absence of time reversal symmetry and hence vanishing contribution from the Cooperon.[1]

---

[1]The sign of the quantum correction in relation to the global symmetry of the Hamiltonian can also be obtained from the random matrix theory (Beenakker, 1997) $\delta\sigma/\sigma_0 = (1 - 2/\beta)/4$, where $\beta = 1, 2, 4$ for the orthogonal, unitary, and symplectic Wigner-Dyson symmetry classes.
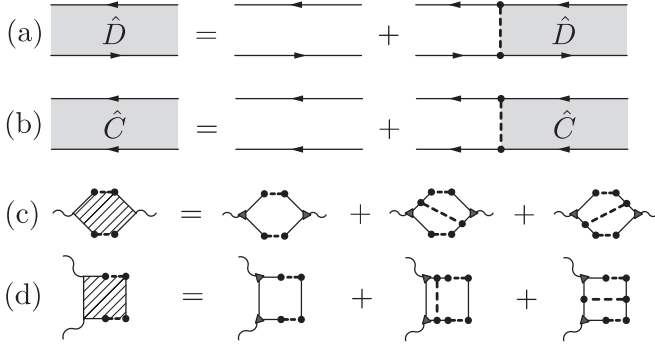
FIG. 9. Diagrammatic representation for (a) diffuson, (b) Cooperon, and dressed Hikami boxes [(c) and (d)]. Adapted from Kharitonov and Efetov, 2008.

Similar to short-range impurities inducing a crossover from symplectic to orthogonal classes, Morpurgo and Guinea (2006) asked if there were other kinds of disorder that could act as pseudomagnetic fields and induce a crossover to the unitary symmetry class leading to the experimental signature of a suppression of weak antilocalization. This was in part motivated by the first experiments on graphene quantum transport showing that the weak localization correction was an order of magnitude smaller than expected (Morozov *et al.*, 2006). They argued that topological lattice defects (Ebbesen and Takada, 1995) (e.g., pentagons and heptagons) and nonplanarity of graphene (commonly referred to as "ripples") would generate terms in the Hamiltonian that looked like a vector potential and correspond to a pseudomagnetic field.

In addition, experiments both on suspended graphene (Meyer *et al.*, 2007) and on a substrate showed that graphene is not perfectly coplanar. It is noteworthy, however, that experiments on a SiO$_2$ substrate showed that these ripples were correlated with the height fluctuations of the substrate and varied by less than 1 nm (Ishigami *et al.*, 2007), while graphene on mica was even smoother with variations of less than 0.03 nm (Lui *et al.*, 2009). On the other hand, one could deliberately induce lattice defects (Chen, Cullen *et al.*, 2009) or create controlled ripples by straining graphene before cooling and exploiting graphene's negative thermal expansion coefficient (Balandin *et al.*, 2008; Bao *et al.*, 2009).

Just as a real magnetic field, these terms would break the time reversal symmetry (TRS) in a single valley (while preserving the TRS of the combined system). If $\tau_i \gg \tau_\phi$, then the two valleys are decoupled, these defects would cause a crossover to the unitary symmetry class, and the resulting Cooperon (Fig. 9) would vanish. For example, considering the case of lattice defects, the disorder Hamiltonian would be given by $\mathcal{U}^G = (1/4)[\sigma_x \otimes \sigma_z] \nabla [\partial_y u_x(\mathbf{r}) - \partial_x u_y(\mathbf{r})]$, where $\mathbf{u}(\mathbf{r})$ is the lattice strain vector induced by the defect. One notes that this term in the Hamiltonian has the form of an effective magnetic field $+B$ in the K valley and $-B$ in the K' valley (Morpurgo and Guinea, 2006). In the absence of intervalley coupling, this would suppress weak antilocalization when the effective magnetic field $|B|$ is larger than the field B^* discussed in Sec. II.A.

3. Magnetoresistance and mesoscopic conductance fluctuations

As discussed, at low energies and in the absence of disorder, graphene is described by two decoupled Dirac cones located at points K and K' in the Brillouin zone. Within each cone, one has a pseudospin space corresponding to wave function amplitudes on the A and B sublattice of the honeycomb lattice. The two-valley Hamiltonian is then the outer product of two SU(2) spin spaces $KK' \otimes AB$. The most generic Hamiltonian in this space of 4×4 Hermitian matrices can be parametrized by the generators of the group U(4) (Aleiner and Efetov, 2006; Altland, 2006; McCann *et al.*, 2006):

$$\mathcal{H} = \hbar v_F \boldsymbol{\Sigma} \mathbf{p} + \mathbb{1}_4 u_0(\mathbf{r}) + \sum_{s,l=x,y,z} \Sigma_s \Lambda_l u_{sl}(\mathbf{r}), \quad (2.13)$$

where $\boldsymbol{\Sigma} = (\Sigma_x, \Sigma_y, \Sigma_z) = (\sigma_z \otimes \sigma_x, \sigma_z \otimes \sigma_y, \mathbb{1}_2 \otimes \sigma_z)$ is the algebra of the sublattice SU(2) space (recall that the outer product is in the space $KK' \otimes AB$, and the $\boldsymbol{\Sigma}$ operator is diagonal in the KK' space). Similarly, $\boldsymbol{\Lambda} = (\sigma_x \otimes \sigma_z, \sigma_y \otimes \sigma_z, \sigma_z \otimes \mathbb{1}_2)$ forms the algebra of the valley-spin space (being diagonal in the AB space).

The Hamiltonian of Eq. (2.13) can be understood in simple terms. The first term is just two decoupled Dirac cones and is equivalent to the disorder-free case discussed earlier, but written here in a slightly modified basis. The second term is identical to $\mathcal{U}^{\text{LR}}$ and as discussed, it represents any long-range diagonal disorder. The last term parametrized by the nine scattering potentials $u_{sl}(\mathbf{r})$ represents all possible types of disorder allowed by the symmetry of the honeycomb lattice. For example, a vacancy would contribute to all terms (including u_0) except u_{xz} and u_{yz}; while bond disorder would contribute to all terms except u_{zz} (Aleiner and Efetov, 2006).

The "diagonal" term $u_0(\mathbf{r})$ is the dominant scattering mechanism for current graphene experiments and originates from long-ranged Coulomb impurities, which is discussed in more detail in Sec. III. Because of the peculiar screening properties of graphene, such long-range disorder cannot be treated using the Gaussian white noise approximation. To circumvent this problem (for both the long-range u_0 and short-range u_{sl} terms), we simply note that for each kind of disorder, there would be a corresponding scattering time $\{\tau_0, \tau_{sl}\}$ that could, in principle, have very different dependence on carrier density.

For the special case of Gaussian white noise, i.e., where $\langle u_{sl}(\mathbf{r}) u_{s'l'}(\mathbf{r}') \rangle = u_{sl}^2 \delta_{s,s'} \delta_{l,l'} \delta(\mathbf{r} - \mathbf{r}')$, we have $\hbar \tau_{sl}^{-1} = \pi D(E_F) u_{sl}^2$. Moreover, one could assume that after disorder averaging, the system is isotropic in the x-y plane. Denoting $\{x, y\} \equiv \perp$, the total scattering time is given by

$$\tau^{-1} = \tau_0^{-1} + \tau_{zz}^{-1} + 2\tau_{\perp z}^{-1} + 2\tau_{z\perp}^{-1} + 4\tau_{\perp\perp}^{-1}. \quad (2.14)$$

These five scattering times could be viewed as independent microscopic parameters entering the theory (Aleiner and Efetov, 2006), or one could further classify scattering times as being either "intervalley" $\tau_i^{-1} = 4\tau_{\perp\perp}^{-1} + 2\tau_{z\perp}^{-1}$ or "intravalley" $\tau_z^{-1} = 4\tau_{\perp z}^{-1} + 2\tau_{zz}^{-1}$. A small contribution from trigonal warping (a distortion to the Dirac cone at the energy scale of the inverse lattice spacing) could be modeled by the perturbative term $H_w \sim \Sigma_x(\boldsymbol{\Sigma}\mathbf{p})\Lambda_z \Sigma_x(\boldsymbol{\Sigma}\mathbf{p})\Sigma_x$, which acts as

an additional source of intravalley scattering (McCann *et al.*, 2006).

The transport properties of the Hamiltonian [Eq. (2.13)] are obtained by calculating the two particle propagator. In general, both the classical contribution (diffusons) and quantum corrections (Cooperons) will be 4×4 matrices defined in terms of the retarded (R) and advanced (A) Green's functions $\mathcal{G}^{R,A}$ as (see also Fig. 9)

$$\mathcal{D}(\omega, \mathbf{r}, \mathbf{r}') = \langle \mathcal{G}^R(\epsilon + \omega, \mathbf{r}, \mathbf{r}') \otimes \mathcal{G}^A(\epsilon, \mathbf{r}', \mathbf{r}) \rangle,$$
$$\mathcal{C}(\omega, \mathbf{r}, \mathbf{r}') = \langle \mathcal{G}^R(\epsilon + \omega, \mathbf{r}, \mathbf{r}') \otimes \mathcal{G}^A(\epsilon, \mathbf{r}, \mathbf{r}') \rangle. \quad (2.15)$$

As discussed in Sec. III.A, the scattering rate is dominated by the diagonal disorder $\tau \approx \tau_0$. Since both this term and the Dirac part of Eq. (2.13) is invariant under the valley SU(2), one can classify the diffussons and Cooperons as "singlets" and "triplets" in the *AB*-sublattice SU(2) space. Moreover, one finds that for both the diffussons and Cooperons, only the valley singlets are gapless, and one can completely ignore the valley triplets whose energy gap scales as τ_0^{-1}. Considering only the sublattice singlet ($j = 0$) and triplet ($j = x, y, z$), one finds (McCann *et al.*, 2006; Fal'ko *et al.*, 2007; Kechedzhi *et al.*, 2008; Kharitonov and Efetov, 2008)

$$\left[-i\omega - \frac{1}{2}v_F^2\tau_0\left(\nabla - \frac{2e\mathbf{A}}{c}\right)^2 + \Gamma^j \right]\mathcal{D}^j(\mathbf{r}, \mathbf{r}') = \delta(\mathbf{r} - \mathbf{r}'),$$
$$\left[-i\omega - \frac{1}{2}v_F^2\tau_0\left(\nabla + \frac{2e\mathbf{A}}{c}\right)^2 + \Gamma^j + \tau_\phi^{-1} \right]\mathcal{C}^j(\mathbf{r}, \mathbf{r}')$$
$$= \delta(\mathbf{r} - \mathbf{r}'), \quad (2.16)$$

with $\Gamma^0 = 0$ (singlet), $\Gamma^x = \Gamma^y = \tau_i^{-1} + \tau_z^{-1}$, and $\Gamma^z = 2\tau_i^{-1}$ (triplet). This equation captures all the differences in the quantum corrections to the conductivity between graphene and usual 2DEGs.

The magnetoresistance and conductance fluctuation properties in graphene follow from this result. The quantum correction to the conductivity is $\delta\sigma \sim N_t^C - N_s^C$, where N_t^C is the number of gapless triplet Cooperon modes and N_s^C is the number of gapless singlet Cooperon modes. In this context, gapped modes do not have a divergent quantum correction and can be neglected. Similarly, the conductance fluctuations are given by $\langle[\delta G]^2\rangle = N_{CD}\langle[\delta G]^2\rangle_{2DEG}$, where N_{CD} counts the total number of gapless Cooperons and diffusons modes, and $\langle[\delta G]^2\rangle_{2DEG}$ is the conductance variance for a conventional 2D electron gas. For a quasi-1D geometry, $\langle[\delta G]^2\rangle_{2DEG} = \frac{1}{15}(2e^2/h)^2$ (Lee and Ramakrishnan, 1985).

We can immediately identify several interesting regimes that are shown schematically in Fig. 10:

(i) *Strong intervalley scattering.* Even with strong short-range disorder (i.e., $\tau_i \ll \tau_\phi$ and $\tau_z \ll \tau_\phi$), both the singlet Cooperon $\mathcal{C}^0$ and the singlet diffuson $\mathcal{D}^0$ remain gapless since $\Gamma^0 = 0$. Contributions from all triplet Cooperons and difussons vanish. In this situation, the quantum corrections to the conductivity in graphene are very similar to the regular 2DEG. The Hamiltonian is in the orthogonal symmetry class discussed earlier and one has weak localization ($\delta\sigma < 0$). Similarly, for conductance fluctuations (typically measured at large magnetic fields), one would have the same result as the nonrelativistic electron gas.
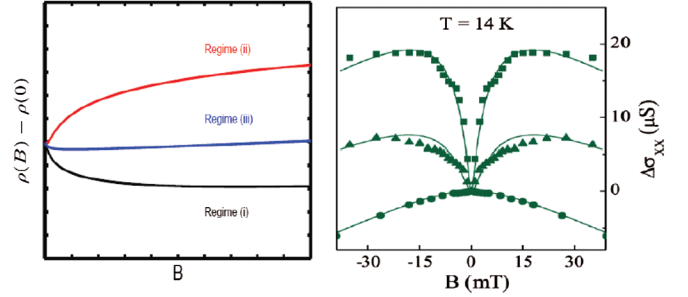

FIG. 10 (color online). Left panel: Schematic of different magnetoresistance regimes. (i) For strong intervalley scattering (i.e. $\tau_i \ll \tau_\phi$ and $\tau_z \ll \tau_\phi$), Eq. (2.18) gives weak localization or $\delta\sigma \sim \rho(B) - \rho(0) < 0$. This is similar to quantum transport in the usual 2DEG. (ii) For weak intervalley scattering (i.e., $\tau_i \gg \tau_\phi$ and $\tau_z \gg \tau_\phi$), one has weak antilocalization, characteristic of the symplectic symmetry class. (iii) For $\tau_i \gg \tau_\phi$, but $\tau_z \ll \tau_\phi$, Eq. (2.18) gives a regime of suppressed weak localization. Right panel: Experimental realization of these three regimes. Graphene magnetoconductance is shown for carrier density (from bottom to top) $n = 2.2 \times 10^{10}$, 1.1×10^{12}, and 2.3×10^{12} cm^{-2}, at $T = 14$ K. The lowest carrier density (bottom curve) has a small contribution from short-range disorder and shows weak antilocalization [i.e., the zero-field conductivity is larger than at finite field. $\sigma(B = 0) = \sigma_0 + \delta\sigma$ and $\sigma(B > B^*) = \sigma_0$, with $\delta\sigma > 0$. B^* is the phase-breaking field]. In contrast, the highest density data (top curve) has a larger contribution of intervalley scattering and shows weak localization, i.e., $\delta\sigma < 0$. From Tikhonenko *et al.*, 2009.

(ii) *Weak short-range disorder.* For $\tau_i \gg \tau_\phi$ and $\tau_z \gg \tau_\phi$, all sublattice Cooperons and diffusons remain gapless at zero magnetic field. One then has $\delta\sigma > 0$ or weak antilocalization (symplectic symmetry). This regime was observed in experiments on epitaxial graphene (Wu *et al.*, 2007). The diffuson contribution to the conductance fluctuations is enhanced by a factor of 4 compared with conventional metals.

(iii) *Suppressed localization regime.* In the case that there is strong short-range scattering $\tau_z \ll \tau_\phi$, but in weak intervalley scattering $\tau_i \gg \tau_\phi$. The Cooperons $\mathcal{C}^x$ and $\mathcal{C}^y$ will be gapped, but $\mathcal{C}^z$ will remain and cancel the effect of the singlet $\mathcal{C}^0$. In this case one would have the suppressed weak localization that was presumably seen in the first graphene quantum transport experiments (Morozov *et al.*, 2006).

Although the discussion above captures the main physics, for completeness we reproduce the results of calculating the dressed Hikami boxes in Fig. 9 (Aleiner and Efetov, 2006; McCann *et al.*, 2006; Kechedzhi *et al.*, 2008; Kharitonov and Efetov, 2008) and using known results (Lee and Ramakrishnan, 1985). The quantum correction to the conductance is

$$\delta g = \frac{2e^2 D}{\pi\hbar} \int \frac{d^2q}{(2\pi)^2}(C^x + C^y + C^z - C^0), \quad (2.17)$$

and for the magnetoresistance

$$\rho(B) - \rho(0) = -\frac{e^2\rho^2}{\pi\hbar}\left[F\left(\frac{B}{B_\phi}\right) - F\left(\frac{B}{B_\phi + 2B_i}\right) \right.$$
$$\left. - 2F\left(\frac{B}{B_\phi + 2B_z}\right)\right], \qquad (2.18)$$

where $B_{\phi,i,z} = (\hbar c/4De)\tau_{\phi,i,z}^{-1}$ and $F(x) = \ln x + \psi(1/2 + 1/x)$, with ψ the digamma function. The function $F(x)$ is the same as for 2DEGs (Lee and Ramakrishnan, 1985); however, the presence of three terms in Eq. (2.18) is unique to graphene. The universal conductance fluctuations are

$$\langle[\delta G]^2\rangle = \sum_{C,D} 3\left[\frac{g_s g_v e^2}{2\pi\hbar}\right]^2 \sum_{i=0}^{3}\sum_{n_x=1}^{\infty}\sum_{n_y=0}^{\infty}\frac{1}{\pi^4 L_x^4}\left[\frac{\Gamma_i}{\pi^2 D} + \frac{n_x^2}{L_x^2}\right.$$
$$\left. + \frac{n_y^2}{L_y^2}\right]^{-2} = N_{CD}\langle[\delta G]^2\rangle_{2\text{DEG}}, \qquad (2.19)$$

with only diffusions contributing for $B > B_\phi \approx B^*$.

In this section we assumed Gaussian white noise correlations to calculate the Green's functions. Since we know that this approximation fails for the semiclassical contribution arising from Coulomb disorder, why can we use it successfully for the quantum transport? It turns out that the quasiuniversal nature of weak localization and conductance fluctuations means that the exact nature of the disorder potential will not change the result. Several numerical calculations using long-range Coulomb potential have checked this assumption (Yan and Ting, 2008). Many of the symmetry arguments discussed here apply to confined geometries such as quantum dots (Wurm *et al.*, 2009). Finally, the diagrammatic perturbation theory discussed here applies only away from the Dirac point. As discussed in Sec. II.C.1, numerically calculated weak (anti)localization corrections remain as expected even at the Dirac point. However, Rycerz *et al.* (2007a) found enhanced conductance fluctuations at the Dirac point, a possible consequence of being in the ballistic to diffusive crossover regime.

As for the experimental situation, in addition to the observation of suppressed localization (Morozov *et al.*, 2006) and antilocalization (Wu *et al.*, 2007), Horsell *et al.* (2009) made a systematic study of several samples fitting the data to Eq. (2.18) to extract τ_ϕ, τ_i, and τ_z. Their data showed a mixture of localization, antilocalization, and saturation behavior. An interesting feature is that the intervalley scattering length $L_i = (D\tau_i)^{1/2}$ is strongly correlated to the sample width (i.e., $L_i \approx W/2$) implying that the edges are the dominant source of intervalley scattering. This feature has been corroborated by Raman studies that show a strong D peak at the edges, but not in the bulk (Graf *et al.*, 2007; Chen, Cullen *et al.*, 2009). The most important finding of Horsell *et al.* (2009) is that the contribution from short-range scattering (τ_z) is much larger than one would expect (indeed, comparable to τ_0). They showed that any predicted microscopic mechanisms such as ripples or trigonal warping that might contribute to τ_z (but not τ_i) were all negligible and could not explain such a large τ_z^{-1}. It remains an open question why $\tau_z^{-1} \gg \tau_i^{-1}$ in the experiments.

4. Ultraviolet logarithmic corrections

The semiclassical Boltzmann transport theory treats the impurities within the first Born approximation. In a diagram-

matic perturbation theory, this is the leading order term in an expansion of $n_i \to 0$. Typically for other conventional metals and semiconductors, one makes a better approximation by trying to include more diagrams that capture multiple scattering off the same impurity. For example, in the self-consistent Born approximation (SCBA) one replaces the bare Green's functions with dressed ones to obtain a self-consistent equation for the self-energy (Bruus and Flensberg, 2004).

In practice, for graphene, one often finds that attempts to go beyond the semiclassical Boltzmann transport theory described in Sec. III.A fare far worse than the simple theory. The theoretical underpinnings for the failure of SCBA was pointed out by Aleiner and Efetov (2006), who argued that the SCBA (a standard technique for weakly disordered metals and superconductors) is not justified for the Dirac Hamiltonian. They demonstrated this by calculating terms to fourth order in perturbation theory, showing that SCBA neglects most terms of equal order. This could have severe consequences. For example, considering only diagonal disorder, the SCBA breaks time reversal symmetry. To further illustrate their point, Aleiner and Efetov (2006) argued that for the full disorder Hamiltonian [Eq. (2.13)], considering three impurity scattering, there are 54 terms to that order, and only 6 are captured by the SCBA.

These terms provide a new divergence in the diagrammatic perturbation series, which is distinct from the weak localization discussed in Sec. II.C.3. Unlike weak localization that for 2D systems diverges as the size ($\delta\sigma \sim \ln[L/\ell]$), this additional divergence occurs at all length scales, and was called "ultraviolet logarithmic corrections." The consequences of this divergence include the logarithmic renormalization of the bare disorder parameters which was studied by Foster and Aleiner (2008) using the renormalization group. For the experimentally relevant case of strong diagonal disorder, the renormalization does not change the physics. However, when all disorder couplings (i.e., intervalley and intravalley) are comparable, e.g., relevant for graphene after ion irradiation, the system could flow to various strong coupling fixed points depending on the symmetry of the disorder potential.

In addition to these considerations, interaction effects could also affect quantum transport (e.g., the Altshuler-Aronov phenomena), particularly in the presence of disorder. Although such interaction effects are probably relatively small in monolayer graphene, they may not be negligible. Interaction effects may certainly be important in determining graphene transport properties near the charge neutral Dirac point (Fritz *et al.*, 2008; Kashuba, 2008; Müller *et al.*, 2008; Bistritzer and MacDonald, 2009).

III. TRANSPORT AT HIGH CARRIER DENSITY

A. Boltzmann transport theory

In this section we review graphene transport for large carrier densities ($n \gg n_i$, n_i is the impurity density), where the system is homogeneous. We discuss in detail the microscopic transport properties at high carrier density using the semiclassical Boltzmann transport theory.

It was predicted that the graphene conductivity limited by short-ranged scatterers (i.e., δ-range disorder) is independent

of the carrier density, because of the linear-in-energy density of states (Shon and Ando, 1998). However, the experiments (Fig. 11) showed that the conductivity increases linearly in the carrier density concentration. To explain this linear-in-density dependence of experimental conductivity, the long-range Coulomb disorder was introduced (Ando, 2006; Cheianov and Fal'ko, 2006a; Nomura and MacDonald, 2006; Hwang *et al.*, 2007a; Nomura and MacDonald, 2007; Trushin and Schliemann, 2008; Katsnelson *et al.*, 2009). The long-range Coulomb disorder also successfully explains several recent transport experiments. Tan, Zhang, Bolotin *et al.* (2007) found the correlation of the sample mobility with the shift of the Dirac point and minimum conductivity plateau width, showing qualitative and semi-quantitative agreement with the calculations with long-range Coulomb disorder [Fig. 11(b)]. Chen, Jang, Adam *et al.* (2008) investigated the effect of Coulomb scatterers on gra-

phene conductivity by intentionally adding potassium ions to graphene in ultrahigh vacuum, qualitatively observing the prediction of the transport theory limited by Coulomb disorder [Fig. 11(c)]. Jang *et al.* (2008) tuned graphene's fine-structure constant by depositing ice on the top of graphene and observed enhanced mobility, which is predicted in the Boltzmann theory with Coulomb disorder [Fig. 11(d) and Chen, Xia, and Tao (2009), Chen, Xia *et al.* (2009), , and Kim, Nah *et al.* (2009)]. The role of remote impurity scattering was further confirmed in the observation of drastic improvement of mobility by reducing carrier scattering in suspended graphene through current annealing (Bolotin, Sikes, Hone *et al.*, 2008; Du *et al.*, 2008). Recent measurement of the ratio of transport scattering time to the quantum scattering time by Hong, Zou, and Zhu (2009) also strongly supports the long-range Coulomb disorder as the main scattering mechanism in graphene (Fig. 12).
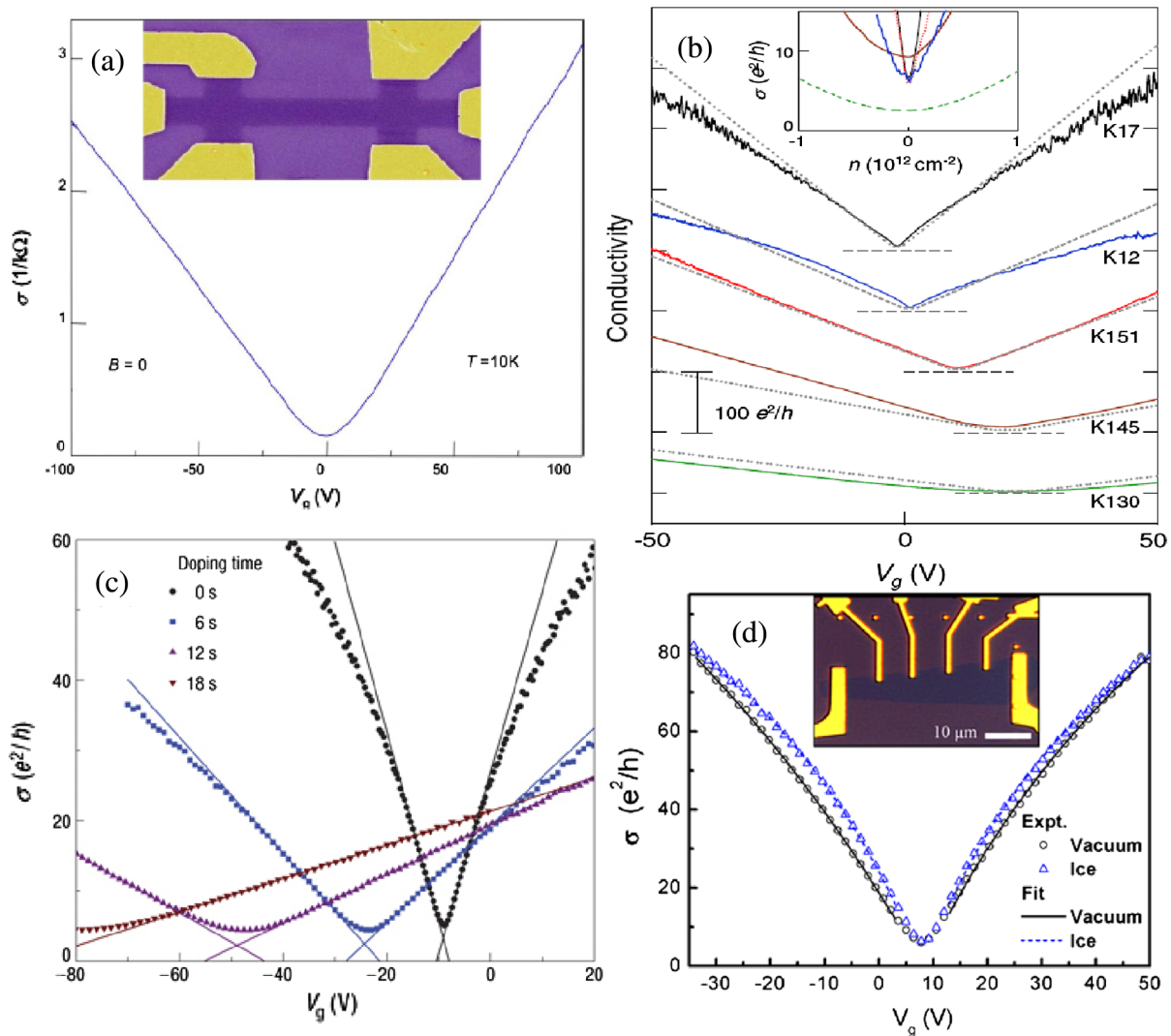

FIG. 11 (color online). (a) The measured conductivity σ of graphene as a function of gate voltage V_g (or carrier density). The conductivity increases linearly with the density. Adapted from Castro Neto *et al.*, 2009. (b) σ as a function of V_g for five different samples For clarity, curves are vertically displaced. The inset shows the detailed view of the density-dependent conductivity near the Dirac point for the data in the main panel. Adapted from Tan, Zhang, Bolotin *et al.*, 2007. (c) σ vs V_g for the pristine sample and three different doping concentrations. Adapted from Chen, Jang, Adam *et al.*, 2008. (d) σ as a function V_g for pristine graphene (circles) and after deposition of 6 monolayers of ice (triangles). Inset: Optical microscope image of the device. Adapted from Jang *et al.*, 2008.
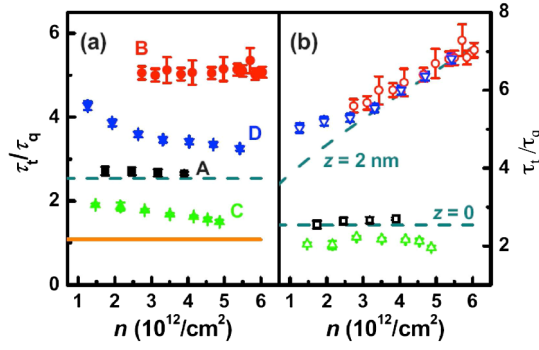
FIG. 12 (color online). The ratio of transport scattering time (τ_t) to quantum scattering time (τ_q) as a function of density for different samples. Dashed (solid) lines indicate the theoretical calculations (Hwang and Das Sarma, 2008e) with Coulomb disorder (δ-range disorder). Adapted from Hong, Zou, and Zhu, 2009.

The conductivity σ (or mobility $\mu = \sigma/ne$) is calculated in the presence of randomly distributed Coulomb impurity charges with the electron-impurity interaction being screened by the 2D electron gas in the random phase approximation (RPA). Even though the screened Coulomb scattering is the most important scattering mechanism, there are additional scattering mechanisms (e.g., neutral point defects) unrelated to the charged impurity scattering. The Boltzmann formalism can treat both effects, where zero-range scatterers are treated with an effective point defect density of n_d. Phonon scattering effects, important at higher temperatures, are treated in the next section. We also discuss other scattering mechanisms which could contribute to graphene transport.

We start by assuming the system to be a homogeneous 2D carrier system of electrons (or holes) with a carrier density n induced by the external gate voltage V_g. When the external electric field is weak and the displacement of the distribution function from thermal equilibrium is small, we may write the distribution function to the lowest order in the applied electric field (**E**) $f_{\mathbf{k}} = f(\epsilon_{\mathbf{k}}) + \delta f_{\mathbf{k}}$, where $\epsilon_{\mathbf{k}}$ is the carrier energy, $f(\epsilon_{\mathbf{k}})$ is the equilibrium Fermi distribution function, and $\delta f_{\mathbf{k}}$ is proportional to the field. When the relaxation time approximation is valid, we have $\delta f_{\mathbf{k}} = -[\tau(\epsilon_{\mathbf{k}})/\hbar]e\mathbf{E} \cdot \mathbf{v}_{\mathbf{k}}[\partial f(\epsilon_{\mathbf{k}})/\partial \epsilon_{\mathbf{k}}]$, where $\mathbf{v}_{\mathbf{k}} = d\epsilon_{\mathbf{k}}/d\mathbf{k}$ is the velocity of carrier and $\tau(\epsilon_{\mathbf{k}})$ is the relaxation time or the transport scattering time, and is given by

$$\frac{1}{\tau(\epsilon_{\mathbf{k}})} = \frac{2\pi}{\hbar} \sum_a \int dz n_i^{(a)}(z) \int \frac{d^2k'}{(2\pi)^2} |\langle V_{\mathbf{k},\mathbf{k}'}(z)\rangle|^2$$
$$\times [1 - \cos\theta_{\mathbf{k}\mathbf{k}'}]\delta(\epsilon_{\mathbf{k}} - \epsilon_{\mathbf{k}'}), \quad (3.1)$$

where $\theta_{\mathbf{k}\mathbf{k}'}$ is the scattering angle between the scattering in and out wave vectors **k** and **k**', $n_i^{(a)}(z)$ is the concentration of the ath kind of impurity, and z represents the coordinate of normal direction to the 2D plane. In Eq. (3.1) $\langle V_{\mathbf{k},\mathbf{k}'}(z)\rangle$ is the matrix element of the scattering potential associated with impurity disorder in the system environment. Within Boltzmann transport theory by averaging over energy, we obtain the conductivity

$$\sigma = \frac{e^2}{2} \int d\epsilon D(\epsilon) \mathbf{v}_{\mathbf{k}}^2 \tau(\epsilon)\left(-\frac{\partial f}{\partial \epsilon}\right), \quad (3.2)$$

and the corresponding temperature-dependent resistivity is given by $\rho(T) = 1/\sigma(T)$. Note that $f(\epsilon_k) = \{1 + \exp[(\epsilon_k - \mu)]/k_B T\}^{-1}$, where the finite temperature chemical potential $\mu(T)$ is determined self-consistently to conserve the total number of electrons. At $T = 0$, $f(\epsilon)$ is a step function at the Fermi energy $E_F \equiv \mu(T = 0)$, and we then recover the usual conductivity formula

$$\sigma = \frac{e^2 v_F^2}{2} D(E_F)\tau(E_F), \quad (3.3)$$

where v_F is the carrier velocity at the Fermi energy.

B. Impurity scattering

The matrix element of the scattering potential is determined by the configuration of the 2D systems and the spatial distribution of the impurities. In general, impurities are located in the environment of the 2D systems. For simplicity, we consider the impurities are distributed completely at random in the plane parallel to the 2D systems located at $z = d$. The location d is a single parameter modeling the impurity configuration. Then the matrix element of the scattering potential of randomly distributed screened impurity charge centers is given by

$$\int dz n_i^{(a)}(z)|\langle V_{\mathbf{k},\mathbf{k}'}(z)\rangle|^2 = n_i \left|\frac{v_i(q)}{\varepsilon(q)}\right|^2 F(q), \quad (3.4)$$

where $q = |\mathbf{k} - \mathbf{k}'|$, $\theta \equiv \theta_{\mathbf{k}\mathbf{k}'}$, n_i is the number of impurities per unit area, $F(q)$ is the form factor associated with the carrier wave function of the 2D system, and $v_i(q) = 2\pi e^2/(\kappa q)e^{-qd}$ is the Fourier transform of the 2D Coulomb potential in an effective background lattice dielectric constant κ. The form factor $F(q)$ in Eq. (3.4) comes from the overlap of the wave function. In 2D semiconductor systems it is related to the quasi-2D nature of systems, i.e., finite width of the 2D systems. The real functional form depends on the details of the quantum structures (i.e., heterostructures, square well, etc.). $F(q)$ becomes unity in the two-dimensional limit (i.e., δ layer). However, in graphene the form factor is related to the chirality, not to the quantum structure since graphene is strictly a 2D layer. In Eq. (3.4), $\varepsilon(q) \equiv \varepsilon(q, T)$ is the 2D finite temperature static RPA dielectric (screening) function and is given by

$$\varepsilon(q, T) = 1 + v_c(q)\Pi(q, T), \quad (3.5)$$

where $\Pi(q, T)$ is the irreducible finite temperature polarizability function and $v_c(q)$ is the Coulomb interaction. For short-ranged disorder, we have

$$\int dz n_i^{(a)}(z)|\langle V_{\mathbf{k},\mathbf{k}'}(z)\rangle|^2 = n_d V_0^2 F(q), \quad (3.6)$$

where n_d is the 2D impurity density and V_0 is a constant short-range (i.e., a δ function in real space) potential strength.

One can also consider the effect on carrier transport by scattering from cluster of correlated charged impurities (Katsnelson *et al.*, 2009), as originally done for 2D

semiconductors by Kawamura and Das Sarma (Kawamura and Das Sarma, 1996; Das Sarma and Kodiyalam, 1998). Without detailed knowledge of the clustering correlations, however, this is little more than arbitrary data fitting.

Because the screening effect is known to be of vital importance for charged impurities (Ando, 2006; Hwang *et al.*, 2007a), we first provide the static polarizability function. It is known that the screening has to be considered to explain the density and temperature dependence of the conductivity of 2D semiconductor systems (Das Sarma and Hwang, 1999, 2005), and the screening property in graphene exhibits significantly different behavior (Hwang and Das Sarma, 2007) from that in conventional 2D metals. Also, significant temperature dependence of the scattering time τ may arise from the screening function in Eq. (3.5). Thus, before we discuss the details of conductivity, we first review screening in graphene and in 2D semiconductor systems.

1. Screening and polarizability

a. Graphene

The polarizability is given by the bare bubble diagram (Ando, 2006; Wunsch *et al.*, 2006; Hwang and Das Sarma, 2007)

$$\Pi(q, T) = -\frac{g}{A}\sum_{\mathbf{k}ss'}\frac{f_{s\mathbf{k}} - f_{s'\mathbf{k}'}}{\varepsilon_{s\mathbf{k}} - \varepsilon_{s'\mathbf{k}'}}F_{ss'}(\mathbf{k}, \mathbf{k}'), \tag{3.7}$$

where $s = \pm 1$ indicate the conduction ($+1$) and valence (-1) bands, respectively, $\mathbf{k}' = \mathbf{k} + \mathbf{q}$, $\varepsilon_{s\mathbf{k}} = s\hbar v_F|\mathbf{k}|$, $F_{ss'}(\mathbf{k}, \mathbf{k}') = (1 + \cos\theta)/2$, and $f_{s\mathbf{k}} = [\exp\{\beta(\varepsilon_{s\mathbf{k}} - \mu)\} + 1]^{-1}$ with $\beta = 1/k_BT$.

After performing the summation over ss', it is useful to rewrite the polarizability as the sum of intraband and interband polarizability $\Pi(q, T) = \Pi^+(q, T) + \Pi^-(q, T)$. At $T = 0$, the intraband (Π^+) and interband (Π^-) polarizability becomes (Ando, 2006; Hwang and Das Sarma, 2007)

$$\tilde{\Pi}^+(q) = \begin{cases} 1 - \frac{\pi q}{8k_F}, & q \leq 2k_F \\ 1 - \frac{1}{2}\sqrt{1 - \frac{4k_F^2}{q^2}} - \frac{q}{4k_F}\sin^{-1}\frac{2k_F}{q}, & q > 2k_F \end{cases}, \tag{3.8a}$$

$$\tilde{\Pi}^-(q) = \frac{\pi q}{8k_F}, \tag{3.8b}$$

where $\tilde{\Pi}^\pm = \Pi^\pm/D_0$, and $D_0 \equiv gE_F/2\pi\hbar^2 v_F^2$ is the density of states (DOS) at the Fermi level. Intraband Π^+ (interband Π^-) polarizability decreases (increases) linearly as q increases, and these two effects exactly cancel out up to $q = 2k_F$, which gives rise to the total static polarizability being constant for $q < 2k_F$ as in the 2DEG (Stern, 1967), i.e., $\Pi(q) = \Pi^+(q) + \Pi^-(q) = D(E_F)$ for $q \leq 2k_F$. In Fig. 13 we show the calculated graphene static polarizability as a function of wave vector. In the large momentum transfer regime, $q > 2k_F$, the static screening increases linearly with q due to the interband transition. In a normal 2D system
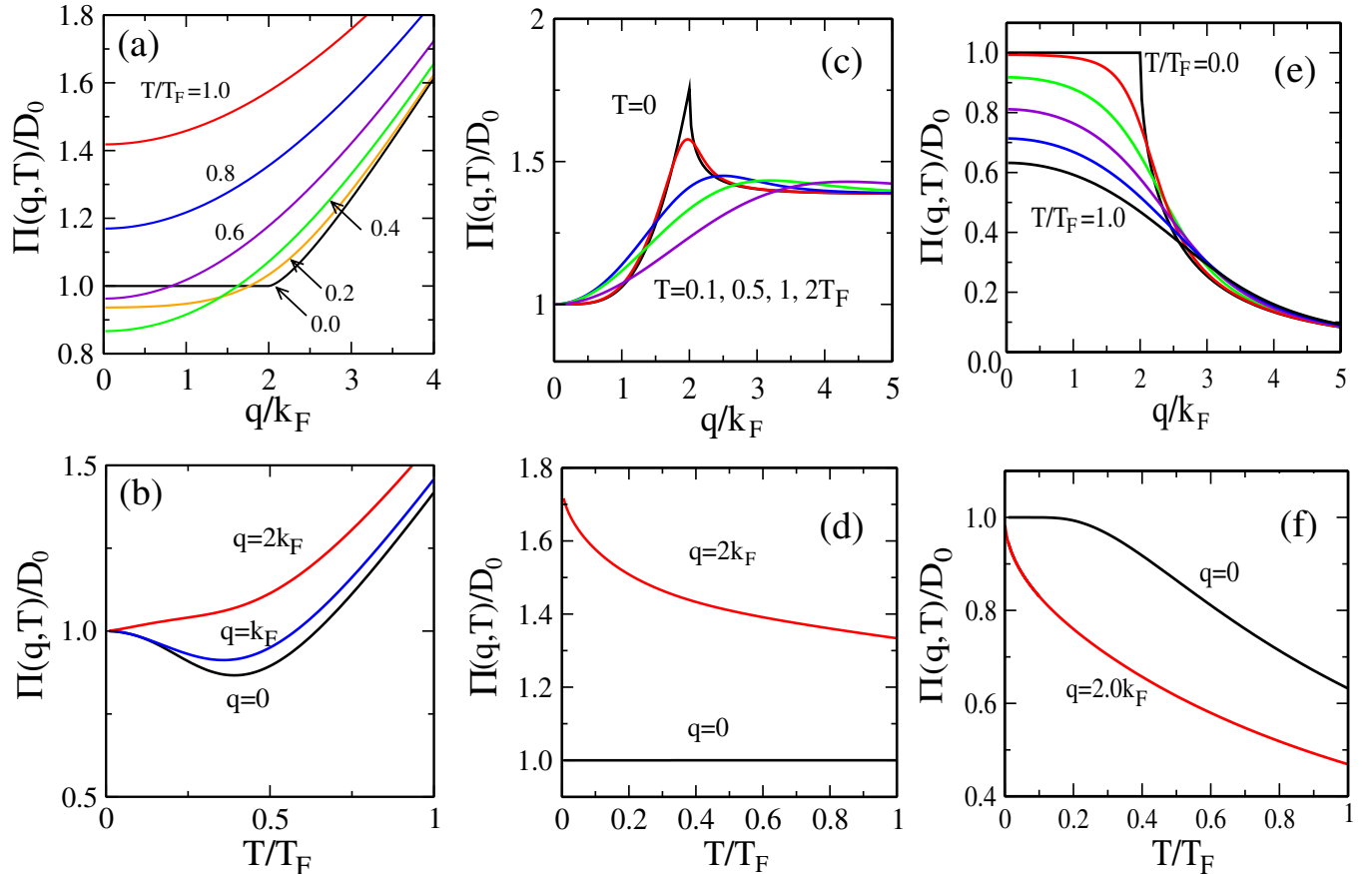

FIG. 13 (color online). Polarizability $\Pi(q, T)$ in units of the density of states at the Fermi level D_0. $\Pi(q, T)$ of monolayer graphene (a) as a function of wave vector for different temperatures and (b) as a function of temperature for different wave vectors. (c), (d) BLG polarizability. (e), (f) The 2DEG polarizability.

the static polarizability falls off rapidly for $q > 2k_F$ with a cusp at $q = 2k_F$ (Stern, 1967). The linear increase of the static polarizability with q gives rise to an enhancement of the effective dielectric constant $\kappa^*(q \to \infty) = \kappa(1 + g_s g_v \pi r_s/8)$ in graphene. Note that in a normal 2D system $\kappa^* \to \kappa$ as $q \to \infty$. Thus, the effective interaction in 2D graphene decreases at short wavelengths due to interband polarization effects. This large wave vector screening behavior is typical of an insulator. Thus, 2D graphene screening is a combination of "metallic" screening (due to Π^+) and "insulating" screening (due to Π^-), leading overall to rather strange screening property, all of which can be traced back to the zero-gap chiral relativistic nature of graphene.

It is interesting to note that the nonanalytic behavior of graphene polarizability at $q = 2k_F$ occurs in the second derivative, $d^2\Pi(q)/dq^2 \propto 1/\sqrt{q^2 - 4k_F^2}$, i.e., the total polarizability, as well as its first derivative, are continuous at $q = 2k_F$. This leads to an oscillatory decay of the screened potential in the real space (Friedel oscillation) which scales as $\phi(r) \sim \cos(2k_F r)/r^3$ (Cheianov and Fal'ko, 2006a; Wunsch *et al.*, 2006). This is in contrast to the behavior of a 2DEG, where Friedel oscillations scale as $\phi(r) \sim \cos(2k_F r)/r^2$. The polarizability also determines the Ruderman-Kittel-Kasuya-Yosida (RKKY) interaction between two magnetic impurities as well as the induced spin density due to a magnetic impurity, while both quantities are proportional to the Fourier transform of $\Pi(q)$. Similar to the screened potential, the induced spin density decreases as r^{-3} for large distances. Again, this contrasts with the r^{-2} behavior found in a 2DEG. For the particular case of intrinsic graphene, the Fourier transform of interband polarizability $[\Pi^-(q)]$ diverges [even though $\Pi(r)$ formally scales as r^{-3}, its magnitude does not converge], which means that intrinsic graphene is susceptible to ferromagnetic ordering in the presence of magnetic impurities due to the divergent RKKY coupling (Brey *et al.*, 2007).

Since the explicit temperature dependence of screening gives rise to significant temperature dependence of the conductivity, we consider the properties of the polarizability at finite temperatures. The asymptotic form of polarizability is given by

$$\tilde{\Pi}(q, T \gg T_F) \approx \frac{T}{T_F} \ln 4 + \frac{q^2}{24k_F^2} \frac{T_F}{T}, \tag{3.9a}$$

$$\tilde{\Pi}(q, T \ll T_F) \approx \frac{\mu(T)}{E_F} = 1 - \frac{\pi^2}{6}\left(\frac{T}{T_F}\right)^2, \tag{3.9b}$$

where $T_F = E_F/k_B$ is the Fermi temperature. In addition, the finite temperature Thomas-Fermi wave vector in the $q \to 0$ long-wavelength limit is given by (Ando, 2006; Hwang and Das Sarma, 2009b)

$$q_s(T \gg T_F) \approx 8\ln(2)r_s k_F\left(\frac{T}{T_F}\right), \tag{3.10a}$$

$$q_s(T \ll T_F) \approx 4r_s k_F\left[1 - \frac{\pi^2}{6}\left(\frac{T}{T_F}\right)^2\right]. \tag{3.10b}$$

The screening wave vector increases linearly with temperature at high temperatures ($T \gg T_F$) but becomes a constant with a small quadratic correction at low temperatures

($T \ll T_F$). In Fig. 13 we show the finite temperature polarizability $\Pi(q, T)$.

b. Bilayer graphene

For bilayer graphene, we have the polarizability of Eq. (3.7) with $\varepsilon_{s\mathbf{k}} = s\mathbf{k}^2/2m$ and $F_{ss'}(\mathbf{k}, \mathbf{k}') = (1 + ss'\cos 2\theta)/2$ due to the chirality of bilayer graphene. At $T = 0$, the polarizability of bilayer graphene (Hwang and Das Sarma, 2008d) is given by

$$\Pi(q) = D_0[f(q) - g(q)\theta(q - 2k_F)], \tag{3.11}$$

where $D_0 = g_s g_v m/2\pi\hbar^2$ is the BLG density of states at the Fermi level and

$$f(q) = \left(1 + \frac{\tilde{q}^2}{2}\right)\sqrt{1 - \frac{4}{\tilde{q}^2}} + \log\frac{\tilde{q} - \sqrt{\tilde{q}^2 - 4}}{\tilde{q} + \sqrt{\tilde{q}^2 - 4^2}}, \tag{3.12a}$$

$$g(q) = \frac{1}{2}\sqrt{4 + \tilde{q}^4} - \log\left[\frac{1 + \sqrt{1 + \tilde{q}^4/4}}{2}\right], \tag{3.12b}$$

where $\tilde{q} = q/k_F$.

In Fig. 13 the wave vector dependent BLG polarizability is shown. For MLG, intraband and interband effects in polarizability exactly cancel out up to $q = 2k_F$, which gives rise to the total static polarizability being constant for $q < 2k_F$. However, for BLG the cancellation of two polarizability functions is not exact because of the enhanced backscattering, so the total polarizability increases as q approaches $2k_F$, which means screening increases as q increases. Thus BLG, in spite of having the same parabolic carrier energy dispersion of 2DEG systems, does not have a constant Thomas-Fermi screening up to $q = 2k_F$ (Hwang and Das Sarma, 2008d; Borghi *et al.*, 2009), which exists in MLG and 2DEG. In the large momentum transfer regime, $q > 2k_F$, the BLG polarizability approaches a constant value, i.e., $\Pi(q) \to N_0 \log 4$, because the interband transition dominates over the intraband contribution in the large wave vector limit. For $q > 2k_F$, the static polarizability falls off rapidly ($\sim 1/q^2$) for 2DEG (Stern, 1967) and for MLG it increases linearly with q (see Sec. III.B.1).

The long-wavelength ($q \to 0$) Thomas-Fermi screening can be expressed as $q_{\text{TF}} = g_s g_v me^2/\kappa\hbar^2$, which is the same form as a regular 2D system and independent of electron concentration. The screening at $q = 2k_F$ is given by $q_s(2k_F) = q_{\text{TF}}[\sqrt{5} - \log\{(1 + \sqrt{5})/2\}]$. Screening at $q = 2k_F$ is about 75% larger than normal 2D Thomas-Fermi (TF) screening, which indicates that in bilayer graphene the scattering by the screened Coulomb potential is much reduced due to the enhanced screening.

A qualitative difference between MLG and BLG polarizability functions is at $q = 2k_F$. Because of the suppression of $2k_F$ backward scattering in MLG, the total polarizability as well as its first derivative are continuous. In BLG, however, large-angle scattering is enhanced due to chirality [i.e., the overlap factor $F_{ss'}$ in Eq. (3.7)], which gives rise to the singular behavior of polarizability at $q = 2k_F$. Even though the BLG polarizability is continuous at $q = 2k_F$, it has a sharp cusp and its derivative is discontinuous at $2k_F$. As $q \to 2k_F$, $d\Pi(q)/dq \propto 1/\sqrt{q^2 - 4k_F^2}$. This behavior is exactly the same as that of the regular 2DEG, which also has a cusp at

$q = 2k_F$. The strong cusp in BLG $\Pi(q)$ at $q = 2k_F$ leads to Friedel oscillations in contrast to the MLG behavior. The leading oscillation term in the screened potential at large distances can be calculated as

$$\phi(r) \sim -\frac{e}{\kappa} \frac{4q_{\text{TF}}k_F^2}{(2k_F + Cq_{\text{TF}})^2} \frac{\sin(2k_F r)}{(2k_F r)^2}, \tag{3.13}$$

where $C = \sqrt{5} - \log[(1 + \sqrt{5})/2]$, which is similar to the 2DEG except for the additional constant C ($C = 1$ for 2DEG), but different from MLG where Friedel oscillations scale as $\phi(r) \sim \cos(2k_F r)/r^3$ (Cheianov and Fal'ko, 2006a; Wunsch *et al.*, 2006).

The enhanced singular behavior of the BLG screening function at $q = 2k_F$ has other interesting consequences related to Kohn anomaly (Kohn, 1959) and RKKY interaction. For intrinsic BLG, the Fourier transform of $\Pi(q)$ simply becomes a δ function, which indicates that the localized magnetic moments are not correlated by the long-range interaction and there is no net magnetic moment. For extrinsic BLG, the oscillatory term in RKKY interaction is restored due to the singularity of polarizability at $q = 2k_F$, and the oscillating behavior dominates at large $k_F r$. At large distances $2k_F r \gg 1$, the dominant oscillating term in $\Pi(r)$ is given by $\Pi(r) \propto \sin(2k_F r)/(k_F r)^2$. This is the same RKKY interaction as in a regular 2DEG.

In Fig. 13 the wave vector dependent BLG polarizability is shown for different temperatures. Note that at $q = 0$, $\Pi(0, T) = N_F$ for all temperatures. For small q, $\Pi(q, T)$ increases as q^4. The asymptotic form of polarizability becomes

$$\tilde{\Pi}(q, T \gg T_F) \approx 1 + \frac{q^2}{6k_F^2} \frac{T_F}{T}, \tag{3.14a}$$

$$\tilde{\Pi}(q, T \ll T_F) \approx 1 + \frac{1}{16} \frac{q^4}{k_F^4} + \frac{\pi^2}{16} \left(\frac{T}{T_F}\right)^2 \frac{q^4}{k_F^4}. \tag{3.14b}$$

More interestingly, the polarizability at $q = 0$ is temperature independent, i.e., the finite temperature Thomas-Fermi wave vector is constant for all temperatures,

$$q_s(T) = q_{\text{TF}}. \tag{3.15}$$

In BLG polarizability at $q = 0$ two temperature effects from the intraband and the interband transition exactly cancel out, which gives rise to the total static polarizability at $q = 0$ being constant for all temperatures.

c. 2D semiconductor systems

The polarizability of ordinary 2D system was first calculated by Stern, and all details can be found in the literature (Stern, 1967; Ando *et al.*, 1982). Here we provide the 2D polarizability for comparison with graphene. The 2D polarizability can be calculated with $\epsilon_{sk} = \hbar^2 \mathbf{k}^2/2m$ and $F_{ss'} = \delta_{ss'}/2$ because of the nonchiral property of the ordinary 2D systems. $\Pi(q)$ at $T = 0$ becomes (Stern, 1967)

$$\Pi(q) = D_0[1 - \sqrt{1 - (2k_F/q)^2} \theta(q - 2k_F)], \tag{3.16}$$

where $D_0 = g_s g_v m/2\pi\hbar^2$ is the 2D density of states at the Fermi level. Since the polarizability is a constant for $q < 2k_F$,

both the long wavelength TF screening and $2k_F$ screening are same, which is given by $q_s = q_{\text{TF}} = g_s g_v m e^2/\kappa\hbar^2$.

The asymptotic form for the regular 2D polarizability are given by

$$\tilde{\Pi}(q = 0, T \ll T_F) \approx 1 - e^{-T_F/T}, \tag{3.17a}$$

$$\tilde{\Pi}(q, T \gg T_F) \approx \frac{T_F}{T}\left[1 - \frac{q^2}{6k_F^2} \frac{T_F}{T}\right]. \tag{3.17b}$$

For $q = 0$, in the $T \gg T_F$ limit, we get the usual Debye screening for the regular 2D electron gas system

$$q_s(T \gg T_F) \approx q_{\text{TF}} \frac{T_F}{T}. \tag{3.18}$$

A comparison of Eq. (3.18) with Eqs. (3.10) and (3.15) shows that the high-temperature Debye screening behaviors are different in all three systems just as the low-temperature screening behaviors, i.e., the high-temperature screening wave vector q_s in semiconductor 2D systems decreases linearly with temperature while q_s in MLG increases linearly with temperature and q_s in BLG is independent of temperature.

In Fig. 13 we show the corresponding parabolic 2D polarizability normalized by the density of states at Fermi level, $D_0 = gm/\hbar^2 2\pi$. Note that the temperature dependence of 2D polarizability at $q = 2k_F$ is much stronger than that of graphene polarizability. Since in normal 2D systems the $2k_F$ scattering event is most important for the electrical resistivity, the temperature dependence of polarizability at $q = 2k_F$ completely dominates at low temperatures ($T \ll T_F$). It is known that the strong temperature dependence of the polarizability function at $q = 2k_F$ leads to the anomalously strong temperature-dependent resistivity in ordinary 2D systems (Stern, 1980; Das Sarma and Hwang, 1999).

In the next section the temperature-dependent conductivities are provided due to the scattering by screened Coulomb impurities using the temperature-dependent screening properties of this section.

2. Conductivity

a. Single layer graphene

The eigenstates of single layer graphene are given by the plane wave $\psi_{sk}(\mathbf{r}) = (1/\sqrt{A}) \exp(i\mathbf{k} \cdot \mathbf{r}) F_{sk}$, where A is the area of the system, $s = \pm 1$ indicate the conduction ($+ 1$) and valence ($- 1$) bands, respectively, and $F_{sk}^{\dagger} = (1/\sqrt{2})(e^{i\theta_{\mathbf{k}}}, s)$ with $\theta_{\mathbf{k}} = \tan(k_y/k_x)$ the polar angle of the momentum $\mathbf{k}$. The corresponding energy of graphene for 2D wave vector $\mathbf{k}$ is given by $\epsilon_{sk} = s\hbar v_F |\mathbf{k}|$, and the DOS is given by $D(\epsilon) = g|\epsilon|/(2\pi\hbar^2 v_F^2)$, where $g = g_s g_v$ is the total degeneracy ($g_s = 2$, $g_v = 2$ being the spin and valley degeneracies, respectively). The corresponding form factor $F(q)$ in the matrix elements of Eqs. (3.4) and (3.6) arising from the sublattice symmetry (overlap of wave function) (Ando, 2006; Auslender and Katsnelson, 2007) becomes $F(q) = (1 + \cos\theta)/2$, where $q = |\mathbf{k} - \mathbf{k}'|$, $\theta \equiv \theta_{\mathbf{k}\mathbf{k}'}$. The matrix element of the scattering potential of randomly distributed screened impurity charge centers in graphene is given by

$$|\langle V_{s\mathbf{k}, s\mathbf{k}'}\rangle|^2 = \left|\frac{v_i(q)}{\epsilon(q)}\right|^2 \frac{1 + \cos\theta}{2}, \tag{3.19}$$

and the matrix element of the short-ranged disorder is

$$|\langle V_{s\mathbf{k},s\mathbf{k}'}\rangle|^2 = V_0^2(1 + \cos\theta)/2, \tag{3.20}$$

where V_0 is the strength of the short-ranged disorder potential measured in eV m^2. The factor $1 - \cos\theta$ in Eq. (3.1) weights the amount of backward scattering of the electron by the impurity. In normal parabolic 2D systems (Ando *et al.*, 1982) the factor $1 - \cos\theta$ favors large-angle scattering events. However, in graphene the large-angle scattering is suppressed due to the wave function overlap factor $1 + \cos\theta$, which arises from the sublattice symmetry peculiar to graphene. The energy dependent scattering time in graphene thus gets weighted by an angular contribution factor of $(1 - \cos\theta) \times (1 + \cos\theta)$, which suppresses both small-angle and large-angle scattering contributions in the scattering rate.

Assuming random distribution of charged centers with density n_i, the scattering time τ at $T = 0$ is given by (Adam *et al.*, 2007; Hwang and Das Sarma, 2008e)

$$\frac{1}{\tau} = \frac{r_s^2}{\tau_0}\left\{\frac{\pi}{2} - 4\frac{d}{dr_s}[r_s^2 g(2r_s)]\right\}, \tag{3.21}$$

where $\tau_0^{-1} = 2\sqrt{\pi}n_i v_F/\sqrt{n}$, and $g(x) = -1 + \frac{\pi}{2}x + (1 - x^2)f(x)$ with

$$f(x) = \begin{cases} \frac{1}{\sqrt{1-x^2}}\cosh^{-1}\frac{1}{x} & \text{for } x < 1 \\ \frac{1}{\sqrt{x^2-1}}\cos^{-1}\frac{1}{x} & \text{for } x > 1 \end{cases}. \tag{3.22}$$

Since r_s is independent of the carrier density, the scattering time is simply given by $\tau \propto \sqrt{n}$. With Eq. (3.3), we find the density dependence of graphene conductivity $\sigma(n) \propto n$ because $D(E_F) \propto \sqrt{n}$. For graphene on SiO$_2$ substrate, the
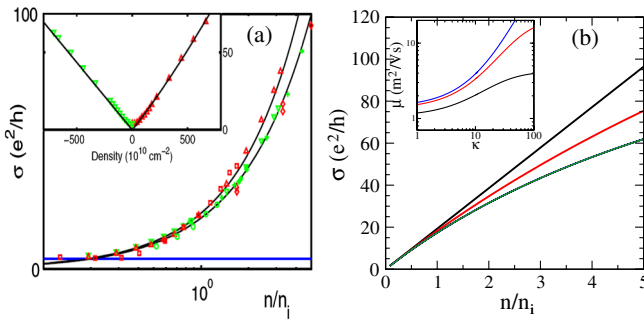

FIG. 14 (color online). (a) Calculated graphene conductivity as a function of carrier density (n_i is an impurity density) limited by Coulomb scattering with experimental data. Solid lines (from bottom to top) show the minimum conductivity of $4e^2/h$, theory for $d = 0$ and 0.2 nm. The inset shows the results in a linear scale assuming that the impurity shifts by $d = 0.2$ nm for positive voltage bias. Adapted from Hwang *et al.*, 2007a. (b) Graphene conductivity calculated using a combination of short- and long-range disorder. In the calculation, $n_d/n_i = 0$, 0.01, and 0.02 (top to bottom) are used. In inset the graphene mobility as a function of dielectric constant (κ) of substrate is shown for different carrier densities $n = 0.1$, 1, and 5×10^{12} cm^{-2} (from top to bottom) in the presence of both long-ranged charged impurity ($n_i = 2 \times 10^{11}$ cm^{-2}) and short-ranged neutral impurity ($n_d = 0.4 \times 10^{10}$ cm^{-2}). $V_0 = 10$ eV nm^2 is used in the calculation.

interaction parameter $r_s \approx 0.8$, then the conductivity is given by $\sigma(n) \approx (20e^2/h)n/n_i$ (Adam *et al.*, 2007). On the other hand, the corresponding energy dependent scattering time of short-ranged disorder is

$$\frac{1}{\tau} = \frac{n_d V_0^2}{\hbar}\frac{E_F}{4(\hbar v_F)^2}. \tag{3.23}$$

Thus, the density dependence of scattering time due to the short-range disorder scattering is given by $\tau(n) \propto n^{-1/2}$. With Eq. (3.3), we find the conductivity to be independent of density for short-range scattering, i.e., $\sigma(n) \propto n^0$, in contrast to charged impurity scattering which produces a conductivity linear in n.

In Fig. 14(a) the calculated graphene conductivity limited by screened charged impurities is shown along with the experimental data (Tan, Zhang, Bolotin *et al.*, 2007; Chen, Jang, Adam *et al.*, 2008). In order to get quantitative agreement with experiment, the screening effect must be included. The effect of remote scatterers which are located at a distance d from the interface is also shown. The main effect of remote impurity scattering is that the conductivity deviates from the linear behavior with density and increases with both the distance d and n/n_i (Hwang *et al.*, 2007a).

For very high-mobility samples, a sublinear conductivity, instead of the linear behavior with density, is found in experiments (Tan, Zhang, Bolotin *et al.*, 2007; Chen, Jang, Adam *et al.*, 2008). Such high quality samples presumably have a small charge impurity concentration n_i, and it is therefore likely that short-range disorder plays a more dominant role. Figure 14(b) shows the graphene conductivity calculated including both charge impurity and short-range disorder for different values of n_d/n_i. For small n_d/n_i, the conductivity is linear in density, which is seen in most experiments, and for large n_d/n_i the total conductivity shows the sublinear behavior. This high-density flattening of the graphene conductivity is a nonuniversal crossover behavior arising from the competition between two kinds of scatterers. In general, this crossover occurs when two scattering potentials are equivalent, that is, $n_i V_i^2 \approx n_d V_0^2$. In the inset of Fig. 14(b) the mobility in the presence of both charged impurities and short-ranged impurities is shown as a function of κ. As the scattering limited by the short-ranged impurity dominates over that by the long-ranged impurity (e.g., $n_d V_0^2 \gg n_i V_i^2$), the mobility is no longer linearly dependent on the charged impurity and approaches its limiting value

$$\mu = \frac{e}{4\hbar}\frac{(\hbar v_F)^2}{n}\frac{1}{n_d V_0^2}. \tag{3.24}$$

The limiting mobility depends only on neutral impurity concentration n_d and carrier density, i.e., long-range Coulomb scattering is irrelevant in this high-density limit.

The temperature-dependent conductivity of graphene arising from screening and the energy averaging defined in Eq. (3.2) is given at low temperatures ($T \ll T_F$) $\sigma(T)/\sigma_0 \approx 1 - C_1(T/T_F)^2$, where $\sigma_0 = e^2 v_F^2 D(E_F)\tau_0/2$ and C_1 is a positive constant depending only on r_s (Hwang and Das Sarma, 2009b). The conductivity decreases quadratically as the temperature increases and shows typical metallic
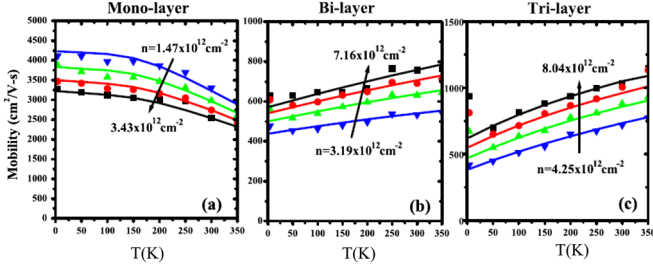
FIG. 15 (color online). Hall mobility as a function of temperature for different hole densities in (a) monolayer graphene, (b) bilayer graphene, and (c) trilayer graphene. The symbols are the measured data and the lines are fits. Adapted from Zhu *et al.*, 2009.

temperature dependence. On the other hand, at high temperatures ($T/T_F \gg 1$), it becomes $\sigma(T)/\sigma_0 \approx C_2(T/T_F)^2$, where C_2 is a positive constant. The temperature-dependent conductivity increases as the temperature increases in the high-temperature regime, which is characteristic of an insulating system. $\sigma_s(T)$ of graphene due to the short-range disorder (with scattering strength V_0) is given by $\sigma_s(T) = \sigma_{s0}/(1 + e^{-\beta\mu})$, where $\sigma_{s0} = e^2 v_F^2 D(E_F)\tau_s/2$ with $\tau_s = (n_d/4\hbar)E_F V_0^2/(\hbar v_F)^2$. In the low-temperature limit the temperature dependence of conductivity is exponentially suppressed, but the high-temperature limit of the conductivity approaches $\sigma_{s0}/2$ as $T \to \infty$, i.e., the resistivity at high temperatures increases up to a factor of 2 compared with the low-temperature limit resistivity.

Recently, the temperature dependence of resistivity of graphene has been investigated experimentally (Tan, Zhang, Stormer, and Kim, 2007; Bolotin, Sikes, Hone *et al.*, 2008; Chen, Jang, Xiao *et al.*, 2008; Zhu *et al.*, 2009). In Fig. 15(a) the graphene mobility is shown as a function of temperature. An effective metallic behavior at high density is observed as explained with screened Coulomb impurities. However, it is not obvious whether the temperature-dependent correction is quadratic because phonon scattering also gives rise to a temperature dependence (see Sec. III.C).

b. Bilayer graphene

The eigenstates of bilayer graphene can be written as $\psi_{s\mathbf{k}} = e^{i\mathbf{k}\mathbf{r}}(e^{-2i\theta_\mathbf{k}}, s)/\sqrt{2}$, and the corresponding energy is given by $\epsilon_{s\mathbf{k}} = s\hbar^2 k^2/2m$, where $\theta_\mathbf{k} = \tan^{-1}(k_y/k_x)$ and $s = \pm 1$ denote the band index. The corresponding form factor $F(q)$ of Eqs. (3.4) and (3.6) in the matrix elements arising from the sublattice symmetry of bilayer graphene becomes $F(q) = (1 + \cos2\theta)/2$, where $q = |\mathbf{k} - \mathbf{k}'|$, $\theta \equiv \theta_{\mathbf{k}\mathbf{k}'}$. Then the matrix element of the scattering potential of randomly distributed screened impurity charge centers in graphene is given by (Koshino and Ando, 2006; Nilsson *et al.*, 2006b; Katsnelson, 2007; Adam and Das Sarma, 2008a; Nilsson *et al.*, 2008)

$$|\langle V_{s\mathbf{k},s\mathbf{k}'}\rangle|^2 = |v_i(q)/\varepsilon(q)|^2(1 + \cos2\theta)/2. \quad (3.25)$$

The matrix element of the short-ranged disorder is given by $|\langle V_{s\mathbf{k},s\mathbf{k}'}\rangle|^2 = V_0^2(1 + \cos2\theta)/2$, and the corresponding energy dependent scattering time becomes $\tau^{-1}(\epsilon_k) = n_d V_0^2 m/\hbar^3$. The density-dependent conductivity for screened

Coulomb disorder is given by $\sigma(n) \sim n^2$ in the weak screening limit ($q_0 = q_{\text{TF}}/2k_F \ll 1$) or for the unscreened Coulomb disorder, and in the strong screening limit ($q_0 \gg 1$) $\sigma(n) \sim n$. In general for screened Coulomb disorder $\sigma(n) \sim n^\alpha$ (Das Sarma *et al.*, 2010), where α is density dependent and varies slowly changing from 1 at low density to 2 at high density. Increasing temperature, in general, suppresses screening, leading to a slight enhancement of the exponent α. For short-range disorder $\sigma(n) \sim n$.

Figure 16 shows the experiment of BLG conductivity. In Fig. 17(a) the density-dependent conductivities both for screened Coulomb disorder and for short-range disorder are shown. For screened Coulomb disorder, the conductivity shows superlinear behavior, which indicates that pure Coulomb disorder, which dominates mostly in MLG transport, cannot explain the density-dependent conductivity as seen experimentally (see Fig. 16) (Morozov *et al.*, 2008; Xiao *et al.*, 2010). The density dependence of the conductivity with both types of disorder present is approximately linear over a wide density range, which indicates that BLG carrier transport is controlled by two distinct and independent physical scattering mechanisms, i.e., screened Coulomb disorder due to random charged impurities in the environment and a short-range disorder. The weaker scattering rate of screened Coulomb disorder for BLG than for MLG is induced by the stronger BLG screening than MLG screening, rendering the effect of Coulomb scattering relatively less important in BLG (compared with MLG).

The temperature-dependent conductivity due to screened Coulomb disorder (Adam and Stiles, 2010; Das Sarma *et al.*, 2010; Hwang and Das Sarma, 2010; Lv and Wan, 2010) is given by $\sigma(T)/\sigma_0 \approx 1 - C_0(T/T_F)$ at low temperatures, where $C_0 = 4\log2/(C + 1/q_0)$ with $q_0 = q_{\text{TF}}/2k_F$, and $\sigma(T) \approx \sigma_1(T/T_F)^2$ at high temperatures. When the dimensionless temperature is very small ($T/T_F \ll 1$), a linear-in-T metallic T dependence arises from the temperature
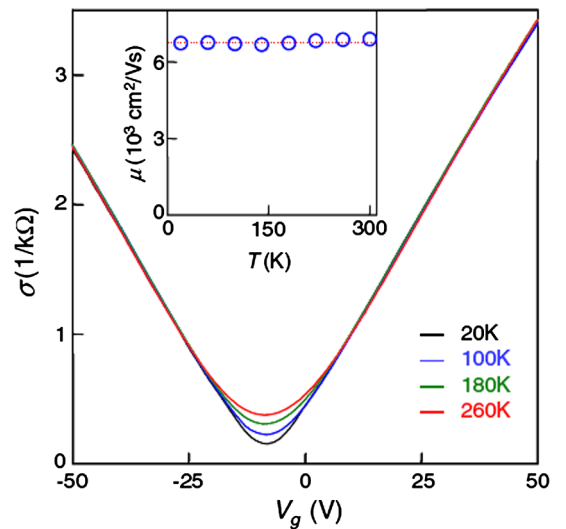

FIG. 16 (color online). The measured conductivity of bilayer graphene as a function of gate voltage V_g (or carrier density). The measured conductivity increases linearly with the density. Adapted from Morozov *et al.*, 2008.
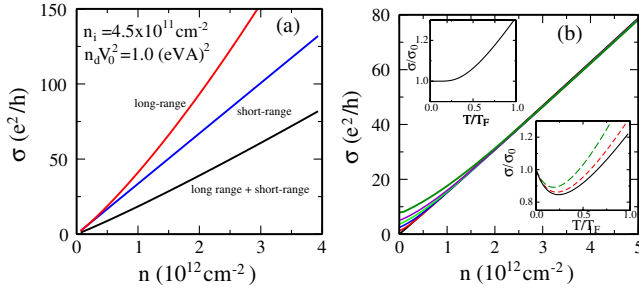
FIG. 17 (color online). (a) Density dependence of bilayer graphene conductivity with two scattering sources: screened long-range Coulomb disorder and short-ranged neutral disorder. (b) Density dependence of BLG conductivity for different temperatures: $T = 0$, 50, 100, 150, 200, and 300 K (from bottom to top). Top inset shows σ as a function of T in presence of short-range disorder. Bottom inset shows σ as a function of T in presence of screened Coulomb disorder for different densities $n = [5, 10, 30] \times 10^{11}$ cm^{-2} (from bottom to top). Adapted from Das Sarma *et al.*, 2010.

dependence of the screened charge impurity scattering, i.e., the thermal suppression of the $2k_F$ peak associated with backscattering (see Fig. 13). For the short-ranged scattering, the temperature dependence only comes from the energy averaging and the conductivity becomes $\sigma(T) = \sigma(0)[1 + t\ln(1 + e^{-1/t})]$, where $t = T/T_F$. At low temperatures the conductivity is exponentially suppressed, but at high temperatures it increases linearly.

Figure 17(b) shows the finite temperature BLG conductivity as a function of n. The temperature dependence is very weak at higher densities as observed in recent experiments (Morozov *et al.*, 2008). At low densities, where T/T_F is not too small, there is a strong insulating-type T dependence arising from the thermal excitation of carriers (which is exponentially suppressed at higher densities) and energy averaging, as observed experimentally (Morozov *et al.*, 2008). Note that for BLG $T_F = 4.23\tilde{n}$ K, where $\tilde{n} = n/(10^{10}$ cm$^{-2})$. In the bottom inset the conductivity due to screened Coulomb disorder is shown as a function of temperature for different densities. At low temperatures ($T/T_F \ll 1$) the conductivity decreases linearly with temperature, but $\sigma(T)$ increases quadratically in high-temperature limit. By contrast, for the short-range disorder σ always increases with T, as shown in the upper inset of Fig. 17(b). Thus for bilayer graphene, the metallic behavior due to screening effects is expected at very low temperatures for low-mobility samples, in which the screened Coulomb disorder dominates. In Fig. 15(b) the temperature dependence of mobility for bilayer graphene is shown. As we expect, the metallic behavior shows up at very low temperatures ($T < 100$ K).

We conclude this section by emphasizing the similarity and the difference between BLG and MLG transport at high densities from the perspective of Boltzmann transport theory considerations. In the MLG the linear density-dependent conductivity arises entirely from Coulomb disorder. However, in the BLG the existence of short-range disorder scattering must be included to explain the linearity because the Coulomb disorder gives rise to a higher power density dependence in conductivity. The importance of short-range scattering in BLG compared with MLG is understandable

based on BLG screening being much stronger than MLG screening leading to the relative importance of short-range scattering in BLG.

c. Semiconductor systems

Transport properties of 2D semiconductor-based parabolic 2D systems (e.g., Si-MOSFETs, GaAs heterostructures, and quantum wells, SiGe-based 2D structures) have been studied extensively over the last 40 years (Ando *et al.*, 1982; Abrahams *et al.*, 2001; Kravchenko and Sarachik, 2004). More recently, 2D transport properties have attracted attention because of the experimental observation of an apparent metallic behavior in the high-mobility low-density electron inversion layer in Si-MOSFET structures (Kravchenko *et al.*, 1994). However, in this review we do not make any attempt at reviewing the whole 2D metal-insulator transition (MIT) literature. Early comprehensive reviews of 2D MIT can be found in the literature (Abrahams *et al.*, 2001; Kravchenko and Sarachik, 2004). More recent perspectives can be found in Das Sarma and Hwang (2005) and Spivak *et al.* (2010). Our goal in this review is to provide a direct comparison of the transport properties of 2D semiconductor systems with those of MLG and BLG, emphasizing similarities and differences.

It is well known that the long-range charged impurity scattering and the short-range surface-roughness scattering dominate, respectively, in the low and high carrier density regimes of transport in 2D semiconductor systems. In Fig. 18 the experimental mobility of Si-MOSFETs is shown as a function of density. As density increases, the measured mobility first increases at low densities, and after reaching the maximum mobility it decreases at high densities. This behavior is typical for all 2D semiconductor systems, even though the mobility of GaAs systems decreases very slowly at high densities. This mobility behavior in density can be explained with mainly two scattering mechanisms as shown in Fig. 18(b). In the low-temperature region phonons do not play much of a role in resistive scattering. At low carrier densities long-range Coulomb scattering by unintentional random charged impurities invariably present in the environment of 2D semiconductor systems dominates the 2D mobility (Ando *et al.*, 1982). However, at high densities as more carriers are pushed to the interface the surface-roughness scattering becomes more significant. Thus transport in 2D semiconductor systems is limited by the same mechanisms as in graphene even though at high densities the unknown short-range disorder in graphene is replaced by the surface-roughness scattering in 2D semiconductor systems. The crucial difference between 2D transport and graphene transport is the existence of the insulating behavior of 2D semiconductor systems at very low densities which arises from the gapped nature of 2D semiconductors. However, the high-density 2D semiconductor transport is not qualitatively different from graphene transport since charged impurity scattering dominates carrier transport in both cases.

The experimentally measured conductivity and mobility for three different systems as a function of density are shown in Figs. 18 and 19. At high densities, the conductivity depends on the density as $\sigma \propto n^\alpha$ with $1 < \alpha < 2$, where $\alpha(n)$ depends weakly on the density for a given system but varies
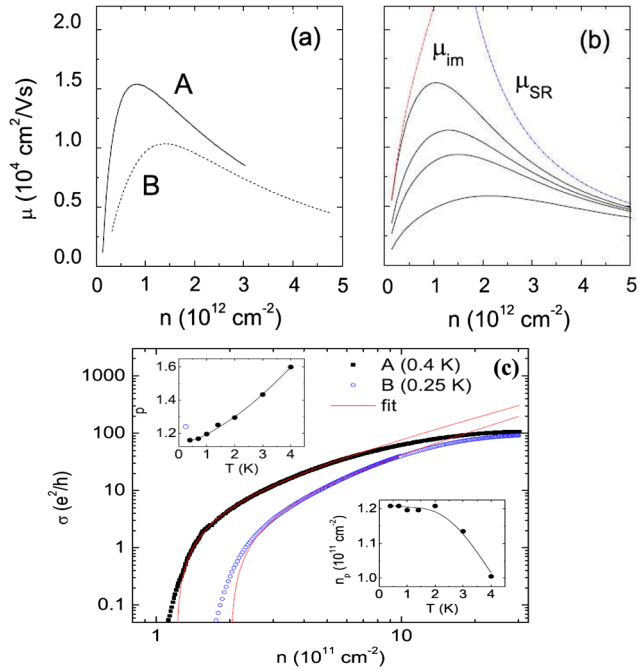
FIG. 18 (color online). (a) Experimental mobility μ as a function of density for two Si-MOSFET samples at a temperature $T = 0.25$ K. (b) Calculated mobility with two different scatterings, i.e., charge impurities and surface-roughness scatterings. (c) Measured conductivity $\sigma(n)$ for Si-MOSFET as a function of electron density n for two different samples. The solid lines are fits to the data of the form $\sigma(n) \propto A(n - n_p)^p$. The upper and lower insets show the exponent p and critical density n_p, respectively, as a function of temperature. Solid lines are a guides for the eyes. Adapted from Tracy *et al.*, 2009.

strongly from one system (e.g. Si-MOSFET) to another (e.g., GaAs). At high densities, before surface-roughness scattering sets in the conductivity is consistent with screened charged impurity scattering for all three systems. As n decreases, $\sigma(n)$ starts decreasing faster with decreasing density and the experimental conductivity exponent α becomes strongly density dependent with its value increasing substantially, and the conductivity vanishes as the density further decreases. To explain this behavior, a density-inhomogeneity-driven percolation transition was proposed (Das Sarma *et al.*, 2005), i.e., the density-dependent conductivity vanishes as $\sigma(n) \propto (n - n_p)^p$ with the exponent $p = 1.2$ being consistent with a percolation transition. At the lowest density, linear screening in a homogeneous electron gas fails qualitatively in explaining the $\sigma(n)$ behavior; whereas, it gives quantitatively accurate results at high densities. As found from direct numerical simulations (Efros, 1988; Nixon and Davies, 1990; Shi and Xie, 2002), homogeneous linear screening of charged impurities breaks down at low carrier densities with the 2D system developing strong inhomogeneities leading to a percolation transition at $n < n_p$. Nonlinear screening dominates transport in this inhomogeneous low carrier density regime. For $n < n_p$, the system is an insulator containing isolated puddles of electrons with no metallic conducting path spanning through the whole system. By contrast, graphene, being gapless, goes from being an electron metal to a hole metal, i.e., the conductivity is always finite for all densities, as the chemical potential passes through the puddle region.

Except for being an insulator at very low densities, the transport behavior of 2D semiconductor systems is not qualitatively different from graphene transport because both systems are governed by the charged impurities. To under-
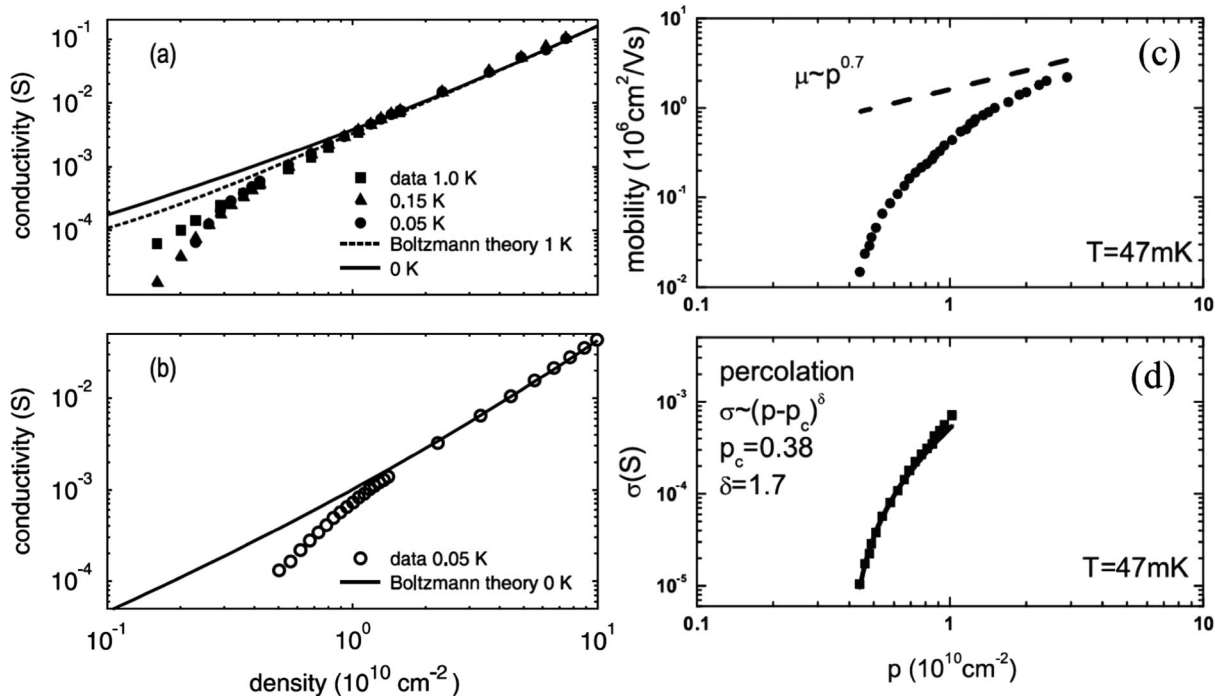
FIG. 19. (a), (b) Experimentally measured (symbols) and calculated (lines) conductivity of two different n-GaAs samples. The high density conductivity limited by the charged impurities fit well to the experimental data. Adapted from Das Sarma *et al.*, 2005. (c) Mobility of p-GaAs 2D system vs density at fixed temperature $T = 47$ mK. (d) The corresponding conductivity vs density (solid squares) along with the fit generated assuming a percolation transition. The dashed line in (c) indicates the $\mu \sim p^{0.7}$ behavior. Adapted from Manfra *et al.*, 2007.

stand the ρ (or σ) behavior at high density, we start with the Drude-Boltzmann semiclassical formula, Eq. (3.2), for 2D transport limited by screened charged impurity scattering (Das Sarma and Hwang, 1999). However, due to the finite extent in the z direction of the real 2D semiconductor system, the Coulomb potential has a form factor depending on the details of the 2D structure. For comparison with graphene, we consider the simplest case of 2D limit, i.e., δ layer. For δ layer 2D systems with parabolic band, the scattering times at $T = 0$ for charged impurity centers with impurity density n_i located at the 2D systems are calculated by

$$\frac{1}{\tau} = \frac{1}{\tau_0}\left\{\pi - 2\frac{d}{dq_0}[q_0^2 f(q_0)]\right\}, \quad (3.26)$$

where $\tau_0^{-1} = 2\pi\hbar(n_i/m)(2/g_s g_v)^2 q_0^2$, $q_0 = q_{\mathrm{TF}}/2k_F$ (q_{TF} is a 2D Thomas-Fermi wave vector), and $f(x)$ is given in Eq. (3.22). Then, the density dependence of conductivity can be expressed as $\sigma(n) \propto n^\alpha$ with $1 < \alpha < 2$. In the strong screening limit ($q_0 \gg 1$) the scattering time becomes

$\tau^{-1} \propto q_0^2 \propto n^{-1}$, then the conductivity behaves as $\sigma(n) \propto n^2$. In the weak screening limit $\tau^{-1} \propto q_0^0 \propto n^0$ and $\sigma(n) \propto n$. These conductivity behaviors are common for 2D systems with parabolic bands and are qualitatively similar to graphene where $\sigma \propto n$ behavior is observed. However, due to the complicated impurity configuration (spatial distribution of impurity centers) and finite width effects of real 2D semiconductor systems the exponent α varies with systems. In general, modulation doped GaAs systems have larger α than Si-MOSFETs due to the configuration of impurity centers.

An interesting transport property of 2D semiconductor systems is the observation of the extremely strong anomalous metallic (i.e., $d\rho/dT > 0$) temperature dependence of the resistivity $\rho(T)$ in the density range just above a critical carrier density n_c where $d\rho/dT$ changes its sign at low temperatures (see Fig. 20), which is not seen in graphene. Note that the experimentally measured $\rho(T)$ of graphene shows very weak metallic behavior at high density due to the weak temperature dependence of screening function. It
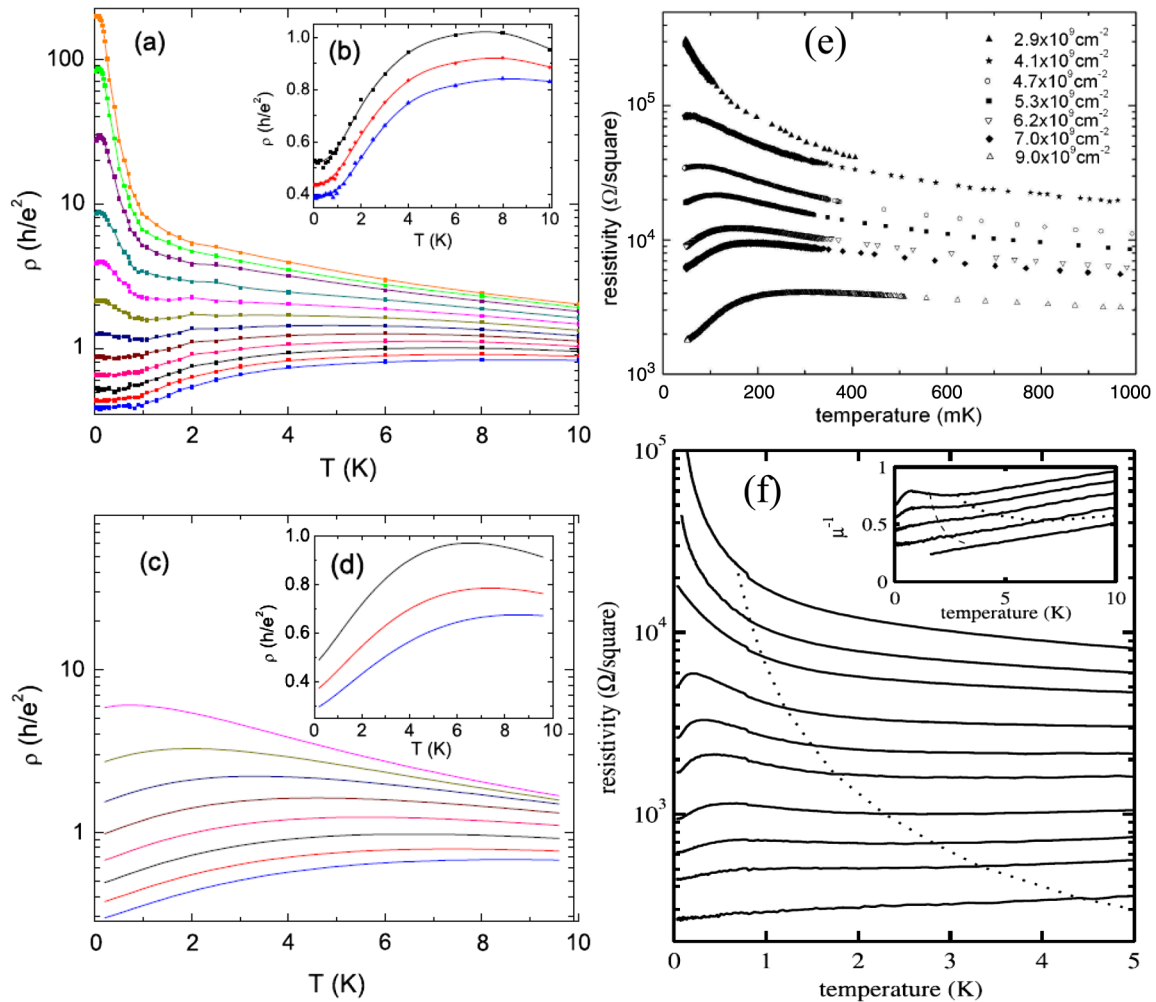

FIG. 20 (color online).   (a) Experimental resistivity ρ of Si-MOSFET as a function of temperature at 2D electron densities (from top to bottom) $n = [1.07, 1.10, 1.13, 1.20, 1.26, 1.32, 1.38, 1.44, 1.50, 1.56, 1.62, \text{and } 1.68] \times 10^{11} \text{ cm}^2$. Inset (b) shows ρ for $n = [1.56, 1.62, \text{and } 1.68] \times 10^{11} \text{ cm}^2$. (c) Theoretically calculated temperature and density-dependent resistivity for sample A for densities $n = [1.26, 1.32, 1.38, 1.44, 1.50, 1.56, 1.62, \text{and } 1.68] \times 10^{11} \text{ cm}^2$ (from top to bottom). Adapted from Tracy *et al.*, 2009. (e) Experimental $\rho(T)$ for n-GaAs (where $n_c = 2.3 \times 10^9 \text{ cm}^{-2}$). The density ranges from 0.16×10^{10} to $1.06 \times 10^{10} \text{ cm}^{-2}$. Adapted from Lilly *et al.*, 2003. (f) Temperature dependence of the resistivity for p-GaAs systems for densities ranging from 9.0×10^9 to $2.9 \times 10^9 \text{ cm}^{-2}$. Adapted from Manfra *et al.*, 2007.

has been suggested (Das Sarma and Hwang, 1999) that the anomalously strong metallic temperature dependence discovered in 2D semiconductor systems arises from the physical mechanism of temperature, density, and wave vector dependent screening of charged impurity scattering in 2D semiconductor structures, leading to a strongly temperature-dependent effective quenched disorder controlling $\rho(T, n)$ at low temperatures and densities. Interaction effects also lead to a linear-T conductivity in 2D semiconductors (Zala *et al.*, 2001).

With temperature-dependent screening function $\varepsilon(q, T)$ in Eq. (3.5), the asymptotic low- (Das Sarma and Hwang, 2003) and high- (Das Sarma and Hwang, 2004) temperature behaviors of 2D conductivity are given by

$$\sigma(t \ll 1) \approx \sigma_0^{2D}[1 - C_1(T/T_F)], \tag{3.27a}$$

$$\sigma(t \gg 1) \approx \sigma_1^{2D}[T/T_F + (3\sqrt{\pi}q_0/4)\sqrt{T_F/T}], \tag{3.27b}$$

where $t = T/T_F$, $\sigma_0^{2D} \equiv \sigma(T = 0)$, $C_1 = 2q_0/(1 + q_0)$, and $\sigma_1^{2D} = (e^2/h)(n/n_i)\pi q_0^2$. Here an ideal 2D electron gas with zero thickness is considered in order to compare with the 2D graphene sheet which also has a zero thickness. It is important to include the temperature-dependent polarizability of Fig. 13 in the calculation in order to get strong temperature-dependent resistivity. Since the most dominant scattering occurs at $q = 2k_F$ and the temperature dependence of screening function at $2k_F$ is strong, the calculated 2D resistivity shows the strong anomalous linear T metallic behavior, which is observed in many different semiconductor systems [e.g. Si-MOSFET Kravchenko *et al.* (1994)]: *p*-GaAs (Noh *et al.*, 2003; Manfra *et al.*, 2007), *n*-GaAs (Lilly *et al.*, 2003), SiGe (Senz *et al.*, 2002), and AlAs (Papadakis and Shayegan, 1998). In addition, for the observation of a large temperature-induced change in resistivity, it is required to have a comparatively large change in the value of the dimensionless temperature $t = T/T_F$, and the strong screening condition, $q_{TF} \gg 2k_F$, which explains why the Si MOS 2D electron system exhibits substantially stronger metallic behavior than the GaAs 2D electron system, as is experimentally observed, since $(q_{TF}/2k_F)_{Si} \approx 10(q_{TF}/2k_F)_{GaAs}$ at similar density.

Before concluding this basic transport theory section of this review, we point out the key qualitative similarities and differences in the transport theory of all systems (i.e., graphene, bilayer graphene, and 2D semiconductor-based parabolic 2D systems). First, the graphene conductivity is qualitatively similar to that of 2D semiconductor systems in the sense that the conductivity at high density of both systems follows the power law in terms of density, $\sigma(n) \sim n^\alpha$. The formal Boltzmann theory for the scattering times is the same in all systems except for the different angular factor arising from chiral properties of graphene. This angular part does not play a role in the density dependence of conductivity, but significantly affects the temperature dependence of conductivity. The explicit differences in the density of states $D(\varepsilon)$ and the dielectric function $\epsilon(q, T)$ also lead to different temperature-dependent conductivities in these systems. The most important qualitative difference between graphene and semiconductor 2D systems occurs at low carrier densities, in which semiconductor 2D systems become insulators, but graphene conductivity is finite for all densities.

C. Phonon scattering in graphene

In this section we review the phonon scattering limited carrier transport in graphene. Lattice vibrations are inevitable sources of scattering and can dominate transport near room temperature. They constitute an intrinsic scattering source, i.e., they limit the mobility at finite temperatures when all extrinsic scattering sources are removed. In general, three different types of phonon scattering are considered: intravalley acoustic and optical phonon scattering which induce the electronic transitions within a single valley, and intervalley phonon scattering that induces electronic transitions between different valleys.

The intravalley acoustic phonon scattering is induced by low energy phonons and is considered an elastic process. The temperature-dependent phonon-limited resistivity (Stauber *et al.*, 2007; Hwang and Das Sarma, 2008a) was found to be linear (i.e., $\rho_{ph} \propto T$) for $T > T_{BG}$, where T_{BG} is the Bloch-Grüneisen (BG) temperature (Kawamura and Das Sarma, 1992), and $\rho_{ph}(T) \sim T^4$ for $T < T_{BG}$. The acoustic phonon scattering gives a quantitatively small contribution in graphene even at room temperature due to the high Fermi temperature of graphene in contrast to 2D semiconductors where room-temperature transport is dominated by phonon scattering (Kawamura and Das Sarma, 1990, 1992). The intravalley optical phonon scattering is induced by optical phonons of low momentum ($q \approx 0$) and very high energy ($\omega_{OP} \approx 200$ meV in graphene) and is negligible. The intervalley scattering can be induced by the emission and absorption of high momentum, high energy acoustic, or optical phonons. In graphene intervalley scattering may be important at high temperatures because of relatively low phonon energy (≈ 70 meV, the out-of-plane acoustic phonon mode at the K point) (Maultzsch *et al.*, 2004; Mounet and Marzari, 2005). Even though the effects of intervalley phonon scattering can explain a crossover (Figs. 21 and 22) observed in experiments in the 150 to 250 K range, more work is needed to validate the model of combined acoustic phonon and out-of-plane acoustic phonon scattering contributing to the temperature-dependent graphene resistivity.

The remote interface polar optical phonons in the substrate (i.e., SiO_2) have recently been considered (Chen, Jang, Xiao *et al.*, 2008; Fratini and Guinea, 2008). Even though these modes are known to be not important in Si-MOSFETs (Hess and Vogl, 1979; Moore and Ferry, 1980), their role in graphene transport seems to be important (Chen, Jang, Xiao *et al.*, 2008; DaSilva *et al.*, 2010). Another possibility considered by Morozov *et al.* (2006) is that the thermal fluctuations (ripplons) of the mechanical ripples invariably present in graphene samples contribute to the graphene resistivity. In addition, Mariani and von Oppen (2008) investigated the role of the flexural (out-of-plane) phonons of free standing graphene membranes which arise from the rotation and reflection symmetries. Flexural phonons make a contribution to the resistivity at low temperatures with an anomalous temperature dependence $\propto T^{5/2} \ln T$.

Before we discuss the theory of electron phonon scattering we mention the current experimental situation for the measurement in graphene of the phonon scattering contribution to the resistivity. Since the experimentally measured resistivity
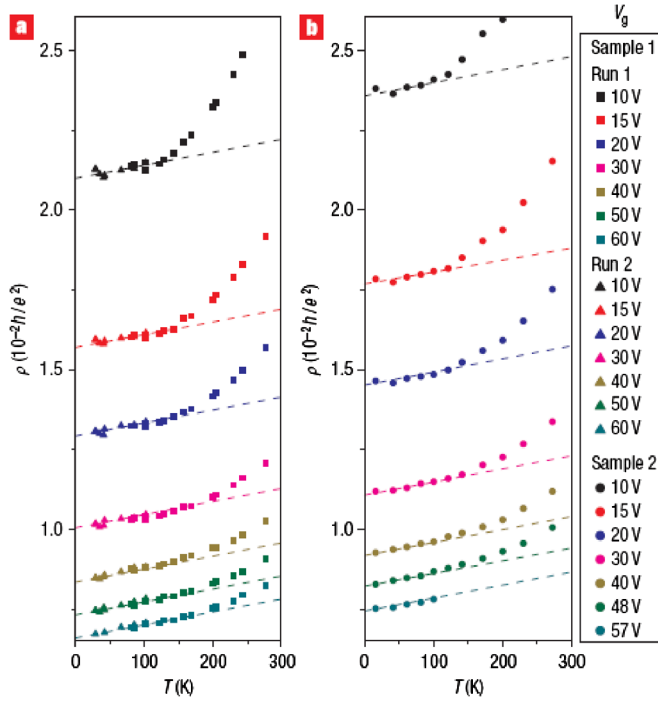
FIG. 21 (color online). Temperature-dependent resistivity of graphene on SiO_2. Resistivity of two graphene samples as a function of temperature for different gate voltages. Dashed lines are fits to the linear T dependence with Eq. (3.32). Adapted from Chen, Jang, Xiao *et al.*, 2008.

in the current graphene samples is completely dominated by extrinsic scattering (impurity scattering described in Sec. III.B), even at room temperatures the experimental extraction of the pure phonon contribution to graphene resistivity is not unique. In particular, the impurity contribution to resistivity also has a temperature dependence arising from Fermi statistics and screening which, although weak, cannot be neglected in extracting the phonon contribution (particu-
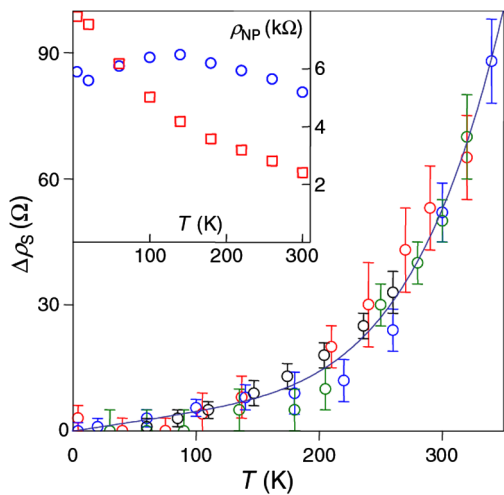

FIG. 22 (color online). Temperature-dependent resistivity for four different MLG samples (symbols). The solid curve is the best fit by using a combination of T and T^5 functions. The inset shows T dependence of maximum resistivity at the neutrality point for MLG and BLG (circles and squares, respectively). Adapted from Morozov *et al.*, 2008.

larly since the total phonon contribution itself is much smaller than the total extrinsic contribution). In addition, the experimental phonon contribution is obtained assuming Matthiessen's rule, i.e., $\rho_{tot} = \rho_{ph} + \rho_i$, where ρ_{tot} is the total resistivity contributed by impurities and defects (ρ_i) and phonons (ρ_{ph}), which is not valid at room temperature (Hwang and Das Sarma, 2008a). Thus, two different groups (Chen, Jang, Xiao *et al.*, 2008; Morozov *et al.*, 2008) (Figs. 21 and 22) have obtained totally different behavior of phonon contribution to resistivity. Morozov *et al.* (2008) found that the temperature dependence is a rather high power (T^5) at room temperatures, and the phonon contribution is independent of carrier density. Chen, Jang, Xiao *et al.* (2008) showed that the extracted phonon contribution is strongly density dependent and is fitted with both linear T from acoustic phonons and Bose-Einstein distribution. Therefore, the phonon contribution, as determined by a simple subtraction, could have large errors due to the dominance of extrinsic scattering.

In this section we describe transport only due to the longitudinal acoustic phonons since either the coupling to other graphene lattice modes is too weak or the energy scales of these (optical) phonon modes are far too high for them to provide an effective scattering channel in the temperature range (5 to 500 K) of our interest. Since graphene is a non-polar material, the most important scattering arises from the deformation potential due to quasistatic deformation of the lattice. Within the Boltzmann transport theory (Kawamura and Das Sarma, 1990; Kawamura and Das Sarma, 1992), the relaxation time due to deformation potential coupled acoustic phonon mode is given by

$$\frac{1}{\tau(\varepsilon)} = \sum_{\mathbf{k}'}(1 - \cos\theta_{\mathbf{k}\mathbf{k}'})W_{\mathbf{k}\mathbf{k}'}\frac{1 - f(\varepsilon')}{1 - f(\varepsilon)}, \qquad (3.28)$$

where $\theta_{\mathbf{k}\mathbf{k}'}$ is the scattering angle between $\mathbf{k}$ and $\mathbf{k}'$, $\varepsilon = \hbar v_F|\mathbf{k}|$, and $W_{\mathbf{k}\mathbf{k}'}$ is the transition probability from the state with momentum $\mathbf{k}$ to the state with momentum $\mathbf{k}'$ and is given by

$$W_{\mathbf{k}\mathbf{k}'} = \frac{2\pi}{\hbar}\sum_{\mathbf{q}}|C(\mathbf{q})|^2\Delta(\varepsilon, \varepsilon'), \qquad (3.29)$$

where $C(\mathbf{q})$ is the matrix element for scattering by acoustic phonons, and $\Delta(\varepsilon, \varepsilon')$ is given by

$$\Delta(\varepsilon, \varepsilon') = N_q\delta(\varepsilon - \varepsilon' + \omega_{\mathbf{q}})$$
$$+ (N_q + 1)\delta(\varepsilon - \varepsilon' - \omega_{\mathbf{q}}), \qquad (3.30)$$

where $\omega_{\mathbf{q}} = \hbar v_{ph}\mathbf{q}$ is the acoustic phonon energy with v_{ph} the phonon velocity and N_q the phonon occupation number $N_q = 1/[\exp(\beta\omega_{\mathbf{q}}) - 1]$. The first (second) term is Eq. (3.30) corresponds to the absorption (emission) of an acoustic phonon of wave vector $\mathbf{q} = \mathbf{k} - \mathbf{k}'$. The matrix element $C(\mathbf{q})$ is independent of the phonon occupation numbers. The matrix element $|C(\mathbf{q})|^2$ for the deformation potential is given by

$$|C(\mathbf{q})|^2 = \frac{D^2\hbar q}{2A\rho_m v_{ph}}\left[1 - \left(\frac{q}{2k}\right)^2\right], \qquad (3.31)$$

where D is the deformation-potential coupling constant, ρ_m is the graphene mass density, and A is the area of the sample.

The scattering of electrons by acoustic phonons may be considered quasielastic since $\hbar\omega_{\mathbf{q}} \ll E_F$, where E_F is the Fermi energy. There are two transport regimes, which apply to the temperature regimes $T \ll T_{BG}$ and $T \gg T_{BG}$, depending on whether the phonon system is degenerate (Bloch-Grüneisen) or nondegenerate [equipartition (EP)]. The characteristic temperature T_{BG} is defined as $k_B T_{BG} = 2\hbar k_F v_{ph}$, which is given, in graphene, by $T_{BG} = 2v_{ph}k_F/k_B \approx 54\sqrt{n}$ K with density measured in units of $n = 10^{12}$ cm^{-2}. The relaxation time in the EP regime is calculated to be (Stauber *et al.*, 2007; Vasko and Ryzhii, 2007; Hwang and Das Sarma, 2008a)

$$\frac{1}{\tau(\varepsilon)} = \frac{1}{\hbar^3} \frac{\varepsilon}{4v_F^2} \frac{D^2}{\rho_m v_{ph}^2} k_B T. \quad (3.32)$$

Thus, in the nondegenerate EP regime ($\hbar\omega_{\mathbf{q}} \ll k_B T$) the scattering rate $[1/\tau(\varepsilon)]$ depends linearly on the temperature. At low temperatures ($T_{BG} \ll T \ll E_F/k_B$) the calculated conductivity is independent of electron density. Therefore, the electronic mobility in graphene is inversely proportional to the carrier density, i.e., $\mu \propto 1/n$. The linear temperature dependence of the scattering time has been reported for nanotubes (Kane *et al.*, 1998) and graphites (Pietronero *et al.*, 1980; Woods and Mahan, 2000; Suzuura and Ando, 2002b).

In the BG regime the scattering rate is strongly reduced by the thermal occupation factors because the phonon population decreases exponentially, and the phonon emission is prohibited by the sharp Fermi distribution. Then, in the low-temperature limit $T \ll T_{BG}$ the scattering time becomes (Hwang and Das Sarma, 2008a)

$$\frac{1}{\langle \tau \rangle} \approx \frac{1}{\pi} \frac{1}{E_F} \frac{1}{k_F} \frac{D^2}{2\rho_m v_{ph}} \frac{4!\zeta(4)}{(\hbar v_{ph})^4} (k_B T)^4. \quad (3.33)$$

Thus, the temperature-dependent resistivity in BG regime becomes $\rho \propto T^4$. Even though the resistivity in the EP regime is density independent, Eq. (3.33) indicates that the calculated resistivity in BG regime is inversely proportional to the density, i.e., $\rho_{BG} \propto n^{-3/2}$ since $\rho \propto [D(E_F)\langle\tau\rangle]^{-1}$. More experimental and theoretical work would be needed for a precise quantitative understanding of phonon scattering effect on graphene resistivity.

D. Intrinsic mobility

Based on the results of previous sections, one can extract the possible (hypothetical) intrinsic mobility of 2D systems when all extrinsic impurities are removed. In Fig. 23 the acoustic phonon-limited mobility is shown for 2D *n*-GaAs system. For lower temperatures, $\mu(T)$ increases by a large factor ($\mu \propto T^{-7}$ for deformation-potential scattering and $\mu \propto T^{-5}$ for piezoelectric scattering) since one is in the Bloch-Grüneisen regime where phonon occupancy is suppressed exponentially (Kawamura and Das Sarma, 1990; Kawamura and Das Sarma, 1992). Thus the intrinsic mobility of semiconductor systems is extremely high at low temperatures ($T < T_{BG}$). For currently available semiconductor samples,
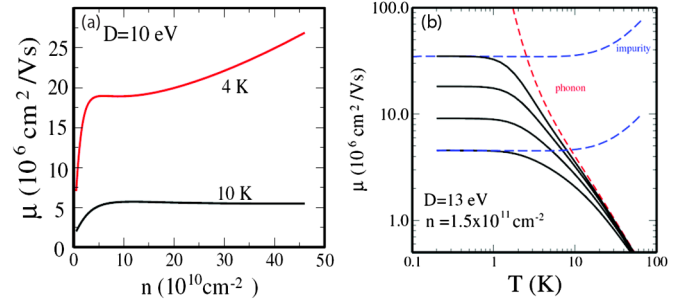
FIG. 23 (color online). (a) Acoustic phonon-limited mobility of *n*-GaAs 2D system as a function of density for two different temperatures. (b) Calculated *n*-GaAs mobility as a function of temperature for different impurity densities. At low temperatures ($T < 1$ K) the mobility is completely limited by impurity scattering. Adapted from Hwang and Das Sarma, 2008b.

the mobility below T_{BG} is completely limited by extrinsic impurity scattering in 2D systems. Above the BG regime (or $T > 4$ K), the mobility is dominated by phonons. In this limit the mobility limited by phonon scattering is much lower than that for charged impurity scattering. Therefore, it will be impossible to raise 2D mobility (for $T > 4$ K) by removing the extrinsic impurities since acoustic phonon scattering sets the intrinsic limit at these higher temperatures (for $T > 100$ K, optical phonons become dominant) (Pfeiffer *et al.*, 1989).

In Fig. 24, the acoustic phonon-limited graphene mobility $\mu \equiv (en\rho)^{-1}$ is shown as functions of temperature and carrier density, which is given by $\mu \gtrsim 10^{10}/D^2\tilde{n}T$ cm^2/V s where D is measured in eV, the temperature T in K, and $\tilde{n}$ carrier density measured in units of 10^{12} cm^{-2}. Thus, the acoustic phonon scattering limited graphene mobility is inversely proportion to T and n for $T > T_{BG}$. Also with the generally accepted values in the literature for the graphene sound velocity and deformation coupling (Chen, Jang, Xiao *et al.*, 2008) (i.e., $v_{ph} = 2 \times 10^6$ cm/s and deformation potential $D = 19$ eV), μ could reach values as high as 10^5 cm^2/V s for lower carrier densities ($n \lesssim 10^{12}$ cm^{-2}) at $T = 300$ K (Hwang and Das Sarma, 2008a; Shishir and Ferry, 2009). For larger (smaller) values of D, μ would be smaller (larger) by a factor of D^2. It may be important to emphasize here that we know of no other system where the intrinsic room-temperature carrier mobility could reach a value as high as 10^5 cm^2/V s, which is also consistent with
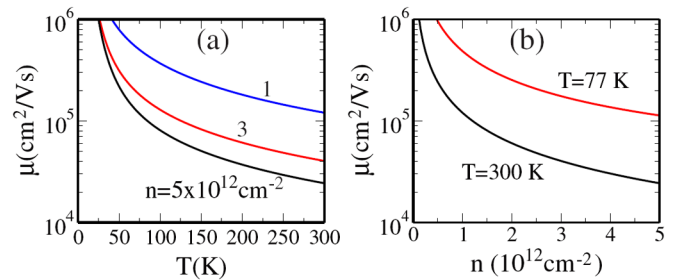

FIG. 24 (color online). Calculated graphene mobility limited by the acoustic phonon with the deformation-potential coupling constant $D = 19$ eV (a) as a function of temperature and (b) as a function of density. Adapted from Hwang and Das Sarma, 2008a.

the experimental conclusion by Chen, Jang, Xiao *et al.* (2008), Morozov *et al.* (2008), and Hong *et al.* (2009). This would, however, require the elimination of all extrinsic scattering, and first steps in this direction have been taken in fabricating suspended graphene samples (Bolotin, Sikes, Jiang *et al.*, 2008; Du *et al.*, 2008). Finally, we point out the crucial difference between graphene and 2D GaAs in phonon-limited mobility. In the 2D GaAS system the acoustic phonon scattering is important below $T = 100$ K and polar optical phonon scattering becomes exponentially more important for $T \gtrsim 100$ K; whereas, in graphene a resistivity linear in T is observed up to very high temperatures (≈ 1000 K) since the relevant optical phonons have very high energy (≈ 2000 K) and are simply irrelevant for carrier transport.

E. Other scattering mechanisms

1. Midgap states

The Boltzmann transport theory developed in Sec. III.A is considered the limit of weak scattering. One can ask about the opposite limit of very strong scattering. The unitarity of the wave functions implies that a potential scatterer can only cause a phase shift in the outgoing wave. Standard treatment of *s*-wave elastic scattering gives the scattering time

$$\frac{\hbar}{\tau_k} = \frac{8n_d}{\pi D(E_k)} \sin^2(\delta_k), \qquad (3.34)$$

where the conductivity is then given by the Einstein relation $\sigma = (2e^2/h)v_F k_F \tau_{k_F}$.

To model the disorder potential induced by a vacancy, Hentschel and Guinea (2007) assumed a circularly symmetric potential with $V(0 < r < R') = \infty$, $V(R' < r < R) = $ const, and $V(R > r) = 0$. This corresponds to a circular void of radius R', and appropriate boundary conditions are chosen to allow for zero-energy states (also called midgap states). By matching the wave functions of incoming and outgoing waves, the scattering phase shift can be calculated as (Hentschel and Guinea, 2007; Guinea, 2008)

$$\delta_k = -\arctan\left(\frac{J_0(kR')}{Y_0(kR')}\right) \overset{k\to 0}{\longrightarrow} -\frac{\pi}{2}\frac{1}{\ln(kR')}, \qquad (3.35)$$

where $J_0(x)$ [$Y_0(x)$] is the zeroth order Bessel function of the first (second) kind. Expanding for small carrier density, one then finds for the conductivity (Stauber *et al.*, 2007)

$$\sigma = \frac{2e^2}{\pi h}\frac{n}{n_d}\ln^2(k_F R'), \qquad (3.36)$$

which other than the logarithmic factor, mimics the behavior of charged impurities, and is linear in carrier density.

In recent experimental work, Chen, Cullen *et al.* (2009) irradiated graphene with He and Ne ions to deliberately create large vacancies in the graphene sheet. They further demonstrated that these vacancies induced by ion irradiation gave rise to a strong D peak in the Raman spectra, inferring that the absence of such a D peak in the pristine graphene signalled the lack of such defects (Fig. 25). Moreover, they demonstrated that while transport in pristine graphene is dominated by charged impurities, after ion irradiation the electron scattering off these vacancies appears consistent with the theory including midgap states [Eq. (3.36)]. In this review, we consider only the case where the disorder changes graphene's transport properties without modifying its fundamental chemical structure (Hwang *et al.*, 2007b; Schedin *et al.*, 2007). The subject of transport in graphane (Sofo *et al.*, 2007; Elias *et al.*, 2009) and other chemical derivatives of graphene is beyond the scope of this work; see, e.g., Robinson *et al.*(2008), Bostwick *et al.* (2009), Cheianov *et al.* (2009), Geim (2009), and Wehling *et al.* (2009a, 2009b).

2. Effect of strain and corrugations

While graphene is often assumed to be an atomically perfect 2D sheet, in reality, graphene behaves more like a membrane. When placed on a substrate, graphene will conform to the surface-roughness developing ripples. Even without a substrate, experiments reveal significant deformations (Meyer *et al.*, 2007), although the theoretical picture is still contentious (Fasolino *et al.*, 2007; Pereira *et al.*,
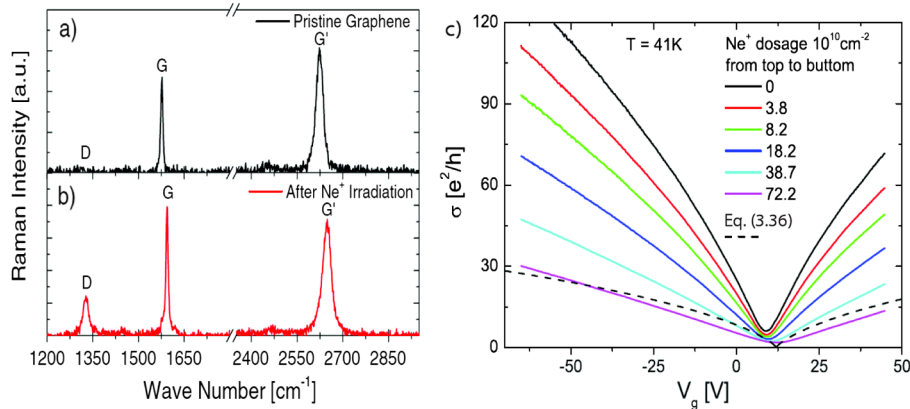
FIG. 25 (color online).   Left panel: Raman spectra (wavelength 633 nm) for (a) pristine graphene and (b) graphene irradiated by 500 eV Ne$^+$ ions that are known to cause vacancies in the graphene lattice. Right panel: Increasing the number of vacancies by ion irradiation caused a transition from the pristine graphene (where Coulomb scattering dominates) to the lower curves where scattering from vacancies dominate. Also shown is a fit to Eq. (3.36) from Stauber *et al.*, 2007 that describes scattering off vacancies that have midgap states. From Chen, Cullen *et al.*, 2009.

2009; Thompson-Flagg *et al.*, 2009). It is nonetheless an important theoretical question to address the nature of electronic scattering off such ripples. Ripples, by their very nature, are correlated long-range fluctuations across the entire sample (i.e. most experiments measuring ripples calculate a height-height correlation function). Yet, for electronic transport, one would like to isolate a "single ripple" and calculate its scattering cross section (assuming that the rest of the sample is flat), and then treat the problem of electrons scattering off ripples as that of random uncorrelated impurities with the cross section of a single ripple. This was the approach followed by Guinea (2008), Katsnelson and Geim (2008), and Prada *et al.* (2010).

With this qualitative picture in mind, one could estimate the transport time due to ripples as

$$\frac{\hbar}{\tau} \approx 2\pi D(E_F)\langle V_q V_{-q}\rangle, \tag{3.37}$$

where V_q is the scattering potential caused by the strain fields of a single ripple.

Introducing a height field $h(\mathbf{r})$ (that measures displacements normal to the graphene sheet), one finds (Katsnelson and Geim, 2008)

$$\langle V_q V_{-q}\rangle \approx \left(\frac{\hbar v_F}{a}\right)^2 \sum_{\mathbf{q}_1, \mathbf{q}_2} \langle h_{\mathbf{q}-\mathbf{q}_1} h_{\mathbf{q}} h_{-\mathbf{q}+\mathbf{q}_2} h_{-\mathbf{q}_2}\rangle$$
$$\times [(\mathbf{q}-\mathbf{q}_1)\cdot\mathbf{q}_1][(\mathbf{q}-\mathbf{q}_2)\cdot\mathbf{q}_2], \tag{3.38}$$

where a is the lattice spacing. Following Ishigami *et al.* (2007), ripple correlations can be parametrized as $\langle [h(r) - h(0)]^2\rangle = r^{2H}$, where the exponent H provides information about the origin of the ripples. An exponent $2H = 1$ indicates that height fluctuation domains have short-range correlations, implying that graphene conforms to the morphology of the underlying substrate, while $2H = 2$ suggests a thermally excitable membrane only loosely bound by Van der Waals forces to the substrate. Ishigami *et al.* (2007) found experimentally that $2H \approx 1.11 \pm 0.013$, implying that graphene mostly conforms to the substrate, but with some intrinsic stiffness. Katsnelson and Geim (2008) showed that this has consequences for transport properties, where for $2H = 1$, $\sigma \sim 1/\ln^2(k_F a)$; for $2H > 1$, $\sigma(n) \sim n^{2H-1}$. For the special case of $2H = 2$ (flexural ripples), this scattering mimics the long-range Coulomb scattering discussed in Sec. III.A. For the experimentally relevant case of $2H \gtrsim 1$, electron scattering off ripples would mimic short-range disorder also discussed in Sec. III.A. Thus, ripple scattering in graphene for $2H \approx 1$ mimic surface-roughness scattering in Si-MOSFET (Ando *et al.*, 1982). We emphasize that these conclusions are at best qualitative, since the approximation of treating the ripples as uncorrelated single impurities is quite drastic. A complete theory for scattering off ripples in graphene is an interesting, and at present and open problem. Ripple scattering effects on graphene transport have a formal similarity to the well-studied problem of interface roughness scattering effects on carrier transport in Si-SiO$_2$ 2D electron systems (Ando *et al.*, 1982; Adam, Hwang, and Das Sarma, 2008; Tracy *et al.*, 2009).

IV. TRANSPORT AT LOW CARRIER DENSITY

A. Graphene minimum conductivity problem

1. Intrinsic conductivity at the Dirac point

One of the most discussed issues in the context of fundamental graphene physics has been the so-called minimum (or minimal) conductivity problem (or puzzle) for intrinsic graphene. In the end, the graphene minimum conductivity problem turns out to be an ill-posed problem, which can only be solved if the real physical system underlying intrinsic (i.e., undoped) graphene is taken into account. An acceptable and reasonably quantitatively successful theoretical solution of the minimum conductivity problem has only emerged in the last couple of years, where the theory has to explicitly incorporate carrier transport in the highly inhomogeneous electron-hole landscape of extrinsic graphene, where density fluctuations completely dominate transport properties for actual graphene samples.

The graphene minimum conductivity problem is the dichotomy between the theoretical prediction of a universal Dirac point conductivity σ_D of undoped intrinsic graphene and the actual experimental sample-dependent nonuniversal minimum of conductivity observed in gated graphene devices at the charge neutrality point with the typical observed minimum conductivity being much larger than the universal prediction.

Unfortunately, σ_D is ill-defined, and depending on the theoretical methods and approximation schemes, many different universal results have been predicted (Fradkin, 1986; Ludwig *et al.*, 1994; Aleiner and Efetov, 2006; Altland, 2006; Peres *et al.*, 2006; Tworzydło *et al.*, 2006; Bardarson *et al.*, 2007; Fritz *et al.*, 2008; Kashuba, 2008):

$$\sigma_D = \frac{4e^2}{\pi h}, \qquad \frac{\pi e^2}{2h}, \qquad 0, \qquad \infty,$$

and other values. The conductivity $\sigma(T, \omega, \epsilon_F, \Gamma, \Delta, L^{-1})$ is in general a function of many variables: temperature (T), frequency (ω), Fermi energy or chemical potential (ϵ_F), impurity scattering strength or broadening (Γ), intervalley scattering strength (Δ), and system size (L). The Dirac point conductivity of clean graphene $\sigma_D(0, 0, 0, 0, 0, 0)$ is obtained in the limit of all the independent variables being zero, and the result depends explicitly on how and in which order these limits are taken. For example, $\omega \to 0$ and $T \to 0$ limit is not necessarily interchangeable with the $T \to 0$ and $\omega \to 0$ limit. In addition, the limit of vanishing impurity scattering ($\Gamma \to 0$) and whether $\Gamma = 0$ or $\Gamma \neq 0$ may also matter. In the ballistic limit ($\Gamma = 0$), the mesoscopic physics of the system size being finite ($1/L \neq 0$) or infinite ($1/L = 0$) seems to matter. The intervalley scattering being finite ($\Delta \neq 0$) or precisely zero ($\Delta \equiv 0$) seems to matter a great deal because the scaling theory of localization predicts radically different results for σ_D, $\sigma_D = 0$ for $\Delta \neq 0$, $\sigma_D = \infty$ for $\Delta = 0$, in the presence of any finite disorder ($\Gamma \neq 0$).

A great deal of the early discussion on the graphene minimum of conductivity problem has been misguided by the existing theoretical work which considered the strict $T = 0$ limit and then taking the $\omega \to 0$ limit. Many theories claim $\sigma_D = 4e^2/(\pi h)$ in this limit, but the typical

experimentally measured value is much larger (and sample dependent), leading to the so-called problem of the missing pi. The limit $\lim_{\omega \to 0} \sigma(\omega, T = 0)$ is, in fact, experimentally irrelevant since for experimental temperatures (even 10 mK), $k_B T \gg \hbar\omega$, and thus the appropriate limiting procedure for dc conductivity is $\lim_{T \to 0} \sigma(\omega = 0, T)$. There is an intuitive way of studying this limit theoretically, which, however, can only treat the ballistic (and therefore, the completely unrealistic disorder-free) limit. We first put $\omega = 0$ and assume $\mu = 0$, i.e., intrinsic graphene. It is then easy to show that at $T \neq 0$, there will be a finite carrier density $n_e = n_h \propto T^2$ thermally excited from the graphene valence band to the conduction band. The algebraic T^2 dependence of thermal carrier density, rather than the exponentially suppressed thermal occupancy in semiconductors, of course follows from the nonexistence of a band gap in graphene. Using the Drude formula for dc conductivity, we write $\sigma_D = ne^2\tau/m \propto T^2\tau(T)/m(T)$, where τ and m are, respectively, the relaxation time and the effective mass. Although the graphene effective mass is zero due to its linear dispersion, an effective definition of effective mass follows from writing $\epsilon = \hbar v_F k = (\hbar^2 k_F^2)/(2m)$, which leads to $m \propto \sqrt{n} \propto T$ (which vanishes as $T \to 0$) by using $k \propto \sqrt{n}$. This then leads to $\sigma_D \sim T\tau(T)$. In the ballistic limit, the only scattering mechanism is the electron-hole scattering, where the thermally excited electrons and holes scatter from each other due to mutual Coulomb interaction. This inelastic electron-hole scattering rate $1/\tau$ is given by the imaginary part of the self-energy which, to the leading order, is given by $1/\tau \sim T$, leading to $\sigma_D \sim T(1/T) \sim$ const in the ballistic limit. There are logarithmic subleading terms which indicate that $\sigma_D(T \to 0)$ grows logarithmically at low temperature in the ballistic limit. The conductivity in this picture, where interaction effects are crucial, is nonuniversal even in the ballistic limit, depending logarithmically on temperature and becoming infinite at $T = 0$. The presence of any finite impurity disorder modifies the whole picture completely. More details along this idea can be found in the literature (Foster and Aleiner, 2008, 2009; Fritz *et al.*, 2008; Kashuba, 2008; Müller *et al.*, 2008).

2. Localization

A fundamental mystery in graphene transport is the absence of any strong localization-induced insulating phase at low carrier density around the Dirac point, where $k_F l \ll 1$ since $k_F \approx 0$ at the charge neutrality point and the transport mean free path l is finite (and small). This is a manifest violation of the Ioffe-Reggel criterion which predicts strong localization for $k_F l \lesssim 1$. By contrast, 2D semiconductor systems always go insulating in the low-density regime. It is conceivable, but does not seem likely, that graphene may go insulating due to strong localization at lower temperatures. Until that happens, the absence of any signature of strong localization in graphene is a fundamental mystery deserving serious experimental attention. Two noteworthy aspects stand out in this context. First, no evidence of strong localization is observed in experiments that deliberately break the *A-B* sublattice symmetry (Chen, Cullen *et al.*, 2009). Thus, the absence of localization in graphene cannot be attributed to the chiral valley symmetry of the Dirac fermions. Second, the

opening of an intrinsic spectral gap in the graphene band structure by using graphene nanoribbons (Han *et al.*, 2007; Adam, Cho *et al.*, 2008) or biased BLG (Oostinga *et al.*, 2008; Zhang, Tang *et al.*, 2009) immediately introduces an insulating phase around the charge neutrality point. These two features indicate that the insulating behavior in graphene and 2D semiconductors is connected more with the existence of a spectral gap than with the quantum localization phenomena.

3. Zero-density limit

It is instructive to think about the intrinsic conductivity as the zero-density limit of the extrinsic conductivity for gated graphene. Starting with the Boltzmann theory high-density result of Sec. III, we see that

$$\sigma_D \equiv \sigma(n \to 0) = \begin{cases} 0 & \text{Coulomb scattering,} \\ C_i & \text{zero-range scattering,} \end{cases} \quad (4.1)$$

where the nonuniversal constant C_i is proportional to the strength of the short-range scattering in the system. We note that the vanishing of the Boltzmann conductivity in the intrinsic zero-density limit for Coulomb scattering is true for both unscreened and screened Coulomb impurities. The nonvanishing of graphene Boltzmann conductivity for zero-range δ function scattering potential in the zero carrier density intrinsic limit follows directly from the gapless linear dispersion of graphene carriers. We emphasize, however, that σ_D is nonuniversal for zero-range scattering.

For further insight into the zero-density Boltzmann limit $T = 0$ for σ, consider Eq. (3.3). In general, $\tau^{-1}(E) \sim D(E)$ since the availability of unoccupied states for scattering should be proportional to the density of states. This immediately shows that the intrinsic limit $E_F(n \to 0) \to 0$ is extremely delicate for graphene because $D(E \to 0) \to 0$, and the product $D\tau$ becomes ill defined at the Dirac point.

We emphasize in this context, as discussed in Sec. I, that as a function of carrier density (or gate voltage), graphene conductivity (at high carrier density) is qualitatively identical to that of semiconductor-based 2DEG. This point needs emphasis because it seems not to be appreciated much in the general graphene literature. In particular, $\sigma(n) \sim n^\alpha$ for both graphene and 2DEG with $\alpha = 1$ for graphene at intermediate density and $\alpha \approx 0.3$ to 1.5 in 2DEG depending on the semiconductor system. At a very high density, $\alpha \approx 0$ (or even negative) for both graphene and 2DEG. The precise nature of density dependence (i.e., value of the exponent α) depends strongly on the nature of scattering potential and screening, and varies in different materials with graphene ($\alpha \approx 1$) falling somewhere in the middle between Si-MOSFETs ($\alpha \approx 0.3$) and modulation doped 2D *n*-GaAs ($\alpha \approx 1.5$). Thus, from the perspective of high-density low-temperature transport properties, graphene is simply a rather low-mobility (comparable to Si-MOSFET, but much lower mobility than 2D GaAs) 2D semiconductor system.

4. Electron and hole puddles

The low-density physics in both graphene and 2D semiconductors is dominated by strong density inhomogeneity ("puddle") arising from the failure of screening. This

inhomogeneity is mostly due to the random distribution of unintentional quenched charged impurity centers in the environment. (In graphene, ripples associated with either intrinsic structural wrinkles or the substrate interface roughness may also make contribution to the inhomogeneity.) At low density, the inhomogeneous puddles control transport phenomena in graphene as well as in 2D semiconductors. Inhomogeneous puddles would also form in doped 3D semiconductors at low carrier densities (Shklovskii and Efros, 1984).

In Sec. IV.C we discuss the details of electron-hole-puddle formation in graphene around the charge neutrality point and describe its implications for graphene transport properties. Here we emphasize the qualitative difference between graphene and 2D semiconductors with respect to the formation of inhomogeneous puddles. In 2D semiconductors, depending on whether the system is electron doped or hole doped, there are only just electron or just hole puddles. At low density, $n \approx 0$, therefore most of the macroscopic sample has little finite carrier density except for the puddle regime. From the transport perspective, the system becomes the landscape of mountains and lakes for a boat negotiating a hilly lake. When percolation becomes impossible, the system becomes an insulator. In graphene, however, there is no gap at the Dirac point, and therefore, the electron (hole) lakes are hole (electron) mountains, and one can always have transport even at zero carrier density. This picture breaks down when a spectral gap is introduced, and gapped graphene should manifest an insulating behavior around the charge neutrality point as it indeed does experimentally.

5. Self-consistent theory

The physical puddle picture discussed above enables one to develop a simple theory for graphene transport at low densities using a self-consistent approximation where the graphene puddle density is calculated by considering the potential and density fluctuations induced by the charged impurities themselves. Such a theory was developed by Adam *et al.* (2007). The basic idea is to realize that at low carrier density $|n| < |n_i|$ the self-consistent screening adjustment between the impurities and the carriers could physically lead to an approximate pinning of the carrier density at $n = n^* \approx n_i$. A calculation within the RPA approximation yields (Adam *et al.*, 2007)

$$\frac{n^*}{n_{imp}} = 2r_s^2 C_0^{RPA}(r_s, a = 4d\sqrt{\pi n^*}), \qquad (4.2)$$

$$C_0^{RPA}(r_s, a) = -1 + \frac{4E_1(a)}{(2 + \pi r_s)^2} + \frac{2e^{-a}r_s}{1 + 2r_s}$$
$$+ (1 + 2r_s a)e^{2r_s a}(E_1[2r_s a]$$
$$- E_1[a(1 + 2r_s)]),$$

where $E_1(z) = \int_z^\infty t^{-1}e^{-t}dt$ is the exponential integral function. This density pinning then leads to an approximately constant minimum graphene conductivity which can be obtained from the high-density Boltzmann theory by putting in a carrier density of n^*. This simple intuitive self-consistent theory is found to be in surprisingly good agreement with all experimental observations (Adam *et al.*, 2007; Chen,

Jang, Adam *et al.*, 2008). In the next section we describe a more elaborate density functional theory and an effective medium approximation to calculate the puddle electronic structure and the resultant transport properties (Rossi and Das Sarma, 2008; Rossi *et al.*, 2009).

B. Quantum to classical crossover

The starting point for the quantum transport properties at the Dirac point discussed in Sec. II.C.1 is the ballistic universal minimum conductivity $\sigma_{min} = 4e^2/(\pi h)$ for clean graphene. The addition of disorder, i.e., including potential fluctuations [given by Eq. (2.10)] that are smooth on the scale of the lattice spacing *increases* the conductivity through weak antilocalization. This picture is in contrast to the semiclassical picture discussed above where the transport properties are calculated at high density using the Boltzmann transport theory and the self-consistent theory is used to handle the inhomogeneities of the carrier density around the Dirac point. This theory predicts that the conductivity *decreases* with increasing disorder strength. Given their vastly different starting points, it is perhaps not surprising that the two approaches disagree.

A direct comparison between the two approaches has not been possible mainly because the published predictions of the Boltzmann approach include screening of the Coulomb disorder potential; whereas, the fully quantum-mechanical calculations are for a noninteracting model using Gaussian disorder. Notwithstanding the fact that screening and Coulomb scattering play crucial roles in transport of real electrons through real graphene, the important question of the comparison between quantum and Boltzmann theories, even for Gaussian disorder, was addressed only recently by Adam, Brouwer, and Das Sarma (2009), where they considered noninteracting Dirac electrons at zero temperature with potential fluctuations of the form shown in Eq. (2.10). They numerically solved the full quantum problem for a sample of finite size $L \gg \xi$ [where ξ is the correlation length of the disorder potential in Eq. (2.10)], for a range of disorder strengths parametrized by K_0.[2]

Typical results for the quantum transport are shown in Fig. 26. For $L \lesssim \xi$, the transport is ballistic and the conductivity given by the universal value $\sigma_{min} = 4e^2/(\pi h)$. For $L \gg \xi$, one is in the diffusive transport regime. For the diffusive regime, Adam, Brouwer, Das Sarma (2009) demonstrated that away from the Dirac point, both the Boltzmann theory and the full quantum theory agree to leading order with

---

[2]Quantum effects are a small correction to the conductivity only if the carrier density n is increased at fixed sample size L. This is the experimentally relevant limit. If the limit $L \to \infty$ is taken at fixed n, quantum effects dominate [see Eq. (2.8)], where the semiclassical theory does not capture the logarithmic scaling of conductivity with system size. Here, we are not considering the conceptually simple question of how quantum transport becomes classical as the phase coherence length decreases, but the more interesting question of how this quantum-Boltzmann crossover depends on the carrier density and disorder strength.
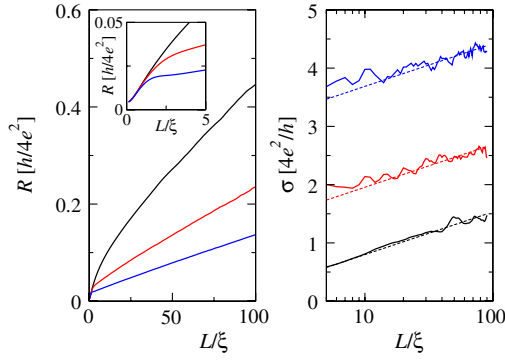
FIG. 26 (color online). Resistance $R = 1/G$ (left) and conductivity (right) obtained using $\sigma = [W dR/dL]^{-1}$ as a function of sample length L. The three curves shown are for $W/\xi = 200$, $K_0 = 2$, and $\pi n \xi^2 = 0$, 0.25, and 1 [from top to bottom (bottom to top) in left (right) panel]. Dashed lines in the right panel show $d\sigma/d \ln L = 4e^2/\pi h$. The inset in the left panel shows the crossover to diffusive transport ($L \gg \xi$).

$$\sigma(n) = \frac{2\sqrt{\pi}e^2}{K_0 h}[(2\pi n\xi^2)^{3/2} + \mathcal{O}(n\xi^2)^{1/2}]. \quad (4.3)$$

While this agreement is perhaps not surprising, it validates the assumptions of both theories and demonstrates that they are compatible at high carrier density. More interesting are the results at the Dirac point. Generalizing the self-consistent Boltzmann theory to the case of a Gaussian correlated disorder potential [Eq. (2.10)], one finds

$$\sigma_{\min}^{\text{SC}} = \frac{2e^2}{\pi h}\left(\exp\left[\frac{-K_0}{2\pi}\right]I_1\left[\frac{K_0}{2\pi}\right]\right)^{-1}, \quad (4.4)$$

where I_1 is the modified Bessel function. Shown in the left panel of Fig. 27 is a comparison of the numerical fully quantum Dirac point conductivity where the weak antilocalization correction has been subtracted $\sigma' = \lim_{L\to\infty}[\sigma(L) - \pi^{-1}\ln(L/\xi)]$ with the semiclassical result [Eq. (4.4)].

The right panel shows the conductivity slightly away from the Dirac point (i.e., at the edge of the minimum conductivity plateau). The numerical calculations at the edge of the plateau are in good quantitative agreement with the self-consistent Boltzmann theory. At the Dirac point, however, the quantum conductivity $\sigma(K_0)$ is found to increase with K_0 for the entire
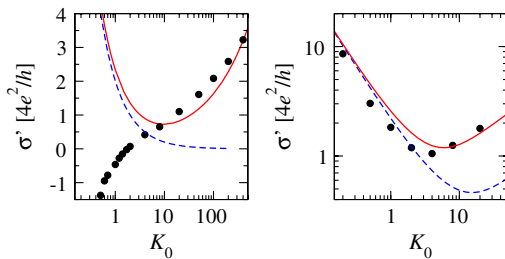

FIG. 27 (color online). Semiclassical conductivity $\sigma' = \lim_{L\to\infty}[\sigma(L) - \pi^{-1}\ln(L/\xi)]$ vs disorder strength at the Dirac point (left) and at carrier density $\pi n = K_0/(\pi\xi)^2$, corresponding to the edge of the minimum conductivity plateau of Adam *et al.* (2007) (right). Data points are from the numerical calculation for $L = 50\xi$ and the (solid) dashed curves represent the (self-consistent) Boltzmann theory. Adapted from Adam, Brouwer, and Das Sarma, 2009.

parameter range considered, which differs from the Boltzmann theory at small K_0. At large K_0, the numerical data follow the trend of the self-consistent theory which predicts $\sigma \sim 2e^2 K_0^{1/2}/(\pi h)$ for $K_0 \gg 10$. This implies that even at the Dirac point, for large enough disorder, the transport is semiclassical and described by the self-consistent Boltzmann transport theory.

For smaller K_0, Fig. 27 shows that upon reducing K_0 below unity, the conductivity first decreases sharply consistent with a renormalization of the mean free path due to the ultraviolet logarithmic divergences discussed in Sec. II.C.4. Upon reducing K_0 further, the Dirac point conductivity saturates at the ballistic value $\sigma_{\min} = 4e^2/\pi h$ (discussed in Sec. II.B.2).

In a closely related work, Lewenkopf *et al.* (2008) numerically simulated a tight-binding model to obtain the conductivity and shot noise of graphene at the Dirac point using a recursive Green's function method. This method was then generalized to calculate the metal-insulator transition in graphene nanoribbons where, as discussed in Sec. II C 2, edge disorder can cause the Anderson localization of electrons (Mucciolo *et al.*, 2009).

The important conclusion of this section is that it provides the criteria for when one needs a full quantum-mechanical solution and when the semiclassical treatment is sufficient. For either sufficiently weak disorder or when the source and drain electrodes are closer than the scattering mean free path, then the quantum nature of the carriers dominates the transport. On the other hand, for sufficiently large disorder, or away from the Dirac point, the electronic transport properties of graphene are semiclassical and the Boltzmann theory correctly captures the most of graphene's transport properties.

C. Ground state in the presence of long-range disorder

In the presence of long-range disorder that does not mix the degenerate valleys, the physics of the graphene fermionic excitations is described by the following Hamiltonian:

$$\mathcal{H} = \int d^2r \Psi_{\mathbf{r}\alpha}^\dagger[-i\hbar v_F \boldsymbol{\sigma}_{\alpha\beta} \cdot \nabla_{\mathbf{r}} - \mu \mathbf{1}]\Psi_{\mathbf{r}\beta}$$
$$+ \frac{e^2}{2\kappa}\int d^2r d^2r' \Psi_{\mathbf{r}\alpha}^\dagger \Psi_{\mathbf{r}\alpha} V(|\mathbf{r}-\mathbf{r}'|)\Psi_{\mathbf{r}'\beta}^\dagger \Psi_{\mathbf{r}'\beta}$$
$$+ \frac{e^2}{2\kappa}\int d^2r V_D(\mathbf{r})\Psi_{\mathbf{r}\alpha}^\dagger \Psi_{\mathbf{r}\alpha}, \quad (4.5)$$

where v_F is the bare Fermi velocity, $\Psi_{\mathbf{r}\alpha}^\dagger$, $\Psi_{\mathbf{r}\alpha}$ are the creation annihilation spinor operators for a fermionic excitation at position $\mathbf{r}$ and pseudospin α, $\boldsymbol{\sigma}$ is the 2D vector formed by the 2×2 Pauli matrices σ_x and σ_y acting in pseudospin space, μ is the chemical potential, $\mathbf{1}$ is the 2×2 identity matrix, κ is the effective static dielectric constant equal to the average of the dielectric constants of the materials surrounding the graphene layer, $V(|\mathbf{r}-\mathbf{r}'|) = 1/||\mathbf{r}-\mathbf{r}'|$ is the Coulomb interaction, and $V_D(\mathbf{r})$ is the bare disorder potential. The Hamiltonian (4.5) is valid as long as the energy of the fermionic excitations is much lower than the graphene bandwidth ≈ 3 eV. Using (4.5), if we know V_D, we can characterize the ground-state carrier density probability close to the Dirac point. In this section we focus on the case when V_D is a disorder potential whose spatial autocorrelation

decays algebraically, such as the disorder induced by ripples or charge impurities.

1. Screening of a single charge impurity

The problem of screening at the Dirac point of a single impurity with charge Ze placed in (or close to) the graphene layer illustrates some of the unique features of the screening properties of massless Dirac fermions. In addition the problem provides a condensed matter realization of the QED phenomenon of ''vacuum polarization'' induced by an external charge (Darwin, 1928; Gordon, 1928; Pomeranchuk and Smorodinsky, 1945; Case, 1950; Zeldovich and Popov, 1972). In the context of graphene the problem was first studied by DiVincenzo and Mele (1984) and recently more in detail by several others (Biswas *et al.*, 2007; Fistul and Efetov, 2007; Fogler *et al.*, 2007; Novikov, 2007b; Pereira *et al.*, 2007; Shytov *et al.*, 2007a, 2007b; Terekhov *et al.*, 2008). The parameter $\beta \equiv Ze^2/(\kappa \hbar v_f) = Zr_s$ quantifies the strength of the coupling between the Coulomb impurity and the massless Dirac fermions in the graphene layer. Neglecting *e-e* interactions for $|\beta| < 1/2$ the Coulomb impurity induces a screening charge that is localized on length scales of the order of the size of the impurity itself (or its distance d from the graphene layer). Even in the limit $|\beta| < 1/2$ the inclusion of the *e-e* interactions induces a long-range tail in the screening charge with sign equal to the sign of the charge impurity (Biswas *et al.*, 2007). For $|\beta| > 1/2$, the Coulomb charge is supercritical, the induced potential is singular (Landau and Lifshitz, 1977), and the solution of the problem depends on the regularization of the wave function at the site of the impurity, $r \to 0$. By setting the wave function to be zero at $r = a$, the induced electron density in addition to a localized $[\delta(\mathbf{r})]$ term, acquires a long-range tail $\sim 1/r^2$ (with sign opposite to the sign of the charge impurity) (Novikov, 2007a; Pereira *et al.*, 2007; Shytov *et al.*, 2007b) and marked resonances appear in the spectral density (Fistul and Efetov, 2007; Shytov *et al.*, 2007a) that should also induce clear signatures in the transport coefficients. Up until now, neither the oscillations in the local density of states nor the predicted signatures in the conductivity (Shytov *et al.*, 2007a) have been observed experimentally. It is likely that in the experiments so far the supercritical regime $|\beta| > 1/2$ has not been reached because of the low Z of the bare charge impurities and renormalization effects. Fogler *et al.* (2007) pointed out, however, that the predicted effects for $|\beta| > 1/2$ are intrinsic to the massless Dirac fermion model that however is inadequate when the small scale cutoff min$[d, a]$ is smaller than $ar_s\sqrt{Z}$.

2. Density functional theory

Assuming that the ground state does not have long-range order (Peres *et al.*, 2005; Dahal *et al.*, 2006; Min, Borghi *et al.*, 2008), a practical and accurate approach to calculate the ground state of many-body problems is the density functional theory (DFT) (Hohenberg and Kohn, 1964; Kohn and Sham, 1965; Kohn, 1999; Giuliani and Vignale, 2005). In this approach the interaction term in the Hamiltonian is replaced by an effective Kohn-Sham (KS) potential V_{KS} that is a functional of the ground-state density $n(\mathbf{r}) = \sum_\sigma \Psi_{\mathbf{r}\sigma}^\dagger \Psi_{\mathbf{r}\sigma}$:

$$\mathcal{H} = \int d^2 r \Psi_{\mathbf{r}\alpha}^\dagger [-i\hbar v_F \sigma_{\alpha\beta} \cdot \nabla_\mathbf{r} - \mu \mathbf{1}]\Psi_{\mathbf{r}\beta}$$
$$+ \int d^2 r \Psi_{\mathbf{r}\alpha}^\dagger V_{KS}[n(\mathbf{r})]\Psi_{\mathbf{r}\alpha}. \tag{4.6}$$

The Kohn-Sham potential is given by the sum of the external potential, the Hartree part of the interaction V_H and an exchange-correlation potential V_{xc} that can only be known approximately. In its original form V_{xc} is calculated within the local density approximation (LDA) (Kohn and Sham, 1965), i.e., V_{xc} is calculated for a uniform liquid of electrons. The DFT-LDA approach can be justified and applied to the study of interacting massless Dirac fermions (Polini, Tomadin *et al.*, 2008). For graphene, the LDA exchange-correlation potential within the RPA approximation is given with very good accuracy by the following expression (González *et al.*, 1999; Katsnelson, 2006; Barlas *et al.*, 2007; Hwang *et al.*, 2007a; Mishchenko, 2007; Vafek, 2007; Polini, Tomadin *et al.*, 2008):

$$V_{xc}(n) = + \frac{r_s}{4}\sqrt{\pi|n|}\text{sgn}(n)\ln\frac{4k_c}{\sqrt{4\pi n}}$$
$$- \frac{gr_s^2\xi(gr_s)}{4}\sqrt{\pi|n|}\text{sgn}(n)\ln\frac{4k_c}{\sqrt{4\pi n}}, \tag{4.7}$$

where g is the spin and valley degeneracy factor ($g = 4$), and k_c is an ultraviolet wave-vector cutoff, fixed by the range of energies over which the pure Dirac model is valid. Without loss of generality, we can use $k_c = 1/a$, where a is the graphene lattice constant, corresponding to an energy cutoff $E_c \approx 3$ eV. Equation (4.7) is valid for $k_F = \sqrt{\pi|n|} \ll k_c$. In Eq. (4.7) ξ is a constant that depends on r_s given by (Polini, Tomadin *et al.*, 2008)

$$\xi(gr_s) = \frac{1}{2}\int_0^{+\infty} \frac{dx}{(1 + x^2)^2(\sqrt{1 + x^2} + \pi gr_s/8)}. \tag{4.8}$$

The terms on the r.h.s. of (4.7) are the exchange and correlation potential, respectively. Note that the exchange and correlation potentials have opposite signs. In Fig. 28 the exchange and correlation potentials and their sum V_{xc} are plotted as a function of n for $r_s = 0.5$. We see that in graphene the correlation potential is smaller than the exchange potential but, contrary to the case of regular parabolic-band 2DEGs, is not negligible. However, from Eq. (4.7) we have that exchange and correlation scale with n in the same way. As a consequence in graphene, the correlation potential can effectively be taken into account by simply rescaling the coefficient of the exchange potential. In Fig. 28 the dotted line shows V_{xc} for a regular parabolic-band 2DEG with effective mass $0.067m_e$ in a background with $\kappa = 4$. The important qualitative difference is that V_{xc} in graphene has the opposite sign than in regular 2DEGs: due to interlayer processes in graphene the exchange-correlation potential penalizes density inhomogeneities contrary to what happens in parabolic-band electron liquids.

Using the DFT-LDA approach, Polini, Tomadin *et al.* (2008) calculated the graphene ground-state carrier density for single disorder realizations of charge impurities and small samples (up to 10×10 nm). The size of the samples is limited by the high computational cost of the approach. For
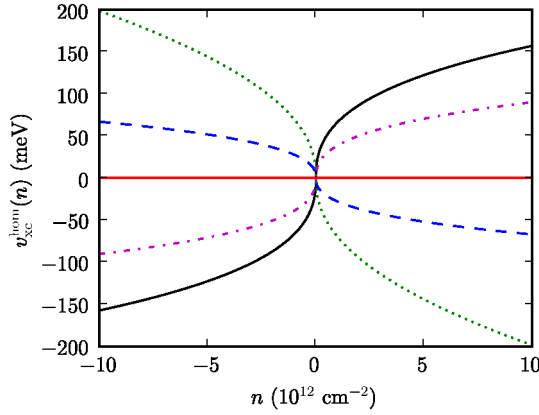
FIG. 28 (color online). Exchange, solid line, and RPA correlation potentials, dashed line, as functions of the density n for $r_s = 0.5$. The dash-dotted line shows the full exchange-correlation potential V_{xc}. The dotted line is the quantum Monte Carlo exchange-correlation potential of a standard parabolic-band 2D electron gas (Attaccalite *et al.*, 2002) with effective mass $0.067m_e$ placed in background with dielectric constant 4. Adapted from Polini, Tomadin *et al.*, 2008.

single disorder realizations, the results of Polini, Tomadin *et al.* (2008) showed that, as predicted (Hwang *et al.*, 2007a), at the Dirac point the carrier density breaks up in electron-hole puddles and that the exchange-correlation potential suppresses the amplitude of the disorder-induced density fluctuations. Given its computational cost, the DFT-LDA approach does not allow the calculation of disordered averaged quantities.

3. Thomas-Fermi-Dirac theory

An approach similar in spirit to the LDA-DFT is the Thomas-Fermi theory (Fermi, 1927; Thomas, 1927; Spruch, 1991; Giuliani and Vignale, 2005). Like DFT, the TF theory is a density functional theory: in the Thomas-Fermi theory the kinetic term is also approximated via a functional of the local density $n(\mathbf{r})$. By Thomas-Fermi-Dirac (TFD) theory, we refer to a modification of the TF theory in which the kinetic functional has the form appropriate for Dirac electrons and in which exchange-correlation terms are included via the exchange-correlation potential proper for Dirac electron liquids as described above for the DFT-LDA theory. The TF theory relies on the fact that if the carrier density varies slowly in space compared to the Fermi wavelength, then the kinetic energy of a small volume with density $n(\mathbf{r})$ is equal, with good approximation, to the kinetic energy of the same volume of a homogeneous electron liquid with density $n = n(\mathbf{r})$. The condition for the validity of the TFD theory is given by the following inequality (Giuliani and Vignale, 2005; Brey and Fertig, 2009b):

$$\frac{|\nabla_{\mathbf{r}} n(\mathbf{r})|}{n(\mathbf{r})} \ll k_F(\mathbf{r}). \tag{4.9}$$

Whenever inequality (4.9) is satisfied, the TFD theory is a computationally efficient alternative to the DFT-LDA approach to calculate the ground-state properties of graphene in presence of disorder. The energy functional $E[n]$ in the TFD theory is given by

$$E[n] = \hbar v_F \left[\frac{2\sqrt{\pi}}{3} \int d^2 r \, \mathrm{sgn}(n) |n|^{3/2} \right.$$
$$+ \frac{r_s}{2} \int d^2 r \int d^2 r' \frac{n(\mathbf{r}) n(\mathbf{r}')}{|\mathbf{r} - \mathbf{r}'|} + \int d^2 r V_{xc}[n(\mathbf{r})] n(\mathbf{r})$$
$$\left. + r_s \int d^2 r V_D(\mathbf{r}) n(\mathbf{r}) - \frac{\mu}{\hbar v_F} \int d^2 r \, n(\mathbf{r}) \right], \tag{4.10}$$

where the first term is the kinetic energy, the second is the Hartree part of the Coulomb interaction, the third is the term due to exchange and correlation, and the fourth is the term due to disorder. The expression for the exchange-correlation potential is given in Eq. (4.7). The carrier ground-state distribution is then calculated by minimizing $E[n]$ with respect to n. Using (4.10), the condition $\delta E/\delta n = 0$ requires

$$\mathrm{sgn}(n)\sqrt{|\pi n|} + \frac{r_s}{2} \int d^2 r \frac{n(\mathbf{r}')}{|\mathbf{r} - \mathbf{r}'|} + V_{xc}[n(\mathbf{r})]$$
$$+ r_s V_D(\mathbf{r}) - \frac{\mu}{\hbar v_F} = 0. \tag{4.11}$$

Equation (4.11) well exemplifies the nonlinear nature of screening in graphene close to the Dirac point: because in graphene, due to the linear dispersion, the kinetic energy per carrier, the first term in (4.11), scales with $\sqrt{n}$ when $\langle n \rangle = 0$ the relation between the density fluctuations δn and the external disorder potential is not linear even when exchange and correlation terms are neglected.

We now consider the case when the disorder potential is due to random Coulomb impurities. In general the charge impurities will be a 3D distribution $C(\mathbf{r})$, however we can assume to a very good approximation $C(\mathbf{r})$ to be effectively 2D. The reason is that for normal substrates such as SiO_2, the charge traps migrate to the surface of the oxide; moreover, any additional impurity charge introduced during the graphene fabrication will be located either on the graphene top surface or trapped between the graphene layer and the substrate. We then assume $C(\mathbf{r})$ to be an effective 2D random distribution located at the average distance d from the graphene layer. An important advantage of this approach is that it limits the number of unknown parameters that enter the theory to two: charge impurity density n_{imp} and d. With this assumption, we have

$$V_D(\mathbf{r}) = \int d\mathbf{r}' \frac{C(\mathbf{r}')}{[|\mathbf{r} - \mathbf{r}'|^2 + d^2]^{1/2}}. \tag{4.12}$$

The correlation properties of the distribution $C(\mathbf{r})$ of the charge impurities are a matter of long-standing debate in the semiconductor community. Because the impurities are charged, one would expect the positions of the impurities to have some correlation; on the other hand, the impurities are quenched (not annealed), they are either imbedded in the substrate or between the substrate and the graphene layer or in the graphene itself. This fact makes it very difficult to know the precise correlation of the charge impurity positions, but it also ensures that to good approximation the impurity positions can be assumed to be uncorrelated:

$$\langle C(\mathbf{r}) \rangle = 0, \quad \langle C(\mathbf{r}_1) C(\mathbf{r}_2) \rangle = n_{imp} \delta(\mathbf{r}_2 - \mathbf{r}_1), \tag{4.13}$$

where the angular brackets denote averaging over disorder realizations. A nonzero value of $\langle C(\mathbf{r}) \rangle$ can be taken into

account simply by a shift of the chemical potential μ. It is easy to generalize the theory to correlated impurities (e.g., impurity clusters) if the correlation function is known.

The parameters n_{imp} and d that enter the theory are reliably fixed by the transport results (see Sec. III.A) at high doping. Transport results at high density indicate that d is of the order of 1 nm; whereas, n_{imp} varies depending on the sample quality but in general is in the range $n_{\mathrm{imp}} = 10^{10}$–$10^{12}$ cm^{-2}, where the lowest limit applies to suspended graphene. The distance d is the physical cutoff for the length scale of the carrier density inhomogeneities. Therefore, to solve Eq. (4.11) numerically, one can use a spatial discretization with unit step of the order of d. For the TFD results presented below, it was assumed $d = 1$ nm and therefore a spatial step $\Delta x = \Delta y = 1$ nm was used.

Figure 29 shows the TFD results for the carrier density distribution at the Dirac point in the presence of charge impurity disorder for a single disorder realization with $n_{\mathrm{imp}} = 10^{12}$ cm^{-2} and $\kappa = 2.5$ corresponding to graphene on SiO$_2$ with the top surface in vacuum (or air). It is immediately clear that as predicted (Hwang *et al.*, 2007a), close to the Dirac point the disorder induced by the charge impurities breaks up the carrier distribution in electron ($n > 0$) and hole ($n < 0$) puddles. The electron-hole puddles are separated by disorder-induced *p-n* junctions (PNJ). Apart from the PNJ, the carrier density is locally always different from zero even though the average density $\langle n \rangle$ is set equal to zero. For this reason, in the presence of disorder it is more correct to refer to the value of the gate voltage for which $\langle n \rangle = 0$ as the charge neutrality point (CNP) rather than Dirac point: the presence of long-range disorder prevents the probing of the physical properties of the Dirac point, i.e., of intrinsic graphene with exactly half filling, zero density, everywhere. The important qualitative results that can be observed even for a single disorder by comparing the results of Figs. 29(b) and 29(c) is that the
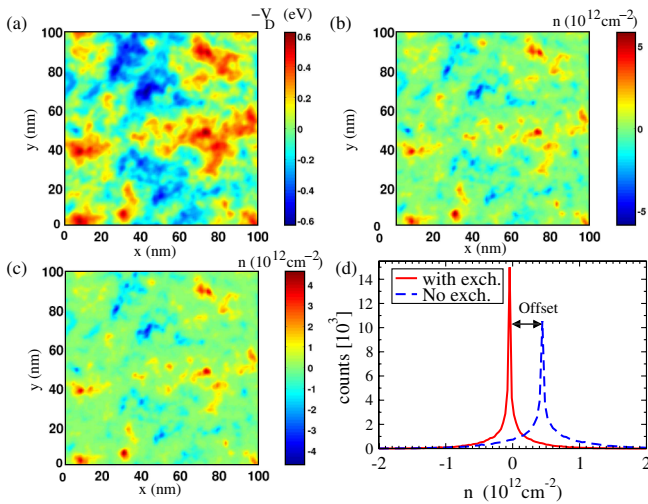
exchange-correlation term suppresses the amplitude of the density fluctuations. This fact is clearly visible in Fig. 29(d) from which we can see that in the presence of exchange correlation the density distribution is much narrower and more peaked around zero. This result, also observed in the DFT-LDA results (Polini, Tomadin *et al.*, 2008), is a consequence of the the fact that as discussed in Sec. IV.C.2 the exchange-correlation potential in graphene, contrary to parabolic-band Fermi liquids, penalizes density inhomogeneities.

In the presence of disorder, in order to make quantitative predictions verifiable experimentally it is necessary to calculate disordered averaged quantities. Using TFD, both the disorder average $\langle X \rangle$ of a given quantity X and its spatial correlation function

$$\delta X^2(\mathbf{r}) \equiv \langle [X(\mathbf{r}) - \langle X \rangle][X(0) - \langle X \rangle] \rangle \qquad (4.14)$$

can be efficiently calculated. For conditions typical in experiments, 500 disorder realizations are sufficient. From $\delta X^2(\mathbf{r})$, one can extract the following quantities:

$$X_{\mathrm{rms}} \equiv \sqrt{\langle [\delta X(0)]^2 \rangle}, \qquad \xi_X \equiv \text{FWHM of } \langle [\delta X(\mathbf{r})]^2 \rangle, \qquad (4.15)$$

respectively the root mean square and the typical spatial correlation of the fluctuations of X. Using the TFD theory, both the spatial correlation function of the screened potential V_{sc} and carrier density are found to decay at long distance as $1/r^3$. This is a consequence of the weak screening properties of graphene and was pointed out by Adam *et al.* (2007) and Galitski *et al.* (2007). From the spatial correlation functions, n_{rms} and $\xi \equiv \xi_n$ are extracted. Figures 30(a) and 30(b) show the calculated n_{rms} and ξ at the Dirac point as a function of n_{imp}. The disorder averaged results show the effect of the exchange-correlation potential in suppressing the amplitude of the density inhomogeneities n_{rms}, and in slightly increasing

FIG. 29 (color online). TFD results as a function of position for a single disorder realization with $\kappa = 2.5$, $d = 1$ nm, and $n_{\mathrm{imp}} = 10^{12}$ cm^{-2}. (a) Bare disorder potential V_D. (b) Carrier density obtained neglecting exchange-correlation terms. (c) Carrier density obtained including exchange-correlation terms. (d) Probability density distribution at the CNP with exchange (solid line) and without (dashed line). Adapted from Rossi and Das Sarma, 2008.

FIG. 30 (color online). TFD disorder averaged results for $\kappa = 2.5$. The solid (dashed) lines show the results obtained including (neglecting) exchange and correlation terms (a) n_{rms} and (b) ξ as a function of n_{imp}. (c) Area A_0 over which $|n(\mathbf{r}) - \langle n \rangle| < n_{\mathrm{rms}}/10$. (d) Average excess charge δQ vs n_{imp}. Adapted from Rossi and Das Sarma, 2008.

their correlation length. The effect of the exchange-correlation potential increases as n_{imp} decreases. At the Dirac point, the quantity ξ can be interpreted as the effective nonlinear screening length. Figure 30 shows that ξ depends weakly on n_{imp}. The reason is that ξ only characterizes the spatial correlation of the regions in which the density is relatively high. If a puddle is defined as a continuous region with same sign charges, then at the CNP the puddles have always a size of the same order of the system size. Inside the puddles there are small areas with high density and size ξ of the order of tens of nanometers for typical experimental conditions, much smaller than the system size L.

This picture is confirmed in Fig. 30(c) in which the disorder averaged area fraction A_0 over which $|n(\mathbf{r}) - \langle n \rangle| < n_{rms}/10$ is plotted as a function of n_{imp}. As n_{imp} decreases A_0 increases reaching more than $1/3$ at the lowest impurity densities. The fraction of area over which $|n(\mathbf{r}) - \langle n \rangle|$ is less than $1/5$ of n_{rms} surpasses 50% for $n_{imp} \lesssim 10^{10}$ cm^{-2}. Figure 30(b) shows the average excess charge $\delta Q \equiv n_{rms} \pi \xi^2$ at the Dirac point as a function of n_{imp}. Note that as defined δQ, especially at low n_{imp}, grossly underestimates the number of charges both in the electron puddles and in the small regions of size ξ. This is because in the regions of size ξ the density is much higher than n_{rms} whereas the electron-hole puddles have a typical size much larger than ξ. Using the estimate $|\nabla n(\mathbf{r})|/n = 1/\xi$ for the small regions and the local value of n inside the regions and, for the electron-hole puddles the estimates

$$n \approx n_{rms}, \qquad |\nabla n(\mathbf{r})| \approx \frac{n_{rms}}{L}, \tag{4.16}$$

we find that the inequality (4.9) is satisfied guaranteeing the validity of the TFD theory even at the Dirac point.

As we move away from the Dirac point more of the area is covered by electron (hole) puddles. However, the density fluctuations remain large even for relatively large values of V_g. This is evident from Fig. 31 where the probability distribution $P(n)$ of the density for different values of $\langle n \rangle$ is shown in Fig. 31(a) and the ratio $n_{rms}/\langle n \rangle$ as a function of $\langle n \rangle$ is shown in Fig. 31(b). The probability distribution $P(n)$ is non-Gaussian (Adam *et al.*, 2007; Galitski *et al.*, 2007; Adam, Hwang *et al.*, 2009). For density $\langle n \rangle \lesssim n_{imp}$, $P(n)$ does not exhibit a single peak around $\langle n \rangle$ but rather a bimodal structure
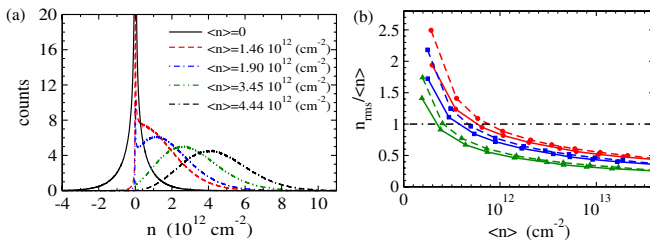

FIG. 31 (color online). (a) Density distribution averaged over disorder for different values of the applied gate voltage assuming $\kappa = 2.5$, $d = 1$ nm and $n_{imp} = 10^{12}$ cm^{-2}. (b) $n_{rms}/\langle n \rangle$ as a function of $\langle n \rangle$ for $d = 1$ nm and different values of n_{imp}: circles, $n_{imp} = 1.5 \times 10^{12}$ cm^{-2}; squares, $n_{imp} = 10^{12}$ cm^{-2}; triangles, $n_{imp} = 5 \times 10^{11}$ cm^{-2}. In (b) the solid (dashed) lines show the results with (without) exchange and correlation terms. Adapted from Rossi and Das Sarma, 2008.

with a strong and narrow peak around zero. The double peak structure for finite V_g provides direct evidence for the existance of puddles over a finite voltage range.

$n_{rms}/\langle n \rangle$ decreases with $\langle n \rangle$, a trend that is expected and that has been observed indirectly in experiments by measuring the inhomogenous broadening of the quasiparticle spectral function (Hong *et al.*, 2009).

In the limit $r_s \ll 1$ it is possible to obtain analytical results using the TFD approach (Fogler, 2009). The first step is to separate the inhomogeneities of the carrier density and screened potential in slow, $\bar{n}$, $\bar{V}_{sc}$, and fast components, δn, δV_{sc}:

$$n(\mathbf{r}) = \bar{n}(\mathbf{r}) + \delta n(\mathbf{r}), \qquad V_{sc}(\mathbf{r}) = \bar{V}_{sc}(\mathbf{r}) + \delta V_{sc}(\mathbf{r}), \tag{4.17}$$

where $\bar{n}$ and $\bar{V}_{sc}$ contain only Fourier harmonics with $k < \Lambda$ where $1/\Lambda$ is the spatial scale below which the spatial variation of n, and V_{sc} are irrelevant for the physical properties measured. For imaging experiments, $1/\Lambda$ is the spatial resolution of the scanning tip and for transport experiments $1/\Lambda$ is of the order of the mean free path. Let $l_{imp} \equiv 1/2r_s\sqrt{n_{imp}}$ and R is the nonlinear screening length. It is assumed that $l_{imp} \lesssim 1/\Lambda \ll R$. With these assumptions and neglecting exchange-correlation terms, from the TFD functional in the limit $\Lambda \ll k_F$ and small nonlinear screening terms compared to the kinetic energy term it follows (Fogler, 2009)

$$\bar{n}(\bar{V}_{sc}) \simeq -\frac{\bar{V}_{sc}|\bar{V}_{sc}|}{\pi(\hbar v)^2} - \frac{\text{sgn}(\bar{V}_{sc})}{2\ell^2} \ln\frac{|\bar{V}_{sc}|}{\hbar v \Lambda}, \tag{4.18}$$

$$|\bar{V}_{sc}| \gg \hbar v \Lambda,$$

with $\bar{V}_{sc}$ given, in momentum space, by

$$\bar{V}_{sc}(\mathbf{k}) = V_D(\mathbf{k}) + \frac{2\pi r_s \hbar v_F}{k} n(\mathbf{k}), \tag{4.19}$$

where we have assumed for simplicity $d = 0$. Equation (4.19) can be approximated by the following asymptotic expressions:

$$\bar{V}_{sc}(\mathbf{k}) = \begin{cases} V_D(\mathbf{k}), & kR \gg 1, \\ V_D(\mathbf{k})\frac{kR}{1+kR}, & kR \ll 1. \end{cases} \tag{4.20}$$

Equations (4.18) and (4.19) define a nonlinear problem that must be solved self-consistently and that in general can only be solved numerically. However, in the limit $r_s \ll 1$ an approximate solution with logarithmic accuracy can be found. Let K_0 be the solution of

$$K_0 = \ln[1/(4r_s K_0)]. \tag{4.21}$$

K_0 is the expansion parameter. To order $\mathcal{O}(K_0^{-1})$, $\bar{V}_{sc}$ can be treated as a Gaussian random potential whose correlator $\delta V_{sc}^2(r)$ can be calculated using Eq. (4.20) to find (Adam *et al.*, 2007; Galitski *et al.*, 2007; Fogler, 2009)

$$K(r) \equiv \delta \bar{V}_{sc}^2(r)$$

$$= \frac{\pi}{2}\left(\frac{\hbar v}{\ell_{imp}}\right)^2 \times \begin{cases} \ln\left(\frac{R}{r}\right), & l_{imp} \ll r \ll R, \\ 2\left(\frac{R}{r}\right)^3, & R \ll r, \end{cases} \tag{4.22}$$

with $R = 1/(4r_sK_0)$. Using Eqs. (4.22) and (4.18) we can find the correlation function for the carrier density (Fogler, 2009):

$$\delta\bar{n}^2(r) = \frac{K_0^2}{2\pi l^4}\left\{3\frac{K(r)}{K(l)}\sqrt{1 - \left(\frac{K(r)}{K(l)}\right)^2} + \left[1 + 2\left(\frac{K(r)}{K(l)}\right)^2\right]\arcsin\frac{K(r)}{K(l)}\right\}. \quad (4.23)$$

The correlation functions given by Eqs. (4.22) and (4.23) are valid in the limit $r_s \ll 1$ but are in qualitative agreement also with the numerical results obtained for $r_s \approx 1$ (Rossi and Das Sarma, 2008).

The location of the disorder-induced PNJ is identified by the isolines $n(\mathbf{r}) = 0$, or equivalently $V_{sc}(\mathbf{r}) = 0$. The CNP corresponds to the "percolation" threshold in which exactly half of the sample is covered by electron puddles and half by hole puddles (note that conventionally the percolation threshold is defined as the condition in which half of the sample has nonzero charge density and half is insulating and so the term percolation in the context of the graphene CNP has a slight different meaning and does not imply that the transport is percolative). At the percolation threshold, all but one PNJ are closed loops. Over length scales d such that $1/\Lambda \ll d \ll R$, V_{sc} is logarithmically rough [Eq. (4.22)] and so the PNJ loops of diameter d have fractal dimension $D_h = 3/2$ (Kondev *et al.*, 2000). At larger d the spatial correlation of V_{sc} decays rapidly [Eq. (4.22)] so that for d larger than R, D_h crosses over to the standard uncorrelated percolation exponent of $7/4$ (Isichenko, 1992).

4. Effect of ripples on carrier density distribution

When placed on a substrate, graphene has been shown (Ishigami *et al.*, 2007; Geringer *et al.*, 2009) to follow with good approximation the surface profile of the substrate, and therefore, it has been shown to have a finite roughness. For graphene on SiO_2, the standard deviation of the graphene height h has been measured to be $\delta h \approx 0.19$ nm with a roughness exponent $2H \approx 1$. More recent experiments (Geringer *et al.*, 2009) have found larger roughness. Even when suspended, graphene is never completely flat, and it has been shown theoretically to possess intrinsic ripples (Fasolino *et al.*, 2007). A local variation of the height profile $h(\mathbf{r})$ can induce a local change of the carrier density through different mechanisms. de Juan *et al.* (2007) considered the change in carrier density due to a local variation of the Fermi velocity due to the rippling and found that assuming $h(\mathbf{r}) = A\exp(-|\mathbf{r}|^2/b^2)$, a variation of 1% and 10% in the carrier density was induced for ratios A/b of order 0.1 and 0.3, respectively. Brey and Palacios (2008) observed that local Fermi velocity changes induced by the curvature associated with the ripples induce charge inhomogeneities in doped graphene but cannot explain the existence of electron-hole puddles in undoped graphene for which the particle-hole symmetry is preserved, and then considered the effect on the local carrier density of a local variation of the exchange energy associated with the local change of the density of carbon atoms due to the presence of ripples. They found that a modulation of the out-of-plane position of the carbon atoms of the order of 1–2 nm over a distance of 10–20 nm induces a modulation in the charge density of the order of 10^{11} cm^2.

Kim and Castro Neto (2008) considered the effect due to the rehybridization of the π and σ orbital between nearest neighbor sites. For the local shift δE_F of the Fermi level, Kim and Castro Neto (2008) found

$$\delta E_F = -\alpha\frac{3a^2}{4}(\nabla^2 h)^2, \quad (4.24)$$

where α is a constant estimated to be approximately equal to 9.23 eV. Recently, Gibertini *et al.* (2010) used the DFT-LDA to study the effect of ripples on the spatial carrier density fluctuations. Transport theories in the presence of topological disorder were considered by Cortijo and Vomediano (2007), Herbut *et al.* (2008), and Cortijo and Vozmediano (2009).

5. Imaging experiments at the Dirac point

The first imaging experiments using STM were done on epitaxial graphene (Brar *et al.*, 2007; Rutter *et al.*, 2007). These experiments were able to image the atomic structure of graphene and reveal the presence of in-plane short-range defects. So far, one limitation of experiments on epitaxial graphene has been the inability to modify the graphene intrinsic doping that is relatively high ($\gtrsim 10^{12}$ cm^{-2}) in most of the samples. This fact has prevented these experiments to directly image the electronic structure of graphene close to the Dirac point. The first scanning probe experiment on exfoliated graphene on SiO_2 (Ishigami *et al.*, 2007) revealed the atomic structure of graphene and the nanoscale morphology. The first experiment that was able to directly image the electronic structure of exfoliated graphene close to the Dirac point was performed by Martin *et al.* (2007) using scanning single-electron transistor (SET), Fig. 32. The breakup of the density landscape in electron-hole puddles as predicted by Adam *et al.* (2007) and Hwang *et al.* (2007a), and shown by the DFT-LDA (Polini, Tomadin *et al.*, 2008), and TFD theory (Rossi and Das Sarma, 2008) is clearly visible.

The result shown in Fig. 32(a), however, does not provide a good quantitative characterization of the carrier density distribution due to the limited spatial resolution of the imaging technique: the diameter of the SET is 100 nm and the distance between the SET and the sample is 50 nm, so the spatial resolution is approximately 150 nm. By analyzing the width in density of the incompressible bands in the quantum Hall regime, Martin *et al.* (2007) were able to extract the amplitude of the density fluctuations in their sample. By fitting the broadened incompressible bands with a Gaussian, Martin *et al.* extracted the value of the amplitude of the density fluctuations, identical for all incompressible bands (Ilani *et al.*, 2004) and found it to be equal to 2.3×10^{11} cm^{-2}. Taking this value to be equal to n_{rms} using the TFD a corresponding value of $n_{imp} = 2.4 \times 10^{11}$ cm^{-2} is found consistent with typical values for the mobility at high density. By calculating the ratio between the density fluctuations amplitude extracted from the broadening of the incompressible bands in the quantum Hall regime and the amplitude extracted from the probability distribution of the density extracted from the imaging results, Martin *et al.* (2007) obtained the upper bound of 30 nm for the characteristic length of the density fluctuations, consistent with the TFD results (Rossi and Das Sarma, 2008).
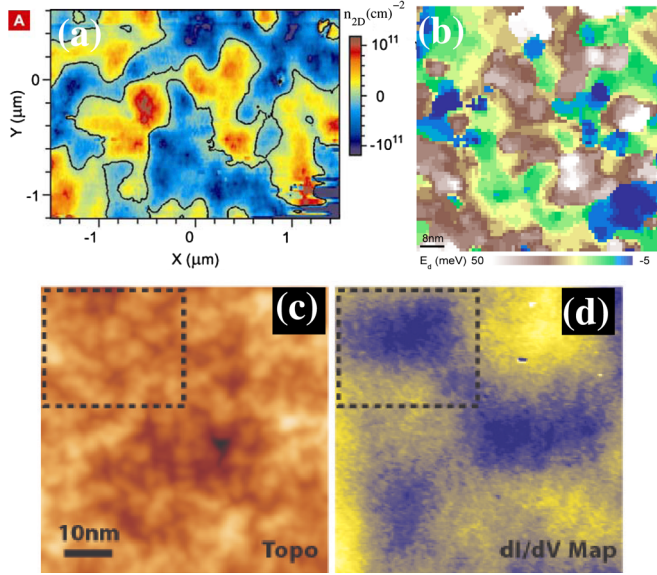
FIG. 32 (color online). (a) Carrier density profile map at the CNP measured with an SET. The contour marks the zero-density contour. Adapted from Martin *et al.*, 2007. (b) Spatial map, on a 80 nm × 80 nm region, of the energy shift of the CNP in BLG from STM dI/dV map. Adapted from Deshpande *et al.*, 2009b. (c) 60 nm × 60 nm constant current STM topography, and (d) simultaneous dI/dV map, at the CNP for MLG, ($V_{bias} = -0.225$ V, $I = 20$ pA). Adapted from Zhang, Tang *et al.*, 2009.

An indirect confirmation of the existence of electron-hole puddles in exfoliated graphene close to the CNP came from the measurement of the magnetic field-dependent longitudinal and Hall components of the resistivity $\rho_{xx}(H)$ and $\rho_{xy}(H)$ (Cho and Fuhrer, 2008). Close to the Dirac point, the measurements showed that $\rho_{xx}(H)$ is strongly enhanced and $\rho_{xy}(H)$ is suppressed, indicating nearly equal electron and hole contributions to the transport current. In addition, the experimental data were found inconsistent with uniformly distributed electron and hole concentrations (two-fluid model) but in excellent agreement with the presence of inhomogeneously distributed electron and hole regions of equal mobility.

The first STM experiments on exfoliated graphene were performed by Zhang, Brar *et al.* (2009). The STM experiments provided the most direct quantitative characterization of the carrier density distribution of exfoliated graphene. Figure 32(c) shows the topography of a 60×60 nm² area of exfoliated graphene, while Fig. 32(d) shows the dI/dV map of the same area. The dI/dV value is directly proportional to the local density of states. We can see that there is no correlation between topography and dI/dV map. This shows that in current exfoliated graphene samples the rippling of graphene, either intrinsic or due to the roughness of the substrate surface, are not the dominant cause of the charge density inhomogeneities. The dI/dV maps clearly reveal the presence of high-density regions with characteristic length of ≈ 20 nm as predicted by the TFD results.

Recently, more experiments have been performed to directly image the electronic structure of both exfoliated single layer graphene (Deshpande, Bao, Miao *et al.* 2009) and

bilayer graphene (Deshpande, Bao, Zhao *et al.*, 2009). In particular, Deshpande, Bao, Miao *et al.* (2009), starting from the topographic data, calculated the carrier density fluctuations due to the local curvature of the graphene layer using Eq. (4.24) and compared them to the fluctuations of the dI/dV map. The comparison shows that there is no correspondence between the density fluctuations induced by the curvature and the ones measured directly. This leads to the conclusion that even though the curvature contributes to a variation in the electrochemical potential, it is not the main factor responsible for the features in the dI/dV map.

The results for BLG of Fig. 32(b) show that close to the CNP the density inhomogeneities are very strong also in BLG and are in semiquantitative agreement with theoretical predictions based on the TF theory (Das Sarma *et al.*, 2010).

Using an SET, Martin *et al.* (2009) imaged the local density of states also in the quantum Hall regime. The disorder carrier density landscape has also been indirectly observed in imaging experiments of coherent transport (Berezovsky *et al.*, 2010; Berezovsky and Westervelt, 2010).

D. Transport in the presence of electron-hole puddles

The previous section showed, both theoretically and experimentally, that close to the Dirac point, in the presence of long-range disorder, the carrier density landscape breaks up in electron-hole puddles. In this situation the transport problem becomes the problem of calculating transport properties of a system with strong density inhomogeneities. The first step is to calculate the conductance of the puddles, G_p, and PNJ, G_{PNJ}.

We have $G_p = \Gamma \sigma$, where Γ is a form factor of order 1 and σ is the puddle conductivity. Away from the Dirac point (see Sec. III.A) the RPA-Boltzmann transport theory for graphene in the presence of random charge impurities is accurate. From the RPA-Boltzmann theory, we have $\sigma = e|\langle n \rangle| \mu(\langle n \rangle, n_{imp}, r_s, d, T)$. For the purposes of this section, it is convenient to explicitly write the dependence of σ on n_{imp} by introducing the function

$$F(r_s, d, T) \equiv \frac{h n_{imp} \mu}{2e} = 2\pi n_{imp} \tau \frac{k_F}{v_F} \qquad (4.25)$$

so that we can write

$$\sigma = \frac{2e^2}{h} \frac{|\langle n \rangle|}{n_{imp}} F(r_s, d, T). \qquad (4.26)$$

Expressions for $F(r_s, d, T)$ at $T = 0$ (or its inverse) were originally given by Adam *et al.* (2007) [see Eq. (3.21)].

We can define a local spatially varying puddle conductivity $\sigma(\mathbf{r})$ if $\sigma(\mathbf{r})$ varies on length scales that are larger than the mean free path l, i.e.,

$$\left| \frac{\nabla \sigma(\mathbf{r})}{\sigma(\mathbf{r})} \right|^{-1} \gg l. \qquad (4.27)$$

By substituting $\langle n \rangle$ with $n(\mathbf{r})$, we then use Eq. (4.26) to define and calculate the local conductivity:

$$\sigma(\mathbf{r}) = \frac{2e^2}{h} \frac{n(\mathbf{r})}{n_{imp}} F(r_s, d, T). \qquad (4.28)$$

Considering that $l = h\sigma/(2e^2 k_F)$ and using Eq. (4.28), then the inequality (4.27) takes the following form:

$$\left| \frac{\nabla n(\mathbf{r})}{n(\mathbf{r})} \right|^{-1} \gg \frac{F(r_s, d, T)}{\sqrt{\pi}} \frac{\sqrt{n}}{n_{\text{imp}}}. \quad (4.29)$$

As shown in the previous sections, at the CNP most of the graphene area is occupied by large electron-hole puddles with size of the order of the sample size L and density of the order of $n_{\text{rms}} \approx n_{\text{imp}}$. For graphene on SiO$_2$, we have $r_s = 0.8$ for which is $F = 10$. Using these facts, we find that the inequality (4.29) is satisfied when

$$L \gg \frac{F(r_s, d, T)}{\sqrt{\pi}} \frac{1}{\sqrt{n_{\text{imp}}}}, \quad (4.30)$$

i.e., when the sample is much larger than the typical in-plane distance between charge impurities. Considering that in experiments on bulk graphene $L > 1 \ \mu$m and $n_{\text{imp}}[10^{10}\text{–}10^{12}] \ \text{cm}^{-2}$, we see that the inequality (4.30) is satisfied. In this discussion we have neglected the presence of the small regions of high density and size ξ. For these regions the inequality (4.30) is not satisfied. However, these regions, because of their high carrier density, steep carrier density gradients at the boundaries, and small size $\xi < l$, are practically transparent to the current carrying quasiparticles and therefore, given that they occupy a small area fraction and are isolated (i.e., do not form a path spanning the whole sample), give a negligible contribution to the graphene resistivity. This fact and the validity of inequality (4.30) for the large puddles ensure that the local conductivity $\sigma(\mathbf{r})$ as given by Eq. (4.28) is well defined. In the limit $r_s \ll 1$ one can use the analytical results for the density distribution to reach the same conclusion (Fogler, 2009).

To calculate the conductance across the PNJ, quantum effects must be taken into account. In particular, as discussed in Sec. II.B for Dirac fermions, we have the phenomenon of Klein tunneling (Klein, 1929; Dombey and Calogeracos, 1999), i.e., the property of perfect transmission through a steep potential barrier perpendicular to the direction of motion. The PNJ conductance G_{PNJ} can be estimated using the results of Cheianov and Fal'ko (2006a) and Zhang *et al.* (2008). The first step is to estimate the steepness of the electrostatic barrier at the PNJ, i.e., the ratio between the length scale D over which the screened potential varies across the PNJ and the Fermi wavelength of the carriers at the side of the PNJ. From the TFD theory, we have that at the sides of the PNJ $n \approx n_{\text{rms}}$ so that $k_F = \sqrt{\pi n_{\text{rms}}}$, and that $D \approx 1/k_F$ so that $k_F D \approx 1$. In this limit, the conductance per unit length of a PNJ g_{PNJ} is given by (Cheianov and Fal'ko, 2006b; Zhang *et al.*, 2008)

$$g_{\text{PNJ}} = \frac{e^2}{h} k_F. \quad (4.31)$$

so that the total conductance across the boundaries of the electron-hole puddles is $G_{\text{PNJ}} = p g_{\text{PNJ}}$ with p the perimeter of the typical puddle (Fogler, 2009; Rossi *et al.*, 2009). Because the puddles have size comparable to the sample size, $p \approx L$, for typical experimental conditions ($L \gtrsim 1 \ \mu$m and $n_{\text{imp}}[10^{10}\text{–}10^{12}] \ \text{cm}^{-2}$) using Eqs. (4.28) and (4.31), we find

$$G_{\text{PNJ}} = \frac{e^2}{h} \sqrt{\pi n_{\text{rms}}} p \gg G_p = \Gamma F(r_s, d, T) \frac{2e^2}{h} \frac{|n_{\text{rms}}|}{n_{\text{imp}}}, \quad (4.32)$$

i.e., $G_{\text{PNJ}} \gg G_p$. In the limit $r_s \ll 1$ the inequality (4.32) is valid for any value of n_{imp} (Fogler, 2009). The inequality (4.32) shows that, in exfoliated graphene samples, transport close to the Dirac point is not percolative: the dominant contribution to the electric resistance is due to scattering events inside the puddles and not to the resistance of the puddle boundaries (Fogler, 2009; Rossi *et al.*, 2009). This conclusion is consistent with the results of Adam, Brouwer, and Das Sarma (2009) in which the graphene conductivity in the presence of Gaussian disorder obtained using a full quantum-mechanical calculation was found to be in agreement with the semiclassical Boltzmann theory even at zero doping provided the disorder is strong enough. Given (i) the random position of the electron-hole puddles, (ii) the fact that because of the inequality (4.30) the local conductivity is well defined, and (iii) the fact that $G_{\text{PNJ}} \gg G_p$, the effective medium theory (EMT) (Bruggeman, 1935; Landauer, 1952; Hori and Yonezawa, 1975) can be used to calculate the electrical conductivity of graphene. The problem of the minimum conductivity at the CNP can be expressed as the problem of correctly averaging the individual puddle conductivity. Using Eq. (4.28), given a carrier density distribution, the conductivity landscape can be calculated.

In the EMT an *effective medium* with homogeneous transport properties equivalent to the bulk transport properties of the inhomogeneous medium is introduced. Starting from the local relation between current $\mathbf{J}$ and electric potential V,

$$\mathbf{J}(\mathbf{r}) = -\sigma(\mathbf{r})\nabla V(\mathbf{r}), \quad (4.33)$$

the effective medium conductivity σ_{EMT} is defined through

$$\langle \mathbf{J}(\mathbf{r}) \rangle = -\sigma_{\text{EMT}} \langle \nabla V(\mathbf{r}) \rangle, \quad (4.34)$$

where the angle bracket denotes spatial and disorder averages. Equations (4.33) and (4.34) along with the condition that in the effective medium the electric field $-\nabla V$ is uniform are sufficient to calculate σ_{EMT}. The derivation of the relation between σ_{EMT} and $\sigma(\mathbf{r})$ using Eqs. (4.33) and (4.34) requires the solution of the electrostatic problem in which a homogeneous region of conductivity $\sigma(\mathbf{r})$ is embedded in an infinite medium of conductivity σ_{EMT}. When the shape of the homogeneous regions, puddles, in the real medium is random the shape of the homogeneous regions used to derive the expression of σ_{EMT} is unimportant, and they can be assumed to be spheres having the same volume as each puddle (Bruggeman, 1935; Landauer, 1952). For a 2D system, the solution of the electrostatic problem gives (Bruggeman, 1935; Landauer, 1952)

$$\int d^2 r \frac{\sigma(\mathbf{r}) - \sigma_{\text{EMT}}}{\sigma(\mathbf{r}) + \sigma_{\text{EMT}}} = 0. \quad (4.35)$$

Equation (4.35) can also be viewed as an approximate resummation of the infinite diagrammatic series for the macroscopic σ using the self-consistent single-site approximation (Hori and Yonezawa, 1975). Disorder averaging Eq. (4.35), we find

$$\left\langle \int d^2 r \frac{\sigma(\mathbf{r}) - \sigma_{EMT}}{\sigma(\mathbf{r}) + \sigma_{EMT}} = 0 \right\rangle \Leftrightarrow \int d\sigma \frac{\sigma - \sigma_{EMT}}{\sigma + \sigma_{EMT}} P(\sigma) = 0,$$

(4.36)

where $P(\sigma)$ is the probability for the local value of σ. Using the relation between the local value σ and the local value of the carrier density n, Eqs. (4.28) and (4.36) can be rewritten in the following form:

$$\int dn \frac{\sigma(n) - \sigma_{EMT}}{\sigma(n) + \sigma_{EMT}} P[n] = 0,$$

(4.37)

where $P[n]$ is the density probability distribution that can be calculated using the TFD theory, Fig. 31. Using the TFD results and Eq. (4.37), the conductivity at the Dirac point and its vicinity can be calculated.

Figure 33(a) shows $\sigma(V_g)$ as obtained using the TFD + EMT theory (Rossi *et al.*, 2009). The theory correctly predicts a finite value of σ very close to the one measured experimentally. At high gate voltages, the theory predicts the linear scaling of σ as a function of V_g. The theory correctly describes the crossover of σ from its minimum at $V_g = 0$ to its linear behavior at high gate voltages. Figure 33(a) also shows the importance of the exchange-correlation term at low gate voltages. The dependence of σ_{min} on n_{imp} is shown in Fig. 33(c). σ_{min} increases as n_{imp} decreases; the dependence of σ_{min} on n_{imp} is weaker if exchange-correlation terms are taken into account. Figure 33(d) shows the dependence of σ_{min} on the inverse mobility $1/\mu \propto n_{imp}$ as measured by Chen, Jang, Adam *et al.* (2008). In this experiment the amount of charge impurities is controlled by potassium doping.

Figure 33(b) shows the results for σ_{min} as a function of r_s. The solid (dashed) line shows the calculated values of σ_{min} including (neglecting) exchange. σ_{min} has a nonmonotonic behavior due to the fact that r_s affects both the carrier density spatial distribution by controlling the strength of the disorder potential, screening, and exchange, and the scattering time τ. The dependence of σ_{min} on r_s has been measured in two recent experiments (Jang *et al.*, 2008; Ponomarenko *et al.*, 2009). In these experiments the fine-structure constant of graphene r_s is modified by placing the graphene on substrates with different κ and/or by using materials with $\kappa \neq 1$ as top dielectric layers. Jang *et al.* (2008) placed graphene on SiO$_2$ and reduced r_s from 0.8 (no top dielectric layer) to 0.56 by placing ice in vacuum as a top dielectric layer. The resulting change of σ_{min} is shown in Fig. 33(b) by the two solid squares. As predicted by the theory, when V_{xc} is included, for this range of values of r_s, σ_{min} is unaffected by the variation of r_s. Overall the results presented by Jang *et al.* (2008) are consistent with charge impurity being the main source of scattering in graphene. Ponomarenko *et al.* (2009) varied r_s by placing graphene on substrates with different dielectric constants and by using glycerol, ethanol, and water as a top dielectric layer. Ponomarenko *et al.* (2009) found very minor differences in the transport properties of graphene with different dielectric layers, thus concluding that charge impurities are not the dominant source of scattering. Currently, the reasons for the discrepancy among the results of Jang *et al.* (2008) and Ponomarenko *et al.* (2009) are not well understood. The experiments are quite different. It must be noted that changing the substrate and the top dielectric layer, in addition to modifying r_s, is likely to modify the amount of disorder seen by the carriers in the graphene layer.
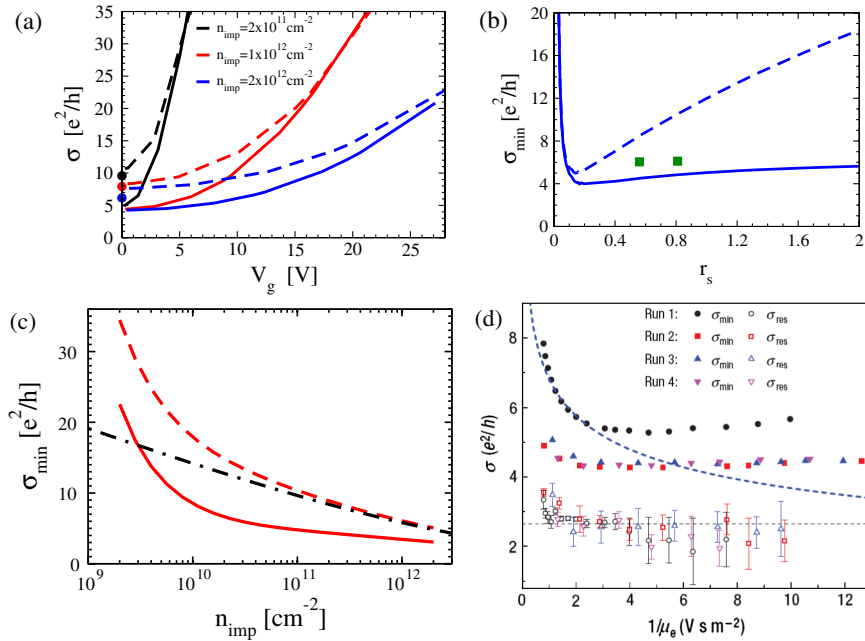

FIG. 33 (color online). Solid (dashed) lines show the EMT-TFD results with (without) exchange. (a) σ as function of V_g for three different values of n_{imp}. The dots at $V_g = 0$ are the results presented by Adam *et al.* (2007) for the same values of n_{imp}. (b) σ_{min} as a function of r_s for $d = 1$ and $n_{imp} = 10^{11}$ cm^{-2}. Solid squares show the experimental results of Jang *et al.* (2008). (c) σ_{min} as a function of n_{imp}, $r_s = 0.8$ and $d = 1$ nm. For comparison the results obtained by Adam *et al.* (2007) are also shown by the dot-dashed line. (d) σ_{min} as a function of the inverse mobility as measured by Chen, Jang, Adam *et al.*, 2008. r_s for $d = 1$ and $n_{imp} = 10^{11}$ cm^{-2}. (a)–(c) Adapted from Rossi *et al.*, 2009. (d) Adapted from Chen, Jang, Adam *et al.*, 2008.

By not modifying the substrate and by placing ice in and ultrahigh vacuum, Jang *et al.* (2008) minimized the change of disorder induced by modifying the top dielectric layer.

The approach presented above based on TFD and EMT theories can be used to calculate other transport properties of MLG and BLG close to the Dirac point. Hwang *et al.* (2009) used the same approach to calculate the thermopower of MLG with results in good agreement with experiments (Checkelsky *et al.*, 2009; Wei *et al.*, 2009; Zuev *et al.*, 2009). Das Sarma *et al.* (2010) used the TFD + EMT approach to calculate the electrical conductivity in BLG. Tiwari and Stroud (2009) used the EMT based on a simple two-fluid model to calculate the magnetoresistance at low magnetic fields of MLG close to the CNP.

It is interesting to consider the case when $G_p \gg G_{\text{PNJ}}$. This limit is relevant, for example, when a gap in the graphene spectrum is opened. Cheianov *et al.* (2007) theoretically studied the limit $G_p \gg G_{\text{PNJ}}$ by considering a random resistor network (RRN) model on a square lattice in which only nearest neighbors and next-nearest neighbor are connected directly. Mathematically, the model is expressed by the following equations for the conductance between the sites (i, j) and (i', j') with $|i - i'| \le 1$, $|j - j'| \le 1$:

$$G_{(i,j)}^{(i+1,j+1)} = g[1 + (-1)^{i+j}\eta_{i,j}]/2; \qquad (4.38)$$

$$G_{(i,j+1)}^{(i+1,j)} = g[1 - (-1)^{i+j}\eta_{i,j}]/2; \qquad (4.39)$$

$$G_{(i,j)}^{(i+1,j)} = G_{(i,j)}^{(i,j+1)} = \gamma g, \qquad \gamma \ll 1, \qquad (4.40)$$

where $\eta_{i,j}$ is a random variable,

$$\eta_{i,j} = \pm 1, \qquad \langle \eta_{i,j} \rangle = p, \qquad \langle \eta_{i,j}\eta_{k,l} \rangle = \delta_{ik}\delta_{jl}, \qquad (4.41)$$

and p is proportional to the doping $\langle n \rangle$. For $\gamma = 0$, $p = 0$ we have percolation. Finite p and γ are relevant perturbations for the percolation leading to a finite correlation length $\xi(p, \gamma)$. On scales much larger than ξ, the RRN is not critical, and consists of independent regions of size ξ so that σ is well defined with scaling (Cheianov *et al.*, 2007) $\sigma(p, \gamma) = [a/\xi(p, \gamma)]^x g$ with $\xi(p, \gamma) \sim a\gamma^{-\gamma}/F(p/p^*)$, $p^* = \gamma^{\mu/\nu}$ and $\nu = 4/3$, $\mu = 1/(h + x)$ where $h = 7/4$ and $x \approx 0.97$ are, respectively, the fractal dimension of the boundaries between the electron-hole puddles and the conductance exponent $\langle G(L) \rangle = (a/L)^x g$ at the percolation threshold (Isichenko, 1992; Cheianov *et al.*, 2007). Figure 34 shows the results obtained solving numerically the RRN defined by Eq. (4.40). The numerical results are well fitted using for $F(p/p^*)$ the function $F(z) = (1 + z^2)^{(\nu/2)}$. Estimating $g \sim (e^2/\hbar)ak_F$ and $\gamma g \sim (e^2/\hbar)(ak_F)^{1/2}$ (Cheianov and Fal'ko, 2006b), Cheianov *et al.* (2007) estimated that

$$\sigma_{\min} \sim \frac{e^2}{\hbar}(a^2\delta n)^{0.41}. \qquad (4.42)$$

From the TFD results, one gets $\delta n \sim n_{\text{imp}}$ and so Eq. (4.42) predicts that $\sigma_{\min}$ should increase with n_{imp}, a trend that is not observed in experiments. The reason for the discrepancy is
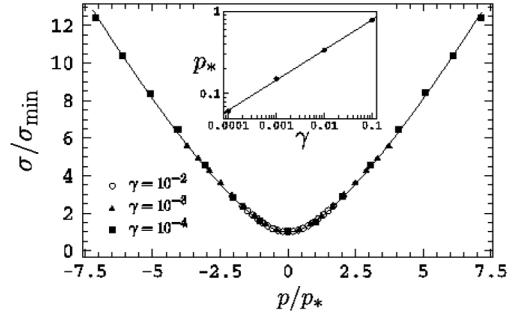

FIG. 34. Collapse of the conductivity data obtained for RRNs with various $-1/2 < p < 1/2$ and values of the parameter γ onto a single curve. Points: numerical results; line: best fit obtained using the equations in the text. Adapted from Cheianov *et al.*, 2007.

due to the fact that for current experiments the relevant regime is expected to be the one for which $G_{\text{PNJ}} \gg G_p$. The minimum conductivity was also calculated for bilayer graphene (Adam and Das Sarma, 2008a; Das Sarma *et al.*, 2010). Other works calculated σ_m using different models and approximations for regimes less relevant for current experiments (Katsnelson, 2006; Cserti, 2007; Cserti *et al.*, 2007; Trushin and Schliemann, 2007; Adam and Das Sarma, 2008a; ; Groth *et al.*, 2008; Trushin *et al.*, 2010).

Although the semiclassical approach presented in this section is justified for most of the current experimental conditions for exfoliated graphene, its precise range of validity and level of accuracy close to the Dirac point can only be determined by a full quantum transport calculation that takes into account the presence of charge impurities. This is still an active area of research and work is in progress to obtain the transport properties of graphene using a full quantum transport treatment (Rossi, Bardarson, Fuhrer, and Das Sarma, 2010).

V. QUANTUM HALL EFFECTS

A. Monolayer graphene

1. Integer quantum Hall effect

The unique properties of the quantum Hall effect in graphene are among the most striking consequences of the Dirac nature of the massless low energy fermionic excitations in graphene. In the presence of a perpendicular magnetic field B electrons (holes) confined in two dimensions are constrained to move in close cyclotron orbits that in quantum mechanics are quantized. The quantization of the cyclotron orbits is reflected in the quantization of the energy levels: at finite B the $B = 0$ dispersion is replaced by a discrete set of energy levels, the Landau levels (LL). For any LL, there are $N_\phi = BA/\phi_0$ degenerate orbital states, where A is the area of the sample and ϕ_0 is the magnetic quantum flux. Quantum Hall effects (MacDonald, 1990; Prange and Girvin, 1990; Das Sarma and Pinczuk, 1996) appear when N is comparable to the total number of quasiparticles present in the system. In the quantum Hall regime the Hall conductivity σ_{xy} exhibits well developed plateaus as a function of carrier density (or correspondingly magnetic field) at which it takes quantized values.

At the same time, for the range of densities for which σ_{xy} is quantized, the longitudinal conductivity σ_{xx} is zero (Laughlin, 1981; Halperin, 1982). For standard parabolic 2DEG (such as the ones created in GaAs and Si quantum wells), the LL have energies energy $\hbar\omega_c(n + 1/2)$, where $n = 0, 1, 2, \ldots$ and $\omega_c = eB/mc$, m being the effective mass, is the cyclotron frequency. Because the low energy fermions in graphene are massless, it is immediately obvious that for graphene we cannot apply the results valid for standard 2DEG (ω_c would appear to be infinite). In order to find the energy levels E_n for the LL the 2D Dirac equation must be solved in the presence of a magnetic field (Jackiw, 1984; Haldane, 1988; Gusynin and Sharapov, 2005; Peres *et al.*, 2006). The result is given by Eq. (1.13a). Differently from parabolic 2DEG, in graphene we have a LL at zero energy. In addition, we have the unconventional Hall quantization rule for σ_{xy} (Zheng and Ando, 2002; Gusynin and Sharapov, 2005; Peres *et al.*, 2006):

$$\sigma_{xy} = g\left(n + \frac{1}{2}\right)\frac{e^2}{h} \tag{5.1}$$

compared to the one valid for regular 2DEGs

$$\sigma_{xy} = gn\frac{e^2}{h} \tag{5.2}$$

shown in Fig. 35, where g is the spin and valley degeneracy. Because in graphene the band dispersion has two inequivalent valleys, $g = 4$ (for GaAs quantum wells we only have the spin degeneracy so that $g = 2$). The additional $1/2$ in
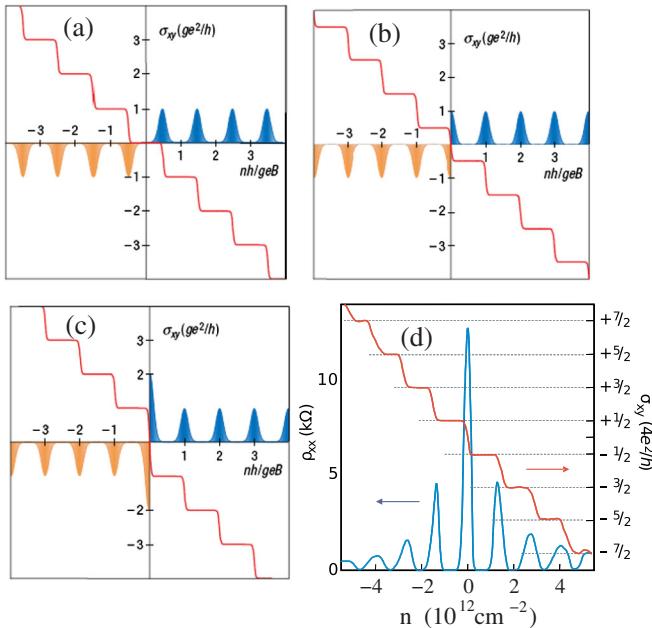

FIG. 35 (color online). Illustration of the integer QHE found in 2D semiconductor systems, (a), incorporated from MacDonald (1990) and Prange and Girvin (1990). (b) Illustration for SLG. (c) Illustration from BLG. The sequences of Landau levels as a function of carrier concentrations n are shown as dark and light peaks for electrons and holes, respectively. Adapted from Novoselov *et al.*, 2006. (d) σ_{xy} and ρ_{xx} of MLG as a function of carrier density measured experimentally at $T = 4$ K and $B = 14$ T. Adapted from Novoselov, Geim *et al.*, 2005.

Eq. (5.1) is the hallmark of the chiral nature of the quasiparticles in graphene. The factor $1/2$ in Eq. (5.1) can be understood as the term induced by the additional Berry phase that the electrons, due to their chiral nature, acquire when completing a close orbit (Mikitik and Sharlai, 1999; Luk'yanchuk and Kopelevich, 2004). Another way to understand its presence is by considering the analogy to the relativistic Dirac equation (Geim and MacDonald, 2007; Yang, 2007). From this equation, two main predictions ensue: (i) the electrons have spin $1/2$ and (ii) the magnetic g factor is exactly equal to 2 for the spin in the nonrelativistic limit. As a consequence the Zeeman splitting is exactly equal to the orbital splitting. In graphene the pseudospin plays the role of the spin and instead of Zeeman splitting, we have "pseudospin splitting" but the same holds true: the pseudospin splitting is exactly equal to the orbital splitting. As a consequence the nth LL can be thought as composed of the degenerate pseudospin-up states of LL n and the pseudospin-down states of LL $n - 1$. For zero mass Dirac fermions, the first LL in the conduction band and the highest LL in the valence band merge contributing equally to the joint level at $E = 0$, resulting in the half-odd-integer quantum Hall effect described by Eq. (5.1). For the $E = 0$ LL, because half of the degenerate states are already filled by holelike (electronlike) particles, we only need $(1/2)N_\phi$ electronlike (holelike) particles to fill the level.

The quantization rule for σ_{xy} has been observed experimentally (Novoselov, Geim *et al.*, 2005; Zhang *et al.*, 2005) as shown in Fig. 35(d). The experimental observation of Eq. (5.1) shows clearly the chiral nature of the massless quasiparticles in graphene.

There is another important experimental consequence of the Dirac nature of the fermions in graphene. Because in graphene E_n scales as $\sqrt{nB}$ [Eq. (1.13a)] rather than linearly as in regular 2DEG [Eq. (1.13c)], at low energies (n) the energy spacing $\Delta_n \equiv E_{n+1} - E_n$ between LL can be rather large. Because the observation of the quantization of σ_{xy} relies on the condition $\Delta_n \gg k_BT$ (T being the temperature), it follows that in graphene the quantization of the LL should be observable at temperatures higher than in regular parabolic 2DEG. This fact has been confirmed by the observation in graphene of the QH effect at room temperature (Novoselov *et al.*, 2007). Graphene is the only known material whose quantum Hall effect has been observed at ambient temperature (albeit at high magnetic fields).

By applying a top gate, p-n junctions (PNJ) can be created in graphene. In the presence of strong perpendicular fields graphene PNJ exhibit unusual fractional plateaus for the conductance that have been studied experimentally by Özyilmaz *et al.* (2007) and Williams *et al.* (2007) and theoretically by Abanin and Levitov (2007). Numerical studies in the presence of disorder have been performed by Long *et al.* (2008), Li and Shen (2008), and Low (2009).

2. Broken-symmetry states

The sequence of plateaus for σ_{xy} given by Eq. (5.1) describes the QH effect due to fully occupied Landau levels including the spin and valley degeneracy. In graphene for the fully occupied LL we have the filling factors $\nu \equiv gN/N_\phi = 4(n + 1/2) = \pm 2, \pm 6, \pm 10, \ldots$ In this section we study the

situation in which the spin or valley, or both, degeneracies are lifted. In this situation QH effects are observable at intermediate filling factors $\nu = 0, \pm 1$ for the lowest LL and $\nu = \pm 3, \pm 4, \pm 5$ for $n = \pm 1$ LL. The difficulty in observing these intermediate QH effects is the lower value of the energy gap between successive split LL. If the gap between successive Landau levels is comparable or smaller than the disorder strength, the disorder mixes adjacent LL preventing the formation of well defined QH plateaus for the Hall conductivity. For the most part of this section, we neglect the Zeeman coupling that turns out to be the lowest energy scale in most of the experimentally relevant conditions.

Koshino and Ando (2007) showed that randomness in the bond couplings and on-site potential can lift the valley degeneracy and cause the appearance of intermediate Landau Levels. Fuchs and Lederer (2007) considered the electron-phonon coupling as the possible mechanism for the lifting of the degeneracy. However, in most of the theories the spin and valley degeneracy is lifted due to interaction effects (Alicea and Fisher, 2006; Goerbig *et al.*, 2006; Gusynin *et al.*, 2006; Nomura and MacDonald, 2006; Yang *et al.*, 2006; Abanin *et al.*, 2007b; Ezawa, 2007, 2008; Herbut, 2007), in particular, electron-electron interactions. When electron-electron interactions are taken into account, the quasiparticles filling a LL can polarize in order to minimize the exchange energy (maximize it in absolute value). In this case, given the SU(4) invariance of the Hamiltonian, the states

$$|\Psi_0\rangle = \prod_{1 \leq i \leq M} \prod_k c_{k,\sigma}^\dagger |0\rangle, \qquad (5.3)$$

where i is the index of the internal states that runs from 1 to $M = \nu - 4(n - 1/2) \leq 4$, and $|0\rangle$ is the vacuum, are exact eigenstates of the Hamiltonian. For a broad class of repulsive interactions, $|\Psi_0\rangle$ is expected to be the exact ground state (Yang *et al.*, 2006, 2007). The state described by $|\Psi_0\rangle$ is a "ferromagnet," sometimes called a QH ferromagnet, in

which either the real spin or the pseudospin associated with the valley degree of freedom is polarized. The problem of broken-symmetry states in the QH regime of graphene is analogous to the problem of "quantum Hall ferromagnetism" studied in regular 2DEG in which, however, normally only the SU(2) symmetry associated with the spin can be spontaneously broken [notice however that for silicon quantum wells the valley degeneracy is also present so that in this case the Hamiltonian is SU(N) ($N > 2$) symmetric]. Because in the QH regime the kinetic energy is completely quenched, the formation of polarized states depends on the relative strength of interaction and disorder. For graphene, Nomura and MacDonald (2006), using the Hartree-Fock approximation, derived a "Stoner criterion" for the existence of polarized states, i.e., QH ferromagnetism, for a given strength of the disorder. Chakraborty and Pietilainen (2007) numerically verified that QH ferromagnetic states with large gaps are realized in graphene. Sheng *et al.* (2007), using exact diagonalization, studied the interplay of long-range Coulomb interaction and lattice effects in determining the robustness of the $\nu = \pm 1$ and ± 3 states with respect to disorder. Nomura *et al.* (2008) studied the effect of strong long-range disorder. Wang *et al.* (2008) performed numerical studies that show that various charge density wave phases can be realized in the partially filled $\nu = \pm 3$ LL.

Experimentally, the existence of broken-symmetry states has been verified by Zhang *et al.* (2006) [Fig. 36(a)], which showed the existence of the intermediate Landau levels with $\nu = 0, \pm 1$ for the $n = 0$ LL and the intermediate level $\nu = \pm 4$ for the $n = 1$ LL that is therefore only partially resolved. Given that the magnetic field by itself does not lift the valley degeneracy, interaction effects are likely the cause for the full resolution of the $n = 0$ LL. On the other hand, a careful analysis of the data as a function of the tilting angle of the magnetic field suggests that the partial resolution of the $n = 1$ LL is due to Zeeman splitting (Zhang *et al.*, 2006).
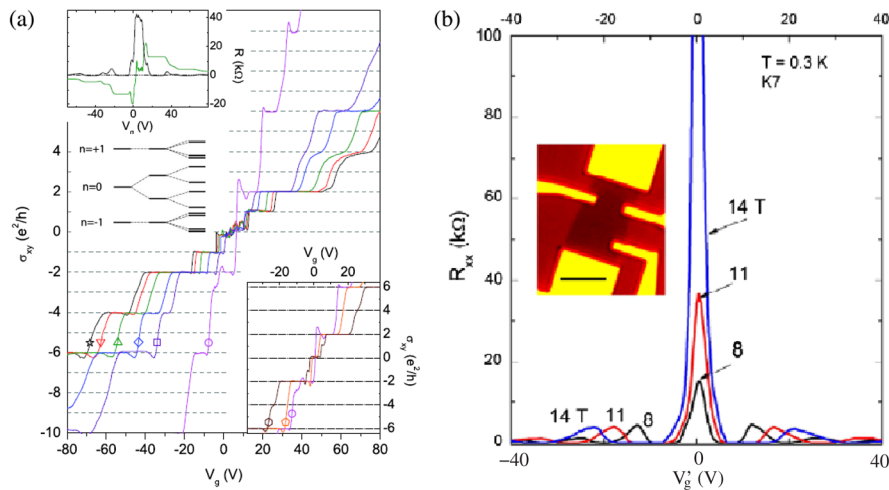

FIG. 36 (color online).   (a) σ_{xy} as a function of gate voltage at different magnetic fields: 9 T (circle), 25 T (square), 30 T (diamond), 37 T (up triangle), 42 T (down triangle), and 45 T (star). All data sets are taken at $T = 1.4$ K, except for the $B = 9$ T curve, which is taken at $T = 30$ mK. Left upper inset: R_{xx} and R_{xy} for the same device measured at $B = 25$ T. Right inset: Detailed σ_{xy} data near the Dirac point for $B = 9$ T (circle), 11.5 T (pentagon), and 17.5 T (hexagon) at $T = 30$ mK. Adapted from Zhang *et al.*, 2006. (b) Longitudinal resistance R_{xx} as a function of gate voltage $V_g' = V_g - V_0$ at 0.3 K and several values of the magnetic field: 8, 11, and 14 T. The inset shows a graphene crystal with Au leads deposited. The bar indicates 5 μm. At $V_g' = 0$, the peak in R_{xx} grows to 190 kΩ at 14 T. Adapted from Checkelsky *et al.*, 2008.

3. The $\nu = 0$ state

In the previous section we have seen that in strong magnetic fields the lowest LL can be completely resolved and the spin and valley degeneracies may be lifted. In particular, an approximate plateau for σ_{xy} appear for $\nu = 0$. This state has been experimentally studied by Jiang *et al.* (2007), Checkelsky *et al.* (2008, 2009), and Giesbers *et al.* (2009); see Fig. 36(b). The state is unique in that the plateau of σ_{xy} corresponds to a maximum of the longitudinal resistivity ρ_{xx} in contrast to what happens for $\nu \neq 0$ where a plateau of σ_{xy} corresponds to zero longitudinal resistivity. In addition, the $\nu = 0$ edge states are not supposed to carry any charge current, but only spin currents (Abanin *et al.*, 2006; Abanin *et al.*, 2007a; Abanin, Novoselov *et al.*, 2007). As pointed out by Das Sarma and Yang (2009), however, the situation is not surprising if we recall the relations between the resistivity tensor and the conductivity tensor:

$$\rho_{xx} = \frac{\sigma_{xx}}{\sigma_{xx}^2 + \sigma_{xy}^2}, \qquad \rho_{xy} = \frac{\sigma_{xy}}{\sigma_{xx}^2 + \sigma_{xy}^2}, \qquad (5.4)$$

and the fact that the quantization of σ_{xy} is associated with the vanishing of σ_{xx}. This can be seen from Laughlin's gauge argument (Laughlin, 1981; Halperin, 1982). Using Eq. (5.4), a possible resolution of the $\nu = 0$ anomaly is obvious: for any finite σ_{xy}, the vanishing of σ_{xx} corresponds to the vanishing of ρ_{xx}; however, for $\sigma_{xy} = 0$, we have $\rho_{xx} = 1/\sigma_{xx}$ so that $\sigma_{xx} \to 0$ implies $\rho_{xx} \to \infty$. This is very similar to the Hall insulator phase in ordinary 2D parabolic-band electron gases. This simple argument shows that the fact that ρ_{xx} seem to diverge for $T \to 0$ for the $\nu = 0$ state is not surprising. However, this argument may not be enough to explain the details of the dependence of $\rho_{xx}(\nu = 0)$ on temperature and magnetic field. In particular, Checkelsky *et al.* (2009) found evidence for a field-induced transition to a strongly insulating state at a finite value of B. These observations suggest that the $\nu = 0$ ground state might differ from the SU(4) eigenstates (5.3) and theoretical calculations proposed that it could be a spin-density wave or charge-density wave (Herbut, 2007; Jung and MacDonald, 2009). It has also been argued that the divergence of $\rho_{xx}(\nu = 0)$ might be the signature of Kekule instability (Nomura *et al.*, 2009; Hou, *et al.*, 2010).

Giesbers *et al.* (2009) interpreted their experimental data using a simple model involving the opening of a field-dependent spin gap. Zhang, Camacho *et al.* (2009) observed a cusp in the longitudinal resistance ρ_{xx} for $\nu \approx 1/2$ and interpreted this as the signature of a transition from a Hall insulating state for $\nu > 1/2$ to a collective insulator, such as a Wigner crystal (Zhang and Joglekar, 2007), for $\nu < 1/2$. No consensus has been reached so far, and more work is needed to understand the $\nu = 0$ state in graphene.

4. Fractional quantum Hall effect

In addition to QH ferromagnetism, the electron-electron interaction is responsible for the fractional quantum Hall effect (FQHE). For the FQHE, the energy gaps are even smaller than for the QH ferromagnetic states. For graphene, the FQHE gaps have been calculated by Apalkov and
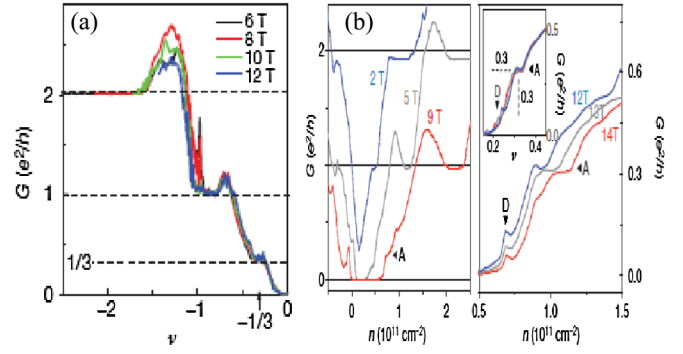

FIG. 37 (color online). Graphene fractional quantum Hall data, from (a) Du *et al.*, 2009 and (b) Bolotin *et al.*, 2009, observed on two probe suspended graphene samples.

Chakraborty (2006) and Toke *et al.* (2006). For the $\nu = 1/3$, the gap has been estimated to be of the order of $0.05e^2/\kappa l_B$, where $l_B \equiv (\hbar c/eB)^{1/2}$ is the magnetic length. Because of the small gap size, the experimental observation of FQHE requires high quality samples. For graphene, very low amount of disorder can be achieved in suspended samples and in these suspended samples two groups (Bolotin *et al.*, 2009; Du *et al.*, 2009) recently observed signatures of the $\nu = 1/3$ fractional quantum Hall state in two-terminal measurements; see Fig. 37. A great deal of work remains to be done in graphene FQHE.

B. Bilayer graphene

1. Integer quantum Hall effect

In bilayer graphene the low energy fermionic excitations are massive, i.e., with good approximation the bands are parabolic. This fact would suggest that the bilayer QH effect in graphene might be similar to the one observed in regular parabolic 2DEG. There are, however, two important differences: the band structure of bilayer graphene is gapless and the fermions in BLG, as in MLG, are also chiral but with a Berry phase equal to 2π instead of π (McCann and Fal'ko, 2006). As a consequence, as shown in Eq. (1.13c), the energy levels have a different sequence from both regular 2DEGs and MLG. In particular, BLG also has a LL at zero energy, however, because the Berry phase associated with the chiral nature of the quasiparticles in BLG is 2π, the step between the plateaus of σ_{xy} across the CNP is twice as large as in MLG [as shown schematically in Fig. 35(c)]. One way to understand the step across the CNP is to consider that in BLG the $n = 0$ and 1 orbital LL are degenerate.

The spin and valley degeneracy factor g in BLG is equal to 4 as in MLG. In BLG the valley degree of freedom can also be regarded as a layer degree of freedom considering that without loss of generality we can use a pseudospin representation in which the K valley states are localized in the top layer and the K' states in the bottom layer. The QH effect has been measured experimentally. Figure 38(a) shows the original data obtained by Novoselov *et al.* (2006). In agreement with the theory the data show a double size step, compared to MLG, for σ_{xy} across the CNP.

2. Broken-symmetry states

As discussed, the $E_n = 0$ LL in BLG has an 8-fold degeneracy due to spin degeneracy, valley (layer) degeneracy, and $n = 0$, $n = 1$ orbital LL degeneracy. The $E_n \neq 0$ LL have only a 4-fold degeneracy due to spin and valley degeneracy. As discussed for MLG, it is natural to expect that the degeneracy of the full LL will be lifted by external perturbations and/or interactions. Similar considerations to the ones made in Sec. V.A.2 for MLG apply here: the splitting can be due to the Zeeman effect (Giesbers *et al.*, 2009), strain-induced lifting of valley degeneracy (Abanin *et al.*, 2007b), or Coulomb interactions. Ezawa (2007) and Barlas *et al.* (2008) considered the splitting of the $E_n = 0$ LL in BLG due to electron-electron interactions and calculated the corresponding charge gaps and filling sequence. As in MLG, the charge gaps of the splitted LLs will be smaller than the charge gap $\hbar\omega_c$ for the fully occupied LLs and so the observation of QH plateaus due to the resolution of the LL requires higher quality samples. This has recently been achieved in suspended BLG samples (Feldman *et al.*, 2009; Zhao *et al.*, 2010) in which the full resolution of the eightfold degeneracy of the zero-energy LL has been observed, Fig. 38(c). By analyzing the dependence of the maximum resistance at the CNP on B and T, Feldman *et al.* (2009) concluded that the observed splitting of the $E_n = 0$ LL cannot be attributed to the Zeeman effect. Moreover, the order in magnetic fields in which the broken-symmetry states appear is consistent with the theoretical predictions of Barlas *et al.* (2008). These facts suggest that in BLG the resolution of the octet zero-energy LL is due to electron-electron interactions.
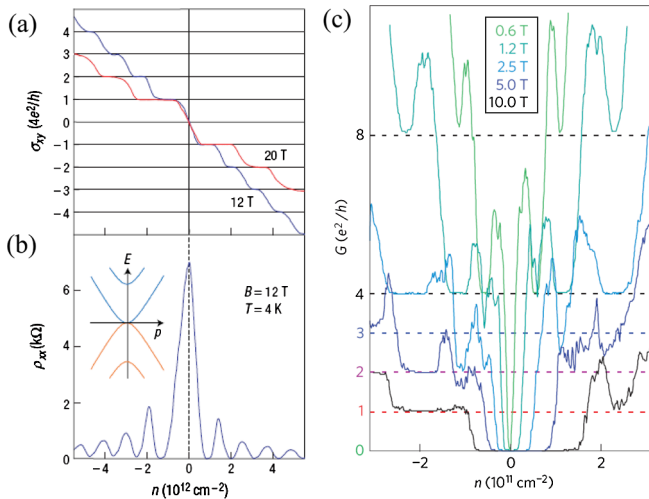

FIG. 38 (color online). (a) Measured Hall conductivity σ_{xy} in BLG as a function of carrier density for $B = 12$ and $B = 20$ T at $T = 4$ K. (b) Measured longitudinal resistivity in BLG at $T = 4$ K and $B = 12$ T. The inset shows the calculated BLG bands close to the CNP. Adapted from Novoselov *et al.*, 2006. (c) Two-terminal conductance, G, as a function of carrier density at $T = 100$ mK for different values of the magnetic field in suspended BLG. Adapted from Feldman *et al.*, 2009.

VI. CONCLUSION AND SUMMARY

In roughly five years, research in graphene physics has made spectacular advances starting from the fabrication of gated variable-density 2D graphene monolayers to the observations of fractional quantum Hall effect and Klein tunneling. The massless chiral Dirac spectrum leads to novel integer quantum Hall effect in graphene with the existence of a $n = 0$ quantized Landau level shared equally between electrons and holes. The nonexistence of a gap in the graphene carrier dispersion leads to a direct transition between electronlike metallic transport to holelike metallic transport as the gate voltage is tuned through the charge neutral Dirac point. By contrast, 2D semiconductors invariably become insulating at low enough carrier densities. In MLG nanoribbons and in BLG structures in the presence of an electric field, graphene carrier transport manifests a transport gap because there is an intrinsic spectral gap induced by the confinement and the bias field, respectively. The precise relationship between the transport and the spectral gap is, however, not well understood at this stage and is a subject of much current activity. Since backscattering processes are suppressed, graphene exhibits weak antilocalization behavior in contrast to the weak localization behavior of ordinary 2D systems. The presence of any short-range scattering, however, introduces intervalley coupling, which leads to the eventual restoration of weak localization. Since short-range scattering, arising from lattice point defects, is weak in graphene, the weak antilocalization behavior is expected to cross over to weak localization behavior only at very low temperatures although a direct experimental observation of such a localization crossover is still lacking and may be difficult.

The observed sequence of graphene integer quantized Hall conductance follows the expected formula $\sigma_{xy} = (4e^2/h) \times (n + 1/2)$, indicating the Berry phase contribution and the $n = 0$ Landau level shared between electrons and holes. For example, the complete lifting of spin and valley splitting leads to the observation of the following quantized Hall conductance sequence $\nu = 0, \pm 1, \pm 2, \ldots$ with $\sigma_{xy} = \nu e^2/h$; whereas, in the presence of spin and valley degeneracy (i.e., with the factor of 4 in the front) one gets the sequence $\nu = \pm 2, \pm 6, \ldots$ The precise nature of the $\nu = 0$ IQHE, which seems to manifest a highly resistive ($\rho_{xx} \rightarrow \infty$) state in some experiments but not in others, is still an open question as is the issue of the physical mechanism or the quantum phase transition associated with the possible spontaneous symmetry breaking that leads to the lifting of the degeneracy. We do mention, however, that similar, but not identical, physics arises in the context of ordinary IQHE in 2D semiconductor structures. For example, the 4-fold spin and valley degeneracy, partially lifted by the applied magnetic field, occurs in 2D Si-(100) based QHE, as already apparent in the original discovery of IQHE by von Klitzing *et al.* (1980). The issue of spin and valley degeneracy lifting in the QHE phenomena is thus generic to both graphene and 2D semiconductor systems, although the origin of valley degeneracy is qualitatively different (Eng *et al.*, 2007; McFarland *et al.*, 2009) in the two cases. The other similarity between graphene and 2DEG QHE is that both systems tend to manifest strongly insulating phases at very high magnetic

field when $\nu \ll 1$. In semiconductor-based high-mobility 2DEG, typically such a strongly insulating phase occurs (Jiang *et al.*, 1990; Jiang *et al.*, 1991) for $\nu < 1/5 - 1/7$; whereas, in graphene the effect manifest near the charge neutral Dirac point around $\nu \approx 0$. Whether the same physics controls either insulating phenomena or not is an open question.

Recent experimental observations of $\nu = 1/3$ FQHE in graphene have created a great deal of excitement. These preliminary experiments involve two-probe measurements on suspended graphene samples where no distinction between ρ_{xx} and ρ_{xy} can really be made. Further advances in the field would necessitate the observation of quantized plateaus in ρ_{xy} with $\rho_{xx} \approx 0$. Since FQHE involves electron-electron interaction effects, with the noninteracting part of the Hamiltonian playing a rather minor role, we should not perhaps expect any dramatic difference between 2DEG and graphene FQHE since both systems manifest the standard $1/r$ Coulomb repulsion between electrons. Two possible quantitative effects distinguishing FQHE in graphene and 2DEG, which should be studied theoretically and numerically, are the different Coulomb pseudopotentials and Landau level coupling in the two systems. Since the stability of various FQH states depends crucially on the minute details of Coulomb pseudopontentials and inter-LL coupling, it is conceivable that graphene may manifest novel FQHE not feasible in 2D semiconductors.

We also note that many properties reviewed here should also apply to topological insulators (Hasan and Kane, 2010), which have only single Dirac cones on their surfaces. Although we now have a reasonable theoretical understanding of the broad aspects of transport in monolayer graphene, much work remains to be done in bilayer and nanoribbons graphene systems.

ACKNOWLEDGMENTS

REFERENCES

Abanin, D., and L. Levitov, 2007, "Quantized Transport in Graphene *p-n* Junctions in Magnetic Field," Science **317**, 641.

Abanin, D. A., P. A. Lee, and L. S. Levitov, 2006, "Spin-filtered edge states and quantum hall effect in graphene," Phys. Rev. Lett. **96**, 176803.

Abanin, D. A., P. A. Lee, and L. S. Levitov, 2007a, "Charge and spin transport at the quantum Hall edge of graphene," Solid State Commun. **143**, 77.

Abanin, D. A., P. A. Lee, and L. S. Levitov, 2007b, "Randomness-induced *XY* ordering in a graphene quantum Hall ferromagnet," Phys. Rev. Lett. **98**, 156801.

Abanin, D. A., and L. S. Levitov, 2008, "Conformal invariance and shape-dependent conductance of graphene samples," Phys. Rev. B **78**, 035416.

Abanin, D. A., K. S. Novoselov, U. Zeitler, P. A. Lee, A. K. Geim, and L. S. Levitov, 2007, "Dissipative quantum Hall effect in graphene near the Dirac point," Phys. Rev. Lett. **98**, 196806.

Abrahams, E., P. W. Anderson, D. C. Licciardello, and T. V. Ramakrishnan, 1979, "Scaling Theory of Localization: Absence of Quantum Diffusion in Two Dimensions," Phys. Rev. Lett. **42**, 673.

Abrahams, E., S. V. Kravchenko, and M. P. Sarachik, 2001, "Metallic behavior and related phenomena in two dimensions," Rev. Mod. Phys. **73**, 251.

Adam, S., P. W. Brouwer, and S. Das Sarma, 2009, "Crossover from quantum to Boltzmann transport in graphene," Phys. Rev. B **79**, 201404.

Adam, S., S. Cho, M. S. Fuhrer, and S. Das Sarma, 2008, "Density Inhomogeneity Driven Percolation Metal-Insulator Transition and Dimensional Crossover in Graphene Nanoribbons," Phys. Rev. Lett. **101**, 046404.

Adam, S., and S. Das Sarma, 2008a, "Boltzmann transport and residual conductivity in bilayer graphene," Phys. Rev. B **77**, 115436.

Adam, S., and S. Das Sarma, 2008b, "Transport in suspended graphene," Solid State Commun. **146**, 356.

Adam, S., E. Hwang, and S. Das Sarma, 2008, "Scattering mechanisms and Boltzmann transport in graphene," Physica E (Amsterdam) **40**, 1022.

Adam, S., E. H. Hwang, V. M. Galitski, and S. Das Sarma, 2007, "A self-consistent theory for graphene transport," Proc. Natl. Acad. Sci. U.S.A. **104**, 18 392.

Adam, S., E. H. Hwang, E. Rossi, and S. Das Sarma, 2009, "Theory of charged impurity scattering in two dimensional graphene," Solid State Commun. **149**, 1072.

Adam, S., and M. D. Stiles, 2010, "Temperature dependence of the diffusive conductivity of bilayer graphene," Phys. Rev. B **82**, 075423.

Akhmerov, A. R., and C. W. J. Beenakker, 2008, "Boundary conditions for Dirac fermions on a terminated honeycomb lattice," Phys. Rev. B **77**, 085423.

Akkermans, E., and G. Montambaux, 2007, *Mesoscopic Physics of Electrons and Photons* (Cambridge University, Cambridge).

Aleiner, I., and K. Efetov, 2006, "Effect of Disorder on Transport in Graphene," Phys. Rev. Lett. **97**, 236801.

Alicea, J., and M. P. A. Fisher, 2006, "Graphene integer quantum Hall effect in the ferromagnetic and paramagnetic regimes," Phys. Rev. B **74**, 075422.

Altland, A., 2006, "Low-Energy Theory of Disordered Graphene," Phys. Rev. Lett. **97**, 236802.

Ando, T., 2006, "Screening Effect and Impurity Scattering in Monolayer Graphene," J. Phys. Soc. Jpn. **75**, 074716.

Ando, T., A. B. Fowler, and F. Stern, 1982, "Electronic Properties of two-dimensional systems," Rev. Mod. Phys. **54**, 437.

Apalkov, V. M., and T. Chakraborty, 2006, "Fractional quantum Hall states of Dirac electrons in graphene," Phys. Rev. Lett. **97**, 126801.

Areshkin, D. A., D. Gunlycke, and C. T. White, 2007, "Ballistic transport in graphene nanostrips in the presence of disorder: Importance of edge effects," Nano Lett. **7**, 204.

Attaccalite, C., S. Moroni, P. Gori-Giorgi, and G. B. Bachelet, 2002, "Correlation Energy and Spin Polarization in the 2D Electron Gas," Phys. Rev. Lett. **88**, 256601.

Auslender, M., and M. I. Katsnelson, 2007, "Generalized kinetic equations for charge carriers in graphene," Phys. Rev. B **76**, 235425.

Avouris, P., Z. H. Chen, and V. Perebeinos, 2007, "Carbon-based electronics," Nature Nanotech. **2**, 605.

Balandin, A., S. Ghosh, W. Bao, I. Calizo, D. Teweldebrhan, F. Miao, and C. N. Lau, 2008, "Extremely High Thermal Conductivity of Graphene: Experimental Study," Nano Lett. **8**, 902.

Bao, W. Z., F. Miao, Z. Chen, H. Zhang, W. Y. Jang, C. Dames, and C. N. Lau, 2009, "Controlled ripple texturing of suspended graphene and ultrathin graphite membranes," Nature Nanotech. **4**, 562.

Bardarson, J. H., J. Tworzydlo, P. W. Brouwer, and C. W. J. Beenakker, 2007, "One-Parameter Scaling at the Dirac Point in Graphene," Phys. Rev. Lett. **99**, 106801.

Barlas, Y., R. Cote, K. Nomura, and A. H. MacDonald, 2008, "Intra-Landau-level cyclotron resonance in bilayer graphene," Phys. Rev. Lett. **101**, 097601.

Barlas, Y., T. Pereg-Barnea, M. Polini, R. Asgari, and A. H. MacDonald, 2007, "Chirality and Correlations in Graphene," Phys. Rev. Lett. **98**, 236601.

Barreiro, A., M. Lazzeri, J. Moser, F. Mauri, and A. Bachtold, 2009, "Transport Properties of Graphene in the High-Current Limit," Phys. Rev. Lett. **103**, 076601.

Bastard, G., 1991, *Wave Mechanics Applied to Semiconductor Heterostructures* (Wiley-Interscience, New York).

Basu, D., M. J. Gilbert, L. F. Register, S. K. Banerjee, and A. H. MacDonald, 2008, "Effect of edge roughness on electronic transport in graphene nanoribbon channel metal-oxide-semiconductor field-effect transistors," Appl. Phys. Lett. **92**, 042114.

Beenakker, C. W. J., 1997, "Random-matrix theory of quantum transport," Rev. Mod. Phys. **69**, 731.

Beenakker, C. W. J., 2006, "Specular Andreev Reflection in Graphene," Phys. Rev. Lett. **97**, 067007.

Beenakker, C. W. J., 2008, "Colloquium: Andreev reflection and Klein tunneling in graphene," Rev. Mod. Phys. **80**, 1337.

Beenakker, C. W. J., and M. Büttiker, 1992, "Suppression of shot noise in metallic diffusive conductors," Phys. Rev. B **46**, 1889.

Berezovsky, J., M. Borunda, E. Heller, and R. Westervelt, 2010, "Imaging coherent transport in graphene (part I): mapping universal conductance fluctuations," Nanotechnology **21**, 274013.

Berezovsky, J., and R. M. Westervelt, 2010, "Imaging coherent transport in graphene (part II): probing weak localization," Nanotechnology **21**, 274014.

Berger, C., *et al.*, 2004, "Ultrathin epitaxial graphite: 2D electron gas properties and a route toward graphene-based nanoelectronics," J. Phys. Chem. B **108**, 19 912.

Berger, C., *et al.*, 2006, "Electronic Confinement and Coherence in Patterned Epitaxial Graphene," Science **312**, 1191.

Biel, B., X. Blase, F. Triozon, and S. Roche, 2009, "Anomalous Doping Effects on Charge Transport in Graphene Nanoribbons," Phys. Rev. Lett. **102**, 096803.

Biel, B., F. Triozon, X. Blase, and S. Roche, 2009, "Chemically Induced Mobility Gaps in Graphene Nanoribbons: A Route for Upscaling Device Performances," Nano Lett. **9**, 2725.

Bistritzer, R., and A. H. MacDonald, 2009, "Hydrodynamic theory of transport in doped graphene," Phys. Rev. B **80**, 085109.

Biswas, R. R., S. Sachdev, and D. T. Son, 2007, "Coulomb impurity in graphene," Phys. Rev. B **76**, 205122.

Blake, P., R. Yang, S. V. Morozov, F. Schedin, L. A. Ponomarenko, A. A. Zhukov, R. R. Nair, I. V. Grigorieva, K. S. Novoselov, and A. K. Geim, 2009, "Influence of metal contacts and charge inhomogeneity on transport properties of graphene near the neutrality point," Solid State Commun. **149**, 1068.

Blanter, Y. M., and I. Martin, 2007, "Transport through normal-metal-graphene contacts," Phys. Rev. B **76**, 155433.

Bolotin, K., K. Sikes, Z. Jiang, G. Fudenberg, J. Hone, P. Kim, and H. Stormer, 2008, "Ultrahigh electron mobility in suspended graphene," Solid State Commun. **146**, 351.

Bolotin, K. I., F. Ghahari, M. D. Shulman, H. L. Stormer, and P. Kim, 2009, "Observation of the Fractional Quantum Hall Effect in Graphene," Nature (London) **462**, 196.

Bolotin, K. I., K. J. Sikes, J. Hone, H. L. Stormer, and P. Kim, 2008, "Temperature-Dependent Transport in Suspended Graphene," Phys. Rev. Lett. **101**, 096802.

Borghi, G., M. Polini, R. Asgari, and A. H. MacDonald, 2009, "Dynamical response functions and collective modes of bilayer graphene," Phys. Rev. B **80**, 241402.

Bostwick, A., J. L. McChesney, K. V. Emtsev, T. Seyller, K. Horn, S. D. Kevan, and E. Rotenberg, 2009, "Quasiparticle Transformation during a Metal-Insulator Transition in Graphene," Phys. Rev. Lett. **103**, 056404.

Bostwick, A., T. Ohta, T. Seyller, K. Horn, and E. Rotenberg, 2006, "Quasiparticle dynamics in graphene," Nature Phys. **3**, 36.

Brandt, N. B., S. M. Chudinov, and Y. G. Ponomarev, 1988, *Modern Problems in Condensed Matter Sciences* (North-Holland, Amsterdam), Vol. 29.1.

Brar, V. W., *et al.*, 2010, "Observation of Carrier-Density-Dependent Many-Body Effects in Graphene via Tunneling Spectroscopy," Phys. Rev. Lett. **104**, 036805.

Brar, V. W., Y. Zhang, Y. Yayon, T. Ohta, J. L. McChesney, A. Bostwick, E. Rotenberg, K. Horn, and M. F. Crommie, 2007, "Scanning tunneling spectroscopy of inhomogeneous electronic structure in monolayer and bilayer graphene on SiC," Appl. Phys. Lett. **91**, 122102.

Brey, L., and H. A. Fertig, 2006, "Electronic states of graphene nanoribbons studied with the Dirac equation," Phys. Rev. B **73**, 235411.

Brey, L., and H. A. Fertig, 2009a, "Emerging Zero Modes for Graphene in a Periodic Potential," Phys. Rev. Lett. **103**, 046809.

Brey, L., and H. A. Fertig, 2009b, "Linear response and the Thomas-Fermi approximation in undoped graphene," Phys. Rev. B **80**, 035406.

Brey, L., H. A. Fertig, and S. Das Sarma, 2007, "Diluted Graphene Antiferromagnet," Phys. Rev. Lett. **99**, 116802.

Brey, L., and J. J. Palacios, 2008, "Exchange-induced charge inhomogeneities in rippled neutral graphene," Phys. Rev. B **77**, 041403(R).

Bruggeman, D. A. G., 1935, "Berechnung verschiedener physikalischer Konstanten von heterogenen Substanzen. I. Dielektrizittskonstanten und Leitfhigkeiten der Mischkrper aus isotropen Substanzen [Engl. Trans.: Computation of Different Physical Constants of Heterogeneous Substances. I. Dielectric Constants and Conductivities of Mixtures of Isotropic Substances.]," Ann. Phys. (Leipzig) **416**, 636.

Bruus, H., and K. Flensberg, 2004, *Many-Body Quantum Theory in Condensed Matter Physics: An Introduction* (Oxford University, Oxford).

Bunch, J. S., A. M. van der Zande, S. S. Verbridge, I. W. Frank, D. M. Tanenbaum, J. M. Parpia, H. G. Craighead, and P. L. McEuen, 2007, "Electromechanical Resonators from Graphene Sheets," Science **315**, 490.

Büttiker, M., 1990, "Scattering theory of thermal and excess noise in open conductors," Phys. Rev. Lett. **65**, 2901.

Calandra, M., and F. Mauri, 2007, "Electron-phonon coupling and electron self-energy in electron-doped graphene: Calculation of angular-resolved photoemission spectra," Phys. Rev. B **76**, 205411.

Carbotte, J. P., E. J. Nicol, and S. G. Sharapov, 2010, "Effect of electron-phonon interaction on spectroscopies in graphene," Phys. Rev. B **81**, 045419.

Case, K. M., 1950, "Singular potentials," Phys. Rev. **80**, 797.

Castro, E. V., K. S. Novoselov, S. V. Morozov, N. M. R. Peres, J. M. B. L. D. Santos, J. Nilsson, F. Guinea, A. K. Geim, and A. H. Castro Neto, 2007, "Biased bilayer graphene: Semiconductor with a gap tunable by the electric field effect," Phys. Rev. Lett. **99**, 216802.

Castro Neto, A. H., F. Guinea, and N. M. R. Peres, 2006, "Drawing conclusions from graphene," Phys. World **19**, 33.

Castro Neto, A. H., F. Guinea, N. M. R. Peres, K. S. Novoselov, and A. K. Geim, 2009, ''The electronic properties of graphene,'' Rev. Mod. Phys. **81**, 109.

Cayssol, J., B. Huard, and D. Goldhaber-Gordon, 2009, ''Contact resistance and shot noise in graphene transistors,'' Phys. Rev. B **79**, 075428.

Chakraborty, T., and P. Pietilainen, 2007, ''Spin configurations and activation gaps of the quantum Hall states in graphene,'' Europhys. Lett. **80**, 37007.

Checkelsky, J. G., L. Li, and N. P. Ong, 2008, ''Zero-Energy State in Graphene in a High Magnetic Field,'' Phys. Rev. Lett. **100**, 206801.

Checkelsky, J. G., L. Li, and N. P. Ong, 2009, ''Divergent resistance at the Dirac point in graphene: Evidence for a transition in a high magnetic field,'' Phys. Rev. B **79**, 115434.

Cheianov, V., and V. Fal'ko, 2006a, ''Friedel oscillations, impurity scattering and temperature dependence of resistivity in graphene,'' Phys. Rev. Lett. **97**, 226801.

Cheianov, V., V. Fal'ko, and B. Altshuler, 2007, ''The Focusing of Electron Flow and a Veselago Lens in Graphene *p-n* Junctions,'' Science **315**, 1252.

Cheianov, V., V. Fal'ko, B. Altshuler, and I. Aleiner, 2007, ''Random Resistor Network Model of Minimal Conductivity in Graphene,'' Phys. Rev. Lett. **99**, 176801.

Cheianov, V., and V. I. Fal'ko, 2006b, ''Selective transmission of Dirac electrons and ballistic magnetoresistance of n-p junctions in graphene,'' Phys. Rev. B **74**, 041403(R).

Cheianov, V. V., V. I. Fal'ko, O. Syljuasen, and B. L. Altshuler, 2009, ''Hidden Kekule ordering of adatoms on graphene,'' Solid State Commun. **149**, 1499.

Chen, F., J. L. Xia, D. K. Ferry, and N. J. Tao, 2009, ''Dielectric Screening Enhanced Performance in Graphene FET,'' Nano Lett. **9**, 2571.

Chen, F., J. L. Xia, and N. J. Tao, 2009, ''Ionic Screening of Charged-Impurity Scattering in Graphene,'' Nano Lett. **9**, 1621.

Chen, J. H., C. Jang, S. Adam, M. S. Fuhrer, E. D. Williams, and M. Ishigami, 2008, ''Charged Impurity Scattering in Graphene,'' Nature Phys. **4**, 377.

Chen, J. H., C. Jang, S. Xiao, M. Ishigami, and M. S. Fuhrer, 2008, ''Intrinsic and Extrinsic Performance Limits of Graphene Devices on SiO2,'' Nature Nanotech. **3**, 206.

Chen, Y. L., *et al.*, 2009, ''Experimental Realization of a Three-Dimensional Topological Insulator, Bi2Te3,'' Science **325**, 178.

Chen, Z. H., Y. M. Lin, M. J. Rooks, and P. Avouris, 2007, ''Graphene nano-ribbon electronics,'' Physica (Amsterdam) **40E**, 228.

Chen, J.-H., W. G. Cullen, C. Jang, M. S. Fuhrer, and E. D. Williams, 2009, ''Defect Scattering in Graphene,'' Phys. Rev. Lett. **102**, 236805.

Cho, S., and M. Fuhrer, 2009, ''Massless and massive particle-in-a-box states in single-and bi-layer graphene,'' Nano Res. **4**, 385.

Cho, S., and M. S. Fuhrer, 2008, ''Charge transport and inhomogeneity near the minimum conductivity point in graphene,'' Phys. Rev. B **77**, 081402.

Cho, S., Y.-F. Chen, and M. S. Fuhrer, 2007, ''Gate-tunable graphene spin valve,'' Appl. Phys. Lett. **91**, 123105.

Cortijo, A., and M. A. H. Vomediano, 2007, ''Effects of topological defects and local curvature on the electronic properties of planar graphene,'' Nucl. Phys. **B763**, 293.

Cortijo, A., and M. A. H. Vozmediano, 2009, ''Minimal conductivity of rippled graphene with topological disorder,'' Phys. Rev. B **79**, 184205.

Cserti, J., 2007, ''Minimal longitudinal dc conductivity of perfect bilayer graphene,'' Phys. Rev. B **75**, 033405.

Cserti, J., A. Csordas, and G. David, 2007, ''Role of the trigonal warping on the minimal conductivity of bilayer graphene,'' Phys. Rev. Lett. **99**, 066802.

Dahal, H. P., Y. N. Joglekar, K. S. Bedell, and A. V. Balatsky, 2006, ''Absence of Wigner crystallization in graphene,'' Phys. Rev. B **74**, 233405.

Danneau, R., F. Wu, M. F. Craciun, S. Russo, M. Y. Tomi, J. Salmilehto, A. F. Morpurgo, and P. J. Hakonen, 2008, ''Shot Noise in Ballistic Graphene,'' Phys. Rev. Lett. **100**, 196802.

Darwin, C. G., 1928, ''The Wave Equations of the Electron,'' Proc. R. Soc. A **118**, 654.

DaSilva, A. M., K. Zou, J. K. Jain, and J. Zhu, 2010, ''Mechanism for Current Saturation and Energy Dissipation in Graphene Transistors,'' Phys. Rev. Lett. **104**, 236601.

Das Sarma, S., A. K. Geim, P. Kim, and A. H. MacDonald, Eds., 2007, *Exploring Graphene: Recent Research Advances, A Special Issue of Solid State Communications* (Elsevier, New York), Vol. 143.

Das Sarma, S., and E. H. Hwang, 1999, ''Charged Impurity-Scattering-Limited Low-Temperature Resistivity of Low-Density Silicon Inversion Layers,'' Phys. Rev. Lett. **83**, 164.

Das Sarma, S., and E. H. Hwang, 2003, ''Low-density finite-temperature apparent insulating phase in two-dimensional semiconductor systems,'' Phys. Rev. B **68**, 195315.

Das Sarma, S., and E. H. Hwang, 2004, ''Metallicity and its low-temperature behavior in dilute two-dimensional carrier systems,'' Phys. Rev. B **69**, 195305.

Das Sarma, S., and E. H. Hwang, 2005, ''The so-called two dimensional metal-insulator transition,'' Solid State Commun. **135**, 579.

Das Sarma, S., and E. H. Hwang, 2009, ''Collective Modes of the Massless Dirac Plasma,'' Phys. Rev. Lett. **102**, 206412.

Das Sarma, S., E. H. Hwang, and Q. Li, 2009, ''Valley-dependent many-body effects in two-dimensional semiconductors,'' Phys. Rev. B **80**, 121303.

Das Sarma, S., E. H. Hwang, and E. Rossi, 2010, ''Theory of carrier transport in bilayer graphene,'' Phys. Rev. B **81**, 161407.

Das Sarma, S., E. H. Hwang, and W.-K. Tse, 2007, ''Many-body interaction effects in doped and undoped graphene: Fermi liquid versus non-Fermi liquid,'' Phys. Rev. B **75**, 121406.

Das Sarma, S., and S. Kodiyalam, 1998, ''Intrinsic dopant correlations and transport properties of mesoscopic modulation-doped heterostructures,'' Semicond. Sci. Technol. **13**, A59.

Das Sarma, S., M. P. Lilly, E. H. Hwang, L. N. Pfeiffer, K. W. West, and J. L. Reno, 2005, ''Two-Dimensional Metal-Insulator Transition as a Percolation Transition in a High-Mobility Electron System,'' Phys. Rev. Lett. **94**, 136401.

Das Sarma, S., and A. Pinczuk, Eds., 1996, *Perspecitive in Quantum Hall Effects* (Wiley, New York).

Das Sarma, S., and K. Yang, 2009, ''The enigma of the $nu = 0$ quantum Hall effect in graphene,'' Solid State Commun. **149**, 1502.

Davies, J. H., 1998, *The Physics of Low-Dimensional Semiconductors: An Introduction* (Cambridge University, New York).

de Heer, W. A., *et al.*, 2010, ''Epitaxial graphene electronic structure and transport,'' J. Phys. D **43**, 374007.

de Juan, F., A. Cortijo, and M. A. H. Vozmediano, 2007, ''Charge inhomogeneities due to smooth ripples in graphene sheets,'' Phys. Rev. B **76**, 165409.

Deshpande, A., W. Bao, F. Miao, C. N. Lau, and B. J. LeRoy, 2009, ''Spatially resolved spectroscopy of monolayer graphene on SiO_2,'' Phys. Rev. B **79**, 205411.

Deshpande, A., W. Bao, Z. Zhao, C. N. Lau, and B. J. LeRoy, 2009, ''Mapping the Dirac point in gated bilayer graphene,'' Appl. Phys. Lett. **95**, 243502.

DiCarlo, L., J. R. Williams, Y. Zhang, D. T. McClure, and C. M. Marcus, 2008, "Shot Noise in Graphene," Phys. Rev. Lett. **100**, 156801.

Dietl, P., G. Metalidis, D. Golubev, P. San-Jose, E. Prada, H. Schomerus, and G. Schön, 2009, "Disorder-induced pseudodiffusive transport in graphene nanoribbons," Phys. Rev. B **79**, 195413.

DiVincenzo, D. P., and E. J. Mele, 1984, "Self-consistent effective-mass theory for intralayer screening in graphite-intercalation compounds," Phys. Rev. B **29**, 1685.

Dombey, N., and A. Calogeracos, 1999, Phys. Rep. **315**, 41.

Dragomirova, R. L., D. A. Areshkin, and B. K. Nikoli, 2009, "Shot noise probing of magnetic ordering in zigzag graphene nanoribbons," Phys. Rev. B **79**, 241401.

Dresselhaus, M. S., and G. Dresselhaus, 2002, "Intercalation compounds of graphite," Adv. Phys. **51**, 1.

Du, X., I. Skachko, and E. Y. Andrei, 2008, "Josephson current and multiple Andreev reflections in graphene SNS junctions," Phys. Rev. B **77**, 184507.

Du, X., I. Skachko, A. Barker, and E. Andrei, 2008, "Suspended Graphene: a bridge to the Dirac point," Nature Nanotech. **3**, 491.

Du, X., I. Skachko, F. Duerr, A. Luican, and E. Y. Andrei, 2009, "Fractional quantum Hall effect and insulating phase of Dirac electrons in graphene," Nature (London) **462**, 192.

Ebbesen, T., and T. Takada, 1995, "Topological and sp3 defect structures in nanotubes," Carbon **33**, 973.

Efros, A. L., 1988, "Non-linear screening and the background density of 2DEG states in magnetic field," Solid State Commun. **67**, 1019.

Elias, D. C., *et al.*, 2009, "Control of Graphene's Properties by Reversible Hydrogenation: Evidence for Graphane," Science **323**, 610.

Emtsev, K. V., *et al.*, 2009, "Towards wafer-size graphene layers by atmospheric pressure graphitization of silicon carbide," Nature Mater. **8**, 203.

Eng, K., R. N. McFarland, and B. E. Kane, 2007, "Integer quantum Hall effect on a six-valley hydrogen-passivated silicon surface," Phys. Rev. Lett. **99**, 016801.

Evers, F., and A. D. Mirlin, 2008, "Anderson transitions," Rev. Mod. Phys. **80**, 1355.

Ezawa, M., 2007, "Supersymmetry and unconventional quantum Hall effect in monolayer, bilayer and trilayer graphene," Physica (Amsterdam) **40E**, 269.

Ezawa, M., 2008, "Supersymmetric structure of quantum Hall effects in graphene," Phys. Lett. A **372**, 924.

Fal'ko, V., A. Geim, S. Das Sarma, A. MacDonald, and P. Kim, 2009, "Preface: Recent Progress in Graphene Studies," Solid State Commun. **149**, 1039.

Fal'ko, V. I., K. Kechedzhi, E. McCann, B. L. Altshuler, H. Suzuura, and T. Ando, 2007, "Weak localization in graphene," Solid State Commun. **143**, 33.

Fang, T., A. Konar, H. Xing, and D. Jena, 2007, "Carrier statistics and quantum capacitance of graphene sheets and ribbons," Appl. Phys. Lett. **91**, 092109.

Fasolino, A., J. H. Los, and M. I. Katsnelson, 2007, "Intrinsic ripples in graphene," Nature Mater. **6**, 858.

Feigel'man, M. V., M. A. Skvortsov, and K. S. Tikhonov, 2008, "Proximity-Induced Superconductivity in Graphene," JETP Lett. **88**, 747.

Feldman, B., J. Martin, and A. Yacoby, 2009, "Broken-symmetry states and divergent resistance in suspended bilayer graphene," Nature Phys. **5**, 889.

Fermi, E., 1927, "Application of statistical gas methods to electronic systems," Rendiconti dell'Accademia Nazionale dei Lincei **6**, 602.

Fernandez-Rossier, J., J. J. Palacios, and L. Brey, 2007, "Electronic structure of gated graphene and graphene ribbons," Phys. Rev. B **75**, 205441.

Ferrari, A. C., 2007, "Raman spectroscopy of graphene and graphite: Disorder, electron-phonon coupling, doping and nonadiabatic effects," Solid State Commun. **143**, 47.

Ferrari, A. C., *et al.*, 2006, "Raman Spectrum of Graphene and Graphene Layers," Phys. Rev. Lett. **97**, 187401.

First, P. N., W. A. de Heer, T. Seyller, C. Berger, J. A. Stroscio, and J.-S. Moon, 2011, "Epitaxial Graphenes on Silicon Carbide," MRS Bull. **35**, 296.

Fistul, M. V., and K. B. Efetov, 2007, "Electromagnetic-field-induced suppression of transport through n-p junctions in graphene," Phys. Rev. Lett. **98**, 256803.

Fogler, M. M., 2009, "Neutrality Point of Graphene with Coplanar Charged Impurities," Phys. Rev. Lett. **103**, 236801.

Fogler, M. M., F. Guinea, and M. I. Katsnelson, 2008, "Pseudomagnetic Fields and Ballistic Transport in a Suspended Graphene Sheet," Phys. Rev. Lett. **101**, 226804.

Fogler, M. M., D. S. Novikov, L. I. Glazman, and B. I. Shklovskii, 2008, "Effect of disorder on a graphene p-n junction," Phys. Rev. B **77**, 075420.

Fogler, M. M., D. S. Novikov, and B. I. Shklovskii, 2007, "Screening of a hypercritical charge in graphene," Phys. Rev. B **76**, 233402.

Foster, M. S., and I. L. Aleiner, 2008, "Graphene via large N: A renormalization group study," Phys. Rev. B **77**, 195413.

Foster, M. S., and I. L. Aleiner, 2009, "Slow imbalance relaxation and thermoelectric transport in graphene," Phys. Rev. B **79**, 085415.

Fradkin, E., 1986, "Critical behavior of disordered degenerate semiconductors. I. Models, symmetries, and formalism," Phys. Rev. B **33**, 3257.

Fratini, S., and F. Guinea, 2008, "Substrate-limited electron dynamics in graphene," Phys. Rev. B **77**, 195415.

Fritz, L., J. Schmalian, M. Müller, and S. Sachdev, 2008, "Quantum critical transport in clean graphene," Phys. Rev. B **78**, 085416.

Fuchs, J. N., and P. Lederer, 2007, "Spontaneous parity breaking of graphene in the quantum Hall regime," Phys. Rev. Lett. **98**, 016803.

Galitski, V., S. Adam, and S. Das Sarma, 2007, "Statistics of random voltage fluctuations and the low-density residual conductivity of graphene," Phys. Rev. B **76**, 245405.

Gallagher, P., K. Todd, and D. Goldhaber-Gordon, 2010, "Disorder-induced gap behavior in graphene nanoribbons," Phys. Rev. B **81**, 115409.

Geim, A. K., 2009, "Graphene: Status and Prospects," Science **324**, 1530.

Geim, A. K., and A. H. MacDonald, 2007, "Graphene: Exploring carbon flatland," Phys. Today **60**, No. 8, 35.

Geim, A. K., and K. S. Novoselov, 2007, "The rise of graphene," Nature Mater. **6**, 183.

Geringer, V., M. Liebmann, T. Echtermeyer, S. Runte, M. Schmidt, R. Ruckamp, M. C. Lemme, and M. Morgenstern, 2009, "Intrinsic and extrinsic corrugation of monolayer graphene deposited on SiO2," Phys. Rev. Lett. **102**, 076102.

Gibertini, M., A. Tomadin, M. Polini, A. Fasolino, and M. I. Katsnelson, 2010, "Electron density distribution and screening in rippled graphene sheets," Phys. Rev. B **81**, 125437.

Giesbers, A. J. M., L. A. Ponomarenko, K. S. Novoselov, A. K. Geim, M. I. Katsnelson, J. C. Maan, and U. Zeitler, 2009, "Gap opening in the zeroth Landau level of graphene," Phys. Rev. B **80**, 201403.

Giovannetti, G., P. A. Khomyakov, G. Brocks, V. M. Karpan, J. van den Brink, and P. J. Kelly, 2008, "Doping Graphene with Metal Contacts," Phys. Rev. Lett. **101**, 026803.

Giuliani, G. F., and G. Vignale, 2005, *Quantum Theory of the Electron Liquid* (Cambridge University, Cambridge).

Goerbig, M. O., R. Moessner, and B. Doucot, 2006, "Electron interactions in graphene in a strong magnetic field," Phys. Rev. B **74**, 161407.

Golizadeh-Mojarad, R., and S. Datta, 2009, "Effect of contact induced states on minimum conductivity in graphene," Phys. Rev. B **79**, 085410.

Gonzalez, J., F. Guinea, and V. A. M. Vozmediano, 1994, Nucl. Phys. **B424**, 595.

González, J., F. Guinea, and M. A. H. Vozmediano, 1999, "Marginal-Fermi-liquid behavior from two-dimensional Coulomb interaction," Phys. Rev. B **59**, R2474.

Gorbachev, R., A. Mayorov, A. Savchenko, D. Horsell, and F. Guinea, 2008, "Conductance of *p-n-p* Graphene Structures with Air-Bridge Top Gates," Nano Lett. **8**, 1995.

Gordon, W., 1928, "Die Energieniveaus des Wasserstoffatoms nach der Diracschen Quantentheorie des Elektrons," Z. Phys. A **48**, 11.

Graf, D., F. Molitor, K. Ensslin, C. Stampfer, A. Jungen, C. Hierold, and L. Wirtz, 2007, "Spatially resolved raman spectroscopy of single- and few-layer graphene," Nano Lett. **7**, 238.

Grimes, C. C., and G. Adams, 1979, "Evidence for a Liquid-to-Crystal Phase Transition in a Classical, Two-Dimensional Sheet of Electrons," Phys. Rev. Lett. **42**, 795.

Groth, C. W., J. Tworzydlo, and C. W. J. Beenakker, 2008, "Electronic shot noise in fractal conductors," Phys. Rev. Lett. **100**, 176804.

Guinea, F., 2008, "Models of electron transport in single layer graphene," J. Low Temp. Phys. **153**, 359.

Gusynin, V. P., V. A. Miransky, S. G. Sharapov, and I. A. Shovkovy, 2006, "Excitonic gap, phase transition, and quantum Hall effect in graphene," Phys. Rev. B **74**, 195429.

Gusynin, V. P., and S. G. Sharapov, 2005, "Unconventional Integer Quantum Hall Effect in Graphene," Phys. Rev. Lett. **95**, 146801.

Gusynin, V. P., and S. G. Sharapov, 2006, "Transport of Dirac quasiparticles in graphene: Hall and optical conductivities," Phys. Rev. B **73**, 245411.

Gusynin, V. P., S. G. Sharapov, and J. P. Carbotte, 2009, "On the universal ac optical background in graphene," New J. Phys. **11**, 095013.

Haldane, F. D. M., 1988, "Model for a Quantum Hall Effect without Landau Levels: Condensed-Matter Realization of the "Parity Anomaly"," Phys. Rev. Lett. **61**, 2015.

Halperin, B. I., 1982, "Quantized hall conductance, current-carrying edge states, and the existence of extended states in a two-dimensional disordered potential," Phys. Rev. B **25**, 2185.

Han, M. Y., J. C. Brant, and P. Kim, 2010, "Electron Transport in Disordered Graphene Nanoribbons," Phys. Rev. Lett. **104**, 056801.

Han, M. Y., B. Ozyilmaz, Y. Zhang, and P. Kim, 2007, "Energy Band-Gap Engineering of Graphene Nanoribbons," Phys. Rev. Lett. **98**, 206805.

Han, W., W. H. Wang, K. Pi, K. M. McCreary, W. Bao, Y. Li, F. Miao, C. N. Lau, and R. K. Kawakami, 2009, "Electron-Hole Asymmetry of Spin Injection and Transport in Single-Layer Graphene," Phys. Rev. Lett. **102**, 137205.

Hasan, M. Z., and C. L. K. Kane, 2010, "Topological Insulators," Rev. Mod. Phys. **82**, 3045.

Hass, J., F. Varchon, J. E. Millán-Otoya, M. Sprinkle, N. Sharma, W. A. de Heer, C. Berger, P. N. First, L. Magaud, and E. H. Conrad, 2008, "Why Multilayer Graphene on 4H-SiC(000

[overline 1]) Behaves Like a Single Sheet of Graphene," Phys. Rev. Lett. **100**, 125504.

Heersche, H. B., P. Jarillo-Herrero, J. B. Oostinga, L. M. K. Vandersypen, and A. F. Morpurgo, 2007, "Bipolar supercurrent in graphene," Nature (London) **446**, 56.

Henriksen, E. A., P. Cadden-Zimansky, Z. Jiang, Z. Q. Li, L. C. Tung, M. E. Schwartz, M. Takita, Y. J. Wang, P. Kim, and H. L. Stormer, 2010, "Interaction-Induced shift of the cyclotron resonance of graphene using infrared spectroscopy," Phys. Rev. Lett. **104**, 067404.

Henriksen, E. A., Z. Jiang, L. C. Tung, M. E. Schwartz, M. Takita, Y. J. Wang, P. Kim, and H. L. Stormer, 2008, "Cyclotron resonance in bilayer graphene," Phys. Rev. Lett. **100**, 087403.

Hentschel, M., and F. Guinea, 2007, "Orthogonality catastrophe and Kondo effect in graphene," Phys. Rev. B **76**, 115407.

Herbut, I. F., 2007, "Theory of integer quantum Hall effect in graphene," Phys. Rev. B **75**, 165411.

Herbut, I. F., V. Juričić, and O. Vafek, 2008, "Coulomb Interaction, Ripples, and the Minimal Conductivity of Graphene," Phys. Rev. Lett. **100**, 046403.

Hess, K., and P. Vogl, 1979, "Remote polar phonon scattering in silicon inversion layers," Solid State Commun. **30**, 807.

Hikami, S., A. I. Larkin, and Y. Nagaoka, 1980, "Spin-Orbit Interaction and Magnetoresistance in the Two Dimensional Random System," Prog. Theor. Phys. **63**, 707.

Hill, E., A. Geim, K. Novoselov, F. Schedin, and P. Blake, 2006, "Graphene Spin Valve Devices," IEEE Trans. Magn. **42**, 2694.

Hohenberg, P., and W. Kohn, 1964, "Inhomogeneous Electron Gas," Phys. Rev. **136**, B864.

Hong, X., A. Posadas, K. Zou, C. H. Ahn, and J. Zhu, 2009, "High-Mobility Few-Layer Graphene Field Effect Transistors Fabricated on Epitaxial Ferroelectric Gate Oxides," Phys. Rev. Lett. **102**, 136808.

Hong, X., K. Zou, and J. Zhu, 2009, "Quantum scattering time and its implications on scattering sources in graphene," Phys. Rev. B **80**, 241415.

Hori, M., and F. Yonezawa, 1975 J. Math. Phys. (N.Y.) **16**, 352.

Horsell, D. W., A. K. Savchenko, F. V. Tikhonenko, K. Kechedzhi, I. V. Lerner, and V. I. Fal'ko, 2009, "Mesoscopic conductance fluctuations in graphene," Solid State Commun. **149**, 1041.

Hou, C.-Y., C. Chamon, and C. Mudry, 2010, "Deconfined fractional electric charges in graphene at high magnetic fields," Phys. Rev. B **81**, 075427.

Hsieh, D., D. Qian, L. Wray, Y. Xia, Y. S. Hor, R. J. Cava, and M. Z. Hasan, 2008, "A topological Dirac insulator in a quantum spin Hall phase," Nature (London) **452**, 970.

Huang, J., D. S. Novikov, D. C. Tsui, L. N. Pfeiffer, and K. W. West, 2006, "Nonactivated transport of strongly interacting two-dimensional holes in GaAs," Phys. Rev. B **74**, 201302.

Huard, B., N. Stander, J. A. Sulpizio, and D. Goldhaber-Gordon, 2008, "Evidence of the role of contacts on the observed electron-hole asymmetry in graphene," Phys. Rev. B **78**, 121402.

Huard, B., J. A. Sulpizio, N. Stander, K. Todd, B. Yang, and D. Goldhaber-Gordon, 2007, "Transport Measurements Across a Tunable Potential Barrier in Graphene," Phys. Rev. Lett. **98**, 236803.

Huertas-Hernando, D., F. Guinea, and A. Brataas, 2006, "Spin-orbit coupling in curved graphene, fullerenes, nanotubes, and nanotube caps," Phys. Rev. B **74**, 155426.

Huertas-Hernando, D., F. Guinea, and A. Brataas, 2009, "Spin-Orbit-Mediated Spin Relaxation in Graphene," Phys. Rev. Lett. **103**, 146801.

Hwang, E. H., S. Adam, and S. Das Sarma, 2007a, "Carrier transport in 2D graphene layers," Phys. Rev. Lett. **98**, 186806.

Hwang, E. H., S. Adam, and S. Das Sarma, 2007b, "Transport in chemically doped graphene in the presence of adsorbed molecules," Phys. Rev. B **76**, 195421.

Hwang, E. H., and S. Das Sarma, 2007, "Dielectric function, screening and plasmons in 2D graphene," Phys. Rev. B **75**, 205418.

Hwang, E. H., and S. Das Sarma, 2008a, "Acoustic phonon scattering limited carrier mobility in two-dimensional extrinsic graphene," Phys. Rev. B **77**, 115449.

Hwang, E. H., and S. Das Sarma, 2008b, "Limit to two-dimensional mobility in modulation-doped GaAs quantum structures: How to achieve a mobility of 100 million," Phys. Rev. B **77**, 235437.

Hwang, E. H., and S. Das Sarma, 2008c, "Quasiparticle spectral function in doped graphene: Electron-electron interaction effects in ARPES," Phys. Rev. B **77**, 081412.

Hwang, E. H., and S. Das Sarma, 2008d, "Screening, Kohn Anomaly, Friedel Oscillation, and RKKY Interaction in Bilayer Graphene," Phys. Rev. Lett. **101**, 156802.

Hwang, E. H., and S. Das Sarma, 2008e, "Single-particle relaxation time versus transport scattering time in a two-dimensional graphene layer," Phys. Rev. B **77**, 195412.

Hwang, E. H., and S. Das Sarma, 2009a, "Plasmon modes of spatially separated double-layer graphene," Phys. Rev. B **80**, 205405.

Hwang, E. H., and S. Das Sarma, 2009b, "Screening-induced temperature-dependent transport in two-dimensional graphene," Phys. Rev. B **79**, 165404.

Hwang, E. H., and S. Das Sarma, 2010, "Insulating behavior in metallic bilayer graphene: Interplay between density inhomogeneity and temperature," Phys. Rev. B **82**, 081409.

Hwang, E. H., E. Rossi, and S. Das Sarma, 2009, "Theory of thermopower in 2D graphene," Phys. Rev. B **80**, 235415.

Hwang, E. H., B. Y.-K. Hu, and S. Das Sarma, 2007a, "Density Dependent Exchange Contribution to [partial-derivative] mu/[partial-derivative]n and Compressibility in Graphene," Phys. Rev. Lett. **99**, 226801.

Hwang, E. H., B. Y.-K. Hu, and S. Das Sarma, 2007b, "Inelastic carrier lifetime in graphene," Phys. Rev. B **76**, 115434.

Ilani, S., J. Martin, E. Teitelbaum, J. H. Smet, D. Mahalu, V. Umansky, and A. Yacoby, 2004, "The microscopic nature of localization in the quantum Hall effect," Nature (London) **427**, 328.

Ishigami, M., J. H. Chen, W. G. Cullen, M. S. Fuhrer, and E. D. Williams, 2007, "Atomic structure of graphene on SiO$_2$," Nano Lett. **7**, 1643.

Isichenko, M. B., 1992, "Percolation, statistical topography, and transport in random-media," Rev. Mod. Phys. **64**, 961.

Jackiw, R., 1984, "Fractional charge and zero modes for planar systems in a magnetic-field," Phys. Rev. D **29**, 2375.

Jang, C., S. Adam, J.-H. Chen, E. D. Williams, S. Das Sarma, and M. S. Fuhrer, 2008, "Tuning the Effective Fine Structure Constant in Graphene: Opposing Effects of Dielectric Screening on Short- and Long-Range Potential Scattering," Phys. Rev. Lett. **101**, 146805.

Ji, Y., Y. Chung, D. Sprinzak, M. Heiblum, D. Mahalu, and H. Shtrikman, 2003, "An electronic Mach-Zehnder interferomete," Nature (London) **422**, 415.

Jiang, H. W., H. L. Stormer, D. C. Tsui, L. N. Pfeiffer, and K. W. West, 1991, "Magnetotransport studies of the insulating phase around $\nu = 1/5$ Landau-level filling," Phys. Rev. B **44**, 8107.

Jiang, H. W., R. L. Willett, H. L. Stormer, D. C. Tsui, L. N. Pfeiffer, and K. W. West, 1990, "Quantum liquid versus electron solid around $\nu = 1/5$ Landau-level filling," Phys. Rev. Lett. **65**, 633.

Jiang, Z., E. A. Henriksen, L. C. Tung, Y.-J. Wang, M. E. Schwartz, M. Y. Han, P. Kim, and H. L. Stormer, 2007, "Infrared Spectroscopy of Landau Levels of Graphene," Phys. Rev. Lett. **98**, 197403.

Jiao, L. Y., L. Zhang, X. R. Wang, G. Diankov, and H. J. Dai, 2009, "Narrow graphene nanoribbons from carbon nanotubes," Nature (London) **458**, 877.

Józsa, C., T. Maassen, M. Popinciuc, P. J. Zomer, A. Veligura, H. T. Jonkman, and B. J. van Wees, 2009, "Linear scaling between momentum and spin scattering in graphene," Phys. Rev. B **80**, 241403.

Jung, J., and A. H. MacDonald, 2009, "Theory of the magnetic-field-induced insulator in neutral graphene sheets," Phys. Rev. B **80**, 235417.

Kane, C. L., and E. J. Mele, 2005a, "Quantum spin Hall effect in graphene," Phys. Rev. Lett. **95**, 226801.

Kane, C. L., and E. J. Mele, 2005b, "Z2 Topological Order and the Quantum Spin Hall Effect," Phys. Rev. Lett. **95**, 146802.

Kane, C. L., *et al.*, 1998, "Temperature-dependent resistivity of single-wall carbon nanotubes," Europhys. Lett. **41**, 683.

Kashuba, A. B., 2008, "Conductivity of defectless graphene," Phys. Rev. B **78**, 085415.

Katsnelson, M., 2007, "Scattering of charge carriers by point defects in bilayer graphene," Phys. Rev. B **76**, 073411.

Katsnelson, M. I., 2006, "Zitterbewegung, chirality, and minimal conductivity in graphene," Eur. Phys. J. B **51**, 157.

Katsnelson, M. I., 2008, "Optical properties of graphene: The Fermi-liquid approach," Europhys. Lett. **84**, 37001.

Katsnelson, M. I., and A. K. Geim, 2008, "Electron scattering on microscopic corrugations in graphene," Phil. Trans. R. Soc. A **366**, 195.

Katsnelson, M. I., F. Guinea, and A. K. Geim, 2009, "Scattering of electrons in graphene by clusters of impurities," Phys. Rev. B **79**, 195426.

Katsnelson, M. I., K. S. Novoselov, and A. K. Geim, 2006, "Chiral tunneling and the Klein paradox in graphene," Nature Phys. **2**, 620.

Kawamura, T., and S. Das Sarma, 1990, "Temperature dependence of the low-temperature mobility in ultrapure $Al_xGa_{1-x}As$/GaAs heterojunctions: Acoustic-phonon scattering," Phys. Rev. B **42**, 3725.

Kawamura, T., and S. Das Sarma, 1992, "Phonon-scattering-limited electron mobilities in $Al_xGa_{1-x}As$/GaAs heterojunctions," Phys. Rev. B **45**, 3612.

Kawamura, T., and S. Das Sarma, 1996, "Spatial correlation effect of ionized impurities on relaxation and scattering times in high-mobility GaAs heterojunctions," Solid State Commun. **100**, 411.

Kechedzhi, K., O. Kashuba, and V. I. Fal'ko, 2008, "Quantum kinetic equation and universal conductance fluctuations in graphene," Phys. Rev. B **77**, 193403.

Kharitonov, M. Y., and K. B. Efetov, 2008, "Universal conductance fluctuations in graphene," Phys. Rev. B **78**, 033404.

Kim, E., and A. H. Castro Neto, 2008, "Graphene as an electronic membrane," Europhys. Lett. **84**, 57007.

Kim, K. S., Y. Zhao, H. Jang, S. Y. Lee, J. M. Kim, K. S. Kim, J.-H. Ahn, P. Kim, J.-Y. Choi, and B. H. Hong, 2009, "Large-scale pattern growth of graphene films for stretchable transparent electrodes," Nature (London) **457**, 706.

Kim, S., J. Nah, I. Jo, D. Shahrjerdi, L. Colombo, Z. Yao, E. Tutuc, and S. K. Banerjee, 2009, "Realization of a high mobility dual-gated graphene field-effect transistor with Al[sub 2]O[sub 3] dielectric," Appl. Phys. Lett. **94**, 062107.

Klein, O., 1929, "Die reflexion von elektronen an einem potential-sprung nach der relativischen dynamik von Dirac," Z. Phys. **53**, 157.

Kohn, W., 1959, "Image of the Fermi Surface in the Vibration Spectrum of a Metal," Phys. Rev. Lett. **2**, 393.

Kohn, W., 1961, "Cyclotron Resonance and de Haas-van Alphen Oscillations of an Interacting Electron Gas," Phys. Rev. **123**, 1242.

Kohn, W., 1999, "Nobel Lecture: Electronic structure of matter-wave functions and density functionals," Rev. Mod. Phys. **71**, 1253.

Kohn, W., and L. J. Sham, 1965, "Self-Consistent Equations Including Exchange and Correlation Effects," Phys. Rev. **140**, A1133.

Kondev, J., C. L. Henley, and D. G. Salinas, 2000, "Nonlinear measures for characterizing rough surface morphologies," Phys. Rev. E **61**, 104.

Koshino, M., and T. Ando, 2006, "Transport in bilayer graphene: Calculations within a self-consistent Born approximation," Phys. Rev. B **73**, 245403.

Koshino, M., and T. Ando, 2007, "Splitting of the quantum Hall transition in disordered graphenes," Phys. Rev. B **75**, 033412.

Kosynkin, D. V., A. L. Higginbotham, A. Sinitskii, J. R. Lomeda, A. Dimiev, B. K. Price, and J. M. Tour, 2009, "Longitudinal unzipping of carbon nanotubes to form graphene nanoribbons," Nature (London) **458**, 872.

Kravchenko, S. V., G. V. Kravchenko, J. E. Furneaux, V. M. Pudalov, and M. D'Iorio, 1994, "Possible metal-insulator transition at $B = 0$ in two dimensions," Phys. Rev. B **50**, 8039.

Kravchenko, S. V., and M. P. Sarachik, 2004, "Metal-Insulator Transition in Two-Dimensional Electron Systems," Rep. Prog. Phys. **67**, 1.

Kuzmenko, A. B., E. van Heumen, F. Carbone, and D. van der Marel, 2008, "Universal Optical Conductance of Graphite," Phys. Rev. Lett. **100**, 117401.

Landau, L. D., and E. M. Lifshitz, 1977, *Quantum mechanics*, Course in Theoretical Physic Vol. 3 (Pergamon, Oxford).

Landauer, R., 1952, "The Electrical Resistance of Binary Metallic Mixtures," J. Appl. Phys. **23**, 779.

Laughlin, R. B., 1981, "Quantized hall conductivity in 2 dimensions," Phys. Rev. B **23**, 5632.

Lee, C., X. Wei, J. W. Kysar, and J. Hone, 2008, "Measurement of the Elastic Properties and Intrinsic Strength of Monolayer Graphene," Science **321**, 385.

Lee, C. A., R. Sharma, A. D. Radadia, R. I. Masel, and M. S. Strano, 2008, "On-chip micro gas chromatograph enabled by a non-covalently funcationalied single-walled carbon nanotube sensor array," Angew. Chem., Int. Ed. Engl. **47**, 5018.

Lee, E. J. H., K. Balasubramanian, R. T. Weitz, M. Burghard, and K. Kern, 2008, "Contact and edge effects in graphene devices," Nature Nanotech. **3**, 486.

Lee, P. A., and T. V. Ramakrishnan, 1985, "Disordered electronic systems," Rev. Mod. Phys. **57**, 287.

Lemme, M., T. Echtermeyer, M. Baus, and H. Kurz, 2007, "A Graphene Field-Effect Device," IEEE Electron Device Lett. **28**, 282.

Lewenkopf, C. H., E. R. Mucciolo, and A. H. Castro Neto, 2008, "Numerical studies of conductivity and Fano factor in disordered graphene," Phys. Rev. B **77**, 081410.

Li, J., and S. Q. Shen, 2008, "Disorder effects in the quantum Hall effect of graphene *p-n* junctions," Phys. Rev. B **78**, 205308.

Li, X., W. Cai, J. An, S. Kim, S. K. Nah, J, L. Colombo, and R. S. Ruoff, 2009, "Large-Area Synthesis of High-Quality and Uniform Graphene Films on Copper Foils," Science **324**, 1312.

Li, Z., E. Henriksen, Z. Jiang, Z. Hao, M. Martin, P. Kim, H. Stormer, and D. Basov, 2008, "Dirac charge dynamics in graphene by infrared spectroscopy," Nature Phys. **4**, 532.

Liang, W., M. Bockrath, D. Bozovic, J. Hafner, M. Tinkham, and H. Park, 2001, "Fabry-Perot interference in a nanotube electron waveguide," Nature (London) **411**, 665.

Lilly, M. P., J. L. Reno, J. A. Simmons, I. B. Spielman, J. P. Eisenstein, L. N. Pfeiffer, K. W. West, E. H. Hwang, and S. Das Sarma, 2003, "Resistivity of Dilute 2D Electrons in an Undoped GaAs Heterostructure," Phys. Rev. Lett. **90**, 056806.

Liu, G., J. Velasco, W. Bao, and C. Lau, 2008, "Fabrication of graphene *p-n-p* junctions with contactless top gates," Appl. Phys. Lett. **92**, 203103.

Long, W., Q. F. Sun, and J. Wang, 2008, "Disorder-Induced Enhancement of Transport through Graphene *p-n* Junctions," Phys. Rev. Lett. **101**, 166806.

Low, T., 2009, "Ballistic-Ohmic quantum Hall plateau transition in a graphene $p - n$ junction," Phys. Rev. B **80**, 205423.

Low, T., and J. Appenzeller, 2009, "Electronic transport properties of a tilted graphene *p-n* junction," Phys. Rev. B **80**, 155406.

Ludwig, A. W. W., M. P. A. Fisher, R. Shankar, and G. Grinstein, 1994, "Integer quantum Hall transition: An alternative approach and exact results," Phys. Rev. B **50**, 7526.

Lui, C. H., L. Liu, K. F. Mak, G. W. Flynn, and T. F. Heinz, 2009, "Ultraflat graphene," Nature (London) **462**, 339.

Luk'yanchuk, I. A., and Y. Kopelevich, 2004, "Phase analysis of quantum oscillations in graphite," Phys. Rev. Lett. **93**, 166402.

Lutchyn, R. M., V. Galitski, G. Refael, and S. Das Sarma, 2008, "Dissipation-Driven Quantum Phase Transition in Superconductor-Graphene Systems," Phys. Rev. Lett. **101**, 106402.

Lv, M., and S. Wan, 2010, "Screening-induced transport at finite temperature in bilayer graphene," Phys. Rev. B **81**, 195409.

MacDonald, A. H., 1990, *Quantum Hall Effect: A Perspective* (Kluwer Academic, Dordrecht, The Netherlands).

Mak, K. F., C. H. Lui, J. Shan, and T. F. Heinz, 2009, "Observation of an Electric-Field-Induced Band Gap in Bilayer Graphene by Infrared Spectroscopy," Phys. Rev. Lett. **102**, 256405.

Mak, K. F., M. Y. Sfeir, Y. Wu, C. H. Lui, J. A. Misewich, and T. F. Heinz, 2008, "Measurement of the Optical Conductivity of Graphene," Phys. Rev. Lett. **101**, 196405.

Manfra, M. J., E. H. Hwang, S. Das Sarma, L. N. Pfeiffer, K. W. West, and A. M. Sergent, 2007, "Transport and Percolation in a Low-Density High-Mobility Two-Dimensional Hole System," Phys. Rev. Lett. **99**, 236402.

Mariani, E., and F. von Oppen, 2008, "Flexural Phonons in Free-Standing Graphene," Phys. Rev. Lett. **100**, 076801.

Martin, I., and Y. M. Blanter, 2009, "Transport in disordered graphene nanoribbons," Phys. Rev. B **79**, 235132.

Martin, J., N. Akerman, G. Ulbricht, T. Lohmann, J. H. Smet, K. von Klitzing, and A. Yacobi, 2008, "Observation of Electron-hole Puddles in Graphene Using a Scanning Single Electron Transistor," Nature Phys. **4**, 144.

Martin, J., N. Akerman, G. Ulbricht, T. Lohmann, K. von Klitzing, J. H. Smet, and A. Yacoby, 2009, "The nature of localization in graphene under quantum Hall conditions," Nature Phys. **5**, 669.

Maultzsch, J., S. Reich, C. Thomsen, H. Requardt, and P. Ordejón, 2004, "Phonon Dispersion in Graphite," Phys. Rev. Lett. **92**, 075501.

McCann, E., 2006, "Asymmetry gap in the electronic band structure of bilayer graphene," Phys. Rev. B **74**, 161403.

McCann, E., and V. Fal'ko, 2006, "Landau-Level Degeneracy and Quantum Hall Effect in a Graphite Bilayer," Phys. Rev. Lett. **96**, 086805.

McCann, E., K. Kechedzhi, V. I. Fal'ko, H. Suzuura, T. Ando, and B. Altshuler, 2006, "Weak localisation magnetoresistance and valley symmetry in graphene," Phys. Rev. Lett. **97**, 146805.

McClure, J. W., 1964, "Energy band structure of graphite," IBM J. Res. Dev. **8**, 255.

McClure, J. W., 1957, "Band Structure of Graphite and de Haas-van Alphen Effect," Phys. Rev. **108**, 612.

McFarland, R. N., T. M. Kott, L. Y. Sun, K. Eng, and B. E. Kane, 2009, "Temperature-dependent transport in a sixfold degenerate two-dimensional electron system on a H-Si surface," Phys. Rev. B **80**, 161310.

Meyer, J. C., A. K. Geim, M. I. Katsnelson, K. S. Novoselov, T. J. Booth, and S. Roth, 2007, "The structure of suspended graphene sheets," Nature (London) **446**, 60.

Miao, F., S. Wijeratne, Y. Zhang, U. Coskun, W. Bao, and C. Lau, 2007, "Phase Coherent Transport of Charges in Graphene Quantum Billiards," Science **317**, 1530.

Mikitik, G. P., and Y. V. Sharlai, 1999, "Manifestation of Berry's phase in metal physics," Phys. Rev. Lett. **82**, 2147.

Miller, D., K. Kubista, G. Rutter, M. Ruan, W. de Heer, P. First, and J. Stroscio, 2009, "Observing the Quantization of Zero Mass Carriers in Graphene," Science **324**, 924.

Miller, J. B., D. M. Zumbühl, C. M. Marcus, Y. B. Lyanda-Geller, D. Goldhaber-Gordon, K. Campman, and A. C. Gossard, 2003, "Gate-Controlled Spin-Orbit Quantum Interference Effects in Lateral Transport," Phys. Rev. Lett. **90**, 076807.

Min, H., R. Bistritzer, J.-J. Su, and A. H. MacDonald, 2008, "Room-temperature superfluidity in graphene bilayers," Phys. Rev. B **78**, 121401.

Min, H., G. Borghi, M. Polini, and A. H. MacDonald, 2008, "Pseudospin magnetism in graphene," Phys. Rev. B **77**, 041407 (R).

Min, H., and A. H. MacDonald, 2009, "Origin of Universal Optical Conductivity and Optical Stacking Sequence Identification in Multilayer Graphene," Phys. Rev. Lett. **103**, 067402.

Min, H., B. Sahu, S. K. Banerjee, and A. H. MacDonald, 2007, "Ab initio theory of gate induced gaps in graphene bilayers," Phys. Rev. B **75**, 155115.

Mishchenko, E. G., 2007, "Effect of Electron-Electron Interactions on the Conductivity of Clean Graphene," Phys. Rev. Lett. **98**, 216801.

Mishchenko, E. G., 2009, "Dynamic Conductivity in Graphene beyond Linear Response," Phys. Rev. Lett. **103**, 246802.

Moore, B. T., and D. K. Ferry, 1980, "Remote polar phonon scattering in Si inversion layers," J. Appl. Phys. **51**, 2603.

Morozov, S. V., K. S. Novoselov, M. I. Katsnelson, F. Schedin, D. C. Elias, J. A. Jaszczak, and A. K. Geim, 2008, "Giant Intrinsic Carrier Mobilities in Graphene and Its Bilayer," Phys. Rev. Lett. **100**, 016602.

Morozov, S. V., K. S. Novoselov, M. I. Katsnelson, F. Schedin, L. A. Ponomarenko, D. Jiang, and A. K. Geim, 2006, "Strong Suppression of Weak Localization in Graphene," Phys. Rev. Lett. **97**, 016801.

Morpurgo, A. F., and F. Guinea, 2006, "Intervalley Scattering, Long-Range Disorder, and Effective Time-Reversal Symmetry Breaking in Graphene," Phys. Rev. Lett. **97**, 196804.

Moser, J., A. Barreiro, and A. Bachtold, 2007, "Current-induced cleaning of graphene," Appl. Phys. Lett. **91**, 163513.

Mounet, N., and N. Marzari, 2005, "First-principles determination of the structural, vibrational and thermodynamic properties of diamond, graphite, and derivatives," Phys. Rev. B **71**, 205214.

Mucciolo, E. R., A. H. Castro Neto, and C. H. Lewenkopf, 2009, "Conductance quantization and transport gaps in disordered graphene nanoribbons," Phys. Rev. B **79**, 075407.

Mucciolo, E. R., and C. H. Lewenkopf, 2010, "Disorder and Electronic Transport in Graphene," J. Phys. Condens. Matter **22**, 273201.

Mucha-Kruczynski, M., E. McCann, and V. I. Fal'ko, 2010, "Electron-hole asymmetry and energy gaps in bilayer graphene," Semicond. Sci. Technol. **25**, 033001.

Muller, M., J. Schmalian, and L. Fritz, 2009, "Graphene: A Nearly Perfect Fluid," Phys. Rev. Lett. **103**, 025301.

Müller, M., M. Bräuninger, and B. Trauzettel, 2009, "Temperature Dependence of the Conductivity of Ballistic Graphene," Phys. Rev. Lett. **103**, 196801.

Müller, M., L. Fritz, and S. Sachdev, 2008, "Quantum-critical relativistic magnetotransport in graphene," Phys. Rev. B **78**, 115406.

Nair, R. R., P. Blake, A. N. Grigorenko, K. S. Novoselov, T. J. Booth, T. Stauber, N. M. R. Peres, and A. K. Geim, 2008, "Fine Structure Constant Defines Visual Transparency of Graphene," Science **320**, 1308.

Nilsson, J., A. Castro Neto, N. Peres, and F. Guinea, 2006a, "Electron-electron interactions and the phase diagram of a graphene bilayer," Phys. Rev. B **73**, 214418.

Nilsson, J., A. H. Castro Neto, F. Guinea, and N. M. R. Peres, 2006b, "Electronic Properties of Graphene Multilayers," Phys. Rev. Lett. **97**, 266801.

Nilsson, J., A. H. Castro Neto, F. Guinea, and N. M. R. Peres, 2008, "Electronic properties of bilayer and multilayer graphene," Phys. Rev. B **78**, 045405.

Nixon, J. A., and J. H. Davies, 1990, "Potential fluctuations in heterostructure devices," Phys. Rev. B **41**, 7929.

Noh, H., M. P. Lilly, D. C. Tsui, J. A. Simmons, E. H. Hwang, D. Das Sarma, L. N. Pfeiffer, and K. W. West, 2003, "Interaction corrections to two-dimensional hole transport in the *large-rs* limit," Phys. Rev. B **68**, 165308.

Nomura, K., M. Koshino, and S. Ryu, 2007, "Topological Delocalization of Two-Dimensional Massless Dirac Fermions," Phys. Rev. Lett. **99**, 146806.

Nomura, K., and A. H. MacDonald, 2006, "Quantum Hall Ferromagnetism in Graphene," Phys. Rev. Lett. **96**, 256602.

Nomura, K., and A. H. MacDonald, 2007, "Quantum Transport of Massless Dirac Fermions in Graphene," Phys. Rev. Lett. **98**, 076602.

Nomura, K., S. Ryu, and D.-H. Lee, 2009, "Field-Induced Kosterlitz-Thouless Transition in the $N = $ Landau Level of Graphene Landau Level of Graphene," Phys. Rev. Lett. **103**, 216801.

Nomura, K., S. Ryu, M. Koshino, C. Mudry, and A. Furusaki, 2008, "Quantum Hall Effect of Massless Dirac Fermions in a Vanishing Magnetic Field," Phys. Rev. Lett. **100**, 246806.

Novikov, D. S., 2007a, "Elastic scattering theory and transport in graphene," Phys. Rev. B **76**, 245435.

Novikov, D. S., 2007b, "Numbers of donors and acceptors from transport measurements in graphene," Appl. Phys. Lett. **91**, 102102.

Novoselov, K., E. McCann, S. Morozov, V. Falko, M. Katsnelson, U. Zeitler, D. Jiang, F. Schedin, and A. Geim, 2006, "Unconventional quantum Hall effect and Berry's phase of 2pi in bilayer graphene," Nature Phys. **2**, 177.

Novoselov, K. S., A. K. Geim, S. V. Morozov, D. Jiang, Y. Zhang, S. V. Dubonos, I. V. Grigorieva, and A. A. Firsov, 2004, "Electric Field Effect in Atomically Thin Carbon Films," Science **306**, 666.

Novoselov, K. S., A. K. Geim, S. V. Morozov, D. Jiang, Y. Zhang, M. I. Katsnelson, I. V. Grigorieva, S. V. Dubonos, and A. A. Firsov, 2005, "Two-dimensional gas of massless Dirac fermions in graphene," Nature (London) **438**, 197.

Novoselov, K. S., D. Jiang, F. Schedin, T. J. Booth, V. V. Khotkevich, S. V. Morozov, and A. K. Geim, 2005, "Two-dimensional atomic crystals," Proc. Natl. Acad. Sci. U.S.A. **102**, 10451.

Novoselov, K. S., Z. Jiang, Y. Zhang, S. V. Morozov, H. L. Stormer, U. Zeitler, J. C. Maan, G. S. Boebinger, P. Kim, and A. K. Geim, 2007, "Room-Temperature Quantum Hall Effect in Graphene," Science **315**, 1379.

Ohta, T., A. Bostwick, T. Seyller, K. Horn, and E. Rotenberg, 2006, "Controlling the electronic structure of bilayer graphene," Science **313**, 951.

Oostinga, J., H. Heersche, X. Liu, A. Morpurgo, and L. Vandersypen, 2007, "Gate-tunable band-gap in bilayer graphene devices," Nature Mater. **7**, 151.

Orlita, M., *et al.*, 2008, "Approaching the Dirac Point in High-Mobility Multilayer Epitaxial Graphene," Phys. Rev. Lett. **101**, 267601.

Ostrovsky, P. M., I. V. Gornyi, and A. D. Mirlin, 2006, "Electron transport in disordered graphene," Phys. Rev. B **74**, 235443.

Özyilmaz, B., P. Jarillo-Herrero, D. Efetov, D. A. Abanin, L. S. Levitov, and P. Kim, 2007, "Electronic Transport and Quantum Hall Effect in Bipolar Graphene *p-n-p* Junctions," Phys. Rev. Lett. **99**, 166804.

Papadakis, S. J., and M. Shayegan, 1998, "Apparent metallic behavior at $B =$ of a two-dimensional electron system in AlAs," Phys. Rev. B **57**, R15068.

Park, C.-H., F. Giustino, M. L. Cohen, and S. G. Louie, 2007, "Velocity Renormalization and Carrier Lifetime in Graphene from the Electron-Phonon Interaction," Phys. Rev. Lett. **99**, 086804.

Park, C.-H., F. Giustino, C. D. Spataru, M. L. Cohen, and S. G. Louie, 2009, "First-Principles Study of Electron Linewidths in Graphene," Phys. Rev. Lett. **102**, 076803.

Park, C.-H., L. Yang, Y.-W. Son, M. L. Cohen, and S. G. Louie, 2008, "Anisotropic behaviours of massless Dirac fermions in graphene under periodic potentials," Nature Phys. **4**, 213.

Pereira, V. M., A. H. Castro Neto, and N. M. R. Peres, 2009, "Tight-binding approach to uniaxial strain in graphene," Phys. Rev. B **80**, 045401.

Pereira, V. M., J. Nilsson, and A. H. Castro Neto, 2007, "Coulomb Impurity Problem in Graphene," Phys. Rev. Lett. **99**, 166802.

Peres, N. M. R., F. Guinea, and A. H. Castro Neto, 2005, "Coulomb interactions and ferromagnetism in pure and doped graphene," Phys. Rev. B **72**, 174406.

Peres, N. M. R., F. Guinea, and A. H. Castro Neto, 2006, "Electronic properties of disordered two-dimensional carbon," Phys. Rev. B **73**, 125411.

Peres, N. M. R., and T. Stauber, 2008, "Transport in a clean graphene sheet at finite temperature and frequency," Int. J. Mod. Phys. B **22**, 2529.

Peres, N. M. R., T. Stauber, and A. H. Castro Neto, 2008, "The infrared conductivity of graphene on top of silicon oxide," Europhys. Lett. **84**, 38002.

Pfeiffer, L., K. W. West, H. L. Stormer, and K. W. Baldwin, 1989, "Electron mobilities exceeding 10^7 cm^2/V s modulation-doped GaAs," Appl. Phys. Lett. **55**, 1888.

Pietronero, L., S. Strässler, H. R. Zeller, and M. J. Rice, 1980, "Electrical conductivity of a graphite layer," Phys. Rev. B **22**, 904.

Polini, M., R. Asgari, Y. Barlas, T. Pereg-Barnea, and A. MacDonald, 2007, "Graphene: A Pseudochiral Fermi Liquid," Solid State Commun. **143**, 58.

Polini, M., R. Asgari, G. Borghi, Y. Barlas, T. Pereg-Barnea, and A. H. MacDonald, 2008, "Plasmons and the spectral function of graphene," Phys. Rev. B **77**, 081411.

Polini, M., A. Tomadin, R. Asgari, and A. H. MacDonald, 2008, "Density functional theory of graphene sheets," Phys. Rev. B **78**, 115426.

Pomeranchuk, I., and Y. A. Smorodinsky, 1945, "On energy levels in systems with $Z > 137$," J. Phys. USSR **9**, 97.

Ponomarenko, L. A., F. Schedin, M. I. Katsnelson, R. Yang, E. W. Hill, K. S. Novoselov, and A. K. Geim, 2008, "Chaotic dirac billiard in graphene quantum dots," Science **320**, 356.

Ponomarenko, L. A., R. Yang, T. M. Mohiuddin, M. I. Katsnelson, K. S. Novoselov, S. V. Morozov, A. A. Zhukov, F. Schedin, E. W. Hill, and A. K. Geim, 2009, "Effect of a High-kappa Environment on Charge Carrier Mobility in Graphene," Phys. Rev. Lett. **102**, 206603.

Prada, E., P. San-Jose, G. León, M. M. Fogler, and F. Guinea, 2010, "Singular elastic strains and magnetoconductance of suspended graphene," Phys. Rev. B **81**, 161402.

Prange, R. E., and S. M. Girvin, 1990, *The Quantum Hall Effect* (Springer, New York).

Rammer, J., 1988, *Quantum Transport Theory* (Perseus, Reading, MA).

Reich, S., J. Maultzsch, C. Thomsen, and P. Ordejon, 2002, "Tight-binding description of graphene," Phys. Rev. B **66**, 035412.

Robinson, J. P., H. Schomerus, L. Oroszlány, and V. I. Fal'ko, 2008, "Adsorbate-Limited Conductivity of Graphene," Phys. Rev. Lett. **101**, 196803.

Rossi, E., S. Adam, and S. Das Sarma, 2009, "Effective medium theory for disordered two-dimensional graphene," Phys. Rev. B **79**, 245423.

Rossi, E., J. H. Bardarson, P. W. Brouwer, and S. Das Sarma, 2010, "Signatures of Klein tunneling in disordered graphene *p-n-p* junctions," Phys. Rev. B **81**, 121408.

Rossi, E., J. H. Bardarson, M. S. Fuhrer, and S. Das Sarma, 2010, "Quantum motion of electrons and holes in the random puddle landscape of graphene" (unpublished).

Rossi, E., and S. Das Sarma, 2008, "Ground State of Graphene in the Presence of Random Charged Impurities," Phys. Rev. Lett. **101**, 166803.

Rutter, G. M., J. N. Crain, N. P. Guisinger, T. Li, P. N. First, and J. A. Stroscio, 2007, "Scattering and Interference in Epitaxial Graphene," Science **317**, 219.

Rycerz, A., J. Tworzydlo, and C. W. J. Beenakker, 2007a, "Anomalously large conductance fluctuations in weakly disordered graphene," Europhys. Lett. **79**, 57003.

Rycerz, A., J. Tworzydlo, and C. W. J. Beenakker, 2007b, "Valley filter and valley valve in graphene," Nature Phys. **3**, 172.

Ryu, S., C. Mudry, A. Furusaki, and A. W. W. Ludwig, 2007, "Landauer conductance and twisted boundary conditions for Dirac fermions in two space dimensions," Phys. Rev. B **75**, 205344.

Ryu, S., C. Mudry, H. Obuse, and A. Furusaki, 2007, "Z(2) topological term, the global anomaly, and the two-dimensional symplectic symmetry class of anderson localization," Phys. Rev. Lett. **99**, 116601.

San-Jose, P., E. Prada, and D. S. Golubev, 2007, "Universal scaling of current fluctuations in disordered graphene," Phys. Rev. B **76**, 195445.

Schedin, F., A. K. Geim, S. V. Morozov, D. Jiang, E. H. Hill, P. Blake, and K. S. Novoselov, 2007, "Detection of Individual Molecules by Graphene-Based Sensors," Nature Mater. **6**, 652.

Schuessler, A., P. M. Ostrovsky, I. V. Gornyi, and A. D. Mirlin, 2009, "Analytic theory of ballistic transport in disordered graphene," Phys. Rev. B **79**, 075405.

Semenoff, G. W., 1984, "Condensed-Matter Simulation of a Three-Dimensional Anomaly," Phys. Rev. Lett. **53**, 2449.

Senz, V., T. Ihn, T. Heinzel, K. Ensslin, G. Dehlinger, D. Grutzmacher, U. Gennser, E. H. Hwang, and S. Das Sarma, 2002, "Analysis of the resistance of two-dimensional holes in

SiGe over a wide temperature range," Physica E (Amsterdam) **13**, 723.

Sheehy, D. E., and J. Schmalian, 2009, "Optical transparency of graphene as determined by the fine-structure constant," Phys. Rev. B **80**, 193411.

Sheng, L., D. N. Sheng, F. D. M. Haldane, and L. Balents, 2007, "Odd-integer quantum Hall effect in graphene: Interaction and disorder effects," Phys. Rev. Lett. **99**, 196802.

Shi, J., and X. C. Xie, 2002, "Droplet State and the Compressibility Anomaly in Dilute 2D Electron Systems," Phys. Rev. Lett. **88**, 086401.

Shishir, R. S., and D. K. Ferry, 2009, "Intrinsic mobility in graphene," J. Phys. Condens. Matter **21**, 232204.

Shizuya, K., 2010, "Many-body corrections to cyclotron resonance in monolayer and bilayer graphene," Phys. Rev. B **81**, 075407.

Shklovskii, B., and A. Efros, 1984, *Electronic Properties of Doped Semiconductors* (Springer, Berlin).

Shon, N., and T. Ando, 1998, "Quantum Transport in Two-Dimensional Graphite System," J. Phys. Soc. Jpn. **67**, 2421.

Shytov, A. V., M. I. Katsnelson, and L. S. Levitov, 2007a, "Atomic collapse and quasi-Rydberg states in graphene," Phys. Rev. Lett. **99**, 246802.

Shytov, A. V., M. I. Katsnelson, and L. S. Levitov, 2007b, "Vacuum Polarization and Screening of Supercritical Impurities in Graphene," Phys. Rev. Lett. **99**, 236801.

Shytov, A. V., M. S. Rudner, and L. S. Levitov, 2008, "Klein Backscattering and Fabry-Perot Interference in Graphene Heterojunctions," Phys. Rev. Lett. **101**, 156804.

Sinitskii, A., A. A. Fursina, D. V. Kosynkin, A. L. Higginbotham, D. Natelson, and J. M. Tour, 2009, "Electronic transport in monolayer graphene nanoribbons produced by chemical unzipping of carbon nanotubes," Appl. Phys. Lett. **95**, 253108.

Sinitsyn, N. A., J. E. Hill, H. Min, J. Sinova, and A. H. MacDonald, 2006, "Charge and spin Hall conductivity in metallic graphene," Phys. Rev. Lett. **97**, 106804.

Slonczewski, J. C., and P. R. Weiss, 1958, "Band Structure of Graphite," Phys. Rev. **109**, 272.

Sofo, J. O., A. S. Chaudhari, and G. D. Barber, 2007, "Graphane: A two-dimensional hydrocarbon," Phys. Rev. B **75**, 153401.

Sols, F., F. Guinea, and A. H. Castro Neto, 2007, "Coulomb Blockade in Graphene Nanoribbons," Phys. Rev. Lett. **99**, 166803.

Son, Y. W., M. L. Cohen, and S. G. Louie, 2006b, "Half-metallic graphene nanoribbons," Nature (London) **444**, 347.

Son, Y.-W., M. L. Cohen, and S. G. Louie, 2006a, "Energy Gaps in Graphene Nanoribbons," Phys. Rev. Lett. **97**, 216803.

Sonin, E. B., 2008, "Charge transport and shot noise in a ballistic graphene sheet," Phys. Rev. B **77**, 233408.

Sonin, E. B., 2009, "Effect of Klein tunneling on conductance and shot noise in ballistic graphene," Phys. Rev. B **79**, 195438.

Spivak, B., S. V. Kravchenko, S. A. Kivelson, and X. P. A. Gao, 2010, "Colloquium: Transport in strongly correlated two dimensional electron fluids," Rev. Mod. Phys. **82**, 1743.

Spruch, L., 1991, "Pedagogic notes on Thomas-Fermi theory (and on some improvements): atoms, stars, and the stability of bulk matter," Rev. Mod. Phys. **63**, 151.

Stampfer, C., J. Guttinger, S. Hellmueller, F. Molitor, K. Ensslin, and T. Ihn, 2009, "Energy Gaps in Etched Graphene Nanoribbons," Phys. Rev. Lett. **102**, 056403.

Stander, N., B. Huard, and D. Goldhaber-Gordon, 2009, "Evidence for Klein Tunneling in Graphene *p-n* Junctions," Phys. Rev. Lett. **102**, 026807.

Stauber, T., N. M. R. Peres, and A. K. Geim, 2008, "Optical conductivity of graphene in the visible region of the spectrum," Phys. Rev. B **78**, 085432.

Stauber, T., N. M. R. Peres, and F. Guinea, 2007, "Electronic transport in graphene: A semiclassical approach including midgap states," Phys. Rev. B **76**, 205423.

Stauber, T., N. M. R. Peres, and A. H. C. Neto, 2008, "Conductivity of suspended and non-suspended graphene at finite gate voltage," Phys. Rev. B **78**, 085418.

Stern, F., 1967, "Polarizability of a Two-Dimensional Electron Gas," Phys. Rev. Lett. **18**, 546.

Stern, F., 1980, "Calculated Temperature Dependence of Mobility in Silicon Inversion Layers," Phys. Rev. Lett. **44**, 1469.

Stern, F., and S. Das Sarma, 1984, "Electron energy levels in GaAs-Ga1-xAlxAs heterojunctions," Phys. Rev. B **30**, 840.

Stolyarova, E., K. T. Rim, S. Ryu, J. Maultzsch, P. Kim, L. E. Brus, T. F. Heinz, M. S. Hybertsen, and G. W. Flynn, 2007, "High-Resolution Scanning Tunneling Microscopy Imaging of Mesoscopic Graphene Sheets on an Insulating Surface," Proc. Natl. Acad. Sci. U.S.A. **104**, 9209.

Suzuura, H., and T. Ando, 2002a, "Crossover from Symplectic to Orthogonal Class in a Two-Dimensional Honeycomb Lattice," Phys. Rev. Lett. **89**, 266603.

Suzuura, H., and T. Ando, 2002b, "Phonons and electron-phonon scattering in carbon nanotubes," Phys. Rev. B **65**, 235412.

Tan, Y.-W., Y. Zhang, K. Bolotin, Y. Zhao, S. Adam, E. H. Hwang, S. Das Sarma, H. L. Stormer, and P. Kim, 2007, "Measurement of Scattering Rate and Minimum Conductivity in Graphene," Phys. Rev. Lett. **99**, 246803.

Tan, Y.-W., Y. Zhang, H. L. Stormer, and P. Kim, 2007, "Temperature Dependent Electron Transport in Graphene," Eur. Phys. J. Special Topics **148**, 15.

Terekhov, I. S., A. I. Milstein, V. N. Kotov, and O. P. Sushkov, 2008, "Screening of Coulomb Impurities in Graphene," Phys. Rev. Lett. **100**, 076803.

Thomas, L. H., 1927, "The calculation of atomic fields," Proc. Cambridge Philos. Soc. **23** 542.

Thompson-Flagg, R. C., M. J. B. Moura, and M. Marder, 2009, "Rippling of graphene," Europhys. Lett. **85**, 46002.

Tikhonenko, F. V., A. A. Kozikov, A. K. Savchenko, and R. V. Gorbachev, 2009, "Transition between Electron Localization and Antilocalization in Graphene," Phys. Rev. Lett. **103**, 226801.

Titov, M., 2007, "Impurity-assisted tunneling in graphene," Europhys. Lett. **79**, 17004.

Tiwari, R. P., and D. Stroud, 2009, "Model for the magnetoresistance and Hall coefficient of inhomogeneous graphene," Phys. Rev. B **79**, 165408.

Todd, K., H. T. Chou, S. Amasha, and D. Goldhaber-Gordon, 2009, "Quantum Dot Behavior in Graphene Nanoconstrictions," Nano Lett. **9**, 416.

Toke, C., P. E. Lammert, V. H. Crespi, and J. K. Jain, 2006, "Fractional quantum Hall effect in graphene," Phys. Rev. B **74**, 235417.

Tombros, N., C. Jozsa, M. Popinciuc, H. T. Jonkman, and B. J. van Wees, 2007 Nature (London) **448**, 571.

Tracy, L. A., E. H. Hwang, K. Eng, G. A. T. Eyck, E. P. Nordberg, K. Childs, M. S. Carroll, M. P. Lilly, and S. Das Sarma, 2009, "Observation of percolation-induced two-dimensional metal-insulator transition in a Si MOSFET," Phys. Rev. B **79**, 235307.

Trushin, M., J. Kailasvuori, J. Schliemann, and A. H. MacDonald, 2010, "Finite conductivity minimum in bilayer graphene without charge inhomogeneities," Phys. Rev. B **82**, 155308.

Trushin, M., and J. Schliemann, 2007, "Minimum Electrical and Thermal Conductivity of Graphene: A Quasiclassical Approach," Phys. Rev. Lett. **99**, 216602.

Trushin, M., and J. Schliemann, 2008, "Conductivity of graphene: How to distinguish between samples with short and long range scatterers," Europhys. Lett. **83**, 17001.

Tse, W.-K., and S. Das Sarma, 2007, "Phonon-Induced Many-Body Renormalization of the Electronic Properties of Graphene," Phys. Rev. Lett. **99**, 236802.

Tworzydło, J., C. W. Groth, and C. W. J. Beenakker, 2008, "Finite difference method for transport properties of massless Dirac fermions," Phys. Rev. B **78**, 235438.

Tworzydło, J., B. Trauzettel, M. Titov, A. Rycerz, and C. W. J. Beenakker, 2006, "Sub-Poissonian Shot Noise in Graphene," Phys. Rev. Lett. **96**, 246802.

Vafek, O., 2007, "Anomalous Thermodynamics of Coulomb-Interacting Massless Dirac Fermions in Two Spatial Dimensions," Phys. Rev. Lett. **98**, 216401.

Vasko, F. T., and V. Ryzhii, 2007, "Voltage and temperature dependencies of conductivity in gated graphene," Phys. Rev. B **76**, 233404.

von Klitzing, K. V., G. Dorda, and M. Pepper, 1980, "New Method for High-Accuracy Determination of the Fine-Structure Constant Based on Quantized Hall Resistance," Phys. Rev. Lett. **45**, 494.

Wakabayashi, K., M. Fujita, H. Ajiki, and M. Sigrist, 1999, "Electronic and magnetic properties of nanographite ribbons," Phys. Rev. B **59**, 8271.

Wallace, P. R., 1947, "The Band Theory of Graphite," Phys. Rev. **71**, 622.

Wang, H., D. N. Sheng, L. Sheng, and F. D. M. Haldane, 2008, "Broken-symmetry states of dirac fermions in graphene with a partially filled high landau level," Phys. Rev. Lett. **100**, 116802.

Wehling, T. O., M. I. Katsnelson, and A. I. Lichtenstein, 2009a, "Adsorbates on graphene: Impurity states and electron scattering," Chem. Phys. Lett. **476**, 125.

Wehling, T. O., M. I. Katsnelson, and A. I. Lichtenstein, 2009b, "Impurities on graphene: Midgap states and migration barriers," Phys. Rev. B **80**, 085428.

Wei, P., W. Z. Bao, Y. Pu, C. N. Lau, and J. Shi, 2009, "Anomalous Thermoelectric Transport of Dirac Particles in Graphene," Phys. Rev. Lett. **102**, 166808.

Williams, J. R., L. DiCarlo, and C. M. Marcus, 2007, "Quantum Hall Effect in a Graphene p-n Junction," Science **317**, 638.

Wilson, M., 2006, "Electrons in atomically thin carbon sheets behave like massless particles," Phys. Today **59**, No. 1, 21.

Woods, L. M., and G. D. Mahan, 2000, "Electron-phonon effects in graphene and armchair (10,10) single-wall carbon nanotubes," Phys. Rev. B **61**, 10 651.

Wu, X., X. Li, Z. Song, C. Berger, and W. A. de Heer, 2007, "Weak Antilocalization in Epitaxial Graphene: Evidence for Chiral Electrons," Phys. Rev. Lett. **98**, 136801.

Wunsch, B., T. Stauber, F. Sols, and F. Guinea, 2006, "Dynamical polarization of graphene at finite doping," New J. Phys. **8**, 318.

Wurm, J., A. Rycerz, I. Adagideli, M. Wimmer, K. Richter, and H. U. Baranger, 2009, "Symmetry Classes in Graphene Quantum Dots: Universal Spectral Statistics, Weak Localization, and Conductance Fluctuations," Phys. Rev. Lett. **102**, 056806.

Xiao, S., J.-H. Chen, S. Adam, E. D. Williams, and M. S. Fuhrer, 2010, "Charged impurity scattering in bilayer graphene," Phys. Rev. B **82**, 041406.

Yan, X.-Z., and C. S. Ting, 2008, "Weak Localization of Dirac Fermions in Graphene," Phys. Rev. Lett. **101**, 126801.

Yang, K., 2007, "Spontaneous symmetry breaking and quantum Hall effect in graphene," Solid State Commun. **143**, 27.

Yang, K., S. Das Sarma, and A. H. MacDonald, 2006, "Collective modes and skyrmion excitations in graphene SU quantum Hall ferromagnets," Phys. Rev. B **74**, 075423.

Yang, L., C.-H. Park, Y.-W. Son, M. L. Cohen, and S. G. Louie, 2007, "Quasiparticle Energies and Band Gaps in Graphene Nanoribbons," Phys. Rev. Lett. **99**, 186801.

Young, A., and P. Kim, 2009, "Quantum interference and Klein tunnelling in graphene heterojunctions," Nature Phys. **5**, 222.

Zala, G., B. N. Narozhny, and I. L. Aleiner, 2001, "Interaction corrections at intermediate temperatures: Longitudinal conductivity and kinetic equation," Phys. Rev. B **64**, 214204.

Zeldovich, W., and V. S. Popov, 1972, "Electronic-structure of superheavy atoms," Sov. Phys. Usp. **14**, 673.

Zhang, C. H., and Y. N. Joglekar, 2007, "Wigner crystal and bubble phases in graphene in the quantum Hall regime," Phys. Rev. B **75**, 245414.

Zhang, L., J. Camacho, H. Cao, Y. P. Chen, M. Khodas, D. E. Kharzeev, A. M. Tsvelik, T. Valla, and I. A. Zaliznyak, 2009, "Breakdown of the $N = 0$ quantum Hall state in graphene: Two insulating regimes," Phys. Rev. B **80**, 241412.

Zhang, L., and M. Fogler, 2008, "Nonlinear Screening and Ballistic Transport in a Graphene *p-n* Junction," Phys. Rev. Lett. **100**, 116804.

Zhang, Y., V. Brar, C. Girit, A. Zettl, and M. Crommie, 2009, "Origin of spatial charge inhomogeneity in graphene," Nature Phys. **5**, 722.

Zhang, Y., V. W. Brar, F. Wang, C. Girit, Y. Yayon, M. Panlasigui, A. Zettl, and M. F. Crommie, 2008, "Giant Phonon-induced Conductance in Scanning Tunneling Spectroscopy of Gate-tunable Graphene," Nature Phys. **4**, 627.

Zhang, Y., Z. Jiang, J. P. Small, M. S. Purewal, Y.-W. Tan, M. Fazlollahi, J. D. Chudow, J. A. Jaszczak, H. L. Stormer, and P. Kim, 2006, "Landau-Level Splitting in Graphene in High Magnetic Fields," Phys. Rev. Lett. **96**, 136806.

Zhang, Y., Y.-W. Tan, H. L. Stormer, and P. Kim, 2005, "Experimental observation of the quantum hall effect and Berry's phase in graphene," Nature (London) **438**, 201.

Zhang, Y. B., T. T. Tang, C. Girit, Z. Hao, M. C. Martin, A. Zettl, M. F. Crommie, Y. R. Shen, and F. Wang, 2009, "Direct observation of a widely tunable bandgap in bilayer graphene," Nature (London) **459**, 820.

Zhao, Y., P. Cadden-Zimansky, Z. Jiang, and P. Kim, 2010, "Symmetry Breaking in the Zero-Energy Landau Level in Bilayer Graphene," Phys. Rev. Lett. **104**, 066801.

Zheng, Y. S., and T. Ando, 2002, "Hall conductivity of a two-dimensional graphite system," Phys. Rev. B **65**, 245420.

Zhou, S. Y., G. H. Gweon, A. V. Fedorov, P. N. First, W. A. D. Heer, D. H. Lee, F. Guinea, A. H. C. Neto, and A. Lanzara, 2007, "Substrate-induced bandgap opening in epitaxial graphene," Nature Mater. **6**, 770.

Zhu, W., V. Perebeinos, M. Freitag, and P. Avouris, 2009, "Carrier scattering, mobilities, and electrostatic potential in monolayer, bilayer, and trilayer graphene," Phys. Rev. B **80**, 235402.

Zuev, Y. M., W. Chang, and P. Kim, 2009, "Thermoelectric and Magnetothermoelectric Transport Measurements of Graphene," Phys. Rev. Lett. **102**, 096807.